

# **Applications of a Unique Nopoldiol- Benzoxaborolate Cross-link in Biomaterials**

by

Di Wu

A thesis submitted in partial fulfillment of the requirements for the degree of

Master of Science

Department of Chemistry

University of Alberta

© Di Wu, 2019

## Abstract

A novel nopoldiol-benzoxaborolate cross-link formed by a bioorthogonal click reaction between nopoldiol- and benzoxaborole-based components was developed for the preparation of biomaterials such as hydrogels and nanogels. In contrast to the traditional boronic ester-based cross-links, this hydrolytically stable, acid-resistant, and bioorthogonal cross-link provides an innovative strategy for the preparation of highly stable and widely applicable biomaterials.

In Chapter 2, the application of this chemistry towards an in situ forming, self-healing, and bioorthogonal hydrogel is described. The resulting hydrogel shows a number of advantages, such as fast gelation process, self-healing within a wide range of pH (8.5–1.5), polyol-resistant properties, and reactive oxygen species (ROS)-responsive properties. In addition, the biomedical applications of this hydrogel system were demonstrated by pH-responsive release of an anti-cancer drug (doxorubicin) and 3D encapsulation of live cells.

Furthermore, efforts on the development of a nanogel-based drug carrier for the encapsulation of another anti-cancer drug, capecitabine (CAPE), are presented in Chapter 3. Nopoldiol-benzoxaborolate cross-links were included in nanogels to produce a more stable drug carrier with ROS-responsive properties. Then, the application of a polymer–drug covalent binding strategy was evaluated in the conjugation of benzoxaborole-based polymer and CAPE through boronic ester formation. Although the nanogels demonstrated pH- and ROS- controlled release of CAPE, a more efficient encapsulation method needs to be explored further.

## Preface

Chapter 2 of this thesis has been published in *Chemistry of Materials* (*Chem. Mater.* 2019, ASAP) as Wu, D.; Wang, W.; Diaz-Dussan D.; Peng, Y.-Y; Chen, Y.; Narain, R.; Hall, D. G., “In Situ Forming, Dual-Crosslink Network, Self-Healing Hydrogel Enabled by a Bioorthogonal Nopoldiol–Benzoxaborolate Click Reaction with a Wide pH Range”. Prof. D. G. Hall and Prof. R. Narain were the supervisory authors, and I was involved actively with the conception and project creation. I wrote the manuscript with assistance from Prof. D. G. Hall. I was responsible for the experiments, including monomer synthesis, polymer synthesis and optimization, arylboronic acids–diols binding studies, oxidative degradation studies, hydrogel stability studies, drug release studies, cytotoxicity studies, and scanning electron microscopy (SEM) imaging. Wenda Wang was involved in all the rheological studies, including gelation time measurements, dynamic oscillatory frequency sweep tests, and step-strain tests. Diana Diaz-Dussan was involved partly in 3D cell encapsulation tests, confocal microscope imaging, and calculation of cell viability for hydrogel-encapsulated cells. Yi-Yang Peng was responsible for the measurement of polymer molecular weights using Gel Permeation Chromatography (GPC). Dr. Yangjun Chen was responsible for the synthesis of a key monomer (**GAEMA**) and providing ideas for drug release experiments.

Chapter 3 of this thesis is based on non-published work initiated by Prof. D. G. Hall and Prof. R. Narain. As the sole experimentalist, I was responsible for monomer synthesis, polymer synthesis, drug encapsulation and release studies, SEM imaging, and Alizarin Red S (ARS) assays.

## Acknowledgment

I would like to express my greatest appreciation to my supervisor, Prof. D. G. Hall, for his enormous support and patient guidance throughout my graduate studies. His invaluable advice and trust in my work have given me tremendous motivation and confidence to constantly persevere in my research projects. He is not only my academic supervisor but also a life mentor who always provided firm support when I faced difficulties. I am also thankful to my co-supervisor Prof. R. Narain for his constructive suggestions and guidance throughout my graduate studies.

I would like to extend my appreciation towards the Hall group members, past and present, for their immense support and encouragement. I am especially thankful to Dr. Michele Boghi and Dr. Burcin Akgun, who mentored me with the greatest patience and kindness when I first started my graduate studies. I also want to thank my closest friend in the department, Hwee Ting Ang, for guiding me on my studies, supporting me mentally, providing invaluable suggestions on my research projects, and most importantly, making lunch for me twice a week. I am thankful to those who have provided advice while I was writing my dissertation: Dr. Marco Paladino, Jasmine Bhangu, Xiangyu Li, Hwee Ting Ang, Jason Rygus, Helen Clement, Mohamad Estaitie, Carl Estrada, and Le Xuan Wang. A special thanks to a warm-hearted and extremely friendly individual, Dr. Anna D. Jordan, for her help in editing my thesis.

I also would like to thank my colleges in the Narain group, past and present, for their cooperation on my research projects. Specifically, I am thankful for the help provided by Wenda Wang, Diana Diaz-Dussan, Yi-Yang Peng, and Dr. Yangjun Chen. In regard to the Scientific Staff, I am particularly thankful to Mark Miskolzie (NMR), Prof. H. Zeng (rheometer), Li Peng (nanoFAB staff, FESEM imaging), and staff in Imaging Faculty Cross Cancer Institute (confocal laser scanning microscope). A special thanks to Gareth Lambkin (lab manager of biological services), who trained me on cell culture techniques and the use of scientific equipment with tremendous patience and friendship.

Last but not least, I would like to thank my parents for bringing me into the world and providing me with a good education. I also thank my grandparents for giving me the warmest love throughout my life. Their unconditional support is my greatest motivation while seeking a beautiful but also challenging life miles away from home.

## Table of Contents

<b>Chapter 1. Introduction: Recent Advances in Hydrogel Cross-linking Methods and the Applications of Arylboronic Acids/Esters in Biomaterials .....</b>	<b>1</b>
<b>1.1 Introduction to Hydrogels and Their Cross-linking Methods.....</b>	<b>1</b>
1.1.1 Brief History of Hydrogels .....	2
1.1.2 In Situ Hydrogel Cross-linking Methods.....	3
1.1.2.1 Physical in situ forming hydrogels.....	5
1.1.2.2 Chemical in situ forming hydrogels .....	7
1.1.3 Self-healing Hydrogels .....	9
1.1.4 Bioorthogonal and Click Chemistry in Hydrogels .....	10
1.1.5 Review of Arylboronic Acids/Esters-containing Hydrogels .....	12
1.1.5.1 Conventional arylboronic acid/ester-based hydrogels .....	12
1.1.5.2 Benzoxaborole for Hydrogels .....	13
1.1.5.3 Summary of the properties of arylboronic acids/esters-based hydrogels..	14
<b>1.2 Introduction of Nanoparticles Based on Arylboronic Acids/Esters for Cancer Therapy.....</b>	<b>16</b>
1.2.1 Nanoparticles as Anti-cancer Drug Carriers.....	16
1.2.2 Arylboronic Acids/Esters as Building Blocks for Nanomedicine in Cancer Therapy.....	17
<b>1.3 Thesis Objectives .....</b>	<b>20</b>
<b>References.....</b>	<b>22</b>
<b>Chapter 2. In Situ Forming and Dual-cure Self-healing Hydrogel Through a Bioorthogonal Nopoldiol-Benzoxaborolate Click Reaction with a Wide pH Range .....</b>	<b>27</b>
<b>2.1 Introduction.....</b>	<b>27</b>
2.1.1 Nopoldiol-Boronate Chemistry .....	29
<b>2.2 Objective .....</b>	<b>30</b>
<b>2.3 Results and Discussion .....</b>	<b>31</b>
2.3.1 Design of Dual-cure Network (DCN) Hydrogels.....	31

2.3.2 Hydrogel Synthesis – Monomer/Polymer Design & Cytotoxicity .....	32
2.3.2.1 Monomer synthesis and optimization .....	32
2.3.2.2 Polymer design.....	36
2.3.2.3 Polymer screening and optimization via cytotoxicity tests.....	37
2.3.2.4 Fabrication of hydrogels.....	47
2.3.3 Monomeric Binding Studies of Benzoxaborole – Diols from pH 8.5 to 1.5 via NMR.....	49
2.3.4 Detailed Binding Studies of Nopoldiol-Benzoxaborole .....	55
2.3.4.1 Binding studies – <sup>1</sup> H NMR analysis.....	55
2.3.4.2 Binding studies – <sup>11</sup> B NMR analysis.....	56
2.3.4.3 Binding studies – ESI-MS & LC-MS analysis .....	57
2.3.5 Rheological Measurements of Hydrogels.....	59
2.3.5.1 Gelation time determination (kinetics).....	60
2.3.5.2 Dynamic oscillatory frequency sweep (mechanical properties) .....	62
2.3.5.3 Oscillatory strain sweeps and step strain tests (self-healing).....	65
2.3.6 ROS-responsive Degradation Studies.....	69
2.3.7 Bioorthogonality of Hydrogels Towards Polyols .....	73
2.3.8 Hydrogel pH-Responsive Degradation Studies .....	76
2.3.9 pH-responsive Drug Release .....	77
2.3.10 Cytotoxicity and 3D Cell Encapsulation .....	78
<b>2.4 Conclusions</b> .....	<b>80</b>
<b>2.5 Experimental</b> .....	<b>81</b>
2.5.1 General Information.....	81
2.5.1.1 Materials.....	81
2.5.1.2 Characterization and instrumentation.....	82
2.5.2 Chemical Synthesis and Analytical Data.....	83
2.5.2.1 Synthesis of monomers .....	83
2.5.2.2 Synthesis of polymers .....	92
2.5.3 Fabrication of Hydrogels .....	94
2.5.4 Monomeric Binding Studies via NMR .....	94
2.5.4.1 NMR studies.....	94

2.5.4.2 ESI-MS studies.....	96
2.5.5 Rheological Measurements of Hydrogels.....	96
2.5.5.1 Gelation time determination.....	97
2.5.5.2 Dynamic oscillatory frequency sweeps.....	97
2.5.5.3 Oscillatory strain sweeps and step-strain tests .....	97
2.5.6 Stability Studies of Hydrogels.....	98
2.5.6.1 Monomeric ROS-responsive degradation studies via NMR.....	98
2.5.6.2 Stability study of nopoldiol-benzoxaborolate against polyols via NMR ..	99
2.5.7 pH-Responsive drug release .....	99
2.5.8 Cytotoxicity Tests of Polymers and Hydrogels.....	100
2.5.9 3D Cell Encapsulation.....	101
<b>References.....</b>	<b>102</b>
<b>Chapter 3. Benzoxaborole-based Nanogel as a Stable and Stimuli-Sensitive Nanocarrier Towards pH and Oxidation-Responsive Cancer Drug Delivery .....</b>	<b>104</b>
<b>3.1 Introduction.....</b>	<b>104</b>
3.1.1 Attempts at Encapsulating Capecitabine (CAPE) into Nanoparticles Through Covalent Bonds.....	105
<b>3.2 Objective.....</b>	<b>107</b>
<b>3.3 Results and Discussion .....</b>	<b>107</b>
3.3.1 Design of Nanogels.....	107
3.3.1.1 Design and synthesis of monomers.....	111
3.3.1.2 Design and synthesis of polymers.....	112
3.3.2 Nanogel Preparation and Drug Release Methodology .....	114
3.3.3 Attempts at Using <b>LB</b> -based nanoparticles for CAPE Drug Delivery .....	115
3.3.3.1 Homopolymer-based nanoparticles.....	115
3.3.3.2 Copolymer-based nanoparticles .....	118
3.3.4 Attempts at Using <b>PMLB–PMN</b> Nanogels for CAPE Drug Delivery .....	119
3.3.4.1 <b>PMLB–PMN</b> nanogel with 1:1 weight ratio .....	119
3.3.4.2 <b>PMLB–PMN</b> nanogel with various weight ratios.....	121
3.3.5 Polymer–Polymer and Polymer–CAPE Binding Studies via ARS Assays.....	122

<b>3.4 Conclusions and Challenges</b> .....	125
<b>3.5 Experimental</b> .....	126
3.5.1 General Information.....	126
3.5.1.1 Materials.....	126
3.5.1.2 Characterization and instrumentation.....	126
3.5.2 Chemical Synthesis and Analytical Data.....	127
3.5.2.1 Synthesis of monomer.....	127
3.5.2.2 Synthesis of polymers .....	131
3.5.3 ARS Assays .....	134
<b>References</b> .....	135
<b>Chapter 4. Thesis Conclusions and Future Perspectives</b> .....	<b>136</b>
<b>4.1 Thesis Conclusions</b> .....	136
<b>4.2 Future Perspectives</b> .....	137
4.2.1 Fast Hydrogel Degradation.....	137
4.2.2 Encapsulation of Hydrophilic and Neutral Drugs with Nanoparticles .....	139
<b>References</b> .....	139
Bibliography .....	140
Appendices .....	147
<b>Appendix 1: Selected copies of NMR spectra of compounds, polymers, binding studies, and oxidative degradation studies found in Chapter 2.</b> .....	147
<b>Appendix 2: Selected copies of NMR spectra of compounds and polymers found in Chapter 3.</b> .....	187
<b>Appendix 3: Enlarged SEM and CLSM images.</b> .....	194

## List of Tables

<b>Table 1-1:</b>	pH of different human body parts/tissues. ....	6
<b>Table 1-2:</b>	Selected covalent cross-linking reactions to form hydrogels. ....	8
<b>Table 1-3:</b>	Selected dynamic covalent cross-links for self-healing hydrogels. ....	10
<b>Table 2-1:</b>	Screening of <b>polymer 1 (DMA–MAAmBO)</b> made by RAFT polymerization. ....	38
<b>Table 2-2:</b>	Screening of <b>polymer 2 (MPC/DMA–nopoldiol – LAEMA)</b> made by RAFT polymerization. ....	38
<b>Table 2-3:</b>	Screening of <b>PEGMA</b> -containing polymers made by free-radical polymerization. ....	41
<b>Table 2-4:</b>	Comparisons of cytotoxicity between <b>DMA</b> -based polymer and <b>PEGMA</b> -based polymer. ....	44
<b>Table 2-5:</b>	Characterizations of the final synthetic polymers. ....	46
<b>Table 2-6:</b>	Fabrication of DCN and SN hydrogels by mixing <b>polymer 1</b> and <b>polymer 2</b> . ....	47
<b>Table 2-7:</b>	Results of benzoxaborolate formation between <b>MAAmBO</b> and various diols. . ....	50
<b>Table 2-8:</b>	Summary of molar ratios of reactive components in hydrogels and the resulting gelation time. ....	60
<b>Table 2-9:</b>	Summary of <b>2-2 – nopoldiol</b> conversion % to benzoxaborolate <b>2-16</b> under 0, 1, 5, 10 mM of H <sub>2</sub> O <sub>2</sub> solution after 20 and 45 min. ....	73

<b>Table 2-10:</b>	Demonstration and results of bioorthogonality tests towards endogenous sugars. ....	74
<b>Table 2-11:</b>	Calculation method of conversion% to benzoxaborolate. ....	95
<b>Table 3-1:</b>	Incubation and drug release conditions for <b>PLB</b> -based homopolymer nanoparticles.....	117
<b>Table 3-2:</b>	Incubation and drug release conditions for <b>PMLB</b> -based copolymer nanoparticles. ....	118
<b>Table 3-3:</b>	Incubation and drug release conditions for <b>PMLB</b> – <b>PMN</b> 1:1 weight ratio nanogels. ....	120
<b>Table 3-4:</b>	Incubation conditions, polymer weight ratios, and drug release conditions for <b>PMLB</b> – <b>PMN</b> nanogels. ....	122
<b>Table 3-5:</b>	Design of ARS assays for (A) binding between <b>PMLB</b> and <b>PMN</b> , and (B) <b>PMLB</b> and CAPE. ....	134

## List of Figures

<b>Figure 1-1:</b>	(A) Graphic demonstration of hydrogels and (B) contact lens as an example of hydrogels. ....	1
<b>Figure 1-2:</b>	Graphical summary of commonly used physical and chemical strategies for in situ hydrogels. ....	4
<b>Figure 1-3:</b>	Structure of poly(N-isopropylacrylamide) (pNIPAAm) and graphic illustration of a temperature-driven phase transition. ....	5
<b>Figure 1-4:</b>	Structure of poly(methacrylic acid) (PMAA) and graphic illustration of pH-dependent gel swelling/degradation. ....	6
<b>Figure 1-5:</b>	Complexation between arylboronic acids and diols in the aqueous phase. ....	12
<b>Figure 1-6:</b>	Summary of the comments on the properties of benzoxaborole-based hydrogels. ....	15
<b>Figure 1-7:</b>	Demonstration of cancer targeted drug delivery with stimuli-responsive nanomedicine and the differences in healthy and cancerous cells. ....	17
<b>Figure 1-8:</b>	Properties of arylboronic acid/ester and their corresponding applications in nanomedicines for cancer therapy. ....	18
<b>Figure 1-9:</b>	Proposed hydrogel cross-linking methods involving nopoldiol moieties. ....	20
<b>Figure 1-10:</b>	Proposed nanogel drug encapsulation strategy using nopoldiol-benzoxaborolate as cross-links and benzoxaborole-CAPE for covalent polymer-drug conjugation. ....	21

<b>Figure 2-1:</b>	Relationships between in situ forming, self-healing, and bioorthogonal properties of the hydrogels, and some examples of hydrogel cross-links. ....	28
<b>Figure 2-2:</b>	Depiction of the dual-cure network (DCN) system and the features of sugar-benzoxaborolate and nopoldiol-benzoxaborolate cross-links. ....	31
<b>Figure 2-3:</b>	Monomer candidates and the design of polymers. ....	37
<b>Figure 2-4:</b>	Illustration of polymer optimization by changing the backbone from <b>DMA</b> to <b>PEGMA</b> and the estimated weight ratios of backbone/functionalities of <b>polymer 2</b> . ....	41
<b>Figure 2-5:</b>	Graphic results of MTT assays of the polymers in Table 2-3. ....	43
<b>Figure 2-6:</b>	Graphic illustration of the design and preparation of benzoxaborolate-based single and dual-cure network hydrogels. ....	48
<b>Figure 2-7:</b>	Representative <sup>1</sup> H NMR spectra for the binding studies of <b>MAAmBO</b> and diols under different pH conditions. ....	54
<b>Figure 2-8:</b>	Detailed <sup>1</sup> H NMR spectra of nopoldiol-benzoxaborolate ( <b>2-14</b> and <b>2-15</b> ) formation at pH 8.5 to 1.5. ....	56
<b>Figure 2-9:</b>	<sup>11</sup> B NMR of <b>MAAmBO</b> (in orange) and <b>MAAmBO – nopoldiol</b> mixture (in blue) at pH 8.5 to 1.5. ....	57
<b>Figure 2-10:</b>	ESI-MS spectra of <b>MAAmBO – nopoldiol</b> mixture at (A) pH 7.4 and (B) pH 1.5. ....	58
<b>Figure 2-11:</b>	LC-MS spectra of <b>MAAmBO – nopoldiol</b> mixture at pH 1.5. ....	59
<b>Figure 2-12:</b>	Rheological measurements of the gelation process of hydrogel <b>PBNG</b> , <b>PBG</b> , <b>PBN</b> and <b>PBN'</b> . ....	61
<b>Figure 2-13:</b>	Gelation of fast in situ forming hydrogel <b>PBNG</b> (10 w/v%) at pH 7.4. ....	61

<b>Figure 2-14:</b>	Structures of polymers <b>PB</b> and <b>PB'</b> . .....	62
<b>Figure 2-15:</b>	Rheological measurements of the gelation process of hydrogels <b>PB'NG</b> , <b>PB'G</b> , <b>PB'N</b> , and <b>PB'N'</b> . .....	62
<b>Figure 2-16:</b>	(A) Dynamic oscillatory frequency sweeps of hydrogels ( <b>PBNG</b> , <b>PBG</b> , <b>PBN</b> and <b>PBN'</b> ) in 10 w/v%. (B) Dynamic oscillatory frequency sweeps of 10 w/v% <b>PBNG</b> at pH 7.4 to 1.5. ....	64
<b>Figure 2-17:</b>	SEM image of hydrogels: (A) <b>PBNG</b> at pH 7.4, (B) <b>PBN</b> at pH 7.4, (C) <b>PBG</b> at pH 7.4, (D) <b>PBNG</b> at pH 1.5. Hydrogels were all made in 10 w/v% and freeze-dried 16 h after gelation. Scale bars are equal to 20 $\mu\text{m}$ . ....	65
<b>Figure 2-18:</b>	Macroscopic demonstration of self-healing property of 10 w/v% <b>PBNG</b> at pH 7.4. ....	65
<b>Figure 2-19:</b>	Oscillatory strain sweep results of hydrogel <b>PBNG</b> at pH (A) 8.5, (B) 7.4, (C) 5.2, and (D) 1.5. ....	67
<b>Figure 2-20:</b>	Step strain tests of hydrogel <b>PBNG</b> at pH (A) 8.5, (B) 7.4, (C) 5.2, and (D) 1.5. ....	68
<b>Figure 2-21:</b>	(A) Oscillatory strain sweeps and (B) step strain tests of hydrogel <b>PBN</b> (10 w/v%) at pH 7.4. ....	68
<b>Figure 2-22:</b>	H <sub>2</sub> O <sub>2</sub> -responsive degradation profile of hydrogel <b>PBNG</b> (10 w/v%) with 1, 5, and 10 mM of H <sub>2</sub> O <sub>2</sub> . ....	69
<b>Figure 2-23:</b>	<sup>1</sup> H NMR spectra of <b>2-2</b> , <b>nopoldiol</b> , mixtures of <b>2-2</b> – <b>nopoldiol</b> with of 0, 1, 5, 10 mM of H <sub>2</sub> O <sub>2</sub> solution after 20 min, and the standard <sup>1</sup> H NMR spectra of side product <b>2-18</b> . ....	71

<b>Figure 2-24:</b>	$^1\text{H}$ NMR spectra of <b>2-2</b> , <b>nopoldiol</b> , mixtures of <b>2-2</b> – <b>nopoldiol</b> with of 0, 1, 5, 10 mM of $\text{H}_2\text{O}_2$ solution after 45 min, and the standard $^1\text{H}$ NMR spectra of side product <b>2-18</b> . ....	72
<b>Figure 2-25:</b>	Degradation profiles of <b>PBNG</b> , <b>PBG</b> and <b>PBN</b> under polyol solution of 30 mM D-glucose and 15 mM D-fructose. ....	73
<b>Figure 2-26:</b>	$^1\text{H}$ NMR spectrum of (A) <b>MAAmBO</b> – <b>nopoldiol</b> (original), (B) <b>MAAmBO</b> – <b>nopoldiol</b> with 30 mM D-glucose, and (C) <b>MAAmBO</b> – <b>nopoldiol</b> with 15 mM D-fructose. ....	76
<b>Figure 2-27:</b>	Hydrogel degradation profile of 10 w/v% (A) <b>PBNG</b> , and (B) <b>PBN</b> , respectively, at pH 7.4 to 1.5. ....	77
<b>Figure 2-28:</b>	pH-Responsive doxorubicin (Dox) drug release. (A) Cumulative Dox release profile of hydrogel <b>PBNG</b> (10 w/v%) at pH 7.4 to 1.5. (B) Picture of hydrogels at pH 7.4 to 1.5 after 48 h of drug releasing. (C) Graphic description of DN hydrogel <b>PBNG</b> pH-responsive drug release. ....	78
<b>Figure 2-29:</b>	Cytotoxicity assays and 3D cell encapsulation images. MTT assay of (A) individual polymers ( <b>PB</b> and <b>PNG</b> ), and (B) hydrogel extract of <b>PBNG</b> . (C) 2D and 3D images of Live/Dead assay of HeLa cells cultured in <b>PBNG</b> (10 w/v%) for 24 and 48 h. (D) Cell viability of the encapsulated cells (measured with the confocal microscope images, n = 4). ....	79
<b>Figure 2-30:</b>	Calibration curve of Dox at pH 7.4, 5.2, and 1.5. ....	100
<b>Figure 2-31:</b>	Live and dead control images of Hela cells cultured on cell culture plate. ....	102
<b>Figure 3-1:</b>	Chemical structure of capecitabine. ....	105

<b>Figure 3-2:</b>	Reported methods for covalent bond-mediated polymer–drug conjugates to form nanoparticles. ....	106
<b>Figure 3-3:</b>	Graphic illustration of the design and preparation of benzoxaborolate-based CAPE nanocarriers. ....	108
<b>Figure 3-4:</b>	Comparison of stability of micelles and nanogels upon dilution. ....	109
<b>Figure 3-5:</b>	Proposed pathways of pH and ROS dual-responsive degradation of nanogels. ....	110
<b>Figure 3-6:</b>	Structures of <b>MAAmBO</b> and <b>LB</b> and a graphic illustration of <b>MAAmBO</b> - and <b>LB</b> -based polymer–drug conjugation. ....	111
<b>Figure 3-7:</b>	Graphical representation of nanogel preparations and nanogel drug release methods. ....	115
<b>Figure 3-8:</b>	Proposed Structure (micelles) and SEM images of homopolymer-based nanoparticles from <b>PLB</b> . ....	116
<b>Figure 3-9:</b>	CAPE cumulative release profiles using homopolymer-based nanoparticles ( <b>PLB</b> ). ....	117
<b>Figure 3-10:</b>	CAPE cumulative release profiles using copolymer-based nanoparticles ( <b>PMLB</b> ). ....	119
<b>Figure 3-11:</b>	Structures of polymer <b>PMLB</b> and <b>PMN</b> , and SEM images of <b>PMLB</b> – <b>PMN</b> nanogels. ....	120
<b>Figure 3-12:</b>	CAPE cumulative release profiles using <b>PMLB</b> – <b>PMN</b> 1:1 weight ratio nanogels. ....	121
<b>Figure 3-13:</b>	CAPE cumulative release profiles using <b>PMLB</b> – <b>PMN</b> nanogels with various weight ratios. ....	122

**Figure 3-14:** Demonstration of ARS assays for benzoxaborole–diol binding tests. ....123

**Figure 3-15:** ARS assays for (A) binding between **PMLB** and **PMN** in concentration of [ARS]:[benzoxaborole]:[**nopoldiol**] = 1:3.4:0.7 and 1:3.4:3.5, (B) binding between **PMLB** and CAPE in concentration of [ARS]:[benzoxaborole]:[CAPE] = 1:3.4:12 and 1:3.4:24. [ARS] = 700  $\mu$ M, PBS pH 7.4 buffer, excitation: 450 nm. ....124

## List of Schemes

<b>Scheme 1-1:</b>	Formation of a benzoxaborolate between benzoxaborole and diol. ....	13
<b>Scheme 2-1:</b>	(A) Previously reported click boronate formation. (B) Previously reported synergic click boronate formation. (C) New design of nopoldiol-benzoxaborolate condensation that applied for hydrogel cross-linking. ..	29
<b>Scheme 2-2:</b>	Synthesis of monomer 5-methacrylamido-1,2-benzoxaborole ( <b>MAAmBO</b> ). .....	32
<b>Scheme 2-3:</b>	Synthesis of (1 <i>R</i> )-(-)-nopoldiol-methacrylamido-diol ( <b>nopoldiol</b> ). .....	33
<b>Scheme 2-4:</b>	Synthesis of 2-gluconamidoethyl methacrylamide ( <b>GAEMA</b> ) and 2-lactobionaidoethyl methacrylamide ( <b>LAEMA</b> ). .....	33
<b>Scheme 2-5:</b>	Synthesis of compound <b>2-4</b> to <b>MAAmBO</b> and the structure of the potential impurity <b>MAAmBO'</b> . .....	35
<b>Scheme 2-6:</b>	Synthesis of polymer <b>PB</b> , <b>PB'</b> , <b>PBN</b> , <b>PG</b> , <b>PN</b> , and <b>PN'</b> . .....	45
<b>Scheme 2-7:</b>	Oxidative degradation of mixtures of <b>2-2</b> , <b>nopoldiol</b> and <b>2-16</b> by H <sub>2</sub> O <sub>2</sub> . .....	70
<b>Scheme 3-1:</b>	Synthesis of monomer 2-(2-(2-methacrylamidoethoxy)ethoxy)-benzoxaborole ( <b>LB</b> ). .....	112
<b>Scheme 3-2:</b>	Synthesis of polymers <b>PMLB</b> and <b>PMN</b> . .....	113
<b>Scheme 4-1:</b>	Proposed modification of nopoldiol-benzoxaborolate cross-links with UV-sensitive <i>o</i> -nitrobenzyl ( <b>NB</b> ) moiety. ....	138

## List of Abbreviations

5-FU	5-fluorouracil
ACN	acetonitrile
ACVA	4,4'-azobis(4-cyanovaleric acid)
AEMA	2-aminoethyl methacrylamide hydrochloride
APBA	acrylamidophenylboronic acid
ARS	Alizarin Red S
calcd.	calculated
CAPE	capecitabine
CD	cyclodextrin
CLSM	confocal laser scanning microscope
CMC	critical micelle concentration
comp m	complex multiplet
conc.	concentration
CTP	4-cyanopentanoic acid dithiobenzoate
d	doublet
DA	Diels–Alder
DCM	dichloromethane
DCN	dual-cure network
dd	doublet of doublets
ddd	doublet of doublet of doublets
dddd	doublet of doublet of doublet of doublets
dhept	doublet of heptlet
DMA	<i>N,N'</i> -dimethylacrylamide
DMEM	dulbecco modified eagle medium
DMSO	dimethyl sulfoxide
Dox	doxorubicin
DP	degree of polymerization
ECM	extracellular matrices

EDA	ethylenediamine
EDA·2HCl	ethylenediamine dihydrochloride
EDTA	ethylenediaminetetraacetic acid
EPR	enhanced permeability and retention
ESI	electrospray ionization
ESI-MS	electrospray ionization–mass spectrometry
FBS	fetal bovine serum
FESEM	field emission scanning electron microscopy
g	grams
G'	storage modulus
G''	loss modulus
GAEMA	2-gluconamidoethyl methacrylamide
GPC	gel permeation chromatography
GSH	glutathione
h	hour
HATU	hexafluorophosphate azabenzotriazole tetramethyl uronium
HRMS	high-resolution mass spectra
Hz	hertz
IEDDA	inverse-electron demand Diels–Alder cycloaddition
IR	infrared
LAEMA	2-lactobionaidoethyl methacrylamide
LB	2-(2-(2-methacrylamidoethoxy)ethoxy)-benzoxaborole
LC-MS	liquid chromatography–mass spectrometry
LCST	lower critical solution temperature
M	molar
<i>m/z</i>	mass-to-charge ratio
m <sup>2</sup>	square meter
MAAmBO	5-methacrylamido-1,2-benzoxaborole
MAPBA	3-methacrylamido phenylboronic acid
mg	milligrams
MHz	mega Hertz

min	minutes
mL	milliliter
mM	millimolar
mm	millimetre
mmol	millimole
$M_n$	number average molecular weights
mol	mole
m.p.	melting point
MPC	2-methacryloyloxyethyl phosphorylcholine
MW	molecular weight
$M_w$	weight average molecular weights
$\mu\text{L}$	microliter
$\mu\text{m}$	micrometer
$\mu\text{M}$	micromolar
NMR	nuclear magnetic resonance spectroscopy
O.D.	optical density
Pa	pascal
PB	poly(PEGMA- <i>st</i> -MAAmBO)
PB'	poly(PEGMA- <i>st</i> -MAPBA) (PB')
PBA	phenylboronic acid
PBS	phosphate buffered saline
PDEAAm	poly( <i>N,N</i> -diethylacrylamide)
PDI	polydispersity
PDMA	poly( <i>N,N'</i> -dimethylacrylamide)
PEG	polyethylene glycol
PEGMA	poly(ethylene glycol) methyl ether methacrylate
PG	poly(PEGMA- <i>st</i> -GAEMA)
pHEMA	poly(2-hydroxyethyl methacrylate)
PLB	polyLB
PLGA	poly(D,L-lactide-co-glycolide)
Plys	polylysine

PMAA	poly(methacrylic acid)
PMLB	poly(MPC- <i>st</i> -LB)
PMN	poly(MPC- <i>st</i> -nopoldiol)
PN	poly(PEGMA- <i>st</i> -nopoldiol)
PN'	poly(PEGMA- <i>st</i> -nopoldiol)
PNG	poly(PEGMA- <i>st</i> -nopoldiol- <i>st</i> -GAEMA)
pNIPAAm	poly( <i>N</i> -isopropylacrylamide)
PVA	poly(vinyl alcohol)
q	quartet
r.t.	room temperature
rad/s	radian per second
RAFT	reversible addition–fragmentation chain-transfer
ROS	reactive oxygen species
SA	sialic acid
SEM	scanning electron microscope
siRNA	small interfering RNA
SN	single network
Sol	solution
SPAAC	strain-promoted azide-alkyne cycloaddition
<i>st</i>	statistical
t	triplet
td	triplet of doublet
TEA	triethylamine
TEMED	tetramethylethylenediamine
TFA	trifluoroacetic acid
THF	tetrahydrofuran
UV	ultraviolet
vs	versus
w/v	weight/volume
$W_i$	initial weight
$W_f$	final weight

wt

weight

# Chapter 1

## Introduction: Recent Advances in Hydrogel Cross-linking Methods and the Applications of Arylboronic Acids/Esters in Biomaterials

### 1.1 Introduction to Hydrogels and Their Cross-linking Methods

Throughout history, there have been continuous efforts to exploit animal and plant based natural substances for practical applications.<sup>1</sup> With the advancement of chemistry and materials science, humans have developed technologies to synthesize new compounds, which were used to make synthetic materials to fulfill their specific demands (e.g., surgery, pharmacology, and tissue engineering).<sup>1</sup> Among the synthetic materials, significant progress has been made in a type of soft material, known as hydrogels. Hydrogels are constructed from three-dimensional water-swollen polymer networks, which can absorb large amounts of water while retaining macromolecular network structures that consist of cross-links between polymers (Figure 1-1).<sup>2</sup> Nowadays, hydrogels stand at the center of biomaterials for various biomedical applications owing to their unique and appealing features, such as softness, hydrophilicity, biodegradability, biocompatibility, and their extracellular matrix (ECM)-like structures.<sup>3</sup>

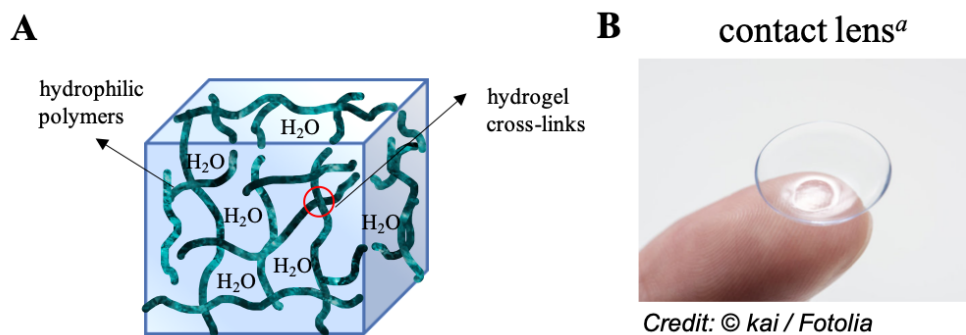


**Figure 1-1.** (A) Graphic demonstration of hydrogels and (B) contact lens as an example of hydrogels.  
<sup>a</sup><https://www.sciencedaily.com/releases/2018/09/180921082952.htm>

To fulfill the diverse requirements of modern biomedical applications, including implantation in regenerative medicine, wound healing, and controlled drug delivery, hydrogels are expected to possess more intelligent properties. Specifically, a desirable hydrogel should exhibit the following features:

- 1) Fast in situ gelation under physiological conditions to minimize invasive surgical procedures during implantations.
- 2) Autonomous self-healing upon gel fractures to maintain the integrity of materials.
- 3) Highly selective cross-linking reactions to avoid unspecific binding towards endogenous polyols (e.g., glucose) and/or cellular functional groups (e.g.,  $-\text{NH}_2$ ,  $-\text{SH}$ , and  $-\text{CHO}$ ) to ensure the bioorthogonality of the gelation reaction and the resulting hydrogels.

In this section, the aforementioned in situ forming, self-healing, and bioorthogonal properties will be discussed in detail (Section 1.1.2 to Section 1.1.4). Furthermore, the role of arylboronic acids/esters in hydrogel preparation/performance also will be addressed (Section 1.1.5).

### **1.1.1 Brief History of Hydrogels**

In 1894, the term ‘hydrogel’ first appeared in the literature to depict a type of inorganic salt-based colloidal gel.<sup>4</sup> In 1960, Wichterle and Lim first reported a water-swollen hydrogel cross-linked by macromolecular polymers for the use of contact lenses, and it became a milestone as the first generation of hydrogels.<sup>5</sup> In the following few decades, hydrogels were made from relatively simple chemically cross-linked synthetic polymers, such as poly(2-hydroxyethyl methacrylate) (pHEMA), poly(vinyl alcohol) (PVA), and poly(ethylene glycol) (PEG).<sup>6-9</sup>

The second generation of hydrogels emerged at the beginning of the 1970s, when scientists started to shift the focus of research from relatively straightforward water-swollen hydrogels to environmental-responsive hydrogels. External triggers, such as pH, temperature, or biomolecules, can be used to initiate the gel formation, gel degradation, or drug release.<sup>10-20</sup> Most of the pH-responsive and temperature-responsive physical hydrogels were cross-linked via ionic and hydrophobic interactions, respectively. Unfortunately, these cross-links involving non-covalent bonds are generally weak and unstable, thus hampering the mechanical performance of the resulting hydrogels.<sup>10</sup>

It was not until the mid-1990s, that the third generation of hydrogels was developed, based on stronger physical interactions, such as stereocomplexation,<sup>21-22</sup> host-guest interaction,<sup>22</sup> metal-ligand coordination,<sup>15-16</sup> and peptide interactions.<sup>10,23</sup> These hydrogels exhibit enhanced and finely-tuned mechanical, thermal, and degradation properties.<sup>10</sup>

Starting from the 2010s, the increased understanding and insights in organic chemistry initiated a variety of chemically cross-linked hydrogels and opened a new era of ‘smart hydrogels’. These chemically cross-linked/modified networks endow the hydrogels with not only enhanced mechanical properties but also a wider scope of stimuli-responsiveness (e.g., pH, temperature, electric field, magnetic field, ionic strength of the solution, reactive oxygen species, and biological molecules).<sup>3</sup>

### **1.1.2 In Situ Hydrogel Cross-linking Methods**

In situ forming polymeric formulations are defined as the processes of injecting into the body the liquid precursors, which then undergo gelation to form solid hydrogels.<sup>24</sup> Historically, hydrogels were pre-formed prior to delivery to the target sites in patients through invasive surgical implantation processes.<sup>25</sup> In the late 1990s, R. Langer and co-workers reported the first in situ forming hydrogels via transdermal injection. Liquid polymer precursors were injected through a small diameter needle, followed by photo-induced polymerization of liquid precursors to solid hydrogels through light penetration in the skin.<sup>26</sup>

Nowadays, in situ forming hydrogels have been used for homogenous encapsulation of therapeutic agents, cells, and biomacromolecules.<sup>27-28</sup> Owing to the superiority of this in situ sol-gel (solution to gel) transition, this system has been applied widely to the field of cell therapy, tissue engineering, immunomodulation, and in vitro diagnostics.<sup>29</sup> This strategy lowers the cost of implantation procedures and reduces the discomfort and risk for the patients. Also, the efficient in situ gel formation aids the tissue regeneration by molding the materials into the shape of the targeted cavity, minimizing the migration of materials, and mitigating the dilution of materials from tissue fluid.<sup>25-26, 30-31</sup> Like native tissues, such hydrogels possess tissue-like mechanical properties and high water-absorbing capabilities; their porous structures can transport oxygen, nutrients, and wastes to maintain cellular functions.<sup>30,32</sup> Therefore, these engineered hydrogel scaffolds have been recognized as a promising synthetic

extracellular matrix (ECM) that could support cell proliferation in the abovementioned biomedical applications.<sup>30, 33</sup>

The common methods for in situ forming hydrogels consist of both physical and chemical in situ cross-linking (Figure 1-2). The hydrogel precursors should be fluid enough to be injected through a standard needle, followed by a solidification triggered by temperature, pH, supramolecular interactions, excitations from light, or covalent binding between a pair of complementary functional groups (shown in Figure 1-2, i–v).

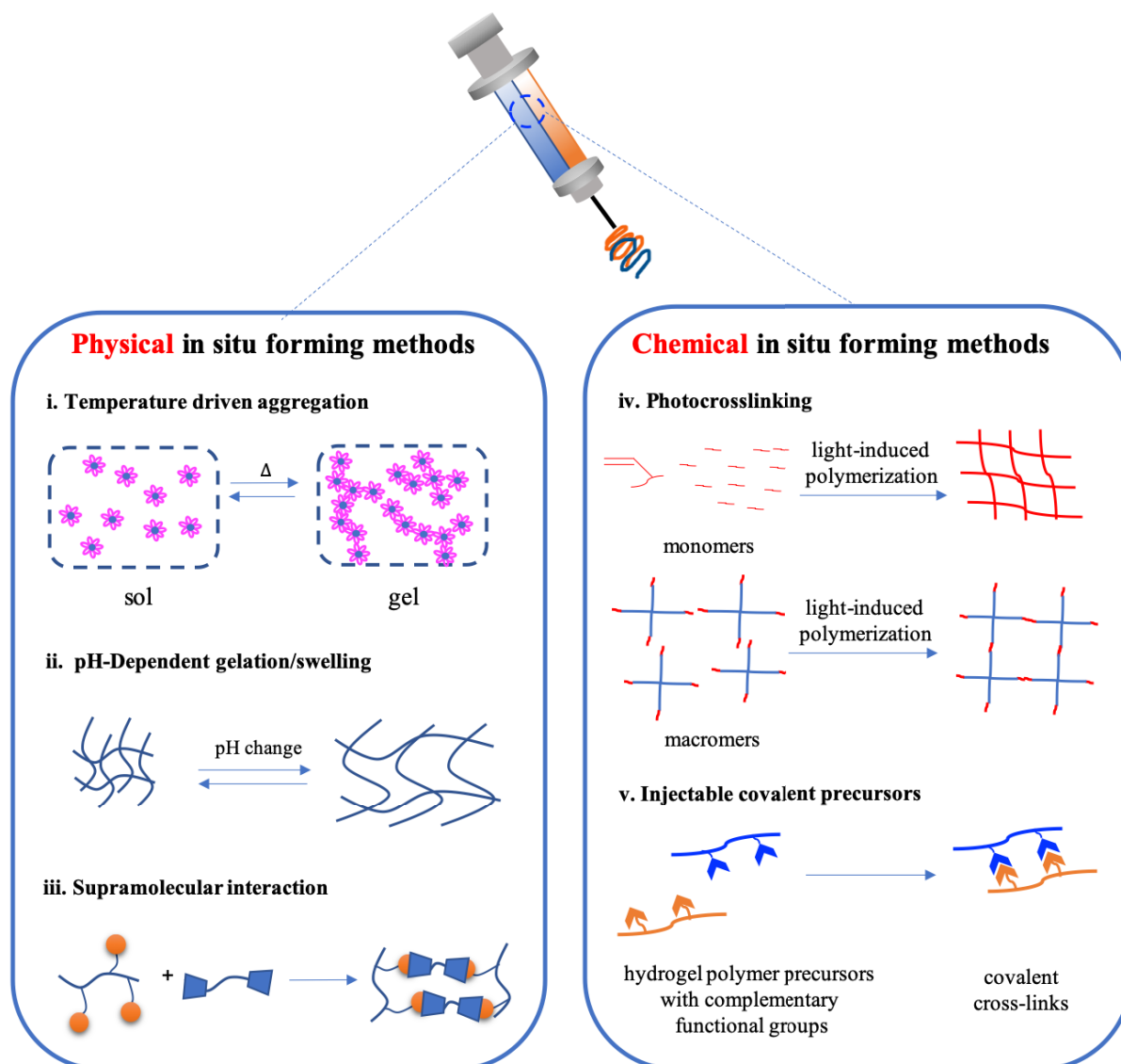


**Figure 1-2.** Graphical summary of commonly used physical and chemical strategies for in situ hydrogels.

### 1.1.2.1 Physical in situ forming hydrogels

#### i) Temperature-driven aggregation (Figure 1-2, i)

Temperature is generally a stable factor in the human body. It is regulated homeostatically throughout the body and does not vary significantly among patients.<sup>25</sup> In addition, the temperatures during the ex vivo material preparations are readily controllable, and therefore, the temperature-driven in situ gelation was one of the earliest strategies for in situ forming hydrogels. In 1968, Heskins and Guillet first reported the heat-triggered phase transition from solution to gel of poly(*N*-isopropylacrylamide) (pNIPAAm) when the temperature exceeded the lower critical solution temperature (LCST) of the polymers.<sup>34</sup> In the case of  $T$  (temperature)  $>$  LCST, the intermolecular hydrogen bonding between pNIPAAm chains is more favorable than the water/amide hydrogen bonding due to the entropy effect, therefore, the polymeric chains are aggregated/annealed into insoluble hydrogel networks (Figure 1-3).<sup>6</sup> Since then, researchers discovered a variety of thermo-responsive polymers and copolymers, such as poly(*N,N*-diethylacrylamide) (PDEAAm),<sup>35</sup> poly(D,L-lactide-co-glycolide) (PLGA)/(PEG) triblock copolymers,<sup>36</sup> and poly(MEO<sub>2</sub>MA-co-OEGMA),<sup>37</sup> with improved LCST tunability, biodegradability, and biocompatibility.

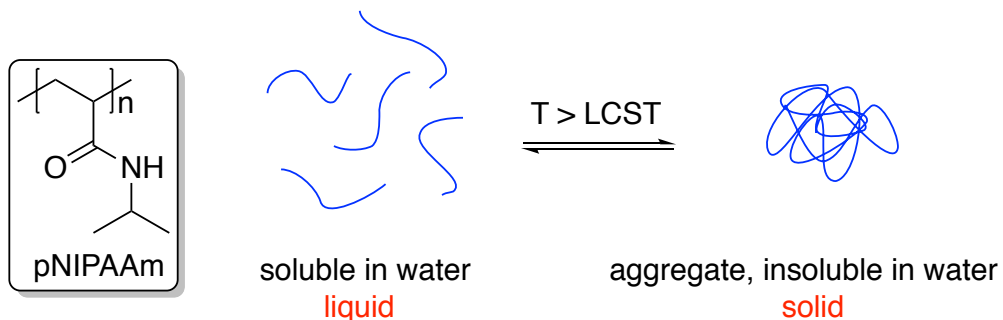


**Figure 1-3.** Structure of poly(*N*-isopropylacrylamide) (pNIPAAm) and graphic illustration of a temperature-driven phase transition.

#### ii) pH-Dependent gelation/swelling/degradation (Figure 1-2, ii)

Despite the physiological pH of the human body being around 7.4, local pH values in different human body parts/tissues vary from a pH of 1.2 (in stomach) to 8.9 (in intestine) (Table 1-1). Therefore, specific pH conditions also can trigger the gelation or the gel swelling/degradation at the site of interest.

**Table 1-1.** pH of different human body parts/tissues.

Fluids Tissue/ Cellular Compartment	pH Ranges <sup>25, 38</sup>
Stomach	1.2–2.0
Duodenum (intestine)	5.0–8.0
Chronic wounds	5.4–8.9
Extracellular matrix in cancerous tissue	6.5–7.2
Lysosomes	4.5–5.0

The pH-responsive behaviors of this type of hydrogels usually are driven by attractive or repulsive forces within the polymer backbones generated by the ionization of acid or base functional groups.<sup>25</sup> Commonly used pH-responsive polymers include acidic polymers, basic polymers, and natural polymers.<sup>39</sup> For example, poly(methacrylic acid) (PMAA), a type of polyacid (acidic polymer), can either receive or donate protons under different pH conditions. Under a higher pH environment, charge repulsion between the carboxylates weakens/disrupts the cross-links, and the gel networks swell/deform as a consequence (Figure 1-4).<sup>39</sup> The ubiquitous pH-sensitive functional groups provide countless possibilities for injectable hydrogels to undergo sol-gel transition at the desired pH.

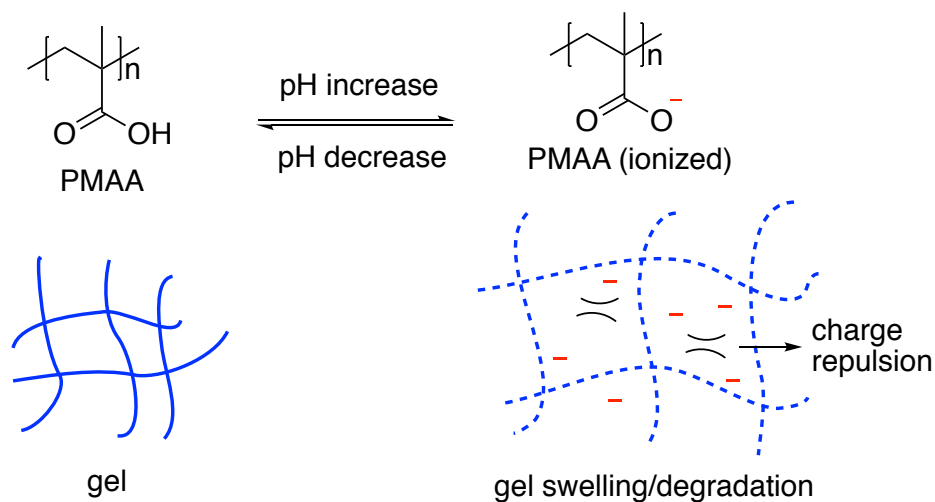


**Figure 1-4.** Structure of poly(methacrylic acid) (PMAA) and graphic illustration of pH-dependent gel swelling/degradation.

### **iii) Supramolecular interaction** (Figure 1-2, iii)

Supramolecular interaction-induced self-assembling has been explored using a variety of complementary interactions,<sup>30</sup> such as ligand-receptor pairs,<sup>40-41</sup> antigen-antibody pairs,<sup>42</sup> and base-pairing interactions.<sup>43</sup> One of the most popular examples is host-guest interaction between the cyclodextrin (CD) family (host molecules) and guest molecules (PEG and adamantane, etc.).<sup>44</sup> CDs are characterized as cyclic oligosaccharides comprised of six to eight D-glucopyranoside units. By mixing the CD-containing polymer with the counterpart of guest-containing polymers, the guest moieties are able to penetrate or be trapped in the hydrophobic inner cavities of the host molecules, resulting in the formation of hydrogel cross-links and networks.

#### **1.1.2.2 Chemical in situ forming hydrogels**

Although the design of physical in situ gelation is relatively straightforward, the non-covalent bonds dominating the networks/cross-links are weak, reversible, inhomogeneous, and highly environment-dependent.<sup>45-46</sup> In contrast, covalent cross-links are a better solution for making a more mechanically robust hydrogel toward a broader range of biomedical applications. To this date, there are two major methods to afford covalent in situ forming hydrogels: photocrosslinking (light-induced cross-linking/polymerization) and injection of covalent precursors (two precursor solutions with complementary functional groups that can interact when mixing).

### **iv) Photocrosslinking** (Figure 1-2, iv)

Light-induced cross-linking/polymerization for in situ forming hydrogels usually follows the following procedure:

- 1) Injection of liquid precursors (monomer or macromer solutions) and photoinitiators (such as ammonium peroxydisulfate and tetramethylethylenediamine (TEMED)).
- 2) UV irradiation to form hydrogel networks through free-radical polymerization in situ.

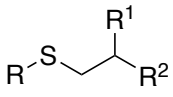
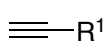
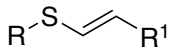
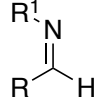
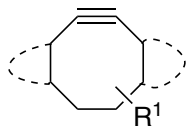
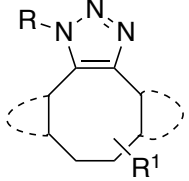
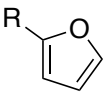
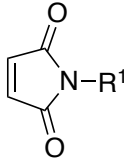
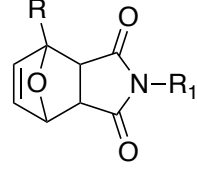
Commonly used monomers for photocrosslinking include (meth)acrylate derivatives, vinyl compounds, and ether/epoxy groups derivatives.<sup>47</sup> Various photochemical reactions have been developed in recent years, including chain photopolymerizations,<sup>48</sup> thiol-Michael additions,<sup>49-50</sup> thiol-ene/thiol-yne reactions,<sup>49, 51-52</sup> and photo-induced 1,3-dipolar cycloadditions.<sup>53-54</sup>

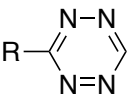
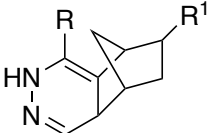
Regardless of the great temporal and spatial control over the gelation process enabled by efficient light irradiation, the high-energy UV light and the potentially toxic photoinitiators may cause damage to the surrounding cells and tissues.<sup>55</sup>

**v) Injectable covalent precursors** (Figure 1-2, v)

Unlike photocrosslinking reactions, covalent precursors generally are considered as two or more polymers that contain pendent binding counterparts on the polymer chains, and not all require light for the binding. By injecting the polymer precursors, the complementary functional groups can conjugate to form new covalent bonds autonomously under aqueous conditions and drive the gelation processes. Some commonly used covalent cross-linking reactions for the formation of hydrogels are shown in Table 1-2.

**Table 1-2.** Selected covalent cross-linking reactions to form hydrogels.

Entry	Cross-linking reaction	Reactant 1	Reactant 2	Cross-link
1	Thiol-ene <sup>56-61</sup>	R-SH		
2	Thiol-yne <sup>62</sup>	R-SH		
3	Schiff base formation <sup>63-65</sup>		H <sub>2</sub> N-R <sup>1</sup>	
4	SPAAC <sup>66-69</sup>	R-N <sub>3</sub>		
5	Diels-Alder reaction (DA) <sup>70-71</sup>			

6	Tetrazine-norbornene IEDDA <sup>72-73</sup>			
---	--	---	--	---

Unfortunately, many of these cross-linking reactions have limitations. For example, thiolene/yne reactions generally require photoinitiators and UV light;<sup>56-62</sup> Schiff base formation is pH-dependent and unspecific (cross-react with cellular amines/aldehydes), impeding the hydrogel's stability and bioorthogonality;<sup>63-65</sup> strain-promoted azide-alkyne cycloadditions (SPAAC) reactions are restricted by their slow reaction rates and complicated reactant synthesis;<sup>66-69</sup> Diels–Alder (DA) reactions require heat and the reaction rate is slow;<sup>70-71</sup> tetrazines are unstable in aqueous medium and may cross-react with cellular thiols,<sup>74-75</sup> and the tetrazine-norbornene inverse-electron demand Diels–Alder cycloaddition (IEDDA) generates N<sub>2</sub> as a byproduct, which may hamper the mechanical properties of the resulting hydrogels.<sup>72-73</sup>

### 1.1.3 Self-healing Hydrogels

For use as biomaterials, it is crucial that the implanted materials can self-heal autonomously upon mechanical damages to maintain the integrity of the networks and their normal functions during and after administration.<sup>76-77</sup> The critical features of self-healing hydrogel networks are ‘dynamic’ and ‘reversible’; namely, the network cross-links can undergo dynamic and reversible bond breaking-reforming reactions.<sup>76</sup>

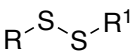
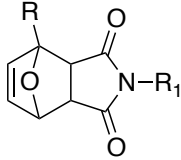
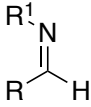
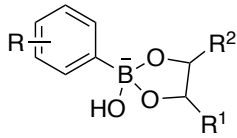
In most cases, physical hydrogels (discussed in Section 1.1.2.1) are characterized as self-healing hydrogels due to their reversible and flexible non-covalent cross-links.<sup>28</sup> Traditional covalent bonds are considered permanent and irreversible; this violates the principle of dynamicity. For example, photocrosslinking reactions produce tight C–C bonds through a radical pathway, and the networks formed are permanent and non-healable. Similarly, strain-promoted azide-alkyne cycloadditions (SPAAC) provide stable cycloaddition adducts, which are also irreversible.

To this end, dynamic covalent bonds have emerged as promising approaches to allow for repair of the damaged hydrogel network, thus achieving hydrogel self-healing properties.<sup>78-80</sup>

As shown in Table 1-3, numerous dynamic covalent polymer network systems have been developed, based on disulfide bonds,<sup>81-85</sup> Diels–Alder reactions,<sup>70-71, 86</sup> transiminations (Schiff base formation),<sup>63-65</sup> and arylboronic ester condensations.<sup>87-89</sup>

It is notable, however, that most of the current self-healing hydrogels suffer from a slow healing process, limited healing conditions (pH, temperature, or light), and unsatisfactory stimuli-responsiveness, which are considered desirable attributes in the development of biomaterials.<sup>79-80</sup> For example, reversible disulfide bond reactions require high pH conditions,<sup>79-80</sup> Diels–Alder reactions usually rely on heat and require a long healing time;<sup>70-71</sup> Schiff bases are not stable and selective in a biological environment;<sup>90</sup> arylboronic ester condensation requires a similar or a higher pH value compared to the pK<sub>a</sub> value of the arylboronic acid.<sup>91</sup> There are ongoing efforts to produce an ideal self-healing hydrogel that can function under a wider range of conditions.

**Table 1-3.** Selected dynamic covalent cross-links for self-healing hydrogels.

<b>Dynamic covalent reaction</b>	Disulfide bond formation	Diels–Alder (DA) reaction	Schiff base	Arylboronic ester condensation
<b>Cross-links</b>				
<b>Self-healing pathway</b>	Disulfide dynamic exchange reactions	Thermo-reversibility	Transimination between aldehydes and amines	Transesterification between arylboronic acids and diols

### 1.1.4 Bioorthogonal and Click Chemistry in Hydrogels

As discussed previously in Section 1.1.2, in situ forming hydrogels are highly desirable for the efficient and homogeneous encapsulation of therapeutic agents or cells, such as anti-cancer drugs, insulin, and cancer cells.<sup>92-95</sup> Therefore, it is critical that throughout the duration of a biomedical treatment, the hydrogel precursors and the in situ gelation process do not

demonstrate cytotoxicity or have unspecific reactions with the encapsulated cargos (e.g., cells and proteins), surrounding tissues, and the biological environment.<sup>96</sup>

To this end, bioorthogonal chemistry has emerged as a desirable solution for the purpose of minimizing the influence of the hydrogel gelation process on its surroundings. As reviewed by Finn and co-workers,<sup>97</sup> this system requires a pair of reactants that possess the following features:

- 1) They are mutually reactive but do not cross-react or interact with endogenous functionalities in a conspicuous way.
- 2) The reaction conditions are mild, and the reactants/products/by-products are benign to the biological environment.
- 3) The reaction is highly specific and efficient.

‘Click reaction’, termed by K. B. Sharpless in 2001, is defined by a set of stringent criteria.<sup>98</sup> Specifically, the reaction has to be modular, wide in scope, high yielding, and generate only harmless byproducts.<sup>98</sup> Recently, click chemistry has emerged as a powerful and advantageous strategy for the in situ fabrication of hydrogels due to its high selectivity and specificity.<sup>61-62, 66, 72, 96-97, 99-102</sup> Among the reactions listed in Table 1-2, thiol-ene, thiol-yne, strain-promoted azide-alkyne cycloadditions (SPAAC), Diels–Alder (DA) reaction, and tetrazine-norbornene inverse-electron demand Diels–Alder cycloaddition (IEDDA) are all recognized as click reactions.

Despite the fact that the definition of a click reaction bears some similarities with the requirements of bioorthogonality, many popular and efficient click reaction strategies to date still suffer from the use of toxic reagents, cross-reactivity towards endogenous functionalities, and specific reaction conditions (UV light or heat) (Section 1.1.2.2). As a result, many click reactions are less than ideal, and their use could impede the development of ‘click hydrogels’ in biomedical applications where a bioorthogonal gelation reaction is needed. Therefore, it is highly desirable to establish new hydrogel cross-linking systems that demonstrate the attributes of both bioorthogonality and click chemistry.

## 1.1.5 Review of Arylboronic Acids/Esters-containing Hydrogels

### 1.1.5.1 Conventional arylboronic acid/ester-based hydrogels

Arylboronic acids have found importance in the construction of hydrogel networks.<sup>103</sup> The process of arylboronic ester formation between arylboronic acids and diols (e.g., glucose, fructose, galactose, and catechol) is intrinsically reversible, thus endowing arylboronic ester-based hydrogel networks with excellent self-healing properties.<sup>103</sup>

It is well known that the binding affinities between the arylboronic acids and conventional diols (e.g., glucose, fructose, and catechol) are poor under near-neutral or acidic conditions.<sup>91</sup> The thermodynamically favored  $sp^3$  boronate complex observed at a higher pH can be explained by the release of angle strain, which results from the  $sp^2$  to  $sp^3$  boron rehybridization (Figure 1-5).<sup>104</sup> This particular pH-dependency of the hydrogel cross-links enriches the stimuli-responsiveness of the hydrogel. However, since the typical  $pK_a$  values of arylboronic acids are reported to range from 8 to 9,<sup>91</sup> this property also hampers the potential of boronic ester formation as a suitable hydrogel cross-linking click reaction, where a hydrogel is required to have fast-gelation time while being stable in physiological conditions as well as being acid-resistant.

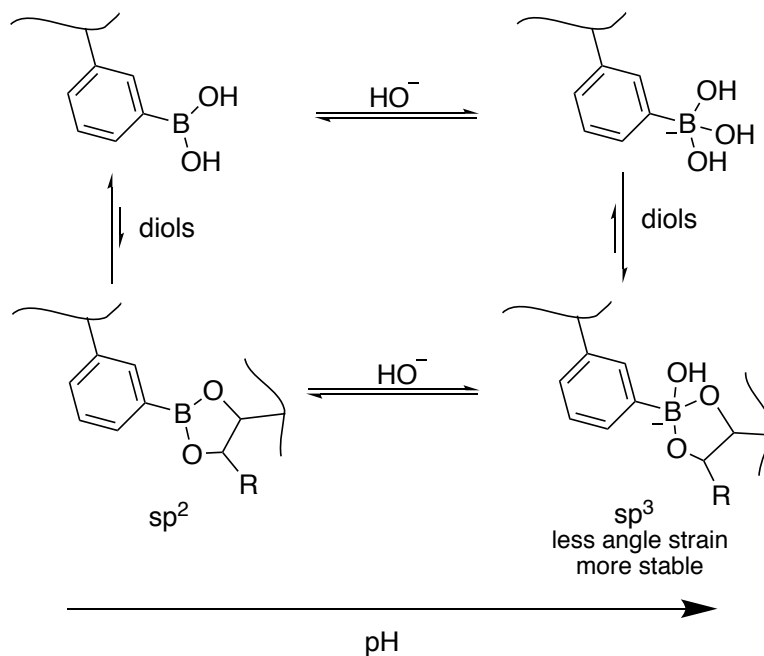
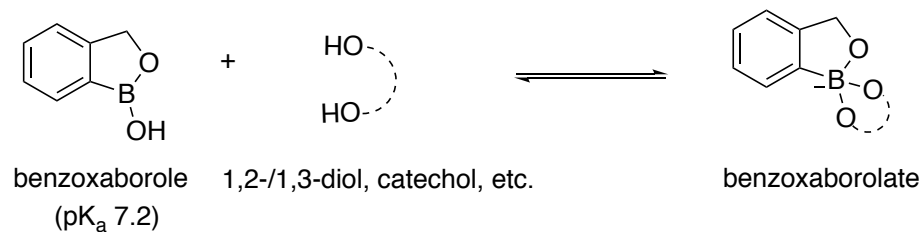


**Figure 1-5.** Complexation between arylboronic acids and diols in the aqueous phase.

Numerous attempts have been made to improve the arylboronic acid/diol binding affinity by lowering the  $pK_a$  of the boronic acid (e.g., with electron withdrawing substituents)<sup>105-107</sup> or through stabilization of the resulting boronates with intra-/inter-molecular interactions (e.g., Wulff-type B–N coordination in *o*-aminomethylarylboronic acids).<sup>108-109</sup> To the best of my knowledge, the lowest gelation at a pH of 4.0 for an arylboronic acid-based hydrogel, which exploited intramolecular B–O coordination in 2-acrylamidophenylboronic acid (2APBA), was reported by Sumerlin and co-workers.<sup>87</sup> Likewise, Kiser and co-workers reported an arylboronic acid/salicylhydroxamic acid-based hydrogel that forms at pH 4.2.<sup>88</sup> An ideal boronate-based hydrogel that can tolerate both neutral and extreme pH conditions remains elusive.

### 1.1.5.2 Benzoxaborole for Hydrogels

Benzoxaborole, a cyclic hemiboronic acid that has a lower  $pK_a$  (7.2) compared to conventional arylboronic acids (8–9) and displays excellent binding affinity towards sugar- and catechol-based polymers under physiological and basic pH has been studied by our group as a promising building block for biomaterials.<sup>110-115</sup> For example, the benzoxaborole monomer was copolymerized with a thermo-sensitive segment NIPAAm, and the resulting copolymers were complexed with cationic glycopolymers to deliver siRNA for gene therapy.<sup>115</sup> More recently, a bioinspired self-healing hydrogel comprised of benzoxaborole/catechol cross-links was utilized for 3D cell encapsulation.<sup>111</sup> The higher binding affinity between benzoxaborole and diols and the enhanced stability of the resulting benzoxaborolate under physiological conditions (Scheme 1-1) make this special hemiboronic acid a promising candidate for hydrogel building blocks.



**Scheme 1-2.** Formation of a benzoxaborolate between benzoxaborole and diol.

### 1.1.5.3 Summary of the properties of arylboronic acids/esters-based hydrogels

As mentioned in Section 1.1.3, 1.1.5.1, and 1.1.5.2, the arylboronic acid-based hydrogels possess a self-healing property at near-neutral or basic pH due to the reversibility of boronic ester formation. The unique boronate-based cross-links also introduce more appealing properties to the hydrogels for biomedical use, such as pH-responsive degradation (acid-triggered degradation), sugar-responsive degradation (e.g., glucose), and reactive oxygen species (ROS)-responsive degradation (e.g.,  $H_2O_2$ ). In spite of the numerous benefits of arylboronic esters, there are some limitations to this strategy in terms of hydrogel stability and bioorthogonality. The properties of arylboronic ester-based hydrogels are summarized and exemplified with benzoxaborole-based hydrogel, the pros and cons of which are shown in Figure 1-6.

Similar to some common dynamic covalent bonds (e.g., Schiff base), the benzoxaborolate formation reaction is also highly reversible under physiological pH conditions (Figure 1-6A). Therefore, although the benzoxaborolate is considered a stronger boronate compared to other traditional arylboronic esters, the resulting hydrogels may lack hydrolytic stability in the aqueous phase, especially for some long-term applications, such as wound dressing and sustainable drug delivery.

The human body is a complex environment that has a variety of pH values ranging between 1.2 and 8.9 depending on the type of body parts and tissues (Table 1-1). Therefore, it is essential that hydrogels can tolerate a wide range of pH conditions and maintain their functions during the injection process and the therapeutic administration. There is no doubt that the pH-dependent formation of arylboronic esters (including benzoxaborolate) provides the hydrogel with added properties of pH-controlled drug release and acid degradability; however, the fast break down of arylboronic ester hydrogel cross-links under even slightly acidic conditions restrict the use of this system in the body environment (Figure 1-6B).

Diabetes is a type of metabolic disorder that is associated with high blood sugar levels over a prolonged period.<sup>116</sup> Owing to the unique sugar binding properties of arylboronic acids, arylboronic acid-based hydrogels have been exploited in the past two decades for glucose-controlled insulin delivery.<sup>117-118</sup> Particularly, a hydrogel cross-linked through arylboronic acid formation could encapsulate insulin in the gel network. Once the glucose level is elevated, the benzoxaborole moieties in cross-links can cross-react with the cellular glucose,

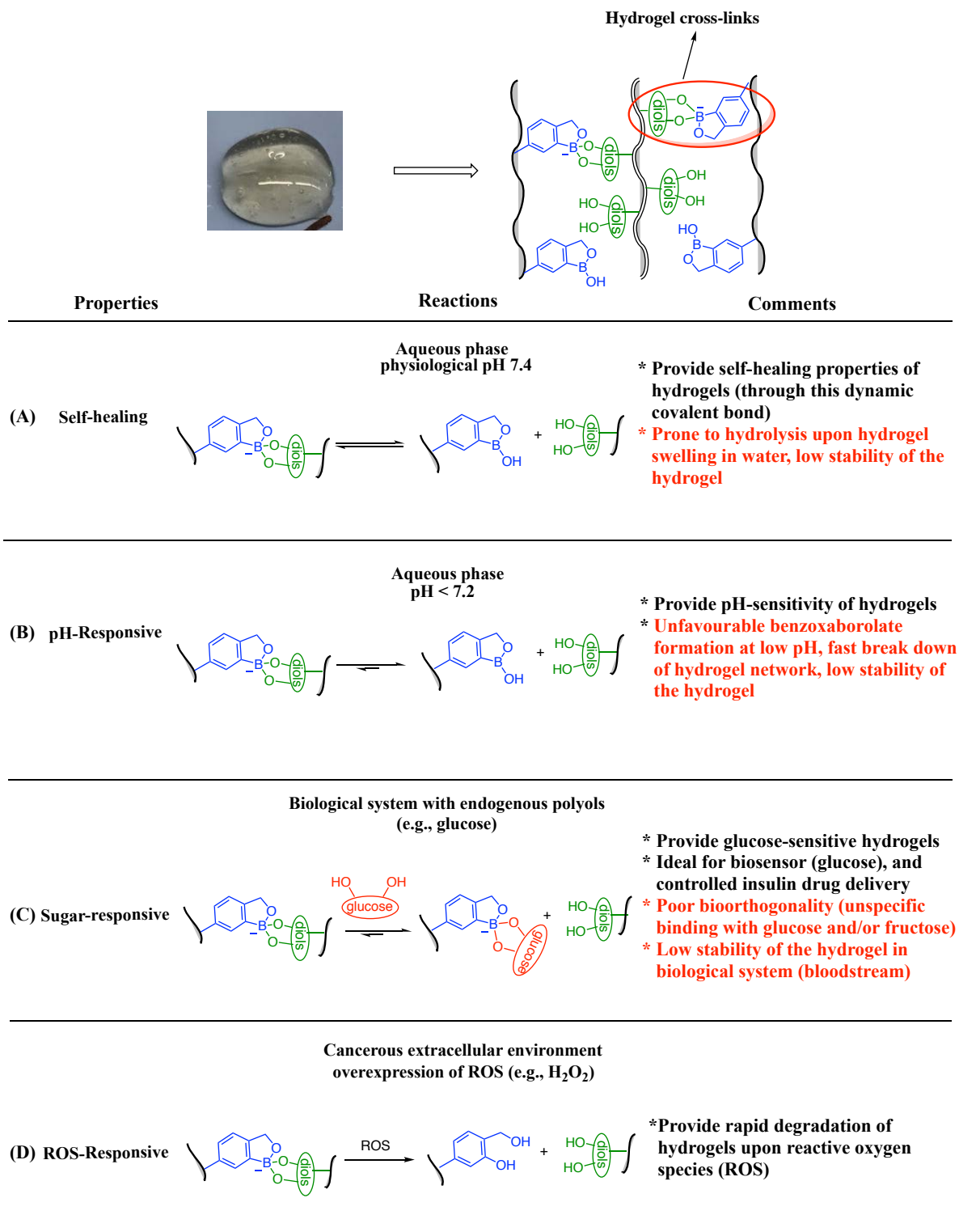


**Figure 1-6.** Summary of the comments on the properties of benzoxaborole-based hydrogels.

thus resulting in the dissociation of the cross-links. Consequently, the gel swells or degrades, and the insulin is released. One drawback of this strategy is that when the hydrogel is placed *in vivo* under normal blood sugar conditions, unspecific binding between the arylboronic acid and endogenous diols could compete with the binding between polymer chains, thus hampering the stability of the hydrogels under physiological conditions (Figure 1-6C).

Oxidative stress, defined as overproduction of ROS, is related to various pathologies, such as cancer/tumor and tissue injury.<sup>119-121</sup> Since the arylboronic acids/esters can undergo oxidative degradation (Figure 1-6D), they have been applied for ROS-responsive probes, prodrugs, and self-immolative dendrimers or polymers in recent years.<sup>120</sup> These unique features provide new insights of the arylboronic acids/esters in a broader range of biomedical applications that relative to oxidative stress.

## **1.2 Introduction of Nanoparticles Based on Arylboronic Acids/Esters for Cancer Therapy**

### **1.2.1 Nanoparticles as Anti-cancer Drug Carriers**

Nanoparticles are defined as solid, colloidal substances that range in size from 10 to 1000 nm in diameter.<sup>122</sup> Nano-sized cancer drug carriers have been shown to be capable of penetrating the tumor sites, and this process was found to be aided by the enhanced permeability and retention (EPR) effect that typically is associated with solid tumors.<sup>123</sup> Nowadays, this nanotechnology has been used to enhance the effectiveness of therapeutic agents by introducing controlled/targeted drug delivery capabilities to nanomedicines for cancer-associated therapy.<sup>122-124</sup>

Controlled/targeted drug delivery systems allow the maintenance of the appropriate dose in target sites for extended periods to ensure that the anti-cancer drug cargoes can accumulate adequately in tumors with minimal side-effects on healthy cells.<sup>122-123, 125</sup> One strategy to afford this outcome is through stimuli-responsive materials. Cancerous cells exhibit abnormal physiological signals compared to normal cells, such as lower pH value,<sup>123</sup> excessive ROS,<sup>119</sup> overexpressed sialic acids,<sup>126</sup> and higher glutathione (GSH) concentration (Figure 1-7).<sup>123</sup>

These intrinsic differences between cancerous and normal cells allow the stimuli-responsive nanomedicines to release the drugs selectively to the targets of interest without interfering with the healthy cells.

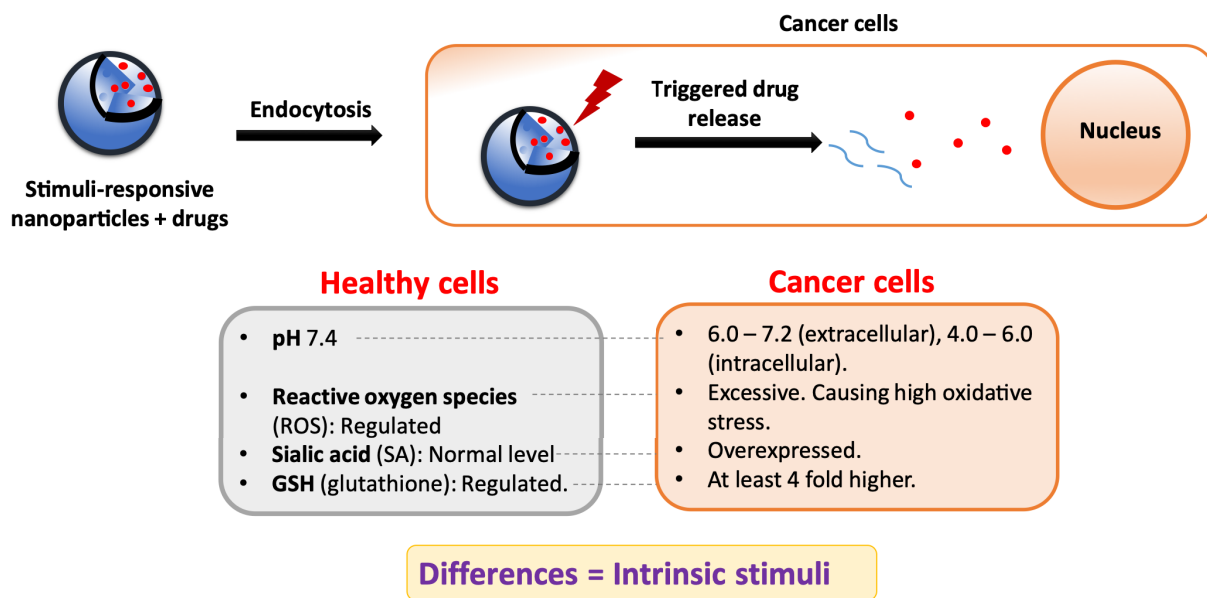


**Figure 1-7.** Demonstration of cancer targeted drug delivery with stimuli-responsive nanomedicine and the differences in healthy and cancerous cells.

## 1.2.2 Arylboronic Acids/Esters as Building Blocks for Nanomedicine in Cancer Therapy

Similar to hydrogels, the unique properties of the arylboronic acids/esters also contribute to the development of stimuli-responsive nanomedicines. As shown in Figure 1-8, the pH-dependent formation of arylboronic ester cross-links, ROS-responsive cross-link degradations, and the strong binding between arylboronic acids and sialic acid enable the nanoparticle to regulate the delivery of encapsulated anti-cancer drugs according to the stimuli mentioned in Section 1.2.1.

Firstly, the boronic ester formation is pH-dependent; therefore, it can be used to trigger the morphological changes of the drug carrier and targeted release of anti-cancer drugs.<sup>126-127</sup> For instance, Liu and co-workers developed acid-degradable prodrug micelles containing arylboronic esters.<sup>125</sup> The arylboronic acid terminated PEG chains detached from the catechol-containing micelles under low pH conditions in tumor tissues, thus resulting in the breakdown

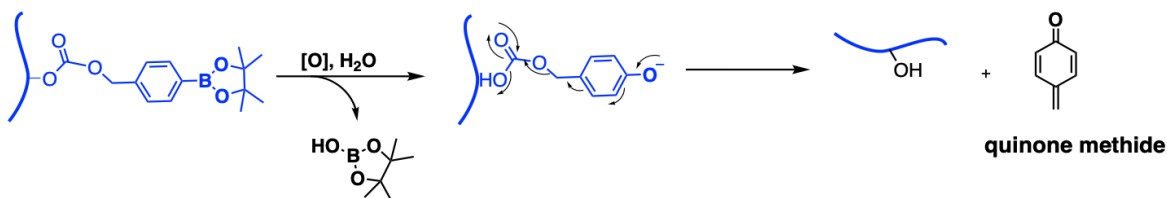
**(a) pH-Responsive binding with diol-containing polymers**

**Applications:** pH-controlled drug delivery.



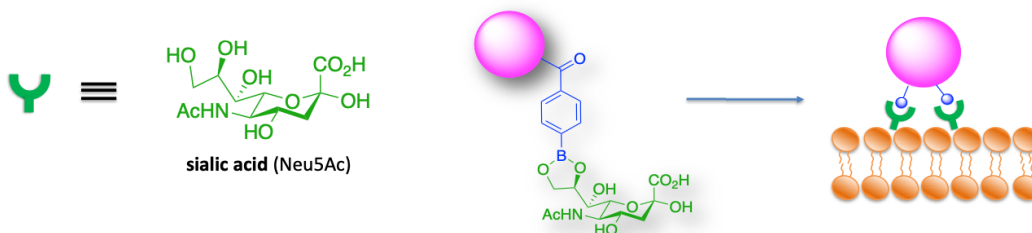
**(b) Oxidative responsive towards reactive oxygen species (ROS)**

**Applications:** ROS-triggered drug delivery.



**(c) Strong binding with sialic acids**

**Applications:** receptor-mediated endocytosis.



**(d) Interactions with diol-containing/electron donor-containing small molecules**

**Applications:** Prodrug.

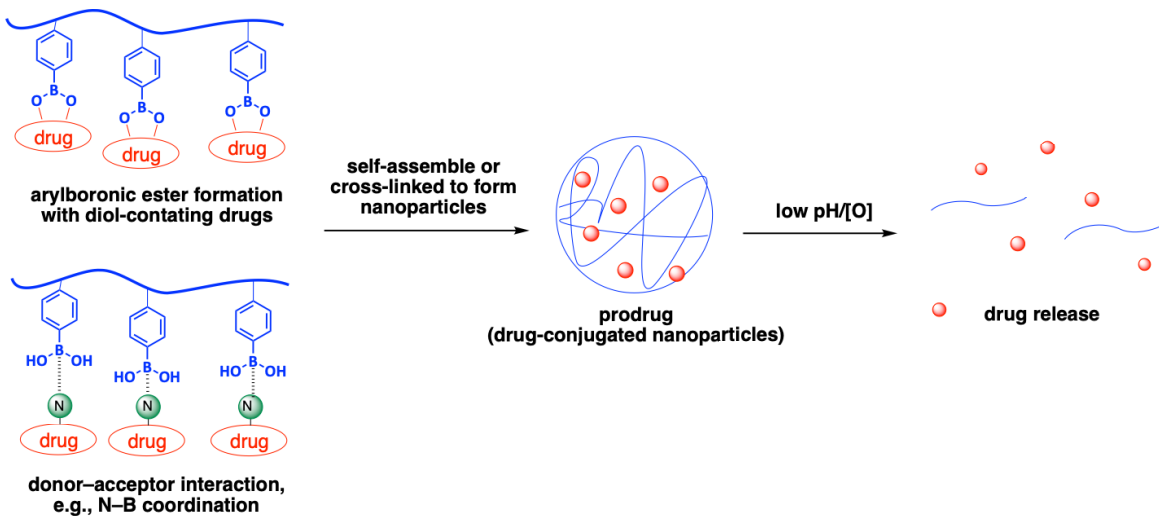


**Figure 1-8.** Properties of arylboronic acid/ester and their corresponding applications in nanomedicines for cancer therapy.

of the drug carriers and release of the drug.

Secondly, the oxidative cleavage of arylboronic esters can be triggered by hydrogen peroxide ( $\text{H}_2\text{O}_2$ ) (Figure 1-8, b), which is generated by glucose oxidase or overproduced ROS (contains peroxides, superoxide, hydroxyl radical, etc.). This property has been used widely for tumor-specific activation.<sup>128-130</sup> For example, Kataoka and co-workers reported a glucose oxidase-loaded therapeutic vesicle containing arylboronic esters, and the resulting nanoparticles have been shown to undergo self-destruction under elevated  $\text{H}_2\text{O}_2$  conditions at tumor sites.<sup>129</sup> This self-destruction mechanism afforded synergistic tumor ablation through the consumption of nutrients ( $\text{O}_2$  and glucose) and the GSH depletion with quinone methide (the by-product of arylboronic ester oxidative cleavage).<sup>129</sup>

Thirdly, arylboronic acid-modified nanoparticles have been shown to be capable of receptor-mediated endocytosis to cancerous cells due to the selective and strong binding between the arylboronic acids and sialic acid that is overexpressed on the surface of tumor cells (Figure 1-8, c).<sup>126, 131-132</sup> For instance, Kataoka and co-workers have used this binding to develop a phenylboronic acid (PBA)-containing nanomedicine with improved cellular recognition and uptakes, thus enhancing the tumor targeting ability of the nanocarriers.<sup>132</sup>

Lastly, the diol binding ability of arylboronic acids and the electrophilicity of the boron atom allows it to conjugate to small molecules that contain either a diol moiety or an electron donor centre (Figure 1-8, d). The polymer–drug complex could self-assemble/cross-link into nanoparticles, which become prodrugs for stimuli-responsive drug delivery with prolonged pharmacokinetics.<sup>133</sup> To be specific, a diol-containing drug can be conjugated on the arylboronic acid-containing polymers through formation of new covalent bonds. For example, Herrera-Alonso and co-workers developed PBA-containing micelles for the delivery of a cis-diol-containing anti-cancer drug, capecitabine.<sup>134</sup> In addition, the N–B electron donor–acceptor interaction also has been exploited in drug delivery. For instance, Yin and co-workers recently investigated PBA-based micelles for the complexation with a primary amine-containing anti-cancer drug, doxorubicin (Dox), through N–B interaction with high efficiency.<sup>135</sup>

Overall, these superior and promising properties of arylboronic acids/esters offer great potential to turn the resulting nanoparticles into smart nanocarriers for more tumor-specific and effective nanomedicines for the clinical diagnosis and treatment of solid tumors.

### 1.3 Thesis Objectives

As described in Section 1.1.5 and 1.2.2, the incorporation of arylboronic acids into hydrogels and nanoparticles provides numerous possibilities and opportunities to improve the properties of biomaterials. In the context of this thesis, the complementary reactants (arylboronic acid and diols) for arylboronic ester formation were designed carefully and embedded into a variety of polymeric network systems to enrich their applications in the field of biomedicine.

Chapter 2 describes a new hydrogel cross-linking system that fulfills all three criteria discussed previously in Section 1.1: in situ forming, self-healing, and bioorthogonal. It describes a benzoxaborolate-based hydrogel combining traditional sugar–benzoxaborole dynamic binding with a novel nopoldiol–benzoxaborole complexation (Figure 1-9). Nopoldiol, a pinanediol derivative, was chosen as one of the diol partners to improve the properties of conventional benzoxaborole-based hydrogels in all aspects of self-healing pH conditions, acid-resistance, stability, bioorthogonality, and mechanical properties. With the

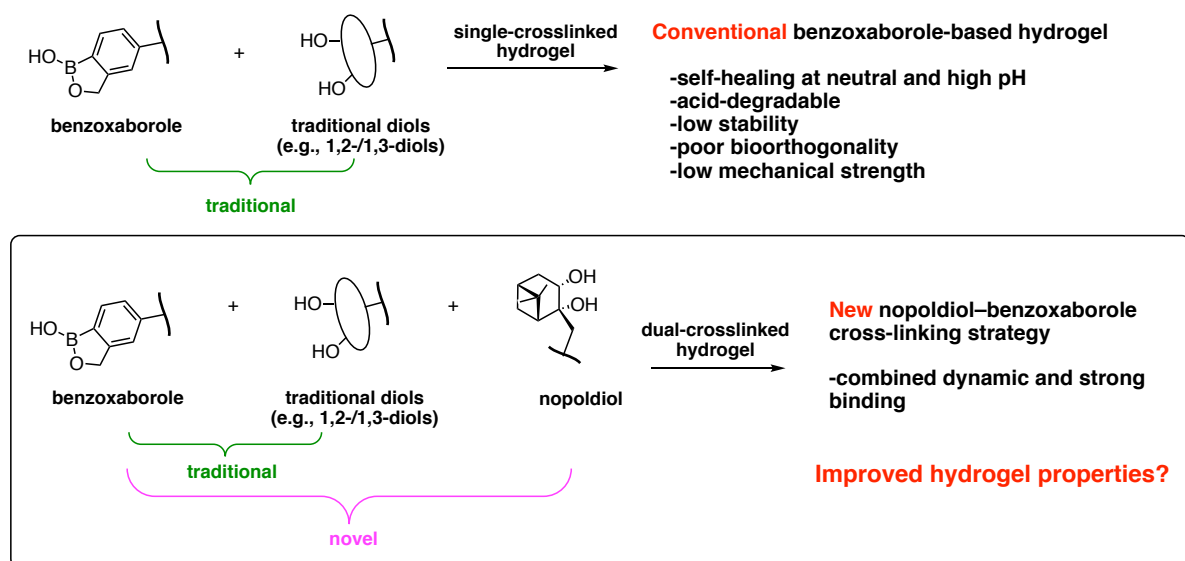


**Figure 1-9.** Proposed hydrogel cross-linking methods involving nopoldiol moieties.

combination of a dynamic sugar-based benzoxaborolate network, the hydrogels are expected also to show good pH-responsiveness, which could ultimately be used for pH-responsive drug delivery of an anti-cancer drug, doxorubicin (Dox). This chapter also presents the suitability

and biocompatibility of this nopoldiol-benzoxaborole formation reaction for cell and tissue engineering by 3D encapsulation of HeLa cells.

Chapter 3 describes the work performed towards the development of a stable nanocarrier for the delivery of an anti-cancer drug, capecitabine (Figure 1-10). A nanogel cross-linked by nopoldiol-benzoxaborolate units was designed to improve the stability of the nanoparticles. In addition, the 1,2-cis diol-containing drug, capecitabine (CAPE), could be conjugated to the excess benzoxaborole moieties on a polymeric network through covalent bond formation with arylboronic esters. Benzoxaborole, with its lower  $pK_a$  (7.2) compared to conventional arylboronic acids (8–9), is expected to form stronger covalent bonds with CAPE, thus improving the encapsulation efficiency and the stability of the resulting nanogel/drug conjugates. Furthermore, nanogel performance in the microenvironment of cancerous cells (low pH and high ROS level) will be studied to access the potential for pH-/ROS-controlled drug release of the resulting nanogel–drug complexes *in vitro*.

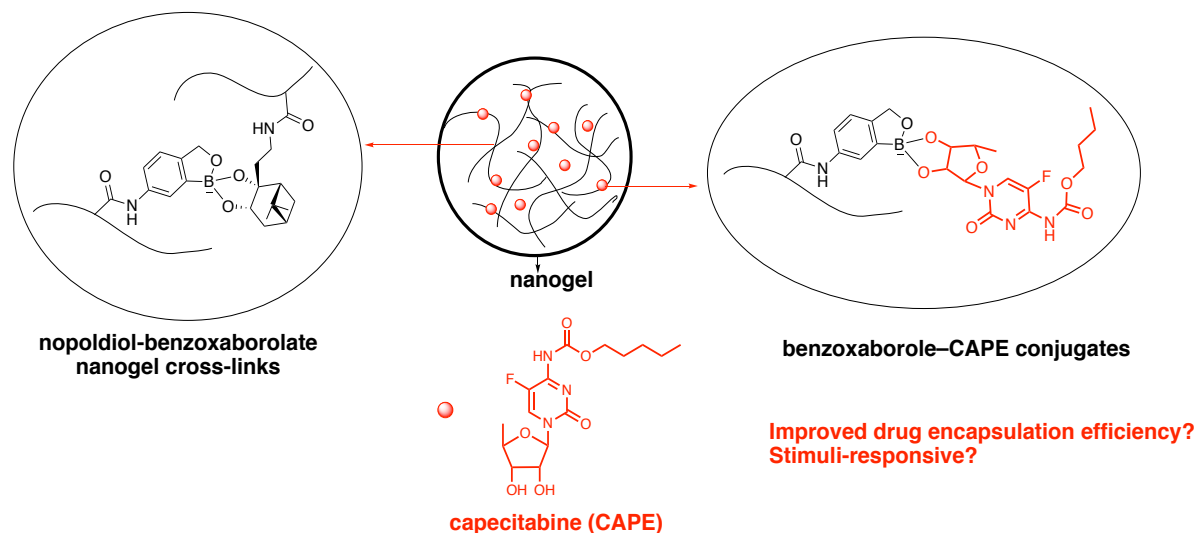


**Figure 1-10.** Proposed nanogel drug encapsulation strategy using nopoldiol-benzoxaborolate as cross-links and benzoxaborole-CAPE for covalent polymer–drug conjugation.

## References

- (1) Vert, M., *Prog. Polym. Sci.* **2007**, *32*, 755–761.
- (2) Gibas, I.; Janik, H., *Chem. Chem. Technol.* **2010**, *4*, 297–304.
- (3) Rizwan, M.; Yahya, R.; Hassan, A.; Yar, M.; Azzahari, A.; Selvanathan, V.; Sonsudin, F.; Abouloula, C., *Polymers* **2017**, *9*, 137.
- (4) Bemmelen, J., *Z Anorg Chem* **1894**, *5*, 466.
- (5) Wichterle, O.; LÍM, D., *Nature* **1960**, *185*, 117–118.
- (6) Buwalda, S. J.; Boere, K. W. M.; Dijkstra, P. J.; Feijen, J.; Vermonden, T.; Hennink, W. E., *J. Control. Release* **2014**, *190*, 254–273.
- (7) King, P. A.; Ward, J. A., *I. J. Polym. Sci. A* **1970**, *8*, 253–262.
- (8) Stafford, J. W., *Die Makromol. Chemie* **1970**, *134*, 57–69.
- (9) Nalbandian, R. M.; Henry, R. L.; Wilks, H. S., *J. of Biomed. Mater. Res.* **1972**, *6*, 583–590.
- (10) Kopecek, J., *J. Polym. Sci. A* **2009**, *47*, 5929–5946.
- (11) Otake, K.; Inomata, H.; Konno, M.; Saito, S., *Macromolecules* **1990**, *23*, 283–289.
- (12) Inomata, H.; Goto, S.; Saito, S., *Macromolecules* **1990**, *23*, 4887–4888.
- (13) Liang-chang, D.; Qi, Y.; Hoffman, A. S., *J. Control. Release* **1992**, *19*, 171–177.
- (14) Sawhney, A. S.; Pathak, C. P.; Hubbell, J. A., *Macromolecules* **1993**, *26*, 581–587.
- (15) Chujo, Y.; Sada, K.; Saegusa, T., *Macromolecules* **1993**, *26*, 6320–6323.
- (16) Chujo, Y.; Sada, K.; Saegusa, T., *Macromolecules* **1993**, *26*, 6315–6319.
- (17) Li, J.; Harada, A.; Kamachi, M., *Polym. J.* **1994**, *26*, 1019.
- (18) Cascone, M. G.; Sim, B.; Sandra, D., *Biomaterials* **1995**, *16*, 569–574.
- (19) Jeong, B.; Bae, Y. H.; Lee, D. S.; Kim, S. W., *Nature* **1997**, *388*, 860.
- (20) Petka, W. A.; Harden, J. L.; McGrath, K. P.; Wirtz, D.; Tirrell, D. A., *Science* **1998**, *281*, 389.
- (21) de Jong, S. J.; De Smedt, S. C.; Wahls, M. W. C.; Demeester, J.; Kettenes-van den Bosch, J. J.; Hennink, W. E., *Macromolecules* **2000**, *33*, 3680–3686.
- (22) Bertin, A., *Macromol. Chem. Phys.* **2012**, *213*, 2329–2352.
- (23) Dinerman, A. A.; Cappello, J.; Ghandehari, H.; Hoag, S. W., *Biomaterials* **2002**, *23*, 4203–4210.
- (24) Madan, M.; Bajaj, A.; Lewis, S.; Udupa, N.; Baig, J., *Indian J. Pharm. Sci* **2009**, *71*, 242.
- (25) Dimatteo, R.; Darling, N. J.; Segura, T., *Adv. Drug Deliv. Rev* **2018**, *127*, 167–184.
- (26) Elisseff, J.; Anseth, K.; Sims, D.; McIntosh, W.; Randolph, M.; Langer, R., *Proc. Natl. Acad. Sci. U.S.A.* **1999**, *96*, 3104.
- (27) Yang, B.; Zhang, Y.; Zhang, X.; Tao, L.; Li, S.; Wei, Y., *Polym. Chem* **2012**, *3*, 3235–3238.
- (28) Choi, B.; Loh, X. J.; Tan, A.; Loh, C. K.; Ye, E.; Joo, M. K.; Jeong, B., *In-Situ Gelling Polymers* **2015**, pp 5–35.
- (29) Seliktar, D., *Science* **2012**, *336*, 1124–1128.
- (30) Yang, J.-A.; Yeom, J.; Hwang, B. W.; Hoffman, A. S.; Hahn, S. K., *Prog. Polym. Sci.* **2014**, *39*, 1973–1986.
- (31) Yu, L.; Ding, J., *Chem. Soc. Rev.* **2008**, *37*, 1473–1481.

- (32) Tibbitt, M. W.; Anseth, K. S., *Biotechnol. Bioeng.* **2009**, *103*, 655–663.
- (33) Lee, K. Y.; Mooney, D. J., *Chem. Rev.* **2001**, *101*, 1869–1880.
- (34) Heskins, M.; Guillet, J. E., *J Macromol. Sci. A* **1968**, *2*, 1441–1455.
- (35) Qiu, Y.; Park, K., *Adv. Drug Deliv. Rev* **2012**, *64*, 49–60.
- (36) Ci, T.; Chen, L.; Yu, L.; Ding, J., *Sci. Rep.* **2014**, *4*, 5473.
- (37) Lutz, J.-F.; Akdemir, Ö.; Hoth, A., *J. Am. Chem. Soc.* **2006**, *128*, 13046–13047.
- (38) Schmaljohann, D., *Adv. Drug Deliv. Rev* **2006**, *58*, 1655–1670.
- (39) Kocak, G.; Tuncer, C.; Büttün, V., *Polym. Chem* **2017**, *8*, 144–176.
- (40) Salem, A. K.; Rose, F. R. A. J.; Oreffo, R. O. C.; Yang, X.; Davies, M. C.; Mitchell, J. R.; Roberts, C. J.; Stolnik-Trenkic, S.; Tendler, S. J. B.; Williams, P. M.; Shakesheff, K. M., *Adv. Mater.* **2003**, *15*, 210–213.
- (41) Foo, C. T. W. P.; Lee, J. S.; Mulyasmita, W.; Parisi-Amon, A.; Heilshorn, S. C., *Proc. Natl. Acad. Sci. U.S.A.* **2009**, *106*, 22067–22072.
- (42) Miyata, T.; Asami, N.; Uragami, T., *J. Polym. Sci. B* **2009**, *47*, 2144–2157.
- (43) Um, S. H.; Lee, J. B.; Park, N.; Kwon, S. Y.; Umbach, C. C.; Luo, D., *Nat. Mater.* **2006**, *5*, 797.
- (44) Li, J.; Loh, X. J., *Adv. Drug Deliv. Rev* **2008**, *60*, 1000–1017.
- (45) Hoffman, A. S., *Adv. Drug Deliv. Rev* **2012**, *64*, 18–23.
- (46) Ding, X.; Wang, Y., *J. Mater. Chem. B* **2017**, *5*, 887–906.
- (47) Blasco, E.; Wegener, M.; Barner-Kowollik, C., *Adv. Mater.* **2017**, *29*, 1604005.
- (48) Odian, G., *Principles of polymerization*. John Wiley & Sons: **2004**.
- (49) Hoyle, C. E.; Bowman, C. N., *Angew. Chem. Int. Ed.* **2010**, *49*, 1540–1573.
- (50) Nair, D. P.; Podgorski, M.; Chatani, S.; Gong, T.; Xi, W.; Fenoli, C. R.; Bowman, C. N., *Chem. Mater.* **2013**, *26*, 724–744.
- (51) Lowe, A. B., *Polym. Chem* **2014**, *5*, 4820–4870.
- (52) Morgan, C.; Magnotta, F.; Ketley, A., *J. Polym. Sci. A* **1977**, *15*, 627–645.
- (53) Agard, N. J.; Prescher, J. A.; Bertozzi, C. R., *J. Am. Chem. Soc.* **2004**, *126*, 15046–15047.
- (54) Baskin, J. M.; Prescher, J. A.; Laughlin, S. T.; Agard, N. J.; Chang, P. V.; Miller, I. A.; Lo, A.; Codelli, J. A.; Bertozzi, C. R., *Proc. Natl. Acad. Sci. U.S.A.* **2007**, *104*, 16793–16797.
- (55) Blasco, E.; Wegener, M.; Barner-Kowollik, C., *Adv. Mater.* **2017**, *29*, 1604005.
- (56) Rydholm, A. E.; Bowman, C. N.; Anseth, K. S., *Biomaterials* **2005**, *26*, 4495–4506.
- (57) Hoyle, C. E.; Lowe, A. B.; Bowman, C. N., *Chem. Soc. Rev.* **2010**, *39*, 1355–1387.
- (58) Shih, H.; Lin, C.-C., *Biomacromolecules* **2012**, *13*, 2003–2012.
- (59) Rydholm, A. E.; Anseth, K. S.; Bowman, C. N., *Acta Biomater.* **2007**, *3*, 449–455.
- (60) Rydholm, A. E.; Reddy, S. K.; Anseth, K. S.; Bowman, C. N., *Polymer* **2007**, *48*, 4589–4600.
- (61) Dong, D.; Li, J.; Cui, M.; Wang, J.; Zhou, Y.; Luo, L.; Wei, Y.; Ye, L.; Sun, H.; Yao, F., *ACS Appl. Mater. Interfaces* **2016**, *8*, 4442–4455.
- (62) Macdougall, L. J.; Truong, V. X.; Dove, A. P., *ACS Macro Lett.* **2017**, *6*, 93–97.
- (63) Saito, H.; Hoffman, A. S.; Ogawa, H. I., *J. Bioact. Compat. Polym.* **2007**, *22*, 589–601.

- (64) Wang, T.; Turhan, M.; Gunasekaran, S., *Polym. Int.* **2004**, *53*, 911–918.
- (65) Tan, H.; Chu, C. R.; Payne, K. A.; Marra, K. G., *Biomaterials* **2009**, *30*, 2499–2506.
- (66) Truong, V. X.; Tsang, K. M.; Simon, G. P.; Boyd, R. L.; Evans, R. A.; Thissen, H.; Forsythe, J. S., *Biomacromolecules* **2015**, *16*, 2246–2253.
- (67) Hodgson, S. M.; McNelles, S. A.; Abdullahu, L.; Marozas, I. A.; Anseth, K. S.; Adronov, A., *Biomacromolecules* **2017**, *18*, 4054–4059.
- (68) Hodgson, S. M.; Bakaic, E.; Stewart, S. A.; Hoare, T.; Adronov, A., *Biomacromolecules* **2016**, *17*, 1093–1100.
- (69) Xu, J.; Fillion, T. M.; Prifti, F.; Song, J., *Chem. Asian J.* **2011**, *6*, 2730–2737.
- (70) Yu, F.; Cao, X.; Li, Y.; Zeng, L.; Zhu, J.; Wang, G.; Chen, X., *Polym. Chem.* **2014**, *5*, 5116–5123.
- (71) García-Astrain, C.; Gandini, A.; Peña, C.; Algar, I.; Eceiza, A.; Corcuera, M.; Gabilondo, N., *RSC Adv.* **2014**, *4*, 35578–35587.
- (72) Truong, V. X.; Ablett, M. P.; Richardson, S. M.; Hoyland, J. A.; Dove, A. P., *J. Am. Chem. Soc.* **2015**, *137*, 1618–1622.
- (73) Alge, D. L.; Azagarsamy, M. A.; Donohue, D. F.; Anseth, K. S., *Biomacromolecules* **2013**, *14*, 949–953.
- (74) Lang, K.; Chin, J. W., *ACS Chem. Biol.* **2014**, *9*, 16–20.
- (75) Patterson, D. M.; Nazarova, L. A.; Prescher, J. A., *ACS Chem. Biol.* **2014**, *9*, 592–605.
- (76) Taylor, D. L.; in het Panhuis, M., *Adv. Mater.* **2016**, *28*, 9060–9093.
- (77) Diba, M.; Spaans, S.; Ning, K.; Ippel, B. D.; Yang, F.; Loomans, B.; Dankers, P. Y.; Leeuwenburgh, S. C., *Adv. Mater. Interfaces* **2018**, *5*, 1800118.
- (78) Shi, Y.-g.; Wang, J.-w.; Li, H.; Hu, G.-f.; Li, X.; Møllerup, S. K.; Wang, N.; Peng, T.; Wang, S., *Chem. Sci.* **2018**, *9*, 1902–1911.
- (79) Wei, Z.; Yang, J. H.; Zhou, J.; Xu, F.; Zrínyi, M.; Dussault, P. H.; Osada, Y.; Chen, Y. M., *Chem. Soc. Rev.* **2014**, *43*, 8114–8131.
- (80) Zou, W.; Dong, J.; Luo, Y.; Zhao, Q.; Xie, T., *Adv. Mater.* **2017**, *29*, 1606100.
- (81) Shu, X. Z.; Liu, Y.; Luo, Y.; Roberts, M. C.; Prestwich, G. D., *Biomacromolecules* **2002**, *3*, 1304–1311.
- (82) Shu, X. Z.; Liu, Y.; Palumbo, F.; Prestwich, G. D., *Biomaterials* **2003**, *24*, 3825–3834.
- (83) Wu, Z.; Zhang, X.; Zheng, C.; Li, C.; Zhang, S.; Dong, R.; Yu, D., *Eur. J. Pharm. Sci.* **2009**, *37*, 198–206.
- (84) Lei, Z. Q.; Xiang, H. P.; Yuan, Y. J.; Rong, M. Z.; Zhang, M. Q., *Chem. Mater.* **2014**, *26*, 2038–2046.
- (85) Kemp, M.; Go, Y.-M.; Jones, D. P., *Free Radic. Biol. Med.* **2008**, *44*, 921–937.
- (86) Wei, Z.; Yang, J. H.; Du, X. J.; Xu, F.; Zrínyi, M.; Osada, Y.; Li, F.; Chen, Y. M., *Macromol. Rapid Commun.* **2013**, *34*, 1464–1470.
- (87) Deng, C. C.; Brooks, W. L. A.; Abboud, K. A.; Sumerlin, B. S., *ACS Macro Lett.* **2015**, *4*, 220–224.
- (88) Roberts, M. C.; Hanson, M. C.; Massey, A. P.; Karren, E. A.; Kiser, P. F., *Adv. Mater.* **2007**, *19*, 2503–2507.
- (89) He, L.; Fullenkamp, D. E.; Rivera, J. G.; Messersmith, P. B., *ChemComm* **2011**, *47*, 7497–7499.

- (90) Medina, S. H., Schneider, J. P. **2017**, *Chemical Ligations in the Design of Hydrogel Materials. In Chemoselective and Bioorthogonal Ligation Reactions* (eds W. R. Algar, P. E. Dawson and I. L. Medintz).
- (91) Yan, J.; Springsteen, G.; Deeter, S.; Wang, B., *Tetrahedron* **2004**, *60*, 11205–11209.
- (92) Hoare, T. R.; Kohane, D. S., *Polymer* **2008**, *49*, 1993–2007.
- (93) Li, J.; Mooney, D. J., *Nat Rev Mater.* **2016**, *1*, 16071.
- (94) Nicodemus, G. D.; Bryant, S. J., *Tissue Eng Part B Rev* **2008**, *14*, 149–165.
- (95) Seliktar, D., *Science* **2012**, *336*, 1124.
- (96) Jiang, Y.; Chen, J.; Deng, C.; Suuronen, E. J.; Zhong, Z., *Biomaterials* **2014**, *35*, 4969–4985.
- (97) McKay, Craig S.; Finn, M. G., *Chem. Biol.* **2014**, *21*, 1075–1101.
- (98) Kolb, H. C.; Finn, M. G.; Sharpless, K. B., *Angew. Chem. Int. Ed.* **2001**, *40*, 2004–2021.
- (99) Fan, Y.; Deng, C.; Cheng, R.; Meng, F.; Zhong, Z., *Biomacromolecules* **2013**, *14*, 2814–2821.
- (100) Xu, J.; Feng, E.; Song, J., *J. Am. Chem. Soc.* **2014**, *136*, 4105–4108.
- (101) Ghanian, M. H.; Mirzadeh, H.; Baharvand, H., *Biomacromolecules* **2018**, *19*, 1646–1662.
- (102) Xu, Z.; Bratlie, K. M., *ACS Biomater. Sci. Eng.* **2018**, *4*, 2276–2291.
- (103) Guan, Y.; Zhang, Y., *Chem. Soc. Rev.* **2013**, *42*, 8106–8121.
- (104) Hall, Dennis G., ed. *Boronic acids: preparation, applications in organic synthesis and medicine*. John Wiley & Sons, **2006**.
- (105) Li, Q.; Lü, C.; Liu, Z., *J. Chromatogr. A* **2013**, *1305*, 123–130.
- (106) Alexeev, V. L.; Das, S.; Finegold, D. N.; Asher, S. A., *Clin. Chem.* **2004**, *50*, 2353.
- (107) Liu, Y.; Ren, L.; Liu, Z., *ChemComm* **2011**, *47*, 5067–5069.
- (108) Wulff, G., *Pure Appl. Chem.* **1982**, *54*, 2093–2102.
- (109) Li, H.; Liu, Y.; Liu, J.; Liu, Z., *ChemComm* **2011**, *47*, 8169–8171.
- (110) Chen, Y.; Wang, W.; Wu, D.; Nagao, M.; Hall, D. G.; Thundat, T.; Narain, R., **2018**, *19*, 596–605.
- (111) Chen, Y.; Diaz-Dussan, D.; Wu, D.; Wang, W.; Peng, Y.-Y.; Asha, A. B.; Hall, D. G.; Ishihara, K.; Narain, R., *ACS Macro Lett.* **2018**, *7*, 904–908.
- (112) Wang, Y.; Li, L.; Kotsuchibashi, Y.; Vshyvenko, S.; Liu, Y.; Hall, D.; Zeng, H.; Narain, R., *ACS Biomater. Sci. Eng.* **2016**, *2*, 2315–2323.
- (113) Kotsuchibashi, Y.; Ebara, M.; Sato, T.; Wang, Y.; Rajender, R.; Hall, D. G.; Narain, R.; Aoyagi, T., *J. Phys. Chem. B* **2015**, *119*, 2323–2329.
- (114) Kotsuchibashi, Y.; Agustin, R. V. C.; Lu, J.-Y.; Hall, D. G.; Narain, R., *ACS Macro Lett.* **2013**, *2*, 260–264.
- (115) Diaz-Dussan, D.; Nakagawa, Y.; Peng, Y.-Y.; C, L. V. S.; Ebara, M.; Kumar, P.; Narain, R., *ACS Macro Lett.* **2017**, *6*, 768–774.
- (116) Alberti, K. G. M. M.; Zimmet, P. Z., *Diabet. Med.* **1998**, *15*, 539–553.
- (117) Shiino, D.; Murata, Y.; Kubo, A.; Kim, Y. J.; Kataoka, K.; Koyama, Y.; Kikuchi, A.; Yokoyama, M.; Sakurai, Y.; Okano, T., *J. Control Release* **1995**, *37*, 269–276.
- (118) Miyata, T.; Uragami, T.; Nakamae, K., *Adv. Drug Deliv. Rev* **2002**, *54*, 79–98.

- (119) Zhang, M.; Song, C.-C.; Su, S.; Du, F.-S.; Li, Z.-C., *ACS Appl. Mater. Interfaces* **2018**, *10*, 7798–7810.
- (120) Zhang, M.; Song, C.-C.; Du, F.-S.; Li, Z.-C., *ACS Appl. Mater. Interfaces* **2017**, *9*, 25905–25914.
- (121) van der Vliet, A.; Janssen-Heininger, Y. M., *J. Cell. Biochem.* **2014**, *115*, 427–435.
- (122) Hasirci, V.; Vrana, E.; Zorlutuna, P.; Ndreu, A.; Yilgor, P.; Basmanav, F. B.; Aydin, E., *J Biomater Sci Polym Ed* **2006**, *17*, 1241–1268.
- (123) Mo, R.; Gu, Z., *Mater. Today* **2016**, *19*, 274–283.
- (124) Chacko, R. T.; Ventura, J.; Zhuang, J.; Thayumanavan, S., *Adv. Drug Deliv. Rev* **2012**, *64*, 836–851.
- (125) Brigger, I.; Dubernet, C.; Couvreur, P., *Adv. Drug Deliv. Rev* **2012**, *64*, 24–36.
- (126) Huang, Y.; Gao, Y.; Chen, T.; Xu, Y.; Lu, W.; Yu, J.; Xiao, Y.; Liu, S., *ACS Biomater. Sci. Eng.* **2017**, *3*, 3364–3375.
- (127) Wang, J.; Zhang, Z.; Wang, X.; Wu, W.; Jiang, X., *J. Control. Release* **2013**, *168*, 1–9.
- (128) Zhang, T.; Chen, X.; Xiao, C.; Zhuang, X.; Chen, X., *Polym. Chem* **2017**, *8*, 6209–6216.
- (129) Li, J.; Dirisala, A.; Ge, Z.; Wang, Y.; Yin, W.; Ke, W.; Toh, K.; Xie, J.; Matsumoto, Y.; Anraku, Y., *Angew. Chem. Int. Ed.* **2017**, *56*, 14025–14030.
- (130) Qiu, F. Y.; Zhang, M.; Ji, R.; Du, F. S.; Li, Z. C., *Macromol. Rapid Commun* **2015**, *36*, 2012–2018.
- (131) Zhang, X.; Chen, B.; He, M.; Zhang, Y.; Peng, L.; Hu, B., *Analyst* **2016**, *141*, 1286–1293.
- (132) Deshayes, S.; Cabral, H.; Ishii, T.; Miura, Y.; Kobayashi, S.; Yamashita, T.; Matsumoto, A.; Miyahara, Y.; Nishiyama, N.; Kataoka, K., *J. Am. Chem. Soc.* **2013**, *135*, 15501–15507.
- (133) Canal, F.; Sanchis, J.; Vicent, M. J., *Curr. Opin. Biotechnol.* **2011**, *22*, 894–900.
- (134) Aguirre-Chagala, Y. E.; Santos, J. L.; Huang, Y.; Herrera-Alonso, M., *ACS Macro Lett.* **2014**, *3*, 1249–1253.
- (135) Lv, S.; Wu, Y.; Cai, K.; He, H.; Li, Y.; Lan, M.; Chen, X.; Cheng, J.; Yin, L., *J. Am. Chem. Soc.* **2018**, *140*, 1235–1238.

## Chapter 2

# In Situ Forming and Dual-cure Self-healing Hydrogel Through a Bioorthogonal Nopoldiol-Benzoxaborolate Click Reaction with a Wide pH Range

The contents of this chapter have been copied and/or adapted from the following publication: In Situ Forming, Dual-Crosslink Network, Self-Healing Hydrogel Enabled by a Bioorthogonal Nopoldiol–Benzoxaborolate Click Reaction with a Wide pH Range. (*Chem. Mater.* 2019, ASAP)

### 2.1 Introduction

Hydrogels are soft biomaterials that are 3D cross-linked with hydrophilic polymeric chains. Hydrogel networks have high water-absorbing capacity and display porous structures.<sup>1</sup> Tremendous progress has been made to develop stimuli-responsive hydrogels with tunable chemical and physical properties, due to an increasing demand of biomaterials for various biomedical applications (regenerative medicine, controlled drug delivery, etc.).<sup>2</sup> As described in Chapter 1 (Section 1.1), there are three major properties for the ideal smart hydrogel: in situ forming, self-healing, and bioorthogonal. Brief definitions of these three requirements are as followed:

- 1) In situ forming: The hydrogel or hydrogel precursors are injectable through a standard needle, and the gelation should occur rapidly after the injection in vivo. (Section 1.1.2)
- 2) Self-healing: The cross-links are composed with dynamic bonds that allow the hydrogel to self-repair any damages autonomously. (Section 1.1.3)
- 3) Bioorthogonal: The hydrogel cross-linking reaction is efficient and only generates non-toxic by-products. The hydrogel must be stable in biological polyols (e.g., glucose) and the hydrogel cross-links/functionalities do not cross-react with endogenous functional groups (e.g., thiols, amines). (Section 1.1.4)

Unfortunately, even the most popular hydrogel cross-linking methods cannot fulfill all of these three requirements in the literal sense. As demonstrated in Figure 2-1, many of the cross-linking approaches that were mentioned in Chapter 1 fully satisfy only two of the three criteria

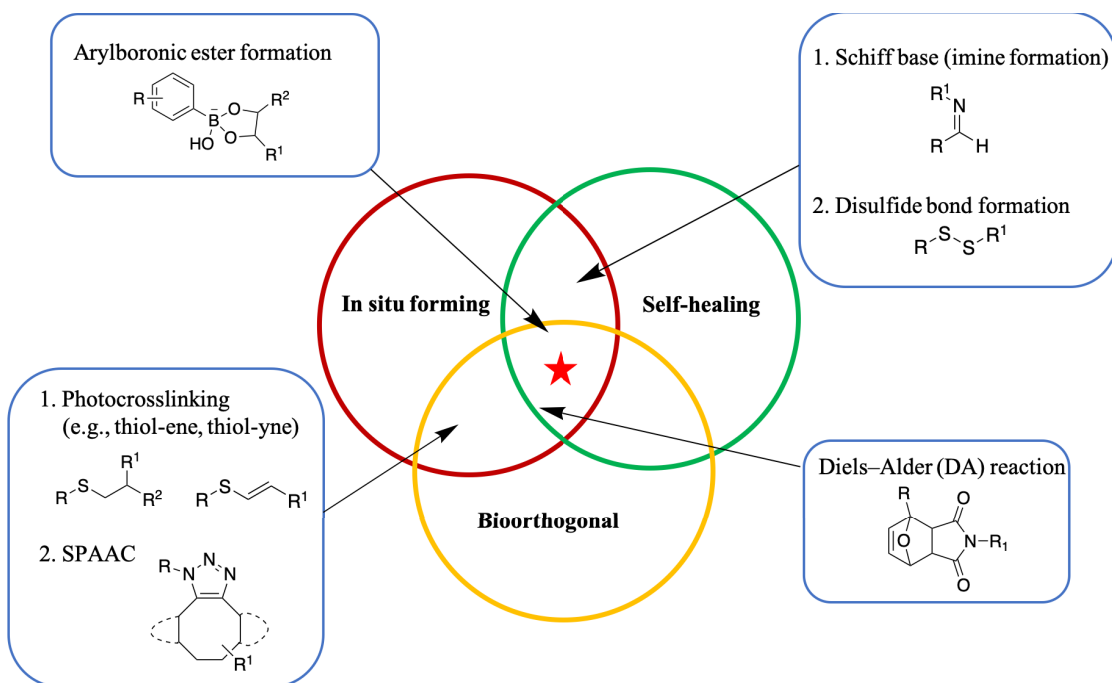


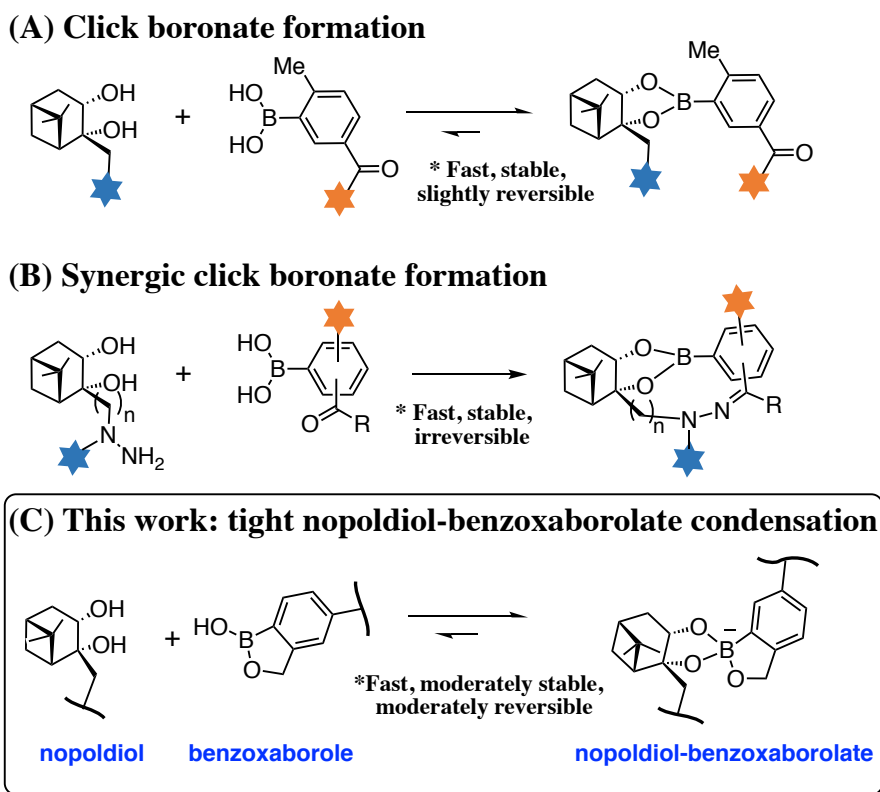
**Figure 2-1.** Relationships between in situ forming, self-healing, and bioorthogonal properties of the hydrogels, and some examples of hydrogel cross-links.

or meet the third one insufficiently. For example, the arylboronic ester formation can be achieved in situ, and the resulting hydrogels are self-healing; however, these reactions are not strictly bioorthogonal due to the competing reactions between the arylboronic acid and biological polyols, even though their binding affinities are very low. Schiff base and disulfide bonds are dynamic, and the resulting hydrogels can form in situ with self-healing properties; however, the imine and disulfide cross-links can easily react with cellular amines and thiols, which disobeys the principle of bioorthogonality. Photocrosslinking reactions and strain-promoted azide-alkyne cycloadditions (SPAAC) produce permanent cross-links, which disables the self-healing properties of the corresponding hydrogels. Lastly, Diels–Alder reaction derived hydrogels are formed in situ and are generally considered bioorthogonal. Whereas they are not strictly self-healing due to their slow reaction rates and their thermo-reversibility; the resulting hydrogels only can self-heal at high temperatures, which is impractical for clinical use.

Altogether, an ideal hydrogel that can meet all of these three criteria at once remains tentative, and the development of this type of cross-linking strategy would be exceptionally desirable for cell/tissue related biomedical applications.

### 2.1.1 Nopoldiol-Boronate Chemistry

Boronate bioorthogonal click chemistry, based on pinanediol derivatives, has been reported recently by our research group and was utilized in protein and cell labeling.<sup>3-4</sup> This new variant of boronic ester meets the standard of both bioorthogonality and click reaction by producing a stable nopoldiol-boronate with high efficiency, high conversion, mild conditions and benign byproducts (Scheme 2-1A, B). However, both of the click boronate formation reactions to access the nopoldiol-boronates are not readily reversible, which is undesirable for the design of a biodegradable and self-healing hydrogel.<sup>5</sup>



**Scheme 2-1.** (A) Previously reported click boronate formation.<sup>3</sup> (B) Previously reported synergic click boronate formation.<sup>4</sup> (C) New design of nopoldiol-benzoxaborolate condensation that applied for hydrogel cross-linking.

On the other hand, the pH conditions (1.0–8.9) of organs/tissues vary in the complex human body (Chapter 1). Therefore, the applicability of hydrogels under a wide range of pH conditions is crucial for in vivo applications, such as localized oral drug release, targeted cancer drug delivery, and wound dressing.<sup>6-7</sup> Unlike many traditional arylboronic esters which degrade readily in acidic pH, the nopoldiol-boronate was found to be very stable even at a pH of 3.<sup>3</sup> This phenomenon indicates that the incorporation of nopoldiol moieties could potentially improve the acid-stability of boronate-containing hydrogels.

Overall, the encouraging studies mention above paved the road for the exploration of a new, reversible, and acid-tolerable hydrogel cross-linking reaction that could afford the resulting nopoldiol-based hydrogel with great self-healing properties, stability, and acid-resistant ability.

## 2.2 Objective

In this work, we aim to exploit the nopoldiol-benzoxaborolate condensation reaction (Scheme 2-1C) for hydrogel cross-linking. Compared to the arylboronic acids shown in Scheme 2-1A and B, benzoxaborole is expected to form nopoldiol-benzoxaborolate with nopoldiol moieties with a higher reversibility due to the strained tetrahedral and spirocyclic arrangement of the benzoxaborolate adduct. Therefore, it is proposed that this improvement on the dynamicity of nopoldiol-benzoxaborolate would benefit the resulting hydrogel's self-healing property. The incorporation of this system to the hydrogel synthesis is expected to enable a bioorthogonal and efficient gelation process and to improve the hydrolytic stability and acid-resistance of the resulting hydrogels. The design of tight forming, but slightly reversible nopoldiol-benzoxaborolates (Scheme 2-1C) as hydrogel cross-links could mitigate the drawbacks of the traditional boronates (discussed in Section 1.1.4) and preserve the unique features of boronate-based hydrogels (oxidative degradability, etc.). However, the exclusive use of these tight cross-links may restrict the stimuli-responsive properties (e.g., pH-sensitivity and sugar-sensitivity) of the resulting hydrogels. Therefore, we intend to combine traditional dynamic sugar-benzoxaborolate cross-links with the rigid nopoldiol-benzoxaborolate cross-links to resolve the problem of stimuli-responsiveness with stability and bioorthogonality, thus advancing the development of the boronate-based hydrogels.

## 2.3 Results and Discussion

### 2.3.1 Design of Dual-cure Network (DCN) Hydrogels

To install the two distinctive benzoxaborolate cross-links in the hydrogel network, we designed a dual-cure network (DCN) system. As the name suggests, the network is made of both dynamic and highly reversible (self-curable) cross-links, as well as the rigid and moderately reversible (self-curable) cross-links (Figure 2-2). As shown in Figure 2-2, the two types of cross-links have complementary features in terms of reversibility, acid resistance, sugar resistance, synthetic approaches, and stability. However, as an inherent benefit of boronates, both nopoldiol- and sugar-benzoxaborolates are sensitive to  $H_2O_2$ .

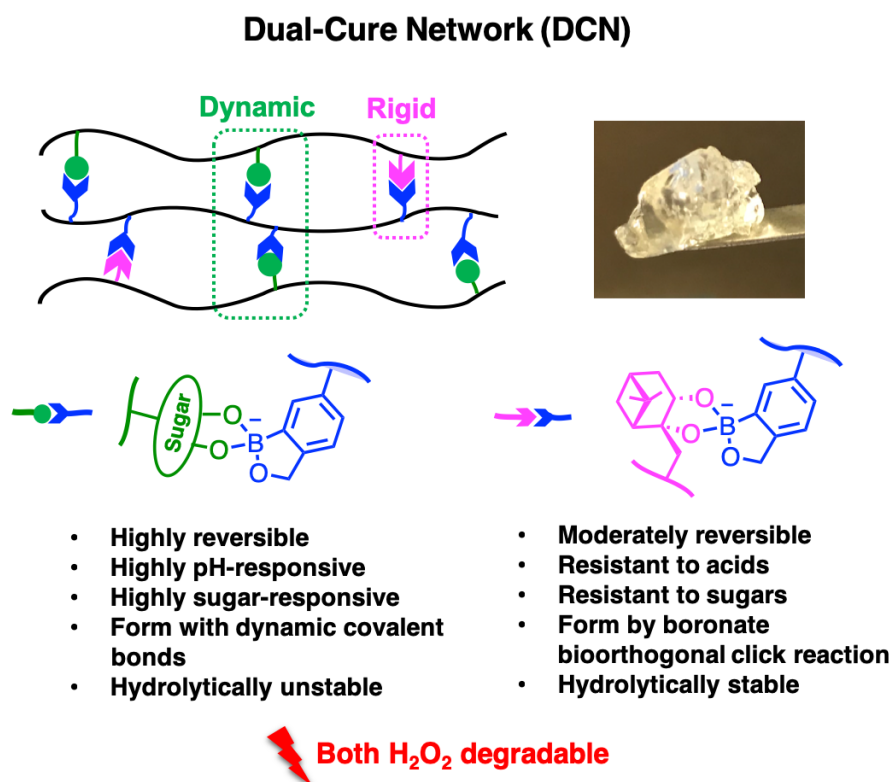


**Figure 2-2.** Depiction of the dual-cure network (DCN) system and the features of sugar-benzoxaborolate and nopoldiol-benzoxaborolate cross-links.

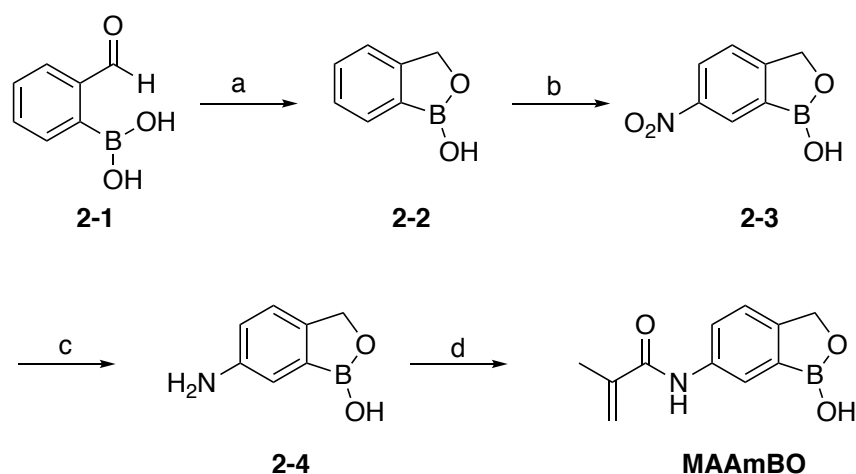
It is proposed that the bioorthogonal click reaction between nopoldiol and benzoxaborole would contribute a rigid, yet slightly reversible network to maintain the integrity of the hydrogel even under low pH conditions and high concentration of sugars (endogenous polyols). On the other hand, the highly flexible and dynamic sugar-benzoxaborolate cross-

links could control the hydrogel pore size through the stimuli-responsive bond cleavage/reforming, therefore preserving the environmental sensitivity of the hydrogel. Furthermore, the formation of DCN hydrogels does not require any external triggers such as heat, initiators, or UV light. Importantly, the benzoxaborolate formation produces water as the only by-product, indicating an excellent bioorthogonal and biocompatible cross-linking reaction for the formation of biomaterials.

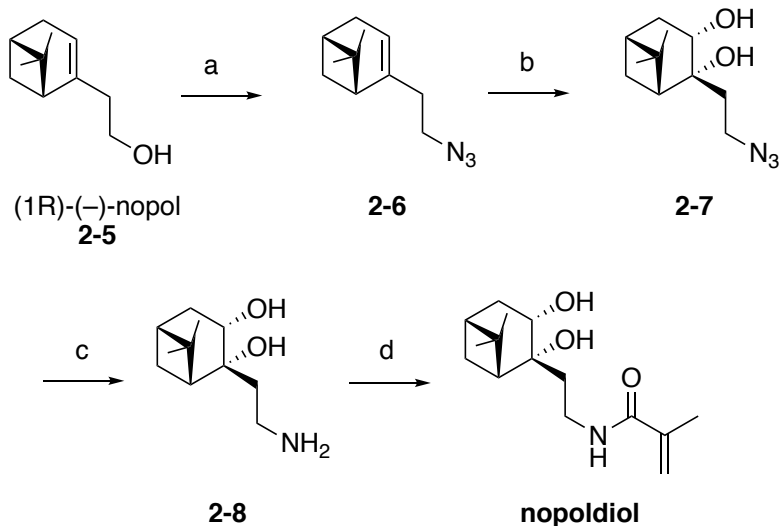
## 2.3.2 Hydrogel Synthesis – Monomer/Polymer Design & Cytotoxicity

### 2.3.2.1 Monomer synthesis and optimization

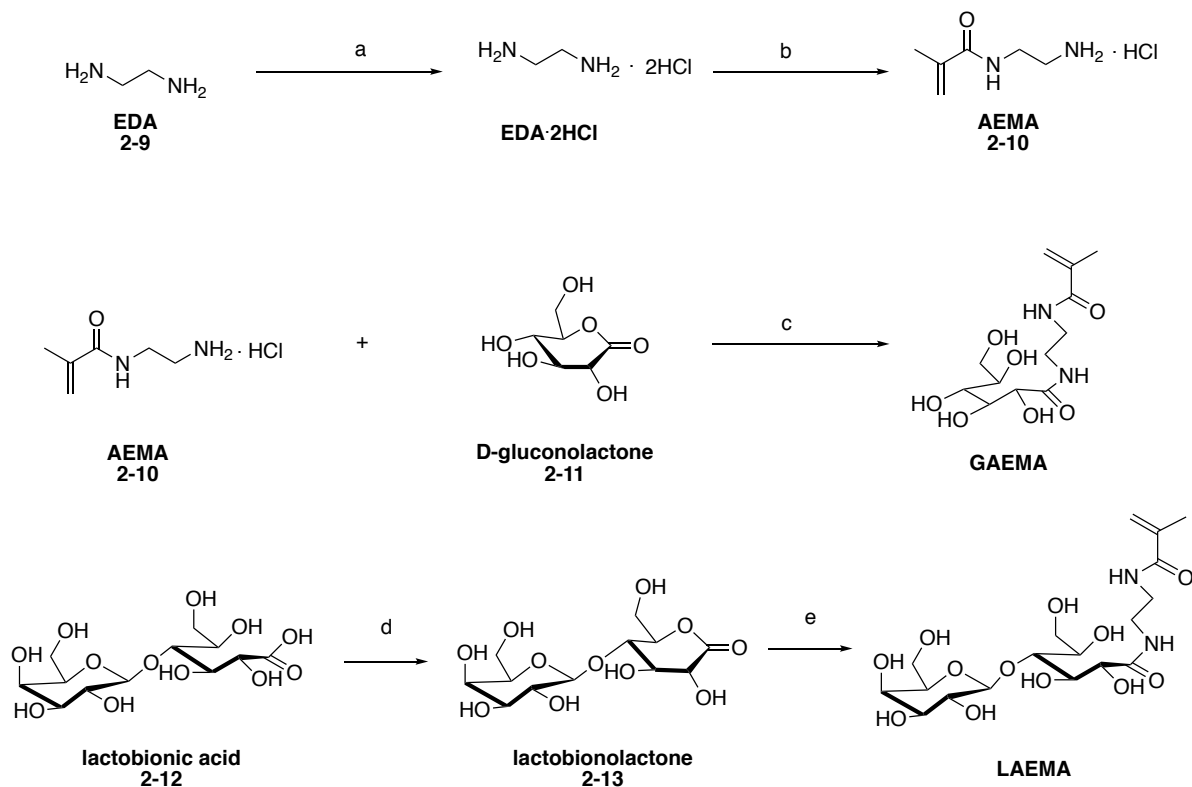
The benzoxaborole-based monomer, 5-methacrylamido-1,2-benzoxaborole (**MAAmBO**), was synthesized according to a previous report, with slight modifications (Scheme 2-2).<sup>8-12</sup> The nopoldiol-based monomer, (1*R*)-(-)-nopoldiol-methacrylamido-diol (**nopoldiol**), was synthesized by an acylation reaction from the nopoldiol-amine precursor (**2-8**), whereas the precursor **2-8** was synthesized according to a previous report (Scheme 2-3).<sup>3-4, 13</sup> Sugar-based monomers, **GAEMA** and **LAEMA**, were synthesized according to the literature (Scheme 2-4).<sup>14, 15-16</sup> A collaborator from Narain Group, Dr. Yangjun Chen, synthesized the compound **GAEMA**.



**Scheme 2-2.** Synthesis of monomer 5-methacrylamido-1,2-benzoxaborole (**MAAmBO**).<sup>8-11</sup> Reaction conditions: (a) NaBH<sub>4</sub>, MeOH, r.t., 2 h, 99% yield, (b) HNO<sub>3</sub> fuming, -40 °C, 1 h, 60–70 % yield, (c) H<sub>2</sub>, Pd/C 10 mol%, THF, r.t., 6 h, quantitative yield, (d) methacryloyl chloride, NaOH/H<sub>2</sub>O, 0 °C then r.t., overnight, 90–98% yield.



**Scheme 2-3.** Synthesis of (1R)-(-)-nopoldiol-methacrylamido-diol (**nopoldiol**).<sup>3-4, 13</sup> Reaction conditions: (a) *p*-toluenesulfonyl chloride pyridine, 0 °C to r.t., 4 h, followed by NaN<sub>3</sub>, DMSO, 80 °C, overnight, 77% yield over two steps, (b) K<sub>2</sub>O<sub>8</sub>•2H<sub>2</sub>O, pyridine, NMR (50%), acetone/water, 65 °C, overnight, 71–81% yield, (c) H<sub>2</sub>, Pd/C 10 mol%, MeOH, r.t., 3 h, (d) methacrylic anhydride, TEA, MeOH, 0 °C to r.t., 54–60% yield over two steps.



**Scheme 2-4.** Synthesis of 2-gluconamidoethyl methacrylamide (**GAEMA**)<sup>15</sup> and 2-lactobionamidoethyl methacrylamide (**LAEMA**).<sup>16</sup> Reaction conditions: (a) HCl, isopropanol, 1 h, 0 °C, 91% yield, (b) EDA, H<sub>2</sub>O, 30 min, r.t., followed by methacrylic anhydride, 0 °C to r.t. overnight, 48% yield, (c) TEA, MeOH, r.t., overnight, 80% yield, (d) TFA, MeOH, 60 °C, overnight, (e) **AEMA**, TEA, MeOH, r.t. 1 to 3 d, 55% yield.

#### Reaction optimization from compound 2-3 to 2-4:

The hydrogenation reaction to yield compound 2-4 suffered from low reaction rate and formation of impurities over a long period of time. A foam-like product was always obtained while using acetic acid as the co-solvent.

There are two main modifications in this hydrogenation step:

##### 1) No acetic acid is needed in the reaction

Many other procedures involve 10% of acetic acid as co-solvent because protic solvents could accelerate the hydrogenation process.<sup>9, 17</sup> However, it was very difficult to remove acetic acid residues through extraction, and chromatography was not an efficient method to purify a large quantity of polar compound, such as compound 2-4. The remaining acetic acid residue resulted in a foam-like product, which also made it inconvenient to handle. Control studies (with and without acetic acid) were conducted and showed that the reaction worked well without the help of acetic acid.

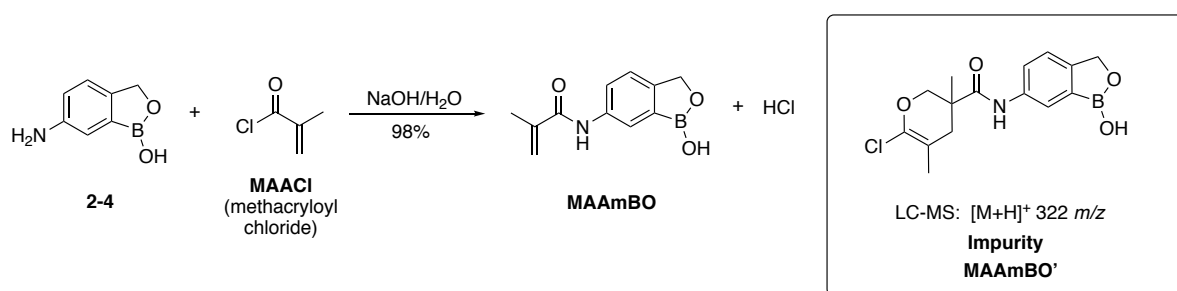
##### 2) Nitric acid residue

The slow reaction rate was suspected to result from the nitric acid residue that remained from the last step (nitration reaction from compound 2-2 to 2-3). A recent report from the literature discussed the impact of nitric acid pretreatment on Pd/C-based hydrogenation reactions to form nitrobenzene, where a small amount of nitric acid could facilitate the reaction, and a too large amount of oxygen-containing substance, such as nitric acid, could inhibit the catalytic activity of the palladium catalyst.<sup>18</sup> To address this problem, compound 2-3 was dissolved in ethyl acetate (add a small amount of methanol if it is not very soluble), followed by an addition of charcoal (about 2 to 5 g). The mixture was stirred at 50°C overnight, and the nitric acid residues could be absorbed. The charcoal was filtered out with celite, and the filtrate was concentrated to dryness to obtain a yellowish solid. As a result, the hydrogenation reaction could be achieved with high efficiency.

#### Reaction optimization from compound 2-4 to MAAmBO:

The literature procedures used equivalence as 2-4: MAACl (methacryloyl chloride): NaOH 1:2:5 or 1:2:4, and involved an acidic work-up by adding concentrated HCl slowly into the reaction mixture to crash out the product.<sup>11, 19</sup> However, a slurry-like product was always

obtained after the addition of concentrated acid, and the product was very sticky and unable to be filtered. By LC-MS analysis, a significant amount of impurity (**MAAmBO'** in Scheme 2-5) was found in the product, and it was believed to be the cause of slurry. Indeed, the literature mentioned that the acidification process has to be very slow to avoid unwanted polymerization during the work-up, and the compound **MAAmBO'** are very likely to be this unwanted side product.



**Scheme 2-5.** Synthesis of compound **2-4** to **MAAmBO** and the structure of the potential impurity **MAAmBO'**.

This unwanted formation of side product could be attributed to the following factors:

1) Impure starting materials

The starting material **MAACl** was found impure by NMR spectrometry. According to the literature, even commercial **MAACl** contains 10–15% of other substances such as the Diels-Alder adduct and the hydrolyzed dimer.<sup>20</sup> Therefore, **MAACl** was distilled prior to the acylation reaction to ensure its purity.

2) Inappropriate work-up (acidification using concentrated HCl)

The acidic work-up with concentrated acid could potentially accelerate the formation of the side product, to be specific, the reaction of the desired product with the excess **MAACl** in the solution. To address this issue, the equivalence of base was changed from 5 to 3 (from **2-4**: **MAACl**: NaOH 1:2:5 to 1:2:3). Interestingly, the product precipitated gradually during the reaction, and no acidic work-up was needed. The base was consumed in the reaction slowly, and the solution pH was just reach neutral, which was sufficient to crash out the acid insoluble **MAAmBO**. The product could be filtered easily as a yellowish powder with high yield and purity.

### 3) Choice of base

It was also suspected that maybe the strong base NaOH was not the optimal base for the reaction. Pyridine, NaHCO<sub>3</sub>, and TEA were used instead of NaOH; however, none to low yield of product was obtained.

Overall, the major modifications of this acylation reaction encompass the distillation of **MAACI** and the proper choice of the equivalence (**2-4: MAACI: NaOH 1:2:3**).

#### Reaction optimization from compound **2-8** to **nopoldiol**:

Monomer **nopoldiol** contains a fairly reactive methacrylamide group, which has a high risk of self-polymerization. The regular process of obtaining the product through solvent evaporation resulted in a severe self-polymerization problem even under ambient conditions. To address this problem, a small amount of hydroquinone (~1 mg, inhibitor) was added to the reaction mixture prior to the solvent evaporation. Then, the reaction crude was purified by flash chromatography, and the fractions were combined and concentrated to ~3 mL in EtOAc at 0 °C using ice bath for rotovap. A small amount of diethyl ether was added into the mixture, and the flask was put in the fridge with an open-neck. Through slow evaporation, **nopoldiol** crystals were obtained overnight or after 24 h with high purity.

#### **2.3.2.2 Polymer design**

With the key components and sugar monomers in hand, we chose a few backbone components for polymers to ensure hydrophilicity and biocompatibility (Figure 2-3). Polyethylene glycol methacrylate (**PEGMA**) is a widely used monomer for hydrogels. PEG-based hydrogels are highly hydrophilic and biocompatible to the surrounding tissue, making them good candidates for biomedical applications.<sup>21-22</sup> 2-Methacryloyloxyethyl phosphorylcholine (**MPC**)-based zwitterionic polymers are emerging as a new class of biocompatible material, which shows bioinspired phospholipid-like structures.<sup>23-24</sup> This particular nature results in superior biocompatibility to cells and blood, as well as antifouling features for surface modification.<sup>23-</sup>  
<sup>24</sup> *N,N'*-Dimethylacrylamide (**DMA**) is one of the most frequently used monomers for the synthesis of polymeric materials interfacing with biological systems. The resulting polymer, poly(*N,N'*-dimethylacrylamide) (**PDMA**) is highly hydrophilic and biocompatible.<sup>25</sup>

Moreover, using **DMA** as the backbone component could be beneficial to polymer cross-linking and/or functioning, because the short length of **DMA** could enable the other adjacent functionalities to become more sterically accessible.

As demonstrated in Figure 2-3, **polymer 1** and **polymer 2** represent the two polymer categories, where **polymer 1** contains **MAAmBO** and a backbone component, and **polymer 2** includes **nopoldiol**, a sugar component, and a backbone component. The two types of polymers are expected to be blended in a designed concentration to form a DCN hydrogel.

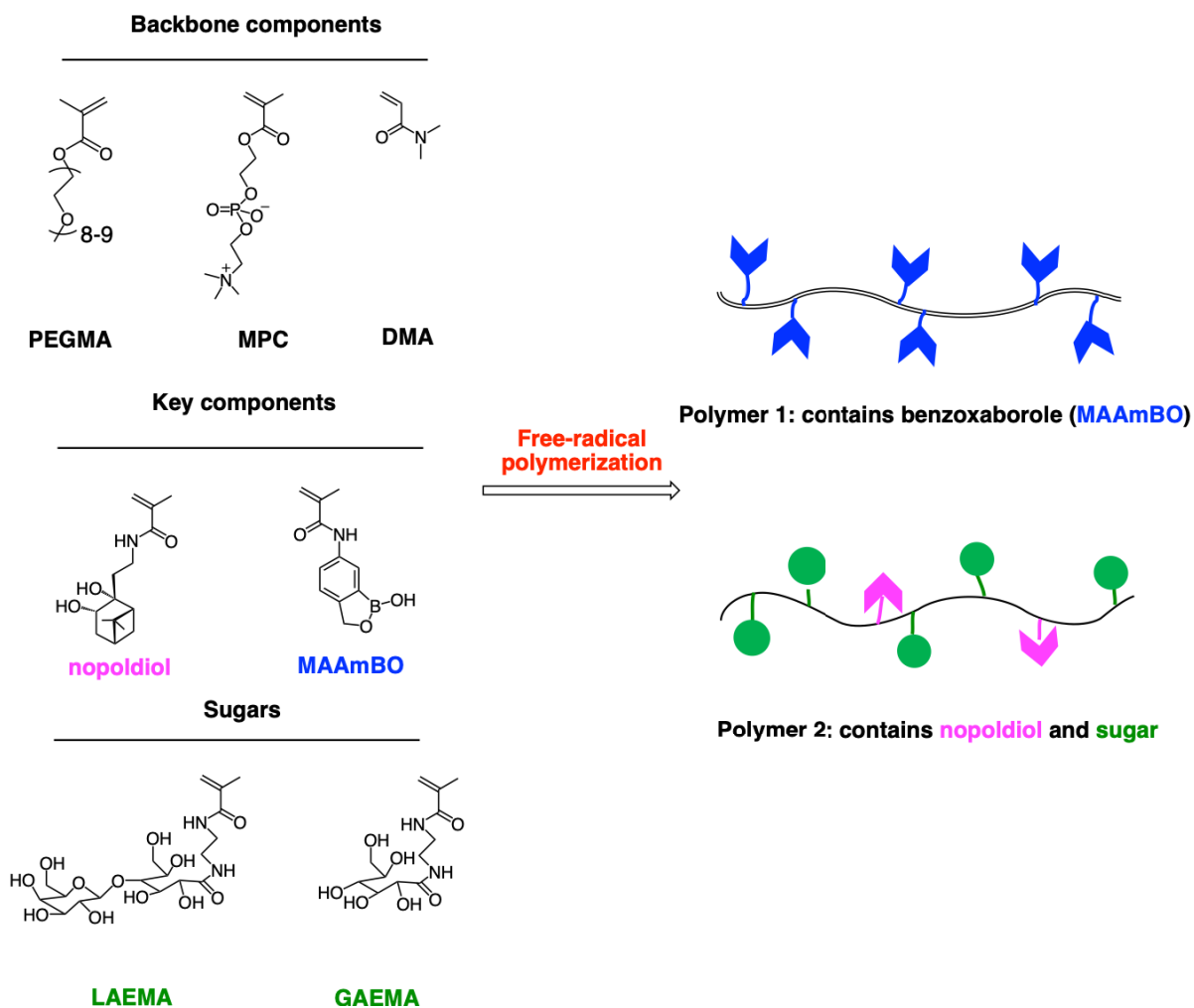


Figure 2-3. Monomer candidates and the design of polymers.

### 2.3.2.3 Polymer screening and optimization via cytotoxicity tests

For biomaterials, biocompatibility or cytocompatibility is exceptionally critical. Ideally, the biopolymers should display a cell viability of > 90% or even 100%. Therefore, we decided to

evaluate the cytotoxicity of the synthetic polymers prior to the other requisite tests. Considering that one of the objectives of this project is to make an acid-resistant hydrogel that can form under an extremely low pH environment, the ability for the hydrogel to gel at pH 1.5 is also a standard. We screened the polymers on their cytotoxicity (through MTT assays) and acid-resistance (gelation with poly(DMA<sub>95</sub>–MAAmBO<sub>5</sub>) at pH 1.5) (Table 2-1 and Table 2-2).

Due to the more readily available sources of DMA and LAEMA, **polymer 1** with DMA and MAAmBO and **polymer 2** with DMA/MPC, LAEMA, and nopoldiol were synthesized first. RAFT polymerization (reversible addition-fragmentation chain-transfer polymerization) was chosen as the synthetic method to polymerize the monomers into well-defined polymers (to afford high polydispersity and a uniform in chain length). However, as shown in Table 2-1 and Table 2-2, the RAFT polymerization resulted in moderate to low yields of 52%–74%. More disappointingly, **polymer 2** showed either poor cell viability or the failure of gelation with standard **polymer 1** (WDH-3-175B) at pH 1.5.

**Table 2-1.** Screening of **polymer 1** (DMA–MAAmBO) made by RAFT polymerization.

Lab Book Code	DMA <sup>a</sup>	MAAmBO <sup>a</sup>	DP <sup>b</sup>	Yield%	Cell viability% <sup>c</sup>
WDH-3-175B	95	5.0	400	52	96
WDH-3-191A	95	5.0	400	66	89

<sup>a</sup>Composition of each component was determined by <sup>1</sup>H NMR in mol%. <sup>b</sup>Designed DP (degree of polymerization) = moles of monomers/moles of RAFT chain transfer agent (CTP), which indicates the number of repeating units in a polymer chain. <sup>c</sup>Cell viability was tested with a polymer solution from concentration 0.01 mg/mol to 2 mg/mol; however, only the viability% at 1 mg/mL was recorded here for easier comparison.

**Table 2-2.** Screening of **polymer 2** (MPC/DMA–nopoldiol – LAEMA) made by RAFT polymerization.

Lab Book Code	MPC <sup>a</sup>	DMA <sup>a</sup>	LAEMA <sup>a</sup>	nopol-diol <sup>a</sup>	DP <sup>b</sup>	Yield %	Cell viability % <sup>c</sup>	Hydrogel formation <sup>d</sup>
WDH-3-165C	44	–	48	8.0	400	73	72	good
WDH-3-165A	51	–	49	–	400	63	56	no

WDH-3-175A	46	–	48	6.0	400	70	80	good
WDH-3-183B	–	53	38	9.0	400	40	50	good
WDH-3-183C	–	54	37	9.0	300	70	45	good
WDH-3-183D	–	58	36	6.0	300	72	60	good
WDH-3-189B	–	76	21	3.0	300	60	80	good
WDH-3-189C	–	56	36	8.0	200	64	59	good
WDH-3-189D	–	77	20	3.0	200	74	72	best
WDH-3-191B	–	76.3	20	3.7	100	51	67	weak
WDH-3-191C	78.7	–	15	6.3	200	66	101	no
WDH-3-191D	82	–	12	6.0	100	58	87	no
WDH-3-195A	–	79	17	4.0	150	69	47	best
WDH-3-195B	73	–	19	8.0	200	41	–	no
WDH-3-195C	69	–	24	7.0	200	67	–	no
WDH-3-195D	–	86	10	4.0	300	43	–	too brittle
WDH-3-200A	82	–	14	4.0	300	42	59	no
WDH-3-200B	–	82	16	2.0	250	45	47	best

WDH-3-200C	78	–	16	6.0	400	66	47	no
------------	----	---	----	-----	-----	----	----	----

<sup>a</sup>Composition of each component was determined by <sup>1</sup>H NMR in mol%. <sup>b</sup>Designed DP (degree of polymerization) = moles of monomers/moles of RAFT chain transfer agent (CTP), which indicates the number of repeating units in a polymer chain. <sup>c</sup>Cell viability was tested with a polymer solution from concentration 0.01 mg/mol to 2 mg/mol; however, only the viability% at 1 mg/mL was recorded here for easier comparison. <sup>d</sup>The ability to gel with the standard **polymer 1** of poly(DMA<sub>95</sub>–MAAmBO<sub>5</sub>) or the appearance of the gel, best/good: moderately hard, can self-heal easily; bad: too brittle, not self-healing; weak: cannot form stable solid, fluid; no: liquid.

Reflecting from the preliminary results from the screening of **polymer 1** and **2** (Table 2-1 and 2-2), the failures were rationalized as follows:

- Two batches of **polymer 1** gave very high cell viability% results; however, all of the batches to form **polymer 2** were pretty toxic, indicating that either **LAEMA** or **nopoldiol** is toxic to cells. Since **LAEMA** is the major component in **polymer 2** compared to **nopoldiol**, it is more likely to be the source of toxicity.
- The molecular weight of polymers (indicated by DP) do not correlate with the cytotoxicity.
- Polymers with a low molecular weight do not form gels or only form weak gels.
- RAFT polymerization is not very efficient for large molecular weight polymers. To make hydrogels, it may not be essential for the polymer precursors to have a well-defined chain length with low polydispersity (PDI). Free-radical polymerization may be a better choice to improve yields.

Therefore, we modified the composition of both polymers by changing the backbone to **PEGMA**, a bulky but flexible monomer (MW: 500 g/mol). By replacing the **DMA** and **MPC** backbone components with **PEGMA**, we expected to lower the weight ratios of the functionalities (**LAEMA** and **nopoldiol**) (Figure 2-4), thus dilute these two components in the ultimate polymers and hydrogels. Satisfactorily, all of the **PEG**-based polymers exhibited high cell viabilities, and the two sugar candidates (**GAEMA** and **LAEMA**) did not show a distinguishable difference (Table 2-3 and Figure 2-5).

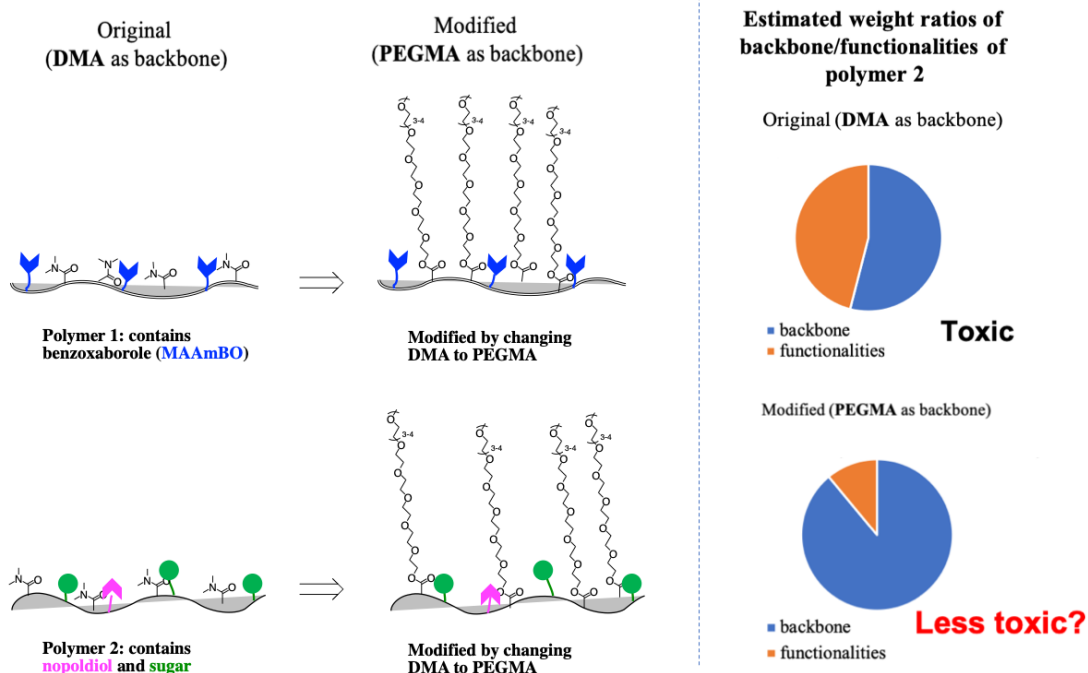


**Figure 2-4:** Illustration of polymer optimization by changing the backbone from **DMA** to **PEGMA** and the estimated weight ratios of backbone/functionalities of **polymer 2**.

**Table 2-3.** Screening of **PEGMA**-containing polymers made by free-radical polymerization.

Lab Book Code	PEG MA <sup>a</sup>	LAEM A <sup>a</sup>	GAE MA <sup>a</sup>	nopol-diol <sup>a</sup>	MAA mBO <sup>a</sup>	DP <sup>b</sup>	Yield %	Cell viability % <sup>c</sup>	Hydrogel formation <sup>d</sup>
WDH-4-29A <sup>e</sup>	85	–	–	–	15	400	69	<b>108</b>	best
WDH-4-29B <sup>f</sup>	83	12	–	5.0	–	400	79	<b>81</b>	best
WDH-4-29C <sup>f</sup>	74	–	20	6.0	–	400	82	<b>96</b>	best
WDH-4-29D <sup>f</sup>	70	–	23	7.0	–	400	85	–	best
WDH-4-29E <sup>f</sup>	85	20	–	5.0	–	300	83	–	best
WDH-4-35A <sup>e</sup>	86	–	–	–	14	200	82	<b>93</b>	best

<b>WDH-4-35B<sup>e</sup></b>	90	–	–	–	20	200	86	–	weak
<b>WDH-4-35C<sup>f</sup></b>	77	–	17	6.0	–	200	80	<b>83</b>	best
<b>WDH-4-35D<sup>f</sup></b>	81	12	–	7.0	–	200	76	<b>83</b>	best

<sup>e</sup>Composition of each component was determined by <sup>1</sup>H NMR in mol%. <sup>b</sup>Designed DP (degree of polymerization) = moles of monomers/moles of initiator (ACVA), which indicates the number of repeating units in a polymer chain. <sup>c</sup>Cell viability was tested with a polymer solution from concentration 0.01 mg/mol to 2 mg/mol; however, only the viability% at 1 mg/mL was recorded here for easier comparison. <sup>d</sup>The ability to gel with the standard **polymer 1** (WDH-4-29A) of poly(PEGMA<sub>85</sub>–MAAmBO<sub>15</sub>) or the appearance of the gel, best: moderately hard, can self-heal easily; weak: cannot for stable solid, fluid. <sup>e</sup>Indicating **polymer 1**. <sup>f</sup>Indicating **polymer 2**.

To investigate the effect of other factors towards cytotoxicity, including a sterilization of polymer solutions and the age (passage number) of cells, two comparison tests were performed. Firstly, polymer WDH-4-35A was sterilized by passing the polymer/DMEM solution through a 0.22 μm filter tip. A parallel control study also was performed (no sterilization) (Figure 2-5). The increasing percent of cell viability confirms the necessity of the sterilization process. Secondly, an old batch of cells (~25 passage number) and a batch of relatively new cells (~10 passage number) were utilized for the cytotoxicity tests. As shown in Figure 2-5, there was no significant difference between the two experiments (WDH-4-35D and WDH-4-35D (old cells)), indicating the irrelevance of cell age.

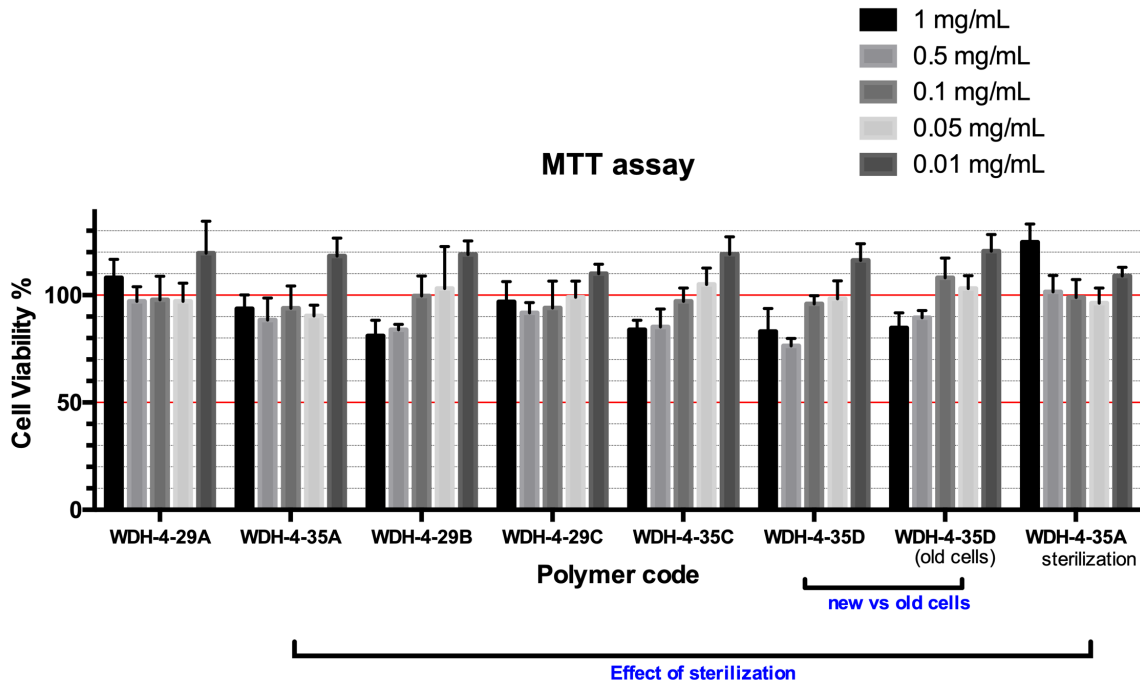


**Figure 2-5.** Graphic results of MTT assays of the polymers in Table 2-3.

To inspect the cause of toxicity further, a representative polymer batch from the **DMA**-backbone method (WDH-4-35D) and **PEGMA**-backbone method (WDH-3-200B) was picked for comparison. As shown in Table 2-4, both polymers contain comparable molar ratios of backbone components (**PEGMA** or **DMA**), **nopoldiol**, and sugars (**LAEMA**). According to the molecular weight of each component, the weight ratios were calculated based on the molar ratios. Clearly, the **PEGMA**-based polymer is much more biocompatible compared to the **DMA**-based polymer (85% and 47% of cell viability, respectively). It is notable that the **LAEMA** moieties constitute nearly half the weight of the polymer WDH-3-200B (46 wt%). This number indicates that the majority of the polymer is **DMA** and **LAEMA**, regardless of the low molar ratios of the **LAEMA** (16 mol%). In contrast, because of the large molecular weight of **PEGMA** (500 g/mol), 12 mol% of **LAEMA** moieties only take up 11 wt% in the resulting polymer. Notably, the molar ratios and weight ratios of **nopoldiol** moieties in both polymers are very small and similar. Thus, the influence of **nopoldiol** to the difference in polymer biocompatibility is considered negligible. These results confirm the assumption that was described earlier in Figure 2-4, where a greater weight ratio of the functionalities (**LAEMA**) is correlated greatly with the toxicity of the polymers. Overall, **PEGMA**-based

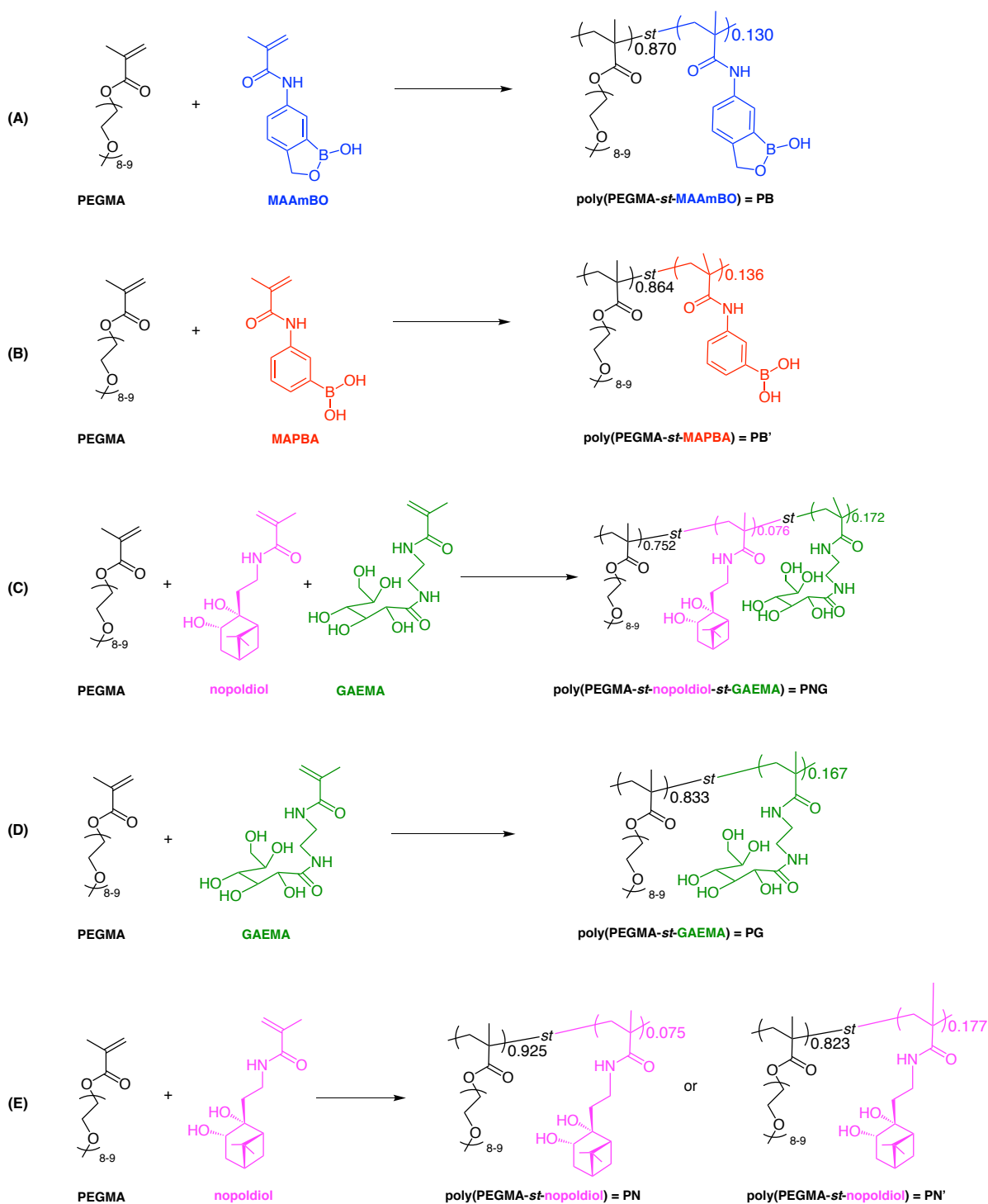
polymers showed significant improvements in the cell viability compared to **DMA**-based polymers, suggesting that **PEGMA** is a better backbone candidate for further studies and applications.

**Table 2-4.** Comparisons of cytotoxicity between **DMA**-based polymer and **PEGMA**-based polymer.

Lab Book Code		DMA	PEGMA	LAEMA	nopol-diol <sup>a</sup>	DP <sup>c</sup>	Method/ Yield%	Cell viability% <sup>d</sup>
<b>WDH-4-35D</b>	mol% <sup>a</sup>	–	81	12	7.0	200	Free radical/ 82	<b>85</b>
	wt% <sup>b</sup>	–	85	<b>11</b>	4.0			
<b>WDH-3-200B</b>	mol% <sup>a</sup>	82	–	16	2.0	250	RAFT/ 45	<b>47</b>
	wt% <sup>b</sup>	51	–	<b>46</b>	3.0			

<sup>a</sup>Composition of each component was determined by <sup>1</sup>H NMR in mol%. <sup>b</sup>Calculated from molecular weight and molar ratio of each components. <sup>c</sup>Designed DP (degree of polymerization) = moles of monomers/moles of initiator (ACVA, Free-radical polymerization), or moles of RAFT chain transfer agent (CTP, RAFT), which indicates the number of repeating units in a polymer chain. <sup>d</sup>Cell viability was tested with a polymer solution from concentration 0.01 mg/mol to 2 mg/mol; however, only the viability% at 1 mg/mL was recorded here for easier comparison.

With the preliminary results in hand, the final combination and the composition of monomers were decided, and a set of **PEGMA**-based polymers was synthesized. To reduce the risk of having a high weight ratio of sugar components, which would likely cause a high cytotoxicity, **GAEMA** was chosen as the sugar component due to its lower molecular weight. As shown in Scheme 2-6 and Table 2-5, polymer **PB** was designed with a fixed molar ratio of **MAAmBO** (13%) to allow sufficient binding with **GAEMA** and **nopoldiol** moieties in the diol-containing polymers. Polymer **PB'**, which contains a comparable composition of **MAPBA** (an arylboronic acid-based monomer) with **MAAmBO** (in polymer **PB**), was designed to study the influence of a different type of traditional arylboronic acid towards



**Scheme 2-6.** Synthesis of polymer **PB**, **PB'**, **PBN**, **PG**, **PN**, and **PN'**. Reaction conditions: 4,4'-azobis(4-cyanovaleric acid) (ACVA), MeOH/H<sub>2</sub>O, 70 °C, 16 h, under nitrogen, (yield 81–93%). DP was designed as 200 in all of the cases. Numbers indicate proportions of each component in the statistical polymers (normalized to 1).

gelation efficiency (Section 2.3.5.1). Polymer **PN** and **PG**, which contained similar proportions of **nopoldiol** and **GAEMA** as polymer **PNG**, respectively, were synthesized to monitor the functions and properties of each component in the resulting hydrogels. Polymer **PN'** and **PG**, which contained similar ratios of **nopoldiol** and **GAEMA** (17.7% and 16.7%, respectively), were also prepared for comparison studies.

Furthermore, the molecular weight of each polymer was determined via GPC (gel permeation chromatography) by a collaborator in the Narain Group, Yi-Yang Peng (Table 2-5). The two polymers in category **polymer 1 (PB and PB')**, and the four polymers in category **polymer 2 (PNG, PG, PN, PN')**, have similar molecular weights. The small differences in molecular weights and PDI resulted from the less controllable chain growth of the free-radical polymerization compared to RAFT polymerization. The cytotoxicity results of the designed polymers are very satisfactory with cell viability close to 100%. The detailed data is shown in Section 2.3.10.

**Table 2-5.** Characterizations of the final synthetic polymers.

Polymer	Composition (mol%) <sup>a</sup>					GPC Characterization <sup>b</sup>		
	PEG MA	GAE MA	nopol- diol	MAAm BO	MA PBA	$M_n$ (10 <sup>3</sup> )/ Da	$M_w$ (10 <sup>3</sup> )/ Da	PDI ( $M_w/M_n$ )
<b>PB<sup>c</sup></b>	87.0	–	–	13.0	–	96.9	293	3.02
<b>PB'<sup>c</sup></b>	86.4	–	–	–	13.6	93.5	174	1.86
<b>PNG<sup>d</sup></b>	75.2	17.2	7.60	–	–	124	327	2.63
<b>PG<sup>d</sup></b>	83.3	16.7	–	–	–	132	237	1.79
<b>PN<sup>d</sup></b>	92.5	–	7.50	–	–	158	264	1.54
<b>PN'<sup>d</sup></b>	82.3	–	17.7	–	–	159	265	1.66

<sup>a</sup>Calculated from signal integrations of the <sup>1</sup>H NMR spectrum by using D<sub>2</sub>O as the NMR solvent. <sup>b</sup>Obtained from aqueous GPC using 0.5 M sodium acetate/acetic acid buffer as the eluent. <sup>c</sup>**polymer 1.** <sup>d</sup>**polymer 2.**

### 2.3.2.4 Fabrication of hydrogels

With the optimal polymers in hand, a set of dual-cure network hydrogels and single network hydrogels was prepared. As shown in Table 2-6, hydrogels formed by mixing **PB** with **PNG**, **PG**, **PN**, and **PN'**, were denoted accordingly as **PBNG**, **PBG**, **PBN**, and **PBN'**; only **PBNG** is a dual-cure network (DCN) hydrogel. The four hydrogels composed by **PB'** (Table 2-6, red) share the same nomenclature. All of the corresponding single network (SN) hydrogels were prepared for control studies. A more straightforward graphic illustration on the preparation of benzoxaborole-containing polymer/hydrogel is shown in Figure 2-6. Specifically, four monomers were polymerized through free-radical polymerization, and then the polymers were mixed in 1:1 weight ratio (concentration of 10 w/v%) to form the corresponding hydrogels. The rigid cross-links were denoted as nopoldiol-benzoxaborolate, while the dynamic cross-links were named as sugar-benzoxaborolate.

**Table 2-6.** Fabrication of DCN and SN hydrogels by mixing **polymer 1** and **polymer 2**.

<b>Hydrogel</b>	<b>Polymer 1</b>	<b>Polymer 2</b>	<b>Hydrogel type</b>
<b>PBNG</b>	PB	PNG	DCN
<b>PBG</b>	PB	PG	SN
<b>PBN</b>	PB	PN	SN
<b>PBN'</b>	PB	PN'	SN
<b>PB'NG</b>	PB'	PNG	DCN
<b>PB'G</b>	PB'	PG	SN
<b>PB'N</b>	PB'	PN	SN
<b>PB'N'</b>	PB'	PN'	SN

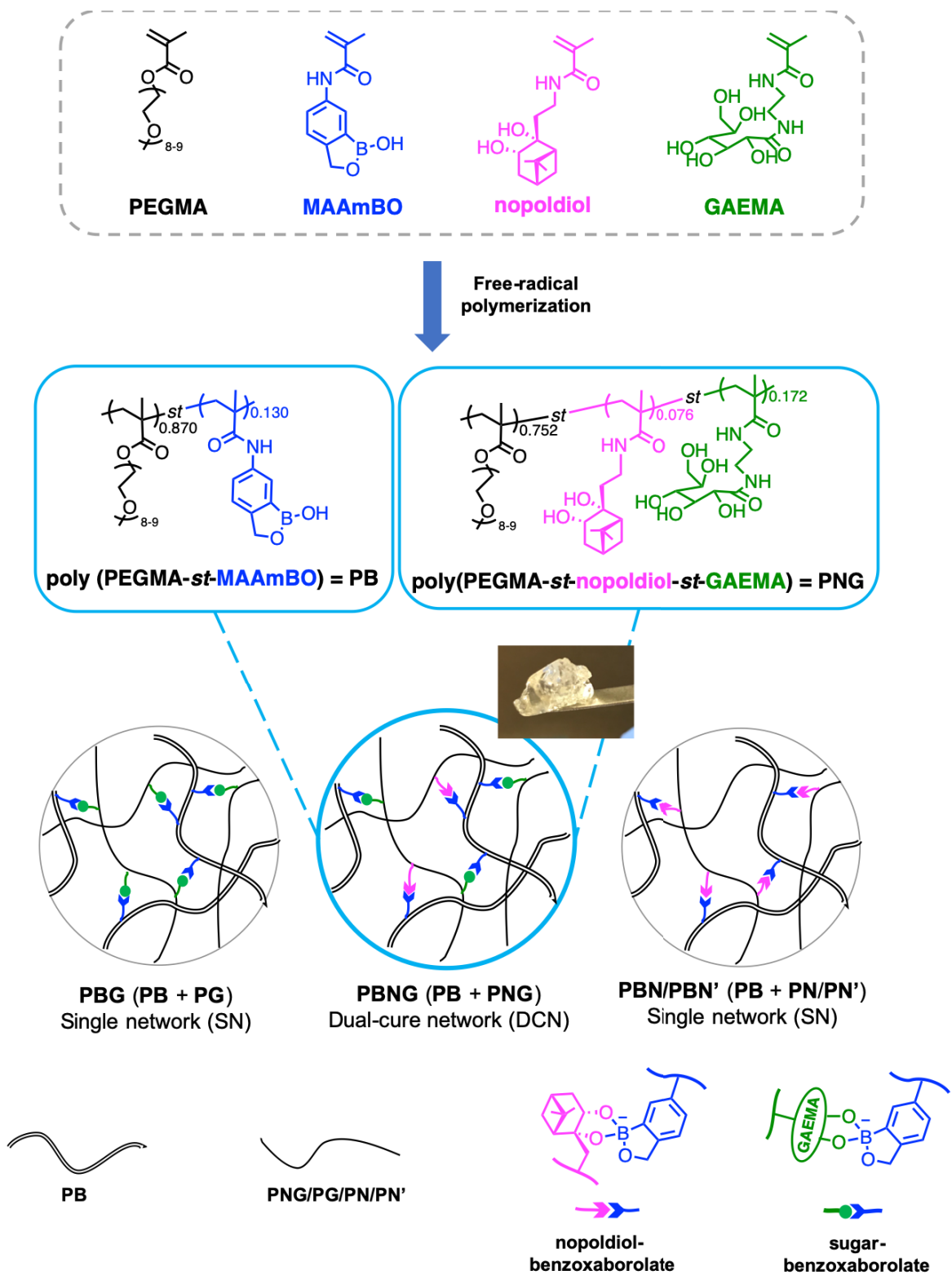


**Figure 2-6.** Graphic illustration of the design and preparation of benzoxaborolate-based single and dual-cure network hydrogels.

### 2.3.3 Monomeric Binding Studies of Benzoxaborole – Diols from pH 8.5 to 1.5 via NMR

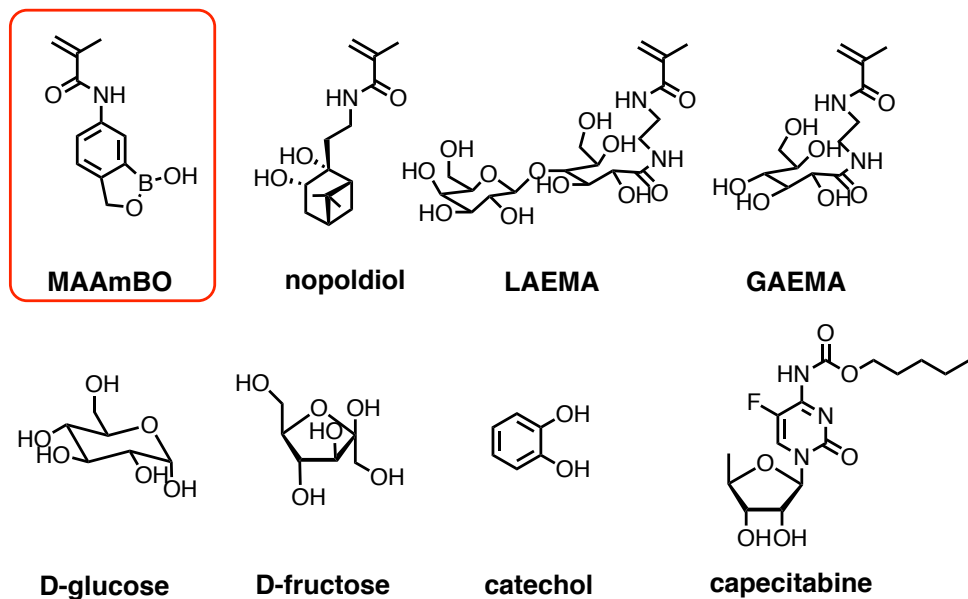
To describe the distinct binding ability of benzoxaborole with **nopoldiol** in a broad pH range, a few diols that are often involved in boronate formation in biomaterial fabrications were tested for comparison. The amount of conversion of the **MAAmBO** and diol compounds to the resulting benzoxaborolates was measured via relative integrations and was calculated based on the following general equation:

Conversion% to benzoxaborole =

$$\frac{\text{integration of new signal}}{\text{integration of original signal} + \text{integration of new signal}} \times 100\% \quad (1)$$

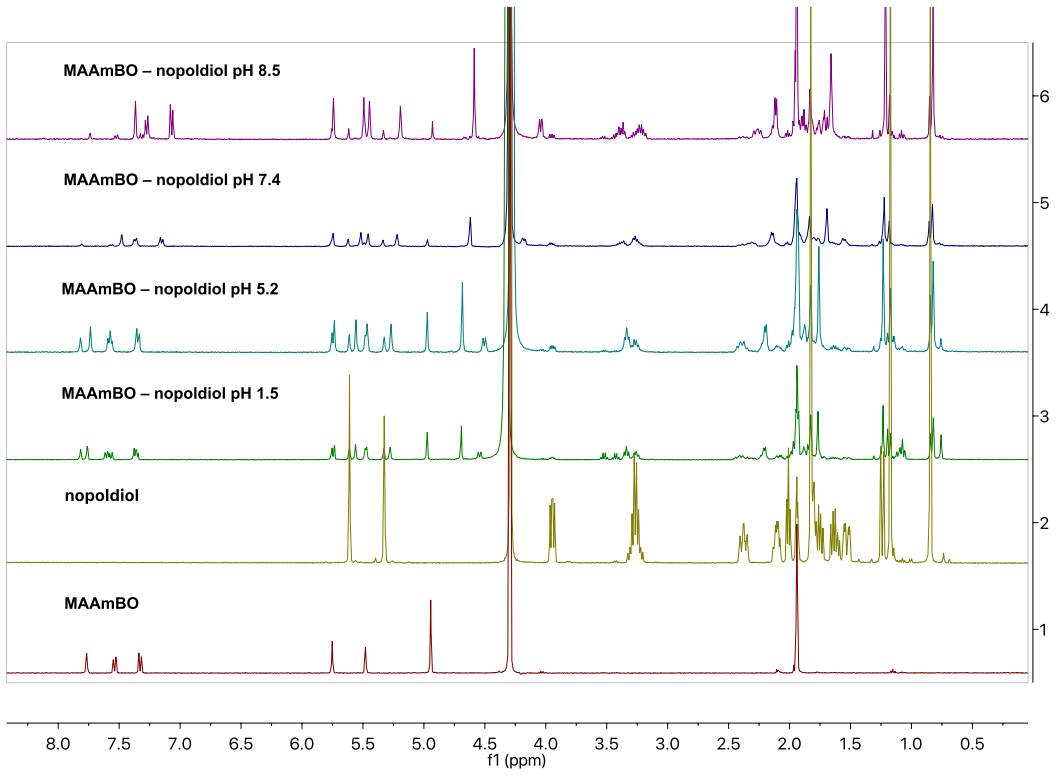
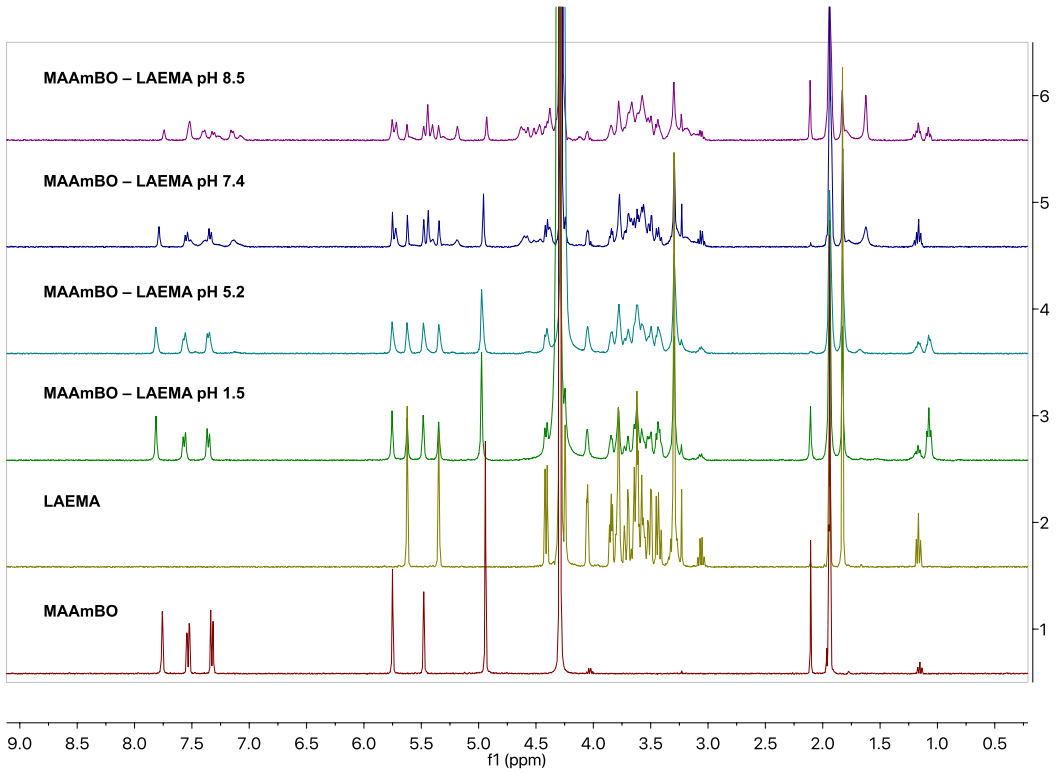
where in most cases, the “new signal” represents the methylene (-**CH<sub>2</sub>**-) on the oxaborole ring of the newly formed benzoxaborolate, and the “original signal” stands for the methylene (-**CH<sub>2</sub>**-) on the oxaborole ring of the free **MAAmBO**. This calculation method was slightly adjusted because of the electronic effect and the complexity of some benzoxaborolates, as described later in Table 2-11. The stacked NMR spectra of benzoxaborolate formation at different pH are shown in Figure 2-7, and separate NMR spectra with integral ratio are described in page 159–180. All of the measurements were performed at least twice, and the final results are displayed as an average (Table 2-7).

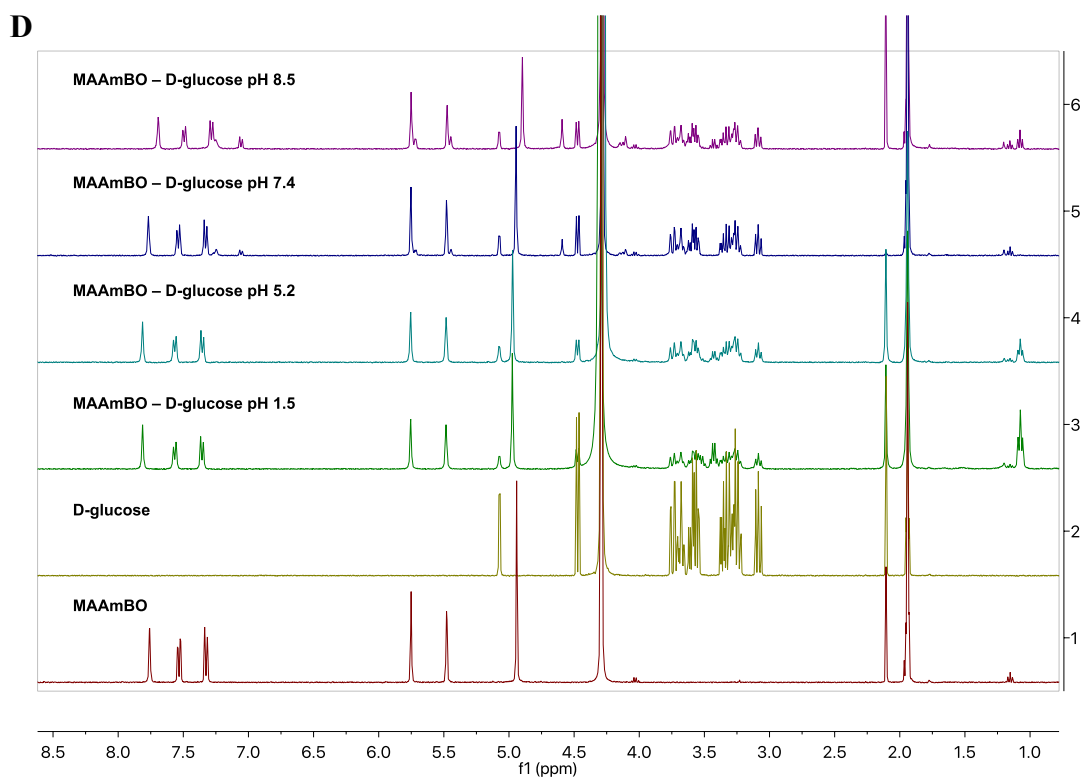
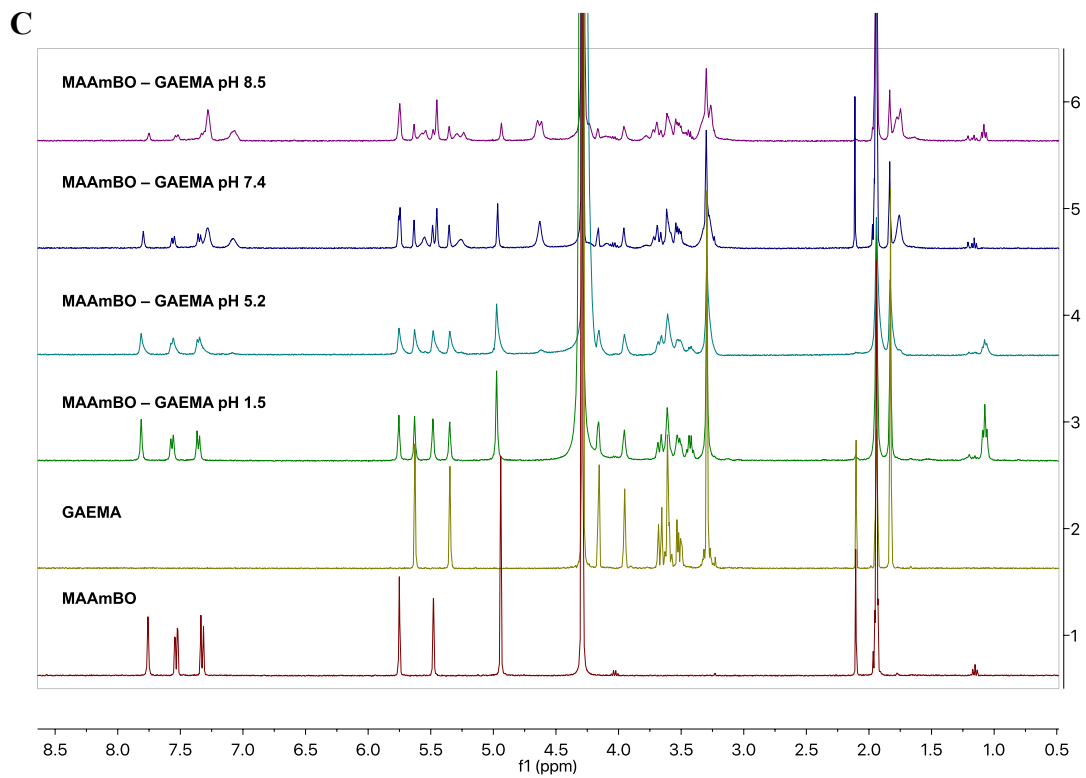
**Table 2-7.** Results of benzoxaborolate formation between **MAAmBO** and various diols.

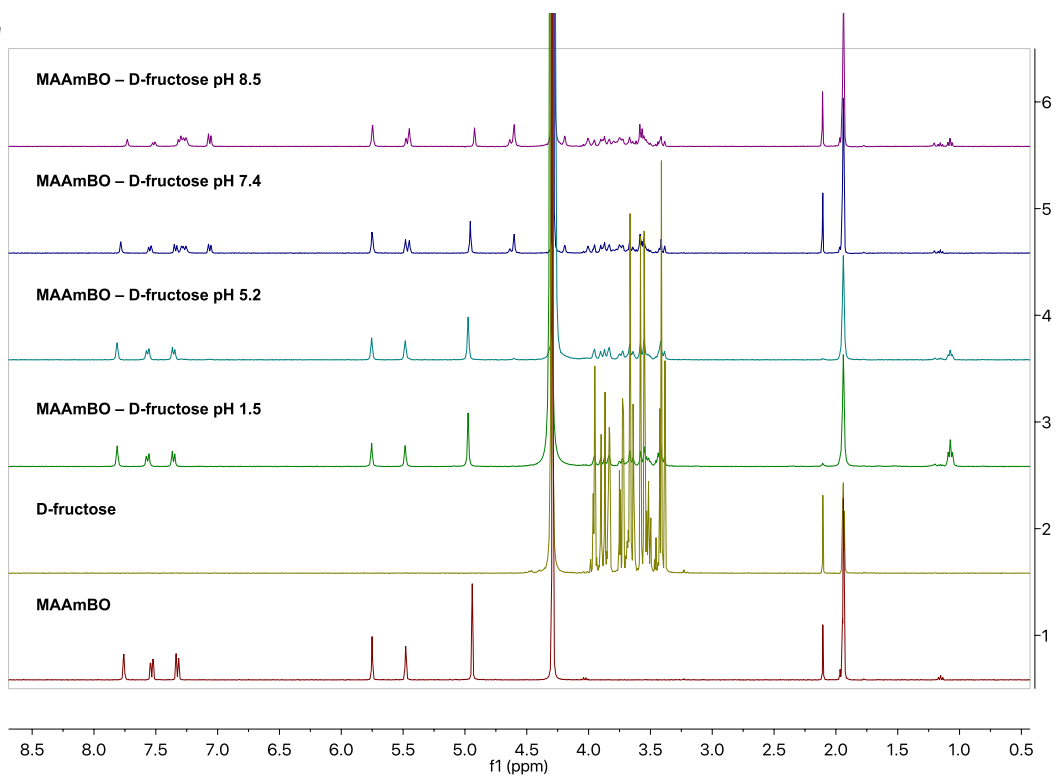
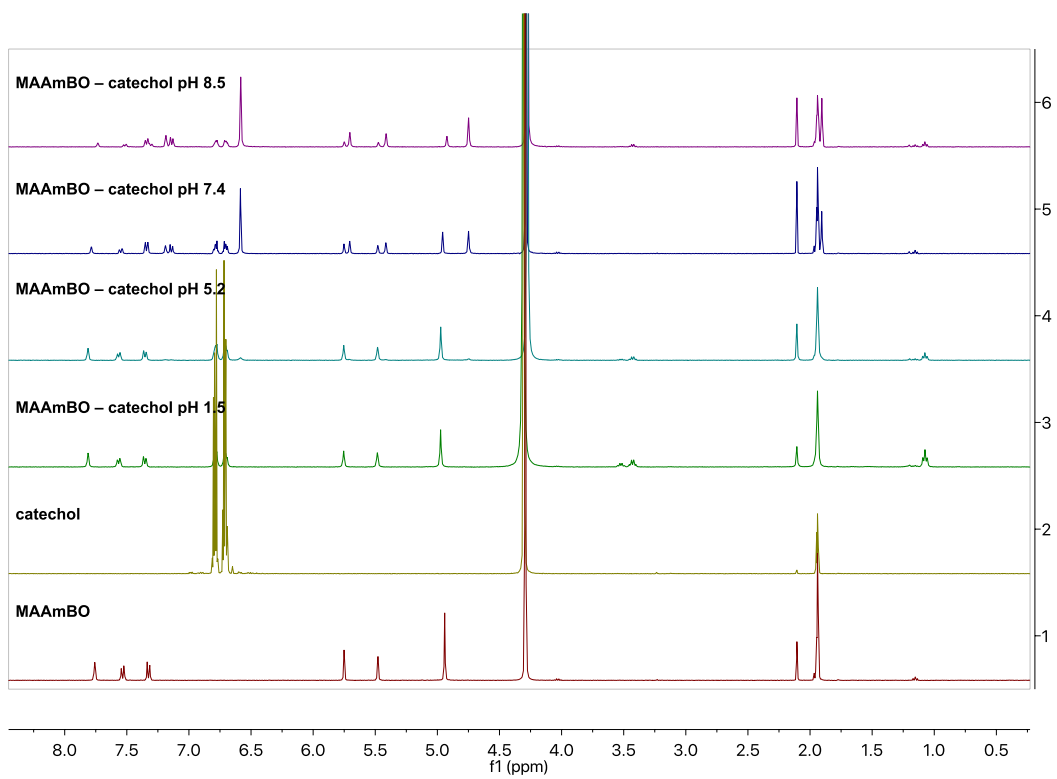


Entry	Diols	Conversion to benzoxaborolate % <sup>a</sup>			
		pH 8.5	pH 7.4	pH 5.2	pH 1.5
1	nopoldiol	86.5	79.6	65.5	59.5
2	nopoldiol <sup>b</sup>	88.2	86.9	84.7	79.9
3	LAEMA	78.2	61.5	9.29	–
4	GAEMA	82.4	64.7	7.38	–
5	D-glucose	29.3	9.90	–	–
6	D-fructose	73.0	51.7	6.33	–
7	catechol	77.4	57.3	9.45	–
8	capecitabine	57.7	38.1	2.91	–

<sup>a</sup>The conversion% of **MAAmBO** and diols to benzoxaborolate was determined by <sup>1</sup>H NMR. <sup>b</sup>Conversion to boronate (%) of mixing **MAPBA** and **nopoldiol**.

**A****B**



**E****F**

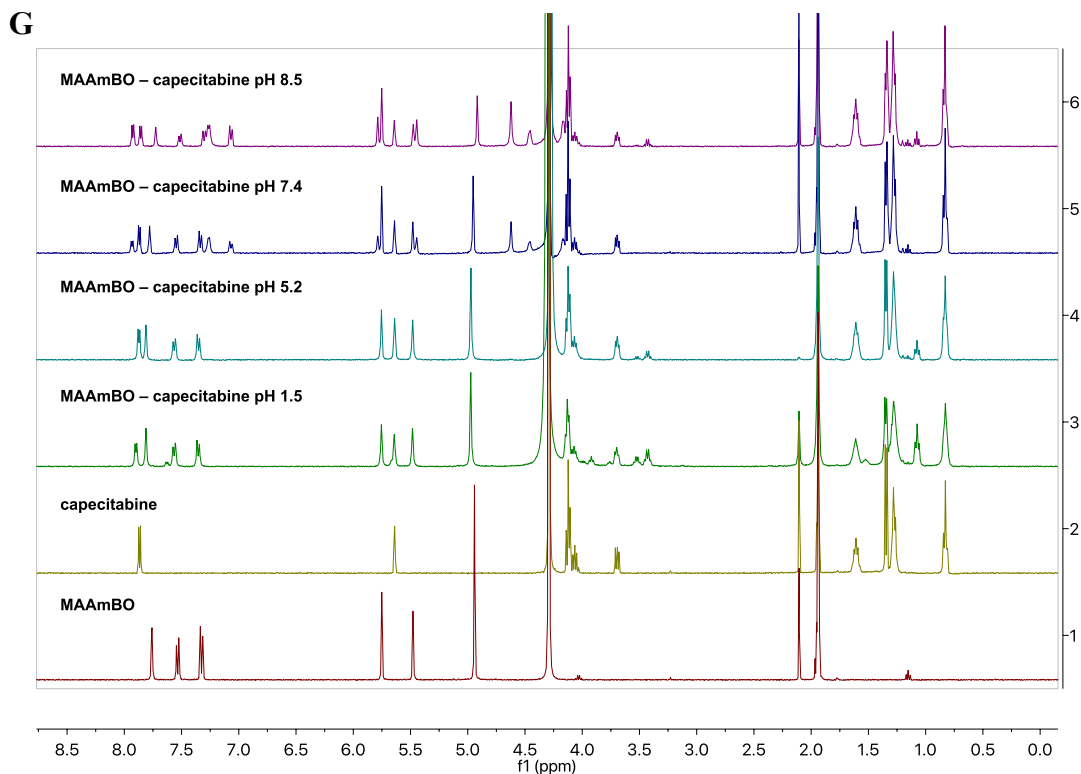


**Figure 2-7.** Representative  $^1\text{H}$  NMR spectra for the binding studies of **MAAmBO** and diols under different pH conditions.

It has been shown in the literature that the benzoxaborolate formation is generally favorable at a higher pH.<sup>26-27</sup> Therefore, it is not surprising that the conversions to the benzoxaborolate complex were found greater under the more basic conditions in all cases (Table 2-7). Even though **nopoldiol** is a rigid cyclic *cis*-diol, it is remarkable that it exhibited strong binding affinities with the **MAAmBO** monomers even at an extremely low pH of 1.5 (59.5% conversion). The abnormal hydrolytic stability of this nopoldiol-benzoxaborolate can be explained by the unfavorable entropy of converting three molecules to two when hydrolyzing a boronic ester composed with a sterically hindered and pre-organized diol.<sup>28</sup> In addition, the structural bulkiness of the **nopoldiol** could slow down the dissociation process by hindering the approach of water. Similarly, 3-methylacrylamido phenylboronic acid (**MAPBA**), a traditional phenylboronic acid, also formed nopoldiol-boronate with high conversion under a wide range of pH; however, the resulting boronate was not as dynamic as nopoldiol-benzoxaborolate (Table 2-7 entry 2), which limits its use in self-healing, pH-responsive, and biodegradable materials. Moreover, **LAEMA**, **GAEMA**, and catechol, which are frequently

used in arylboronic acid-mediated stimuli-responsive biomaterials for the applications of biomolecular recognition,<sup>16</sup> tissue scaffold,<sup>23</sup> and gene therapy were also tested.<sup>29-31</sup> However, these diols exhibited limited binding affinities towards **MAAmBO** at pH 7.4 (~60% conversion), and only a small amount of the benzoxaborolate product was detected even under the slightly acidic conditions. Furthermore, biological polyols, including D-glucose and D-fructose, as well as the ribose-based anti-cancer drug, capecitabine, displayed low to moderate binding with **MAAmBO** under basic and neutral conditions, and negligible affinity at low pH. These monomeric binding results support the unique tightness and acid-tolerance of the nopoldiol-benzoxaborolate complex.

### 2.3.4 Detailed Binding Studies of Nopoldiol-Benzoxaborole

To demonstrate the formation and conformation of nopoldiol-benzoxaborolate between **MAAmBO** and **nopoldiol** further under a wide range of pH values, <sup>1</sup>H NMR, <sup>11</sup>B NMR, ESI-MS, and LC-MS were utilized to analyze the binding.

#### 2.3.4.1 Binding studies – <sup>1</sup>H NMR analysis

As shown clearly in Figures 2-7A and Figure 2-8, a considerable number of new signals appeared under all of the pH conditions, which indicates the formation of nopoldiol-benzoxaborolate. To our surprise, the chemical shifts of the resulting benzoxaborolates were consistent throughout all of the pH conditions, except for the case of nopoldiol-benzoxaborolate (Figure 2-8). For instance, the aromatic proton signal **d** at 7.37 ppm at pH 8.5 was shifted downfield to 7.48 ppm at pH 7.4, and 7.82 ppm under acidic pH (5.2 and 1.5). Similarly, signal **a**, **b**, and **c** also experience a severe downfield shift as pH decreases. We rationalized that under acidic pH, the nopoldiol-benzoxaborolate **2-14** is converted to nopoldiol-benzoxaborolate **2-15** through a ring opening of the oxaborole ring. As a consequence, in the case of **2-15**, the neutral boronic ester (open form of benzoxaborolate) acts as an electron withdrawing group, and the electrons on the aromatic ring are delocalized into the adjacent empty p orbital of the boron atom, thus making the protons more deshielded. It is notable that benzoxaborole ring opening is usually unfavorable;<sup>32</sup> however, in this case, the low pH favors the neutral boronate and the very rigid diol unit is even less likely to open compared to the *o*-hydroxymethyl arm of **MAAmBO**.

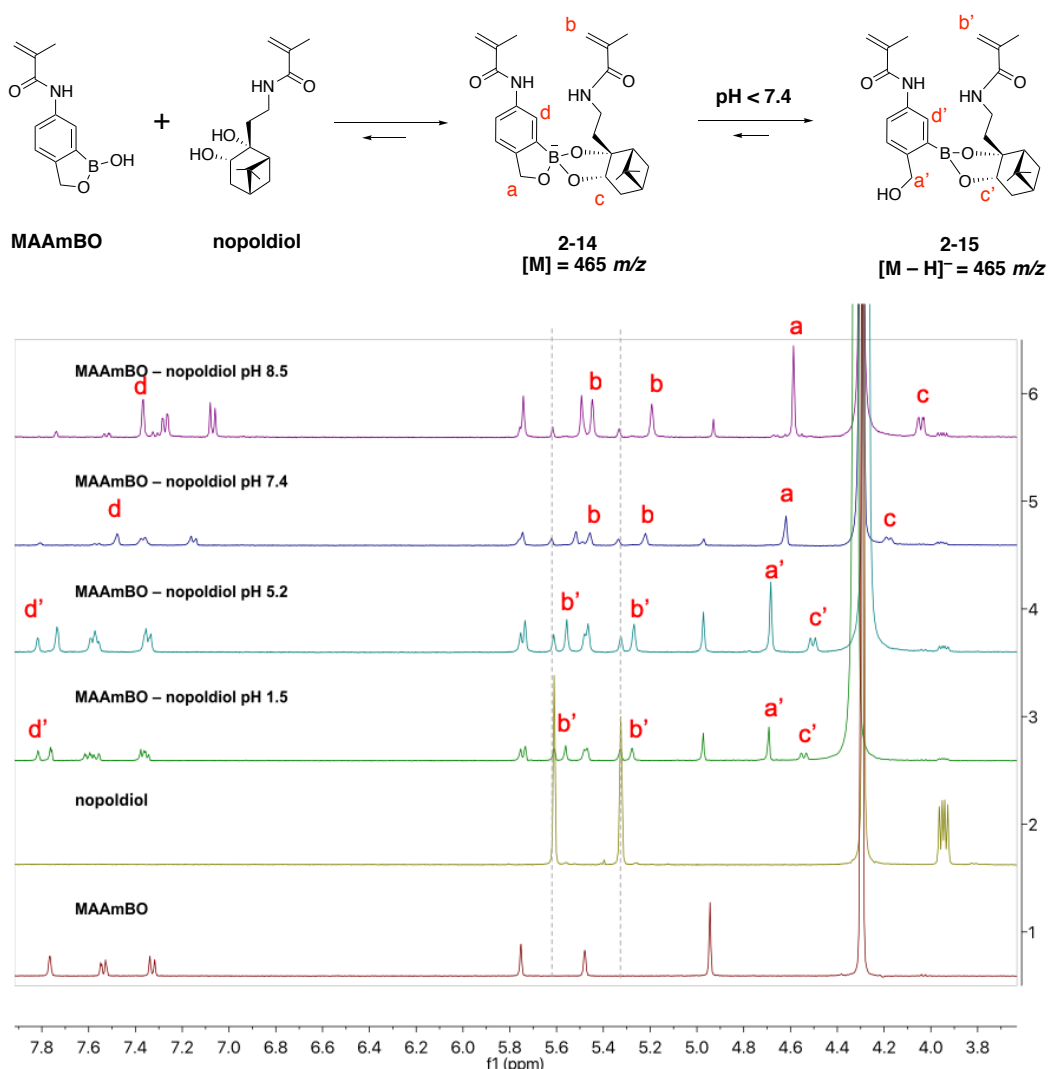


**Figure 2-8.** Detailed <sup>1</sup>H NMR spectra of nopoldiol-benzoxaborolate (**2-14** and **2-15**) formation at pH 8.5 to 1.5.

### 2.3.4.2 Binding studies – <sup>11</sup>B NMR analysis

The hypothesis of the nopoldiol-benzoxaborolate **2-14** ring-opening under acidic condition was further confirmed by <sup>11</sup>B NMR (Figure 2-9). Compared to the MAAmBO monomer alone, the boron signal of the nopoldiol-benzoxaborolate at basic and neutral pH showed a significant upfield shift of ~12 ppm, which implies a strong coordination between the two monomers (MAAmBO and nopoldiol) and a sp<sup>3</sup> configuration of the boron atom in **2-14**. In contrast, the boron chemical shift of the neutral benzoxaborolate **2-15** at lower pH are almost identical to a MAAmBO alone, which confirms a predominantly sp<sup>2</sup> character of the boron in **2-15**.

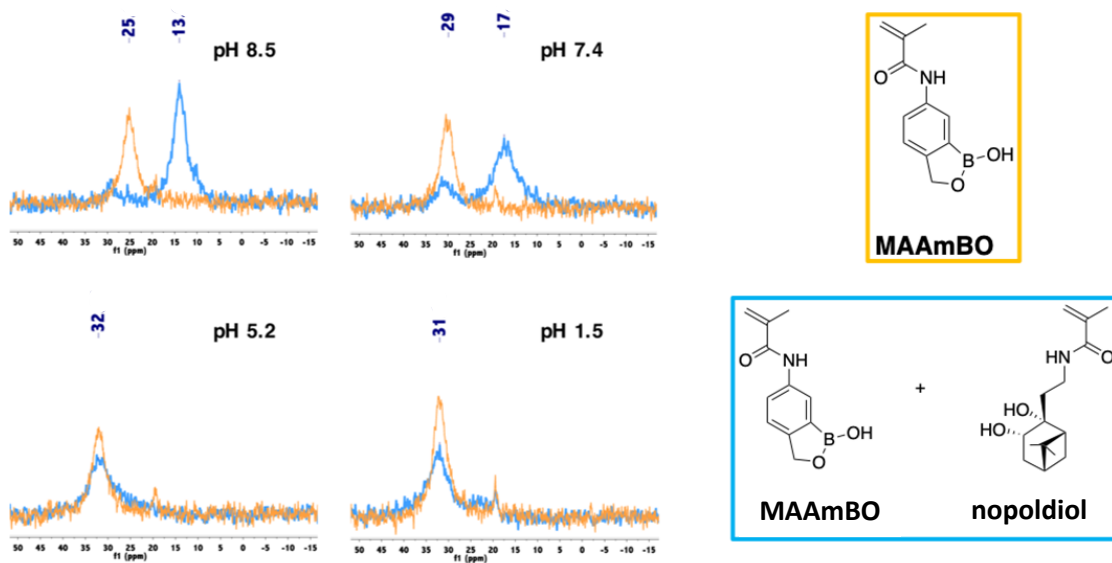


**Figure 2-9.**  $^{11}\text{B}$  NMR of MAAmBO (in orange) and MAAmBO – nopoldiol mixture (in blue) at pH 8.5 to 1.5.

### 2.3.4.3 Binding studies – ESI-MS & LC-MS analysis

The formation of **2-14** and **2-15** at pH 7.4 and 1.5 was observed by ESI-MS analysis (Figure 2-10). To capture the signal of the neutral nopoldiol-benzoxaboronate **2-15** in negative mode, the molecule may lose a proton of a hydroxyl group to display the  $[\text{M} - \text{H}]^-$  signal of 465.2  $m/z$ . The nopoldiol-benzoxaboronate peaks (mass of 465.2  $m/z$ ) were detected in the negative mode in both cases, suggesting the successful formation of the benzoxaboronate.

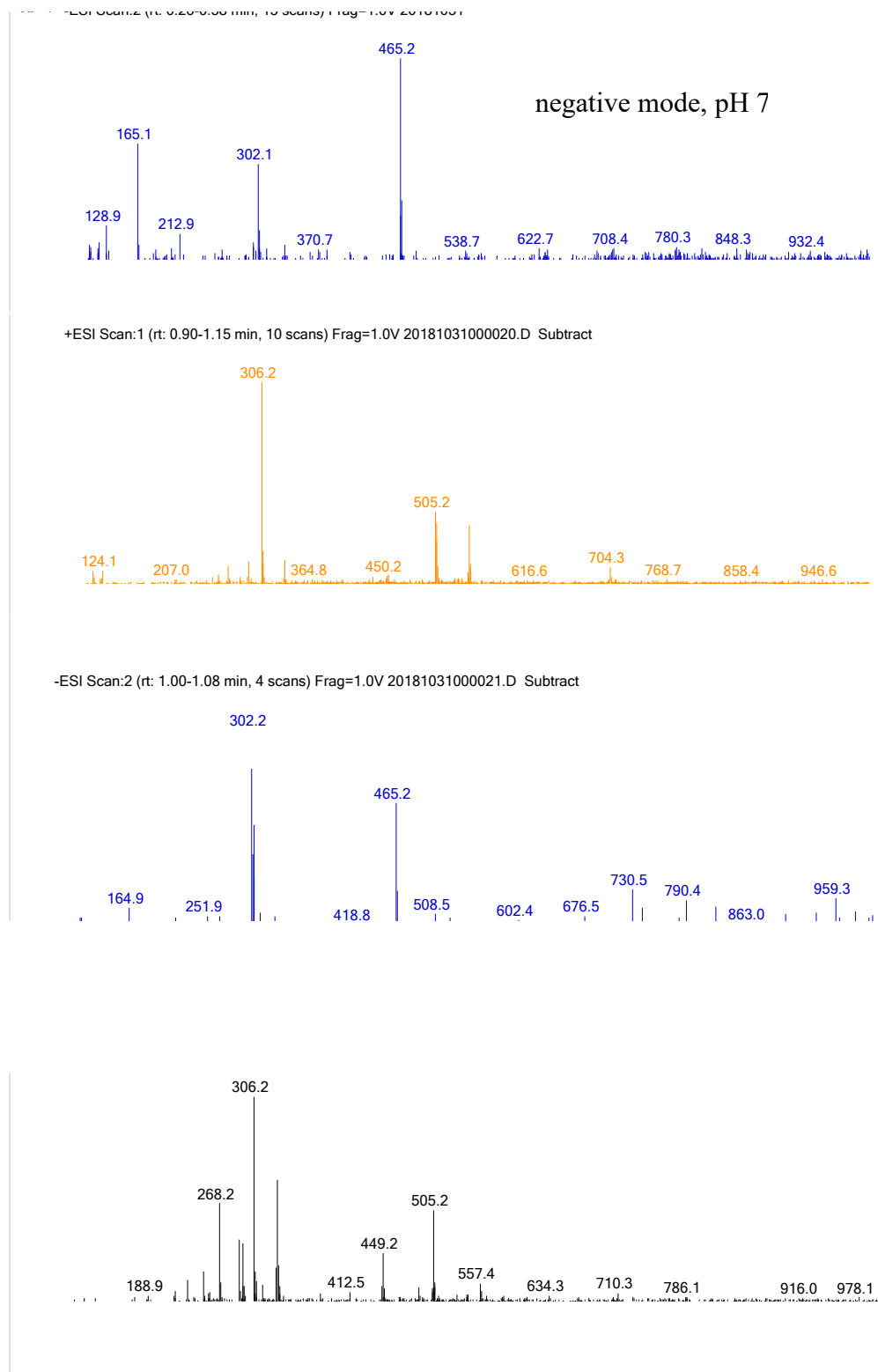


**Figure 2-10.** ESI-MS spectra of MAAmBO – nopoldiol mixture at (A) pH 7.4 and (B) pH 1.5.

Furthermore, to demonstrate that the nopoldiol-benzoxaborolate formation reaction is clean and effective under extreme pH conditions, the nopoldiol-benzoxaborolate formed at pH 1.5 (0.1 mM of both compounds) was subjected to LC-MS analysis after 7 h of incubation (Figure 2-11). The nopoldiol-benzoxaborolate decomposed to the free **MAAmBO** and **nopoldiol** while passing through the column, however, no other degradation product, such as protodeboronation product, was observed. These results suggest that the nopoldiol-benzoxaborolate formation is the only chemical reaction that occurred at the extreme pH of 1.5.

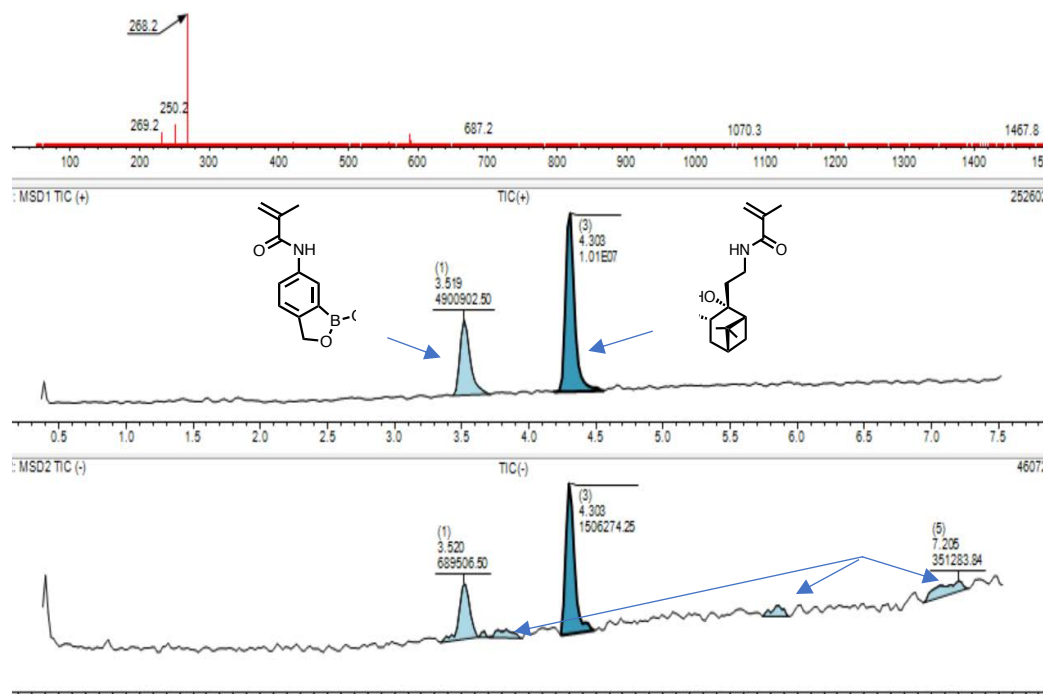


**Figure 2-11.** LC-MS spectra of **MAAmBO – nopoldiol** mixture at pH 1.5.

### 2.3.5 Rheological Measurements of Hydrogels

With encouraging monomer complexation results, the mechanical properties of DCN and SN hydrogels were characterized through a series of rheological measurements. Molar ratios of diols (**nopoldiol** and **GAEMA**) against the aryl boronic acid partners (**MAAmBO** or **MAPBA**) in the abovementioned hydrogels were compared (Table 2-8) to allow a better understanding of the function and influence of each component.

**Table 2-8.** Summary of molar ratios of reactive components in hydrogels and the resulting gelation time.

Entry	Hydrogel <sup>a</sup>	Molar ratio <sup>b</sup>				Gelation time, T (s) <sup>c</sup>
		MAAmBO	MAPBA	nopoldiol	GAEMA	
1	PBNG	1	–	0.60	1.36	26
2	PBG	1	–	–	1.27	204
3	PBN	1	–	0.55	–	230
4	PBN'	1	–	1.37	–	79
5	PB'NG	–	1	0.57	1.29	276
6	PB'G	–	1	–	1.21	427
7	PB'N	–	1	0.53	–	1114
8	PB'N'	–	1	1.30	–	211

<sup>a</sup>All of the hydrogels are formed with 10 w/v% solid content at pH 7.4. <sup>b</sup>Calculated by <sup>1</sup>H NMR. <sup>c</sup>Strain 1%, frequency 1 Hz.

### 2.3.5.1 Gelation time determination (kinetics)

Gelation time is critical for in situ forming hydrogels fabrication process. To minimize the material migration and shorten the implantation procedures, the gelation should occur rapidly after a transdermal injection of liquid polymer precursors through a small needle. In this study, the gelation time was determined via measurements of modulus versus time. A collaborator from the Narain group, Wenda Wang, performed these experiments. Specifically, after mixing the two polymer solutions (**PB** and **PNG/PG/PN/PN'**, 10 w/v%), storage modulus  $G'$  and loss modulus  $G''$  were monitored and the gelation time was defined when the value of the storage modulus  $G'$  exceeded that of the loss modulus  $G''$ . As shown in Table 2-8 and Figure 2-12, the DCN hydrogel **PBNG** exhibited the shortest gelation time of 26 s ( $T_1$ ), which was 7–8 times faster than hydrogels with either **GAEMA** or **nopoldiol** alone ( $T_2$  and  $T_3$ ). Furthermore, compared to **GAEMA**, **nopoldiol** was found to be more essential to the gelation rate, since the gelation process was accelerated markedly by increasing the **nopoldiol** content from a molar ratio of 0.55 to 1.37 ( $T_3$  vs  $T_4$ ). Moreover, with the comparable molar ratios of diol content, hydrogel **PBN'** showed a much shorter gelation time ( $T_4$ ) than that of hydrogel **PBG** ( $T_2$ ). The rapid gelation process also was demonstrated macroscopically by blending the precursor solutions of **PB** containing anti-cancer drug, doxorubicin, with **PNG**. The gelation time was determined simply by vial tilting tests, and the obtained gelation time is even shorter

than what was determined via rheological tests (< 10 s compared to 26 s, respectively) (Figure 2-13).

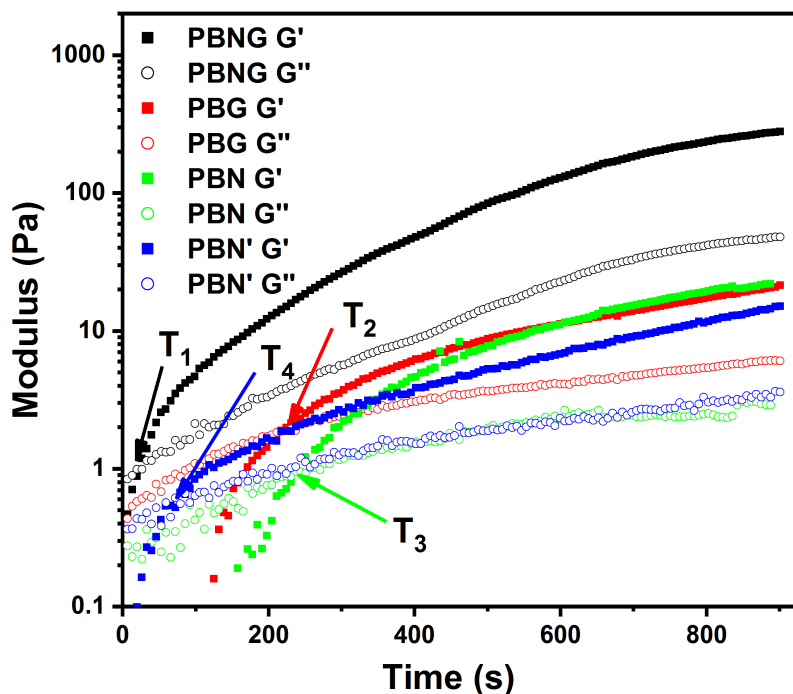


Figure 2-12. Rheological measurements of the gelation process of hydrogel PBNG, PBG, PBN and PBN'.

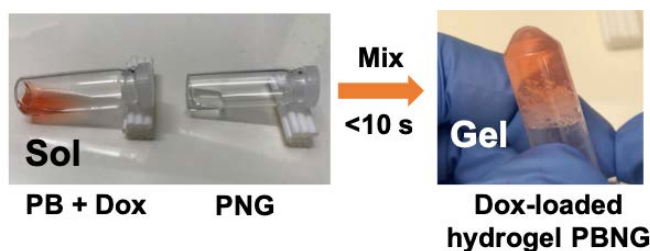
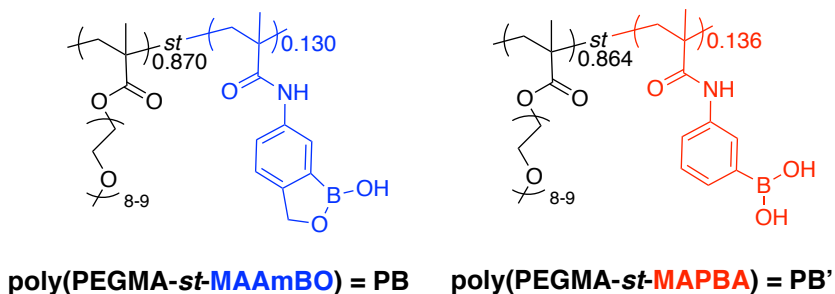


Figure 2-13. Gelation of fast in situ forming hydrogel PBNG (10 w/v%) at pH 7.4.

To describe the advantages of using benzoxaborole, 3-methylacrylamido phenylboronic acid (**MAPBA**), a conventional arylboronic acid, was chosen to replace the **MAAmBO** monomer, and the **MAPBA**-containing polymer is denoted as **PB'** (Figure 2-14). The gelation rates of **PB'** with the diol-containing polymers were assessed to compare with  $T_1$ – $T_4$  (Figure 2-15 and Table 2-8). Unsurprisingly, the gelation time of **MAPBA**-based hydrogels were 2–10 times longer than that of the **MAAmBO**-based hydrogels ( $T_1$ – $T_4$  vs  $T_5$ – $T_8$ ). These

observations can be explained by the lower reactivity of **MAPBA** boron centers towards diol partners, due to its higher  $pK_a$  ( $\sim 9$ ) and its lowered electrophilicity compared to the boron atom in **MAAmBO**. Considering all the results obtained thus far, both **nopoldiol** and **MAAmBO** are crucial to provide an efficient gelation process that meets the criteria for in situ forming hydrogels.



**Figure 2-14.** Structures of polymers **PB** and **PB'**.

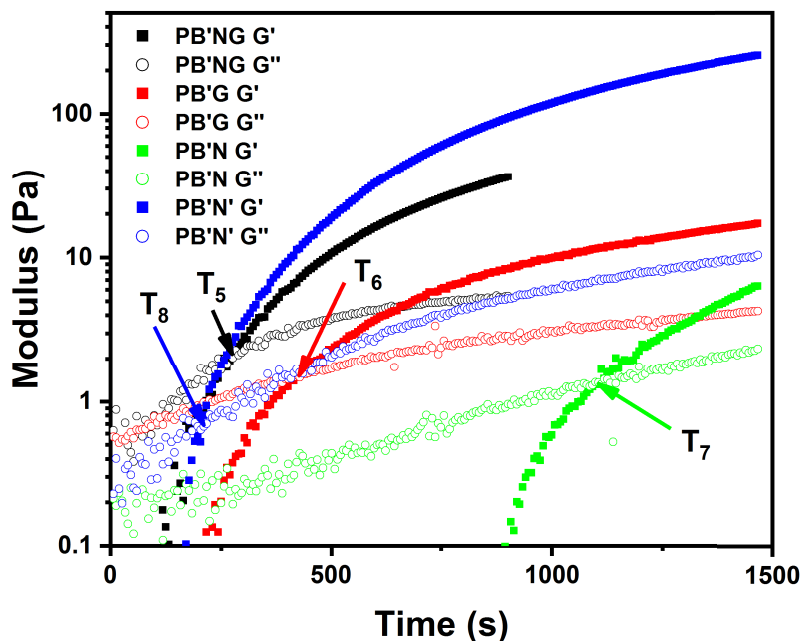
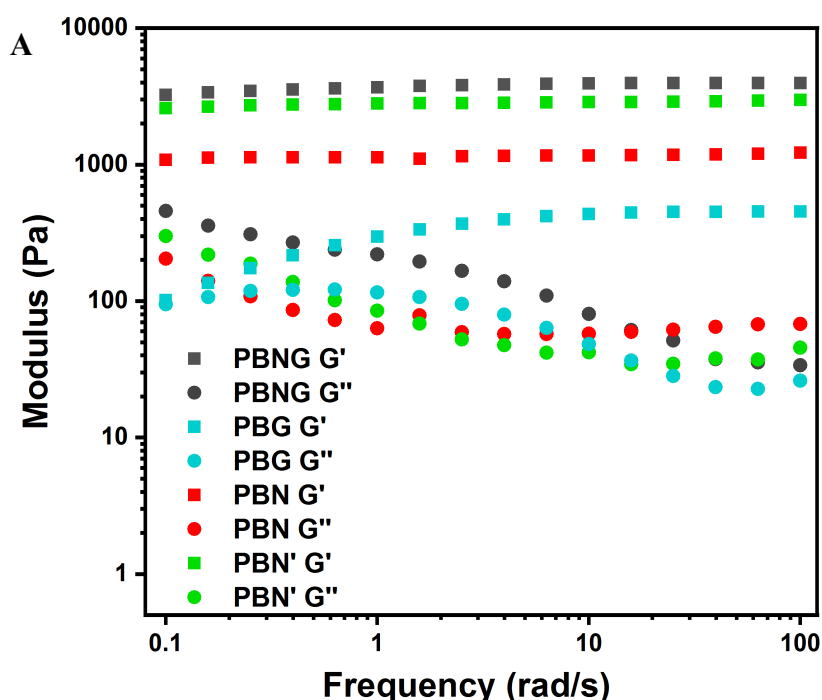


**Figure 2-15.** Rheological measurements of the gelation process of hydrogels **PB'NG**, **PB'G**, **PB'N**, and **PB'N'**.

### 2.3.5.2 Dynamic oscillatory frequency sweep (mechanical properties)

To identify the influence of the hydrogel types and pH conditions on the hydrogels' mechanical strength, dynamic oscillatory frequency sweep tests were carried out. These

experiments were performed by Wenda Wang. Figure 2-16A shows the storage modulus  $G'$  and the loss modulus  $G''$  of the four types of hydrogel (**PBNG**, **PBG**, **PBN**, and **PBN'**). Hydrogel **PBNG**, which contains the highest molar ratios of reactive components, displays the highest storage modulus  $G'$ , namely, the strongest mechanical strength (Table 2-8). On the other hand, hydrogel **PBN** with only 0.55 molar ratio of **nopoldiol** was much stronger than **PBG**, which composes more than twice the diol contents as **PBN**. Next, the hydrogels **PBNG** (10 w/v%) formed at pH 7.4, 5.2, and 1.5 were also subjected to this rheological test to identify the impact of pH conditions on the hydrogel mechanical strength (Figure 2-16B). The  $G'$  value (at  $\gamma = 1\%$ ,  $\omega = 1$  Hz) of **PBNG** was found to be 3896 Pa, 886.4 Pa, and 747.6 Pa at pH 7.4, 5.2, and 1.5, respectively. Clearly, the  $G'$  values of hydrogels at low pH (5.2 and 1.5) were more than four times lower than that of pH 7.4, indicating that the pH-sensitive sugar-benzoxaborolate cross-links and possibly some of the nopoldiol-benzoxaborolate cross-links were dissociated under more acidic conditions. This assumption was also supported by the previous monomer binding studies (Table 2-7), where only  $\sim 15\%$  of the nopoldiol-benzoxaborolates were cleaved at pH 5.2 compared to pH 7.4; whereas nearly all of the sugar-benzoxaborolate complexes with **GAEMA** were dissociated at the same pH.



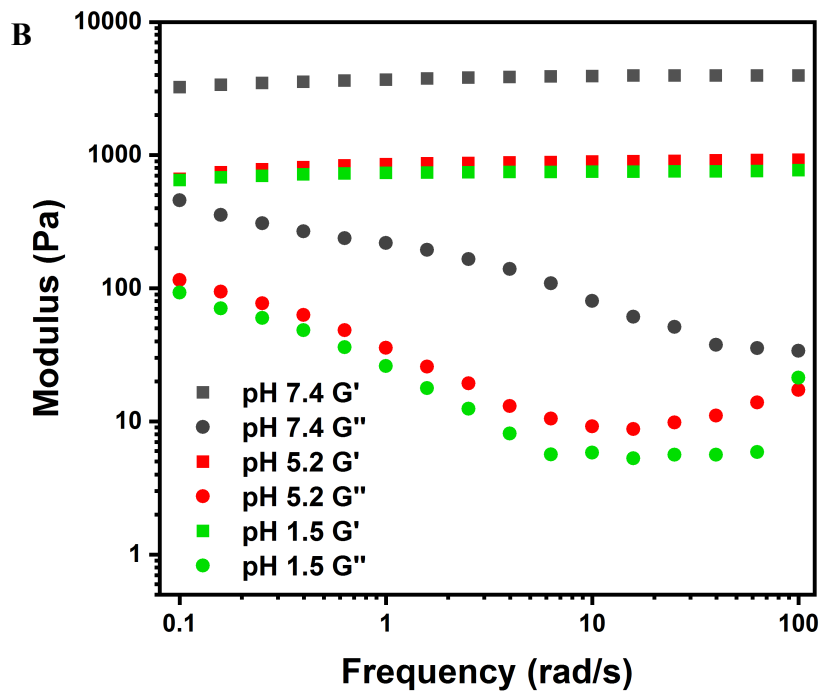


**Figure 2-16.** (A) Dynamic oscillatory frequency sweeps of hydrogels (**PBNG**, **PBG**, **PBN** and **PBN'**) in 10 w/v%. (B) Dynamic oscillatory frequency sweeps of 10 w/v% **PBNG** at pH 7.4 to 1.5.

In addition, the porous structures of **PBNG**, **PBN**, and **PBG** at pH 7.4, as well as **PBNG** at pH 1.5, were characterized by SEM imaging. As shown in Figure 2-17, with a higher storage modulus  $G'$  value and higher pH conditions, the hydrogels exhibit smaller pore sizes and more compact network structures, corroborating their stronger mechanical properties.

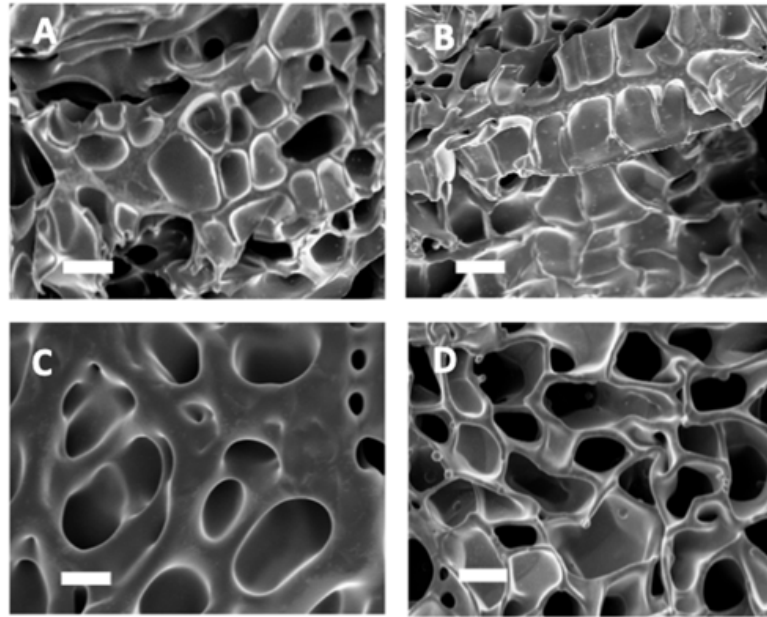


**Figure 2-17.** SEM image of hydrogels: (A) **PBNG** at pH 7.4, (B) **PBN** at pH 7.4, (C) **PBG** at pH 7.4, (D) **PBNG** at pH 1.5. Hydrogels were all made in 10 w/v% and freeze-dried 16 h after gelation. Scale bars are equal to 20  $\mu\text{m}$ .

### 2.3.5.3 Oscillatory strain sweeps and step strain tests (self-healing)

Prior to the rheological measurements, the self-healing property of hydrogel **PBNG** was demonstrated macroscopically by connecting two hydrogel cubes (Dox loaded and non-loaded), followed by 20 s of healing without any external forces (Figure 2-18). The reconstituted hydrogel could be lifted manually and was found to tolerate its own weight, indicating the success of fracture self-repairing.

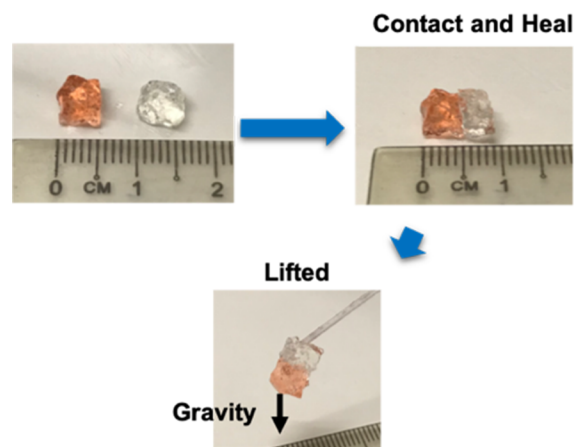


**Figure 2-18.** Macroscopic demonstration of self-healing property of 10 w/v% **PBNG** at pH 7.4.

Differing from permanent covalent bond cross-linked hydrogels, which normally show frequency-independent  $G'$  and  $G''$ , all of the designed hydrogels display variable  $G'$  and  $G''$  values throughout the frequency changes, no matter of the different hydrogel types and pH conditions (shown in Figure 2-16 previously). Furthermore, strain sweep tests and step strain tests were conducted to quantify the hydrogel self-healing behaviors. The optimal hydrogel **PBNG** was chosen to demonstrate the promising self-healing properties in a wide pH range (8.5–1.5) (Figure 2-19 and Figure 2-20). For example, in the case of **PBNG** (10 w/v%) at pH 7.4, the hydrogel was first subjected to strain sweep tests with a linear amplitude sweep of  $\gamma$  (strain%) = 1% to 1000% to identify the linear viscoelastic region. At the critical strain (334%), the storage modulus  $G'$  dropped drastically, whereas the value of loss modulus  $G''$  suppressed that of the storage modulus  $G'$ , indicating gel failure (Figure 2-19 B). Then, a small strain of 1% and a large strain of 400% (a strain greater than the critical strain) was applied cyclically on the hydrogel to evaluate its modulus recovery ability upon exposing in the large strain (gel failure) (Figure 2-20B). Remarkably, after two cycles, almost quantitative  $G'$  and  $G''$  were recovered in all cases, indicating the promising self-healing abilities of **PBNG** under all of the pH conditions tested (8.5–1.5).

Notably, without the help of the dynamic sugar-benzoxaborolates, hydrogel **PBN** with only the nopoldiol-benzoxaborolate cross-links, also exhibits great self-healing properties at pH 7.4 (Figure 2-21). Altogether, despite that the nopoldiol-benzoxaborolate cross-links are considered tough, both sugar-/nopoldiol-benzoxaborolate cross-links demonstrate a certain degree of dynamicity and flexibility, which ultimately results in the promising self-healing properties of the resulting hydrogels.

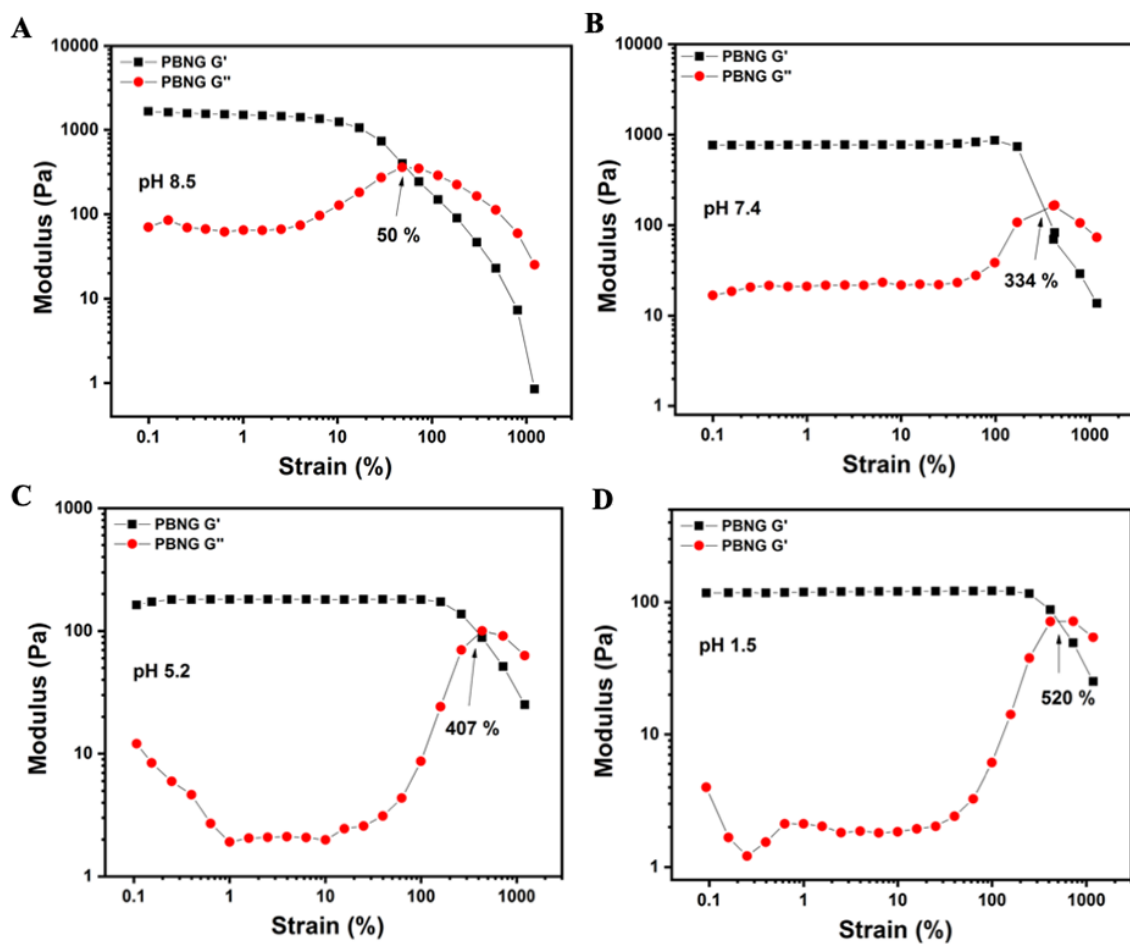


Figure 2-19. Oscillatory strain sweep results of hydrogel PBNG at pH (A) 8.5, (B) 7.4, (C) 5.2, and (D) 1.5.

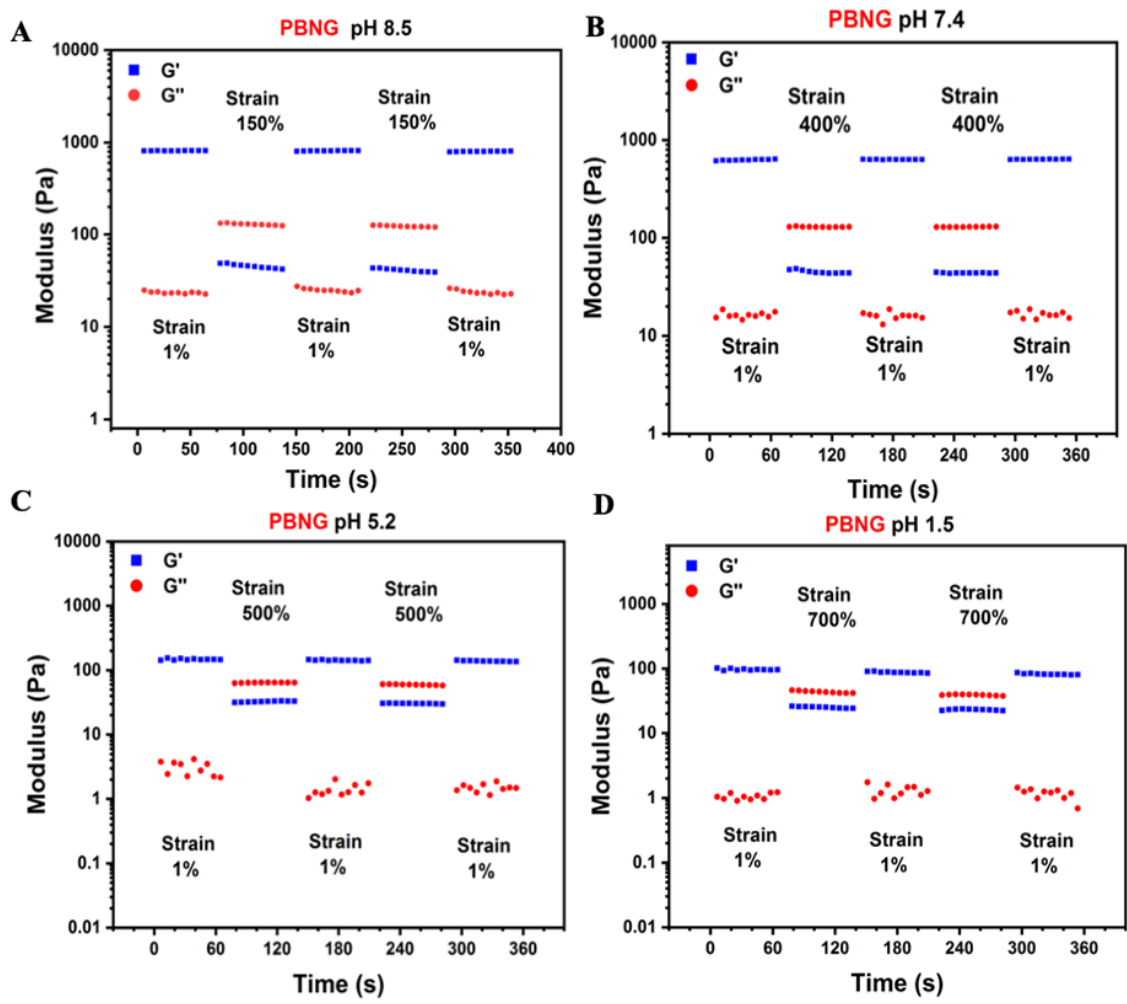


Figure 2-20. Step strain tests of hydrogel PBNG at pH (A) 8.5, (B) 7.4, (C) 5.2, and (D) 1.5.

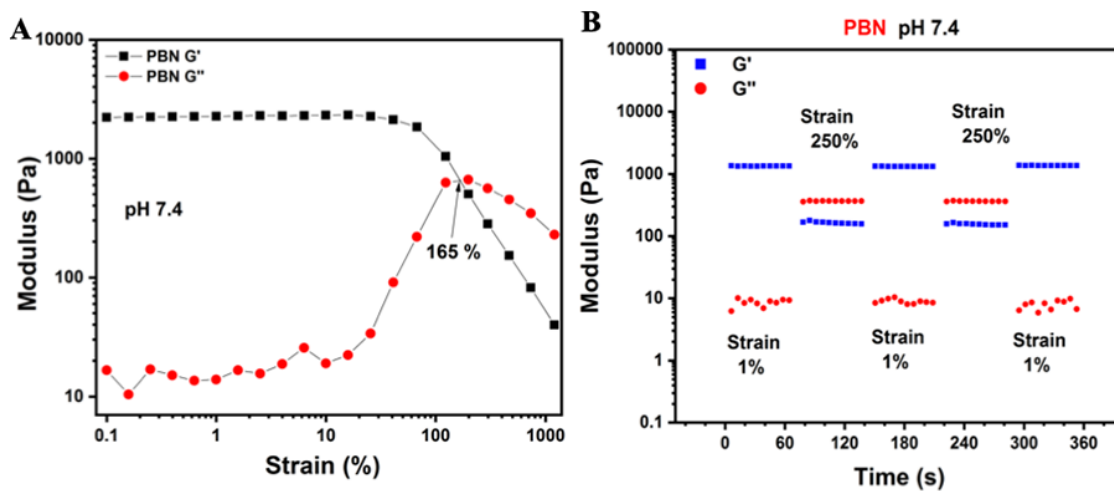
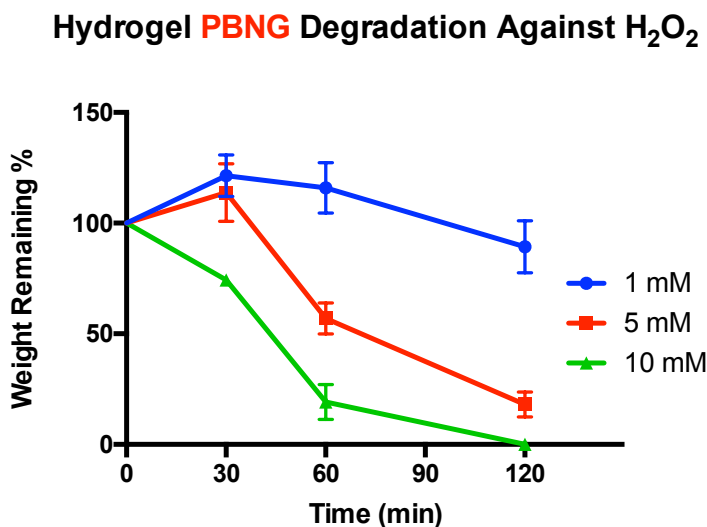


Figure 2-21. (A) Oscillatory strain sweeps and (B) step strain tests of hydrogel PBN (10 w/v%) at pH 7.4.

### 2.3.6 ROS-responsive Degradation Studies

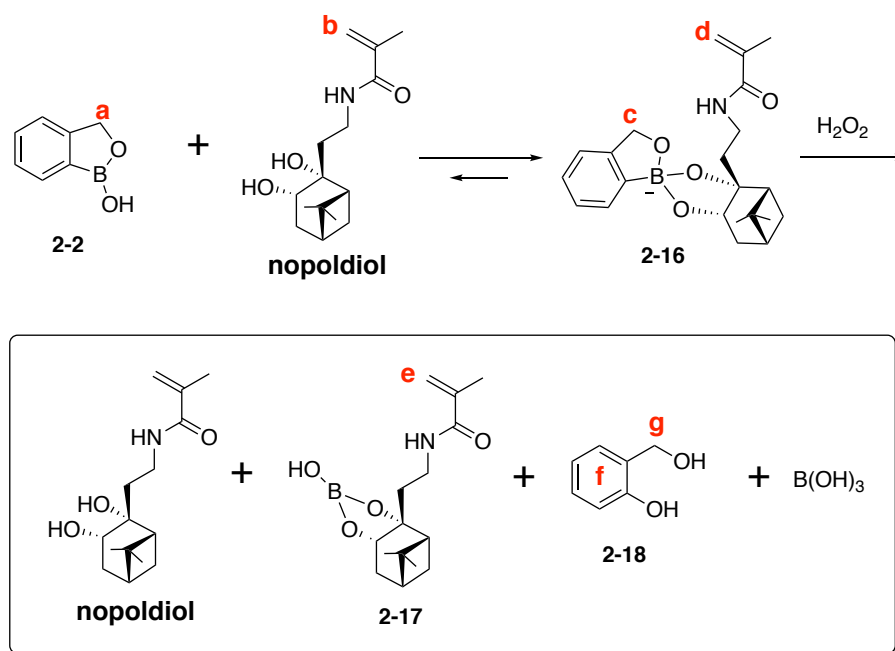
It is well known that the tumor microenvironment and many other pathological conditions are highly correlated with the overexpression of ROS.<sup>1, 33</sup> Therefore, benzoxaborolate cross-linked hydrogels are very attractive for biomedical applications, including ROS-responsive local delivery of therapeutic agents and antioxidative regulation of overproduced ROS. Here, the ROS-responsiveness of the **PBNG** hydrogel was examined by using various concentrations of H<sub>2</sub>O<sub>2</sub> (hydrogen peroxide) solutions as ROS models, and the hydrogel weight changes were monitored. As expected, faster hydrogel degradation was observed in a higher H<sub>2</sub>O<sub>2</sub> concentration, and more complete hydrogel degradation was found over longer exposure times in the H<sub>2</sub>O<sub>2</sub> solutions (Figure 2-22).



**Figure 2-22.** H<sub>2</sub>O<sub>2</sub>-responsive degradation profile of hydrogel **PBNG** (10 w/v%) with 1, 5, and 10 mM of H<sub>2</sub>O<sub>2</sub>.

Furthermore, a model reaction using benzoxaborole (compound **2-2**) and **nopoldiol** monomer as the binding partner was set up to investigate the oxidative-cleavage process of the resulting benzoxaborolate (Scheme 2-6). Thus, H<sub>2</sub>O<sub>2</sub> was added to the mixtures of **2-2** and **nopoldiol** monomer (1:1 molar ratio, 5 mM of each) to reach final concentrations of 1, 5, and 10 mM, respectively, and <sup>1</sup>H NMR was used to monitor the degradation process. As shown in Figure 2-23 and Table 2-9, the conversion to benzoxaborolate complex (**2-16**) was found to decrease from the original level of 63% to 57%, 36%, and 22% under 0, 1, 5, and 10 mM of H<sub>2</sub>O<sub>2</sub>, respectively, after 20 min. The corresponding oxidation product, 2-hydroxybenzyl

alcohol (**2-18**), was found to increase over time, while the **nopoldiol** was released as a free diol or as a boric acid-conjugate (**2-17**). A more complete degradation of **2-16** was found over a longer period of time (45 min), where the conversion to **2-16** further dropped to 52%, 19%, and 11% (Table 2-9). Altogether, these monomer degradation studies further confirmed the efficient benzoxaborolate oxidative cleavage and the fast ROS-responsive degradation features of the resulting hydrogels.



**Scheme 2-7.** Oxidative degradation of mixtures of **2-2**, **nopoldiol** and **2-16** by  $\text{H}_2\text{O}_2$ .

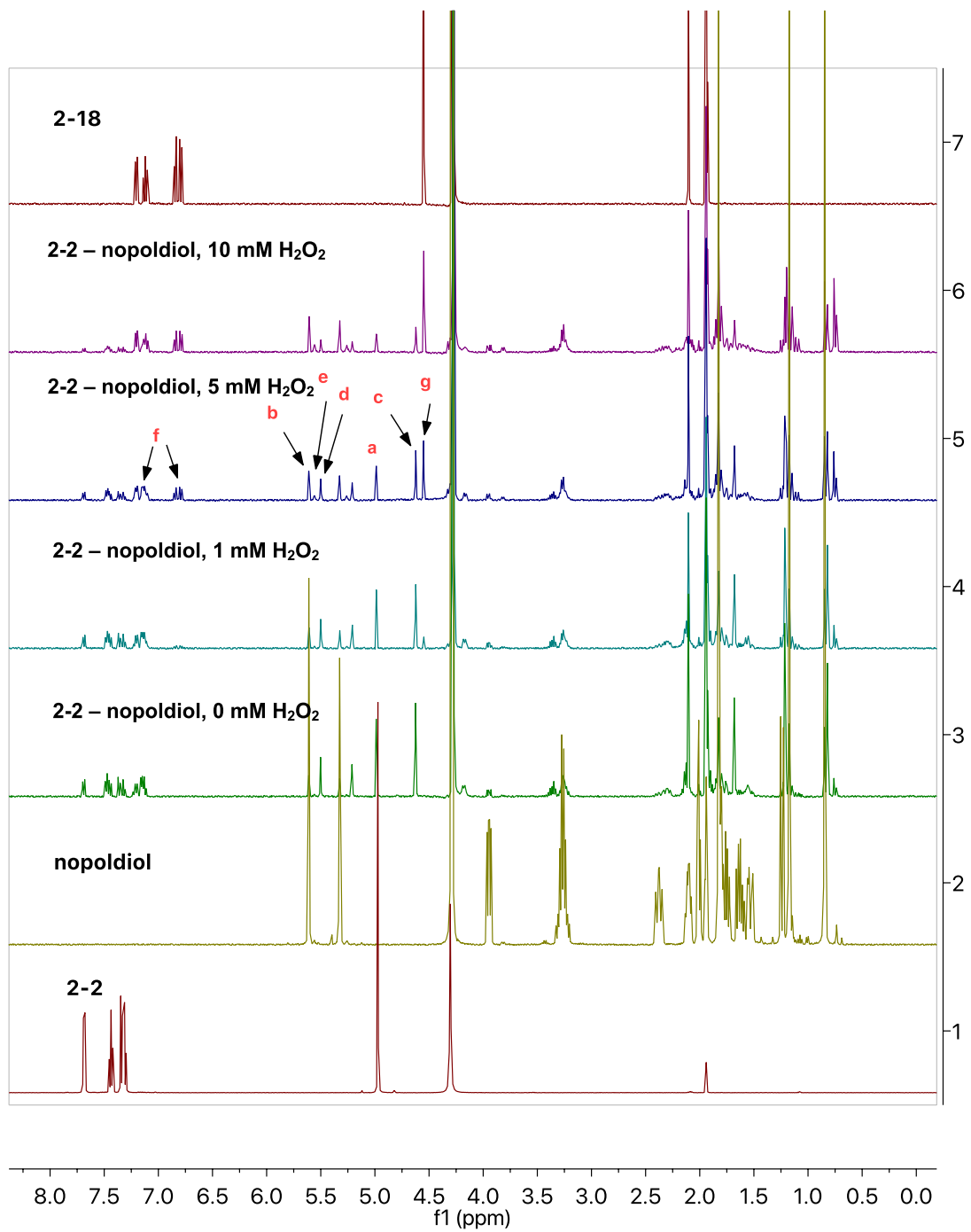


**Figure 2-23.**  $^1\text{H}$  NMR spectra of **2-2**, **nopoldiol**, mixtures of **2-2 - nopoldiol** with of 0, 1, 5, 10 mM of  $\text{H}_2\text{O}_2$  solution after 20 min, and the standard  $^1\text{H}$  NMR spectra of side product **2-18**.

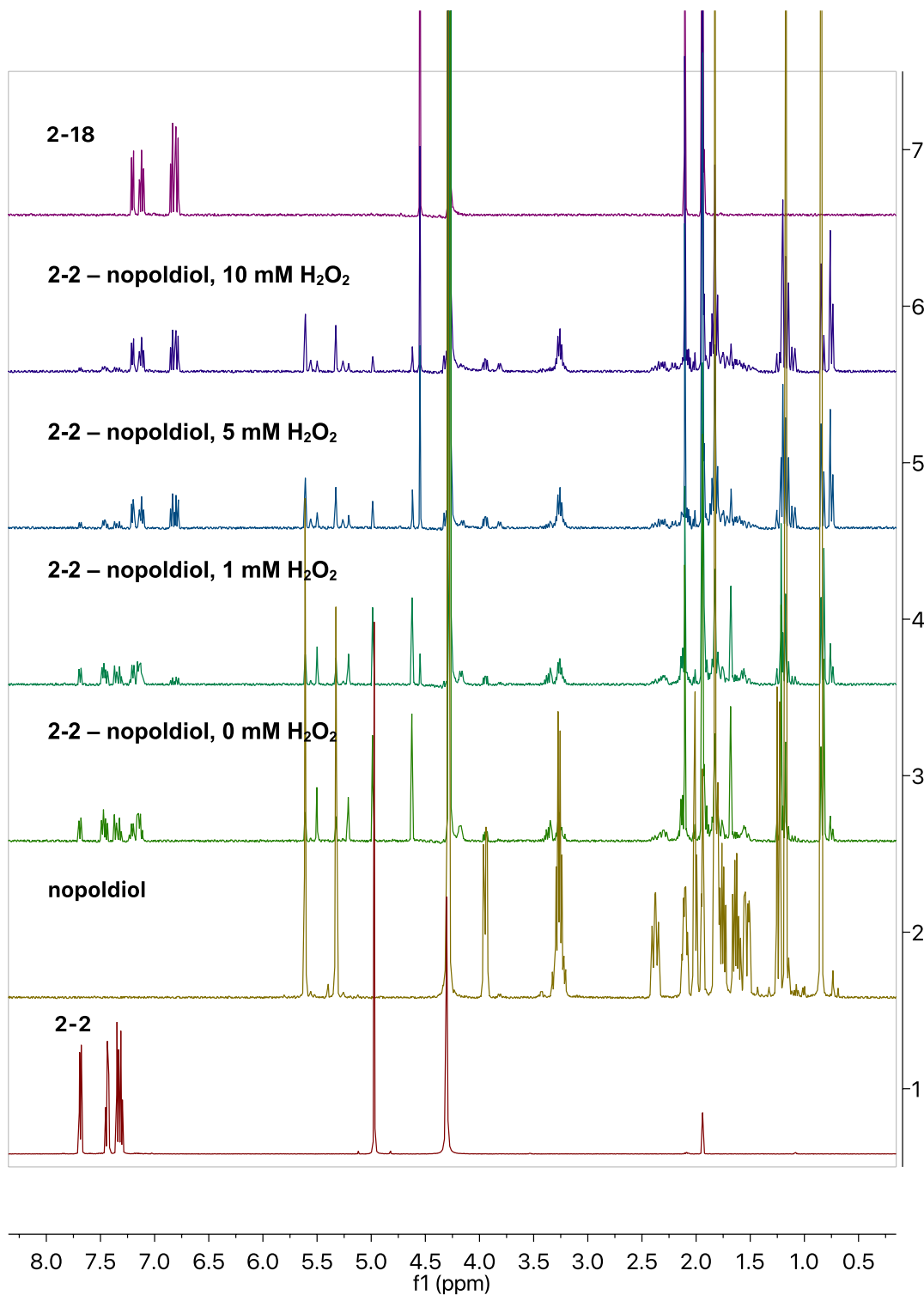


**Figure 2-24.** <sup>1</sup>H NMR spectra of **2-2**, **nopoldiol**, mixtures of **2-2 – nopoldiol** with of 0, 1, 5, 10 mM of H<sub>2</sub>O<sub>2</sub> solution after 45 min, and the standard <sup>1</sup>H NMR spectra of side product **2-18**.

**Table 2-9.** Summary of 2-2 – **nopoldiol** conversion % to benzoxaborolate 2-16 under 0, 1, 5, 10 mM of H<sub>2</sub>O<sub>2</sub> solution after 20 and 45 min.

H <sub>2</sub> O <sub>2</sub> conc. (mM)	0	1	5	10
Time				
20 min	63	57	36	22
45 min		52	19	11

### 2.3.7 Bioorthogonality of Hydrogels Towards Polyols

The bioorthogonality of the system towards endogenous sugars (glucose and fructose) was assessed by immersing the hydrogels into a high concentration of polyols (a mixture of 30 mM D-glucose and 15 mM of D-fructose), and then measure the hydrogel weight changes. Due to the competitive binding of polyols to benzoxaborole, the SN hydrogel **PBG** with only conventional labile sugar-benzoxaborolate cross-links degraded completely after 120 min. In contrast, nopoldiol-benzoxaborolate hydrogels (**PBNG** and **PNG**) could maintain their weights under the same conditions.

#### Hydrogel Stability Against Sugar

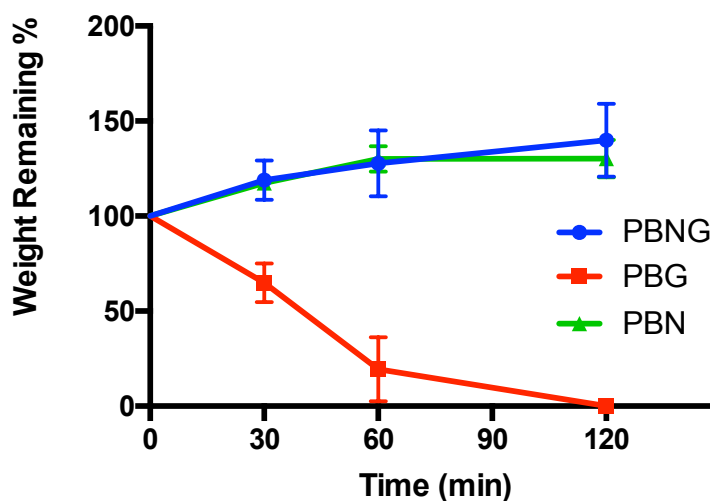
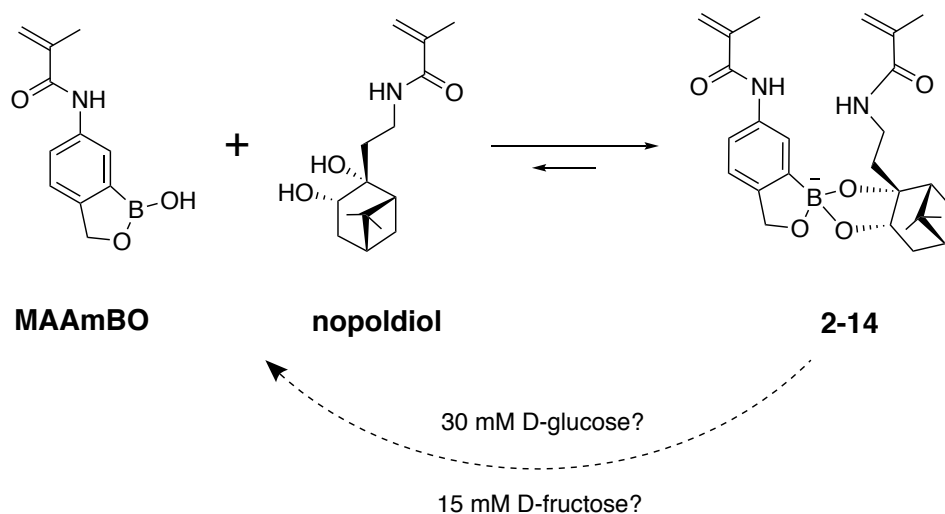


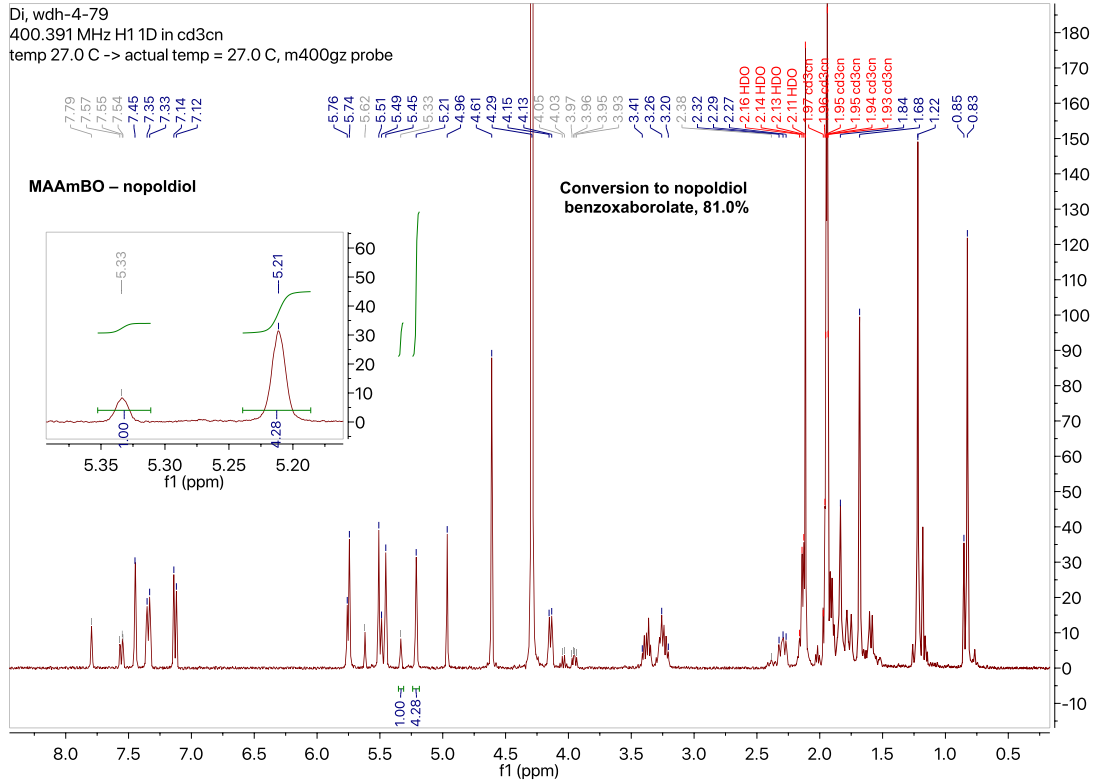
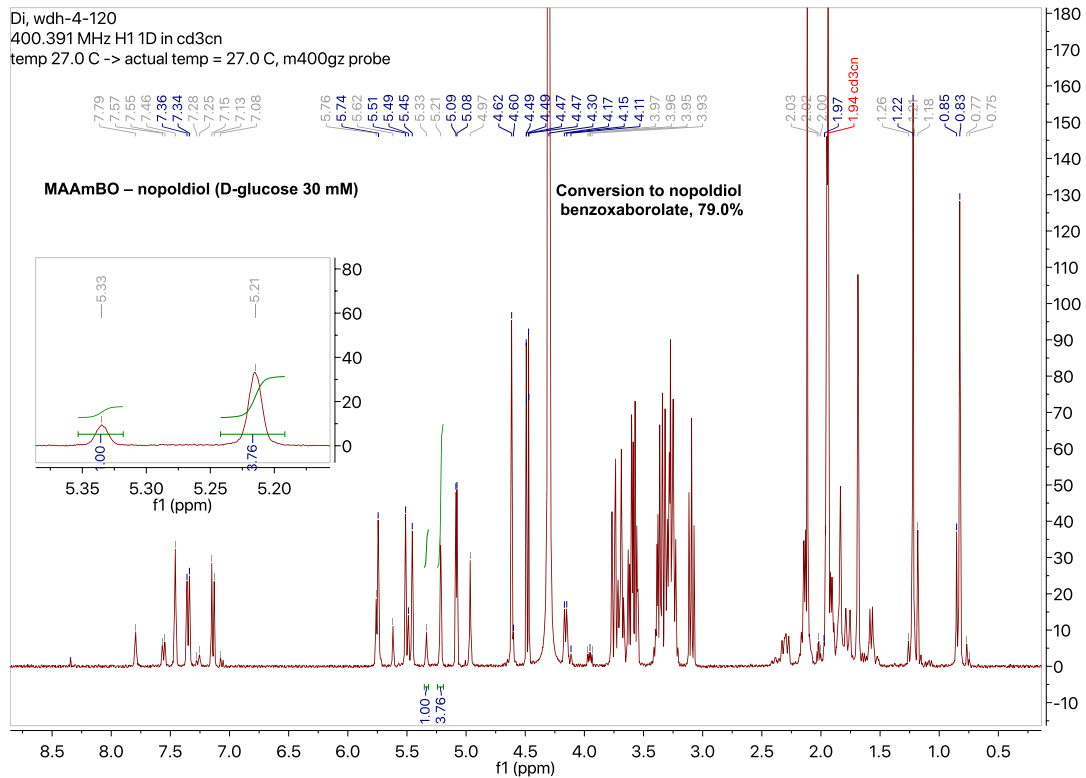
**Figure 2-25.** Degradation profiles of **PBNG**, **PBG** and **PBN** under polyol solution of 30 mM D-glucose and 15 mM D-fructose.

To further describe the bioorthogonality of the nopoldiol-benzoxaborolate cross-links, **MAAmBO** and **nopoldiol** was mixed with D-glucose/D-fructose to reach a final concentration of 10 mM **MAAmBO**, 10 mM **nopoldiol**, and 30 mM D-glucose/15 mM D-fructose. <sup>1</sup>H NMR spectroscopy was used to confirm the extraordinary stability of this nopoldiol-benzoxaborolate system at the monomer level (Table 2-11 and Figure 2-26). Remarkably, 30 mM of D-glucose, which is around four times higher than the diabetic glucose level, did not influence the equilibrium conversion of the monomer **MAAmBO** and **nopoldiol** to nopoldiol-benzoxaborolate **2-14** at pH 7.4 (Table 2-10 and Figure 2-26). Since D-fructose has a greater binding affinity with benzoxaborole, 15 mM of D-fructose caused about 15% of degradation on the nopoldiol boronate **2-14** (Table 10 and Figure 2-26). The high bioorthogonality of the hydrogel **PBNG** could be of great benefit in application such as diabetic wound healing and sustainable insulin/drug delivery, where a stable and glucose-resistant biomaterial is needed.

**Table 2-10.** Demonstration and results of bioorthogonality tests towards endogenous sugars.



Initial conversion% to 2-14	Conversion% to 2-14 after mixing with 30 mM D-glucose	Conversion% to 2-14 after mixing with 15 mM D-fructose
81%	79%	66%

**A****B**

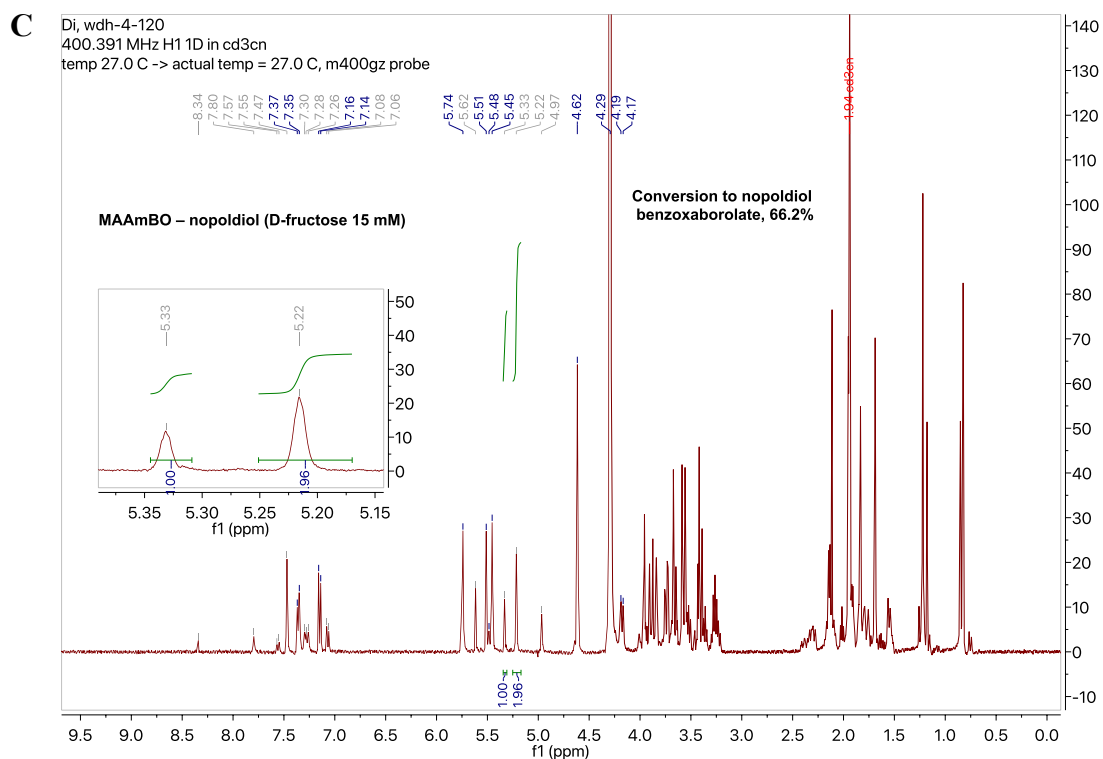


**Figure 2-26.**  $^1\text{H}$  NMR spectrum of (A) MAAmBO – nopoldiol (original), (B) MAAmBO – nopoldiol with 30 mM D-glucose, and (C) MAAmBO – nopoldiol with 15 mM D-fructose.

### 2.3.8 Hydrogel pH-Responsive Degradation Studies

To assess the hydrogel acid-resistance, swelling and degradation behaviors, DCN hydrogel **PBNG** and SN hydrogel **PBN** was immersed in buffers with pH of 7.4, 5.2, and 1.5, and their weights were monitored over time. Both **PBNG** and **PBG** hydrogels could maintain their integrity over several days under acidic conditions (Figure 2-27); however, **PBNG** exhibited twice the lifetime of **PBN** (~20 vs ~10 days). The higher stability of **PBNG** may result from its higher cross-linking density. It is worth mentioning that, unlike other click reactions that form permanent/irreversible bonds, the nopoldiol-benzoxaborolate cross-links can be hydrolyzed gradually in aqueous medium, especially at acidic pH. The monomer studies previously described in Table 2-7 also support this hypothesis of pH-dependent nopoldiol-benzoxaborolate formation, where 86.5% and 59.5% of conversion to benzoxaborolate were observed at pH 8.5 and 1.5, respectively. More interestingly, the **PBNG** hydrogel demonstrated a pH-dependent swelling behavior, a feature that is highly desirable for pH-controlled drug release; the gel swelled faster under more acidic conditions (Figure 2-27A vs

2-27B). This swelling behavior suggests that the highly pH-sensitive sugar-benzoxaborolate cross-links were prone to dissociate faster at lower pH. Consequently, the porous network structures could be enlarged, and thus enabling more water uptake and release of encapsulated cargo.

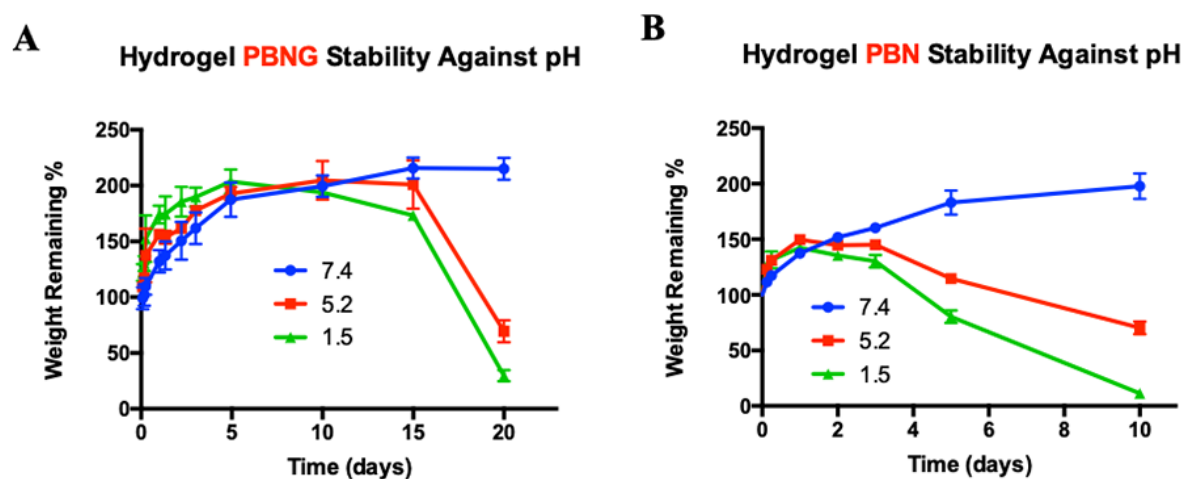


Figure 2-27. Hydrogel degradation profile of 10 w/v% (A) PBNG, and (B) PBN, respectively, at pH 7.4 to 1.5.

### 2.3.9 pH-responsive Drug Release

The previously observed pH-dependent swelling behavior and the acid-resistance of hydrogel PBNG, suggest a potential utility of this DCN hydrogel system in pH-responsive and long-term drug release. Herein, doxorubicin (Dox), a widely used anti-cancer drug, was used to verify the pH-sensitive and sustainable drug release ability of the optimal hydrogel PBNG.

As shown in the cumulative drug release profile (Figure 2-28A), the differences between the drug releasing rates at pH 7.4, 5.2, and 1.5 were distinct. After 8 h, a larger amount of Dox (68.5%) was released under acidic conditions of pH 1.5 compared to 49.2% and 21.8% at pH 5.2 and 7.4, respectively. The cumulative percent of drug release plateaued after 32 h of drug release, and then finally totaled as 89.8%, 79.3%, and 37.5% at pH 1.5, 5.2, and 7.4, respectively, after 48 h. Moreover, distinctive changes in the hydrogel color was observed after 48 h of drug release. As shown in Figure 2-28B, the hydrogel at pH 7.4 displayed the darkest color from the unreleased Dox, and the redness decreased for the gels exposed at lower pH, indicating a faster and more complete drug release under acidic conditions.

As described in Figure 2-28C, at neutral pH, the dual-cure networks provide stable and compact hydrogel structures for the encapsulation of the drug. However, once the hydrogels are exposed to an acidic environment (e.g., tumor sites and gastric environments), the hydrogels could maintain their integrity for long as ~20 days (shown previously in Figure 2-27A), while the acid-cleavable sugar-benzoxaborolate cross-links break up quickly to release the encapsulated drug upon hydrogel pore enlarging. In summary, the potential of DCN hydrogel **PBNG** to be a stable and pH-responsive drug carrier for targeted drug delivery was confirmed by the drug releasing experiments with Dox.

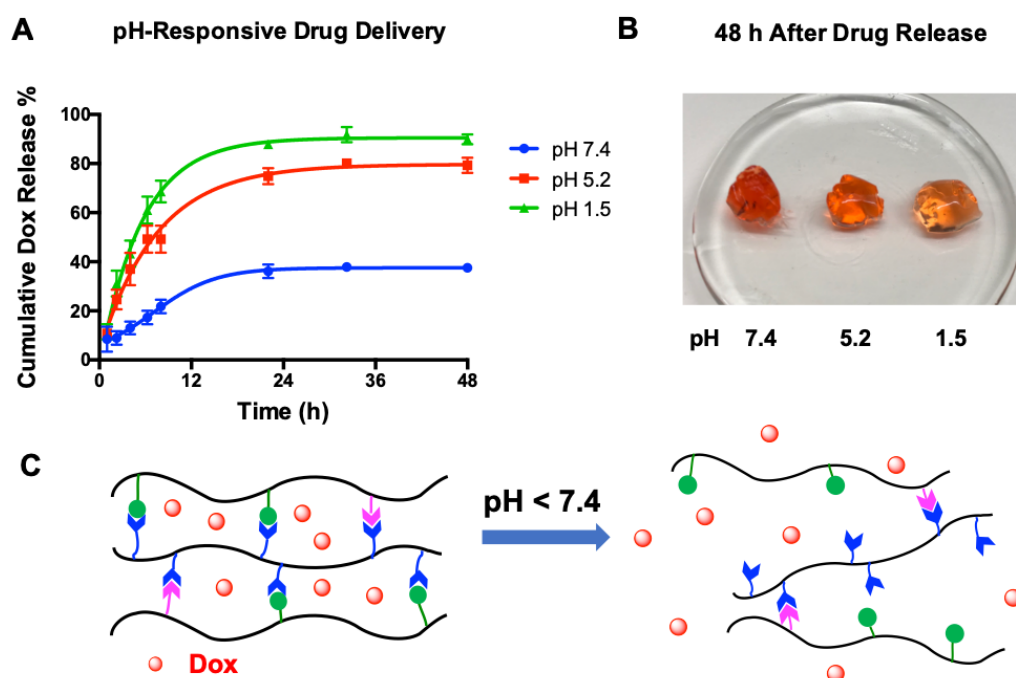


**Figure 2-28.** pH-Responsive doxorubicin (Dox) drug release. (A) Cumulative Dox release profile of hydrogel **PBNG** (10 w/v%) at pH 7.4 to 1.5. (B) Picture of hydrogels at pH 7.4 to 1.5 after 48 h of drug releasing. (C) Graphic description of DN hydrogel **PBNG** pH-responsive drug release.

### 2.3.10 Cytotoxicity and 3D Cell Encapsulation

With an aim to explore the biological potential of the DCN hydrogel, MTT cytotoxicity assays were performed to test the biocompatibility of the individual polymers **PB** and **PNG**. The polymer solutions with concentrations of 0.01–1 mg/mL were incubated with HeLa cells, and almost 100% of cell viability was observed in all cases, except for the highly concentrated polymer **PNG** (1 mg/mL) (Figure 2-29A). Sequentially, the biocompatibility of the hydrogel

**PBNG** was assessed by incubating hydrogel extracts with HeLa cells. The hydrogel extracts were obtained by immersing the hydrogel cubes into the cell culture medium for 24 and 48 h (denoted as 24 h- and 48 h-extract), and the hydrogel/medium ratio was designed as 1:10 and 1:40 to evaluate the effect of hydrogel dilution. Remarkably, more than 95% of cells were found viable with the 24 h-extract, and a slightly lower cell viability of ~86% was observed for the 48 h-extract (1:10 gel/medium ratio), which could be caused by the leaching of unbound or decomposed polymers over this longer period of time (Figure 2-29B). Nevertheless, negligible toxicity was found in both individual polymer and the hydrogel extract, demonstrating the great biocompatibility of the designed biomaterials.

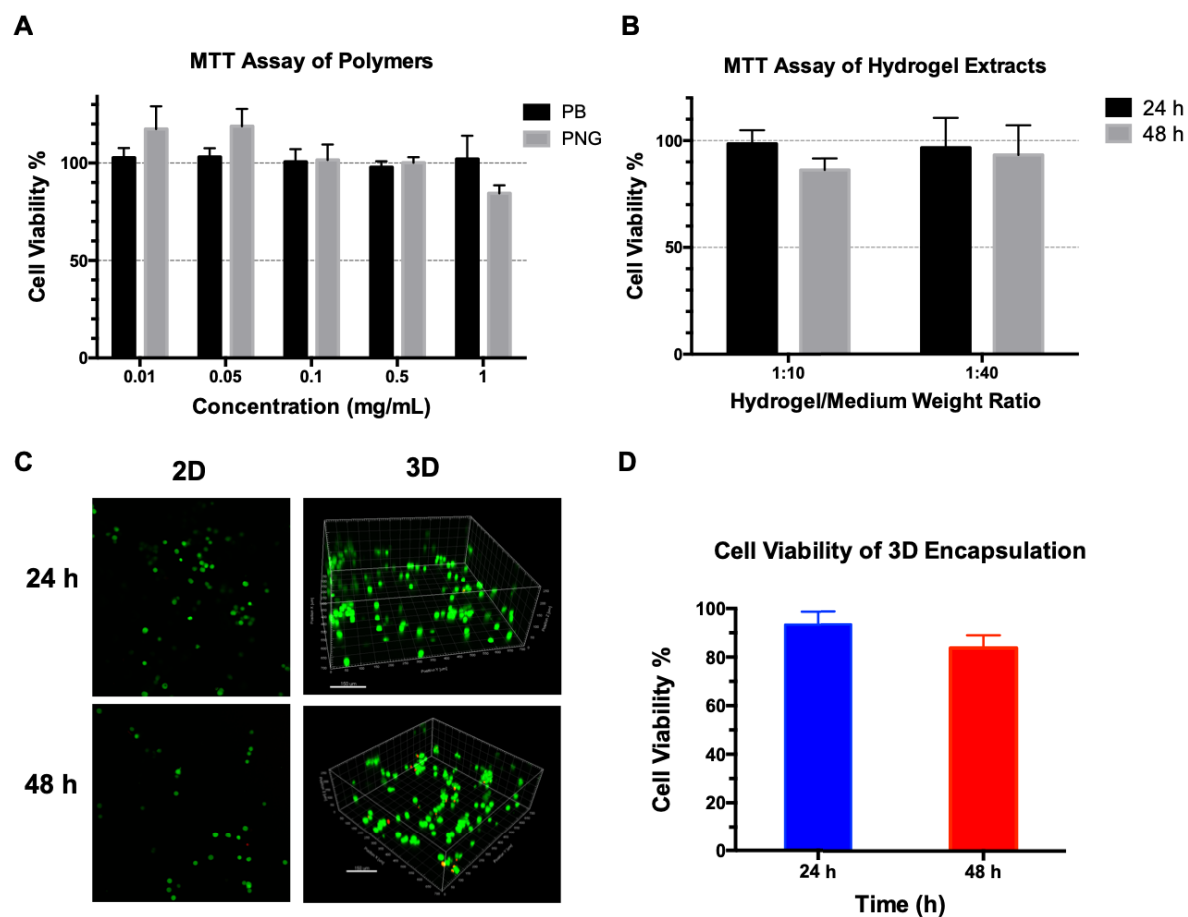


**Figure 2-29.** Cytotoxicity assays and 3D cell encapsulation images. MTT assay of (A) individual polymers (**PB** and **PNG**), and (B) hydrogel extract of **PBNG**. (C) 2D and 3D images of Live/Dead assay of HeLa cells cultured in **PBNG** (10 w/v%) for 24 and 48 h. (D) Cell viability of the encapsulated cells (measured with the confocal microscope images, n = 4).

Hydrogels are recognized as one of the most popular soft materials for extracellular matrices (ECM), due to their similarity with native tissues, such as porous network structures and high water content.<sup>34</sup> Thus, we set out to investigate the potentials of **PBNG**, the optimal hydrogel, for the spontaneous 3D cell encapsulation during the process of in situ gelation. HeLa cells were used for this experiment, and they were distributed homogeneously into the 3D hydrogel network by mixing with the two polymer precursor solutions (**PB** and **PNG**). The encapsulated cells were incubated in the hydrogel networks for 24 and 48 h under a standard cell culture environment. The cells were then stained with live/dead cell kit, and the live (green) and dead (red) cells were visualized by a confocal microscopy. As quantified in Figure 2-29D, 93% and 83% of cells were viable after 24 and 48 h, respectively. A collaborator from the Narain Group, Diana Diaz-Dussan, performed the confocal microscope imaging (both 2D and 3D images in Figure 2-29C) and cell viability analysis for 3D cell encapsulation. These results confirm the ability of the hydrogels to transport nutrients through the porous network structures and to support the cellular functions with the tissue-like ECM microenvironment.

## 2.4 Conclusions

An in situ forming and dual-cure network (DCN) hydrogel, **PBNG**, was designed based on two distinct benzoxaborolate cross-links. The combination of dynamic sugar-benzoxaborolate cross-links and rigid nopoldiol-benzoxaborolate cross-links allows the **PBNG** hydrogel to become self-healing across an exceptionally wide range of pH (8.5 to 1.5), with unusually high tolerance to acid. Furthermore, the nopoldiol-benzoxaborolate bioorthogonal click chemistry endows the desired hydrogel with many attributes, such as an ultra-fast gelation rate (<26 s), benign cross-linking chemistry (light/catalyst-free, water is the only by-product), ROS-responsive degradation, and good resistance towards low pH conditions and biological polyols. The DCN hydrogel exhibits pH-responsive swelling capabilities that contribute to its efficient pH-controlled release of small molecules, as exemplified with the anti-cancer drug doxorubicin (Dox). Moreover, the promising biomedical potential of the DCN hydrogel **PBNG** for cell therapy and tissue engineering is supported by cytotoxicity assays, as well as successful 3D encapsulation and culture of HeLa cells. As novel and unique ‘click’ partners,

**MAAmBO** and **nopoldiol** components could be incorporated easily in diverse polymeric hydrogels to achieve bioorthogonality, acid resistance, ROS-responsiveness, facilitated gelation, and enhanced mechanical properties that could fulfill specific biomedical requirements.

## 2.5 Experimental

### 2.5.1 General Information

#### 2.5.1.1 Materials

All chemical reagents were used as received from their chemical supplier unless specified otherwise. Poly(ethylene glycol) methyl ether methacrylate (**PEGMA**), sodium borohydride, potassium nitrate, methacryloyl chloride, sodium hydroxide (NaOH), (1*R*)-(-)-nopoldiol, pyridine, DMSO, potassium osmate (VI) dihydrate ( $K_2OsO_4 \cdot 2H_2O$ ), 4-methylmorpholine N-oxide (NMO), methacrylic anhydride, hydroquinone, triethylamine (TEA), ethylenediamine (EDA), lactobionic acid, trifluoroacetic acid (TFA), 4,4'-azobis(4-cyanovaleric acid) (ACVA), D-glucose, D-fructose, catechol, capecitabine, hydrogen peroxide ( $H_2O_2$ ), potassium phosphate ( $KH_2PO_4$ ), potassium phosphate dibasic ( $K_2HPO_4$ ), acetic acid, potassium chloride (KCl), sodium chloride (NaCl), thiazolyl blue tetrazolium bromide (MTT), D-gluconolactone, lactobionic acid, and all of the organic solvents were purchased from Sigma-Aldrich. 2-Formylphenylboronic acid and 3-aminophenylboronic acid were purchased from Combi-Blocks. Palladium, 10% on activated carbon, was obtained from Strem. *p*-Toluenesulfonyl chloride was purchased from Alfa Aesar. Sodium azide was purchased from Fisher Scientific. Doxorubicin hydrochloride salt was obtained from LC Laboratories<sup>®</sup>. LIVE/DEAD<sup>™</sup> Cell Imaging Kit was purchased from Thermo Fisher Scientific. All of the cell culture products, including DMEM medium, sodium pyruvate, antibiotic-antimycotic, fetal bovine serum (FBS), and trypsin with EDTA were purchased from Gibco. All of the deuterated NMR solvents, including  $D_2O$ ,  $ACN-d_3$ ,  $DMSO-d_6$ , NaOD, and DCl (in  $D_2O$  solution) were purchased from either Sigma-Aldrich or Cambridge Isotope Laboratories, Inc.

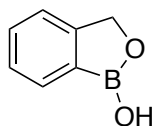
### 2.5.1.2 Characterization and instrumentation

NMR spectra were recorded on INOVA-400, INOVA-500 or INOVA-700 MHz instruments. The residual solvent protons ( $^1\text{H}$ ) of  $\text{CDCl}_3$  (7.26 ppm),  $\text{ACN-d}_3$  (1.94 ppm),  $\text{DMSO-d}_6$  (2.50 ppm), and  $\text{D}_2\text{O}$  (4.79 ppm) were used as internal standards, and the carbon signal ( $^{13}\text{C}$ ) of  $\text{CDCl}_3$  (77.06 ppm) was used as an internal standard. MestReNova software was used to analyze all of the NMR data. The following abbreviations are used in reporting NMR data: s, singlet; d, doublet; t, triplet; app t, apparent triplet; q, quartet; dd, doublet of doublets; ddd, doublet of doublet of doublets; dddd, doublet of doublet of doublet of doublets; dhept, doublet of heptlet; td, triplet of doublet; m, multiplet; comp m, complex multiplet. High-resolution mass spectra (HRMS) using electrospray ionization (ESI), MS-ESI and LC-MS mass spectra were recorded by the University of Alberta Mass Spectrometry Services Laboratory. Optical rotations were measured using a 1-mL cell with a 1-dm length on P.E. 241 polarimeter. Melting points were determined in a capillary tube using a Gallenkamp melting point apparatus and are uncorrected. The number average molecular weights ( $M_n$ ), the weight average molecular weights ( $M_w$ ), and the polydispersity index ( $\text{PDI} = M_w/M_n$ ) of all of the polymers were characterized by Viscotek conventional gel permeation chromatography (GPC) system with two WAT011545 Waters Ultrahydrogel linear columns, using 0.5 M sodium acetate/0.5 M acetic acid buffer as eluent at a flow rate of 1.0 mL/min. The GPC was calibrated by monodisperse pullulan standards ( $M_w = 5900\text{--}404,000$  g/mol). Rheological measurements, including gelation time determination, oscillatory frequency sweeps, oscillatory strain sweep, and step strain tests were measured by AR-G2 rheometer (TA Instruments) with a 20-mm 2.008° cone plate geometry at 25 °C. UV absorbance was measured by SpectraMax® i3x. Scanning electron microscope (Zeiss Sigma FESEM, NanoFAB, University of Alberta) was used to characterize freeze-dried hydrogel structures. 3D cell encapsulation was visualized by a CLSM 710 Meta confocal laser scanning microscope (Carl Zeiss, Jena, Germany). Cell viability assays of encapsulated cells were quantified by Imaris Image Analysis Software.

## 2.5.2 Chemical Synthesis and Analytical Data

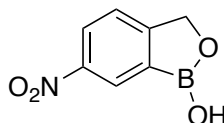
### 2.5.2.1 Synthesis of monomers

Synthesis of 5-methacrylamido-1,2-benzoxaborole (MAAmBO) (Scheme 2-2):



**1-Hydroxy-3H-2,1-benzoxaborole (2-2)**<sup>8</sup>: The title compound was synthesized according to the previous report with slight modifications.<sup>12</sup> 2-Formylphenyl boronic acid (**2-1**) (8.00 g, 53.3 mmol) was dissolved in 120 mL methanol in a single-neck round bottom flask. NaBH<sub>4</sub> (2.02 g, 53.3 mmol) was added slowly, and the reaction was stirred for 2 h. Afterwards, 1 M HCl was added in the reaction mixture to quench the base, and the solution was adjusted to pH < 6. The solvent was removed in vacuo and the residues were extracted by ethyl acetate (4 × 100 mL). The organic phases were combined, dried (MgSO<sub>4</sub>), filtered, and evaporated to give a white solid (7.05 g, 99%). All spectral data corresponded to the literature.<sup>8</sup>

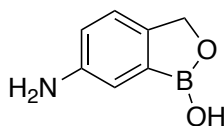
<sup>1</sup>H NMR (400 MHz, DMSO-*d*<sub>6</sub>) δ 7.72 (d, *J* = 7.3 Hz, 1H), 7.46 (td, *J* = 7.4, 1.2 Hz, 1H), 7.40 (d, *J* = 7.6 Hz, 1H), 7.33 (t, *J* = 6 Hz, 1H), 4.97 (s, 2H).



**1-Hydroxy-6-nitro-3H-2,1-benzoxaborole (2-3)**<sup>9-10</sup>: The title compound was synthesized according to the previous report with slight modifications.<sup>9-10</sup> Fuming nitric acid was prepared freshly each time. KNO<sub>3</sub> (40.0 g, 0.400 mol) and concentrated H<sub>2</sub>SO<sub>4</sub> (21.3 mL, 0.400 mol) was added in a single-neck round bottom flask. A heating mantle was used as the heating source, and a distillation apparatus (e.g., still head, condenser, and receiving flask) was connected to the flask. The distillation was performed, and yellowish fuming nitric acid liquid was collected in a cooled (0 °C) receiving flask. A cooling bath (water: methanol = 3:2 volume ratio) was prepared to obtain around -40 °C. Fresh fuming nitric acid (~ 20 mL) was transferred carefully to a pre-cooled round-bottom flask, and the flask was allowed to cool down for 3 min. 5.00 g (37.3 mmol) of starting materials (**2-2**) was added slowly into the flask

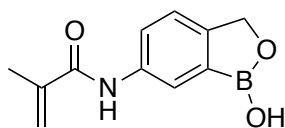
over 5 min with effective stirring. After 2 h, the reaction was quenched by adding crushed ice, and the light-yellow product crashed out. The flask was rinsed with 100 mL distilled water, and the suspension was filtered to obtain a yellow slurry. The wet product was dried under high vacuum overnight, and the product (light-yellow solid) was obtained (4.62 g, 69%). **Notes:** The product could be unreactive in the next step (hydrogenation with Pd/C) if some nitric residue remains. It is recommended to dissolve the product into EtOAc and stir it in the presence of charcoal overnight with heat (50–60 °C). Then, the charcoal was filtered out through celite and the solution was concentrated in vacuo to obtain the pure product (light-yellow solid). All spectral data corresponded to the literature.<sup>10</sup>

<sup>1</sup>H NMR (400 MHz, DMSO-*d*<sub>6</sub>) δ 8.58 (d, *J* = 2.2 Hz, 1H), 8.33 (dd, *J* = 8.4, 2.3 Hz, 1H), 7.70 (d, *J* = 8.4 Hz, 1H), 5.12 (s, 2H).



**1-Hydroxy-3H-2,1-benzoxaborol-6-amine (2-4)**<sup>10</sup>: The title compound was synthesized according to the previous report with slight modifications.<sup>10</sup> Dried starting material **2-3** (2.00 g, 11.2 mmol) was dissolved in 22.4 mL THF. The solution was degassed with nitrogen for 3 min, followed by an addition of 600 mg 5% Pd/C. The reaction mixture was bubbled continuously with hydrogen under atmospheric pressure for about 6 h, while the reaction process was monitored by <sup>1</sup>H NMR. Once the reaction reached completion, the Pd/C was filtered through celite, and the filtrate was concentrated to dryness in vacuo. Product **2-4** was obtained as a yellow solid with high purity and quantitative yield. All spectral data corresponded to the literature.<sup>10</sup>

<sup>1</sup>H NMR (400 MHz, DMSO-*d*<sub>6</sub> + 1 drop of D<sub>2</sub>O) δ 8.89 (s, 1H), 7.03 (d, *J* = 8.1 Hz, 1H), 6.88 (d, *J* = 2.2 Hz, 1H), 6.70 (dd, *J* = 8.1, 2.2 Hz, 1H), 4.96 (s, 2H).

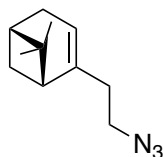


**N-(1-Hydroxy-3H-2,1-benzoxaborol-6-yl)-2-methylprop-2-enamide (MAAmBO)**<sup>11</sup>: The title compound was synthesized according to the previous report with slight modifications.<sup>11</sup>

1-hydroxy-3H-2,1-benzoxaborol-6-amine (**2-4**) (2.00 g, 13.4 mmol) was dissolved in aqueous NaOH solution (1.6 g, 40.2 mmol in 30 mL H<sub>2</sub>O). Freshly distilled methacryloyl chloride (2.61 mL, 26.8 mmol) was added dropwise through a syringe pump at a speed of 1 mL/h at 0 °C. Precipitation formed gradually during the reaction, and the reaction mixture was warmed to ambient temperature and stirred overnight. The suspension was filtered by vacuum filtration and washed with water (50 mL). The product was obtained as a yellowish solid with high purity (2.79 g, 96%). **Notes:** the product could be purified further through recrystallization with hot EtOAc and diethyl ether (pale-yellow solid). All spectral data corresponded to the literature.<sup>11</sup>

<sup>1</sup>H NMR (400 MHz, DMSO)  $\delta$  9.80 (s, 1H), 9.18 (s, 1H), 8.06 (d,  $J = 1.8$  Hz, 1H), 7.67 (dd,  $J = 8.2, 2.1$  Hz, 1H), 7.34 (dd,  $J = 8.2, 0.8$  Hz, 1H), 5.81 (t,  $J = 1.0$  Hz, 1H), 5.50 (dt,  $J = 2.5, 1.2$  Hz, 1H), 4.94 (s, 2H), 1.96 (dd,  $J = 1.6, 0.9$  Hz, 3H).

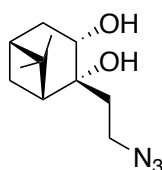
Synthesis of (1R)-(-)-nopoldiol-methacrylamide-diol (**nopoldiol**) (Scheme 2-3):



**(1R,5S)-2-(2-Azidoethyl)-6,6-dimethylbicyclo[3.1.1]hept-2-ene (2-6)**<sup>3</sup>: The title compound was synthesized according to the previous report with slight modifications.<sup>3</sup> Intermediate (1R)-(-)-nopol-tosyl was prepared from commercially available (1R)-(-)-nopol according to the method described earlier.<sup>13</sup> To a solution of (1R)-(-)-nopol (**2-5**) (6.00 g, 36.1 mol), pyridine (9 mL) and *p*-toluenesulfonyl chloride (7.90 g, 41.5 mol) were added at 0 °C. The mixture was stirred for 1 h, and the solution was kept in the fridge for 3 h. TLC was used to monitor the reaction to completion. To the reaction mixture, a solution of concentrated HCl (10 mL) and distilled water (20 mL) was added at 0 °C. The mixture was extracted with diethyl ether (3  $\times$  100 mL). The organic layer was combined and dried with K<sub>2</sub>CO<sub>3</sub> and MgSO<sub>4</sub>, and the mixture was filtered and concentrated in vacuo. The (1R)-(-)-nopol-tosyl (crude yellow oily product) was used immediately for the next step without further purification. To a solution of (1R)-(-)-nopol-tosyl (9.27 g, 28.9 mmol) in DMSO (40 mL), sodium azide (3.75 g, 57.8 mmol) was added at 0 °C under nitrogen. The reaction was carried out at 80 °C and stirred

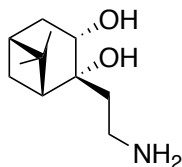
overnight. Distilled water was added, and the aqueous layer was extracted with EtOAc (3 × 100 mL). The combined organic layers were dried with Na<sub>2</sub>SO<sub>4</sub>, filtered, and concentrated in vacuo. The crude product was purified by flash chromatography (hexanes to EtOAc 95:5) to afford product **2-6** as a yellow liquid (5.3 g, 77% yield over two steps). All spectral data corresponded to the literature.<sup>3</sup>

<sup>1</sup>H NMR (400 MHz, CDCl<sub>3</sub>) δ 5.33 (m, 1H), 3.35–3.20 (m, 2H), 2.38 (dt, *J* = 8.6, 5.6 Hz, 1H), 2.33–2.15 (comp m, 4H), 2.10 (m, 1H), 2.02 (app t, *J* = 5.6, 1H), 1.28 (s, 3H), 1.17 (d, *J* = 8.6 Hz, 1H), 0.84 (s, 3H).



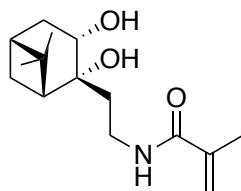
**(1R,2R,3S,5R)-2-(2-Azidoethyl)-6,6-dimethylbicyclo[3.1.1]heptane-2,3-diol (2-7)**<sup>3</sup>: The title compound was synthesized according to the published report with slight modifications.<sup>3</sup> A solution of **2-6** (1.29 g, 6.79 mmol) in acetone/water (10.5/0.774 mL) was prepared in a round bottom flask, followed by an addition of a mixture of NMO 50 wt% in H<sub>2</sub>O (1.05 g NMO, 8.83 mmol, in 1 mL H<sub>2</sub>O) and pyridine (0.660 mL, 8.15 mmol). Lastly, K<sub>2</sub>OsO<sub>4</sub>•2H<sub>2</sub>O (2 mol%, 50.0 mg, 0.136 mmol) was added. The mixture was stirred and refluxed at 65 °C for 24 h under a nitrogen balloon. Then, the reaction mixture was concentrated in vacuo and combined with 60 mL EtOAc. The organic phase was washed with HCl (1 × 60 mL, 1 N), distilled water (1 × 10 mL), and brine (1 × 10 mL), dried with MgSO<sub>4</sub>, filtered, and concentrated in vacuo. The crude residue was purified by flash chromatography (hexanes to EtOAc 4:0 to 0:1), and the product **2-7** was obtained as a yellowish oil (1.24 g, 81%). All spectral data corresponded to the literature.<sup>3</sup>

<sup>1</sup>H NMR (400 MHz, CDCl<sub>3</sub>) δ 4.09 (ddd, *J* = 9.4, 6.2, 5.4 Hz, 1H), 3.65–3.46 (m, 2H), 3.24 (s, 1H), 2.82 (d, *J* = 6.2 Hz, 1H), 2.48 (dddd, *J* = 14.0, 9.5, 3.7, 2.4 Hz, 1H), 2.25–2.16 (m, 1H), 2.06 (app t, *J* = 5.8 Hz, 1H), 1.97–1.87 (comp m, 2H), 1.76–1.61 (m, 2H), 1.39 (d, *J* = 10.4 Hz, 1H), 1.28 (s, 3H), 0.95 (s, 3H).



**(1*R*,2*R*,3*S*,5*R*)-2-(2-Aminoethyl)-6,6-dimethylbicyclo[3.1.1]heptane-2,3-diol (2-8)**<sup>4</sup>: The title compound was synthesized according to the previous report with slight modifications.<sup>4</sup> Starting material **2-7** (1.24 g, 5.51 mmol) was mixed with methanol (35 mL) in a single-neck round bottom flask. An adapter with both a vacuum and a nitrogen inlet was connected on the flask. The reaction mixture was degassed by vacuum for 1 min and then purged with nitrogen. These steps were repeated three times, followed by an addition of 10% Pd/C (62 mg) to the reaction solution. Then, the degassing and purging processes were repeated for another three times, and the nitrogen was replaced with a hydrogen balloon. After 3 h, the hydrogen was removed by vacuum. TLC was used to confirm the completion of the reaction, and the mixture was filtered through celite. The filtrate was concentrated in vacuo to obtain pure product **2-8** (light-yellow liquid) with quantitative yield. The product was used directly for the next step without further purification. All spectral data corresponded to the literature.<sup>4</sup>

<sup>1</sup>H NMR (400 MHz, CDCl<sub>3</sub>) δ 3.99 (ddd, *J* = 9.3, 5.6, 1.1 Hz, 1H), 3.12–3.03 (m, 2H), 2.48–2.38 (m, 1H), 2.22–2.11 (m, 1H), 2.07 (app t, *J* = 6.0 Hz, 1H), 1.92–1.86 (m, 1H), 1.78–1.65 (m, 3H), 1.60–1.53 (m, 1H), 1.47 (d, *J* = 10.2 Hz, 1H), 1.26 (s, 3H), 0.93 (s, 3H).



**N-(2-((1*R*,2*R*,3*S*,5*R*)-2,3-Dihydroxy-6,6-dimethylbicyclo[3.1.1]heptan-2-yl)ethyl)methacrylamide (nopoldiol)**: To a solution of compound **2-8** (0.96 g, 4.82 mmol), methanol (100 mL) and TEA (0.690 mL, 4.82 mmol), 5 mg of hydroquinone was added to prevent self-polymerization of the product. Then, methacrylic anhydride (0.785 mL, 5.30 mmol) was added dropwise through a syringe pump at a speed of 1 mL/h at 0 °C. The reaction mixture was allowed to stir at 0 °C for 3 h, then brought to ambient temperature, and stirred for another 16 h. Next, the reaction mixture was concentrated in vacuo without heating, and the crude mixture was purified by flash chromatography (hexanes to EtOAc 4:1 to 0:1). The

fractions were combined and concentrated to about 3 mL in vacuo at 0 °C, followed by an addition of diethyl ether (2 mL). The open-neck flask was put in the fridge at 4 °C for crystallization. Pale-white crystals (product) formed after 2–48 h, depending on the purity of the collected fractions. The flask was rinsed with cold diethyl ether, and the crystals were collected. The filtrate was concentrated and crystallized again using the same method, and 0.70 g (54%) product (**nopoldiol**) was obtained in total.

m.p. = 89.7–91.0 °C

$R_f$  = 0.25 (hexanes to EtOAc 1:1)

$[\alpha]_D^{20}$ : – 9.2 (*c* 1.052, CHCl<sub>3</sub>)

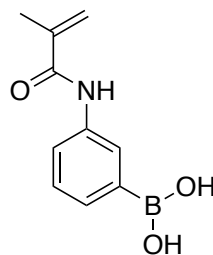
<sup>1</sup>H NMR (498 MHz, CDCl<sub>3</sub>) δ 6.66 (br s, 1H), 5.71 (s, 1H), 5.36–5.28 (s, 1H), 4.08 (dt, *J* = 10.1, 5.4 Hz, 1H), 3.68–3.57 (m, 1H), 3.53 (s, 1H), 3.43 (ddd, *J* = 19.0, 8.4, 4.7 Hz, 1H), 3.20 (d, *J* = 5.8 Hz, 1H), 2.50 (app t, *J* = 11.7 Hz, 1H), 2.23–2.19 (m, 1H), 2.09 (t, *J* = 5.8 Hz, 1H), 1.95 (s, 3H), 1.94–1.83 (m, 2H), 1.76–1.63 (m, 2H), 1.52–1.50 (m, 1H), 1.37 (d, *J* = 10.5 Hz, 1H), 1.27 (s, 3H), 0.92 (s, 3H).

<sup>13</sup>C NMR (126 MHz, CDCl<sub>3</sub>) δ 168.6, 139.7, 119.8, 75.6, 67.7, 52.2, 40.8, 40.5, 38.8, 38.1, 35.4, 27.8, 27.6, 24.3, 18.5.

IR (cast film, cm<sup>-1</sup>): 3350, 2977, 2923, 2869, 1656, 1612, 1534, 1012.

HRMS (ESI) for C<sub>15</sub>H<sub>25</sub>NO<sub>3</sub>: calcd: 267.1834; found: 267.1835.

#### Synthesis of 3-methacrylamido phenylboronic acid (MAPBA):

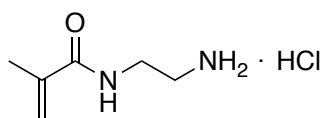


**[3-(2-Methylprop-2-enoylamino)phenyl]boronic acid (MAPBA)**<sup>35</sup>: The title compound was synthesized according to the previous report with slight modifications.<sup>35</sup> Aminophenylboronic acid (0.50 g, 3.65 mmol) was dissolved first in a solution of NaOH (0.438 g, 10.9 mmol NaOH, in 7.5 mL H<sub>2</sub>O). Methacryloyl chloride (0.73 mL, 7.3 mmol) was added dropwise to the reaction mixture through a syringe pump (1 mL/h) at 0 °C. The reaction

was stirred at 0 °C to room temperature overnight, and precipitation formed gradually during the reaction. The reaction suspension was filtered, and the product (**MAPBA**) was washed with cold diethyl ether and dried with high vacuum overnight. The product was obtained as a yellowish solid (0.52 g, 70%). All spectral data corresponded to the literature.<sup>35</sup>

<sup>1</sup>H NMR (498 MHz, DMSO-*d*<sub>6</sub>) δ 9.71 (s, 1H), 7.90 (s, 1H), 7.70 (d, *J* = 8.0 Hz, 1H), 7.48 (d, *J* = 7.3 Hz, 1H), 7.27 (t, *J* = 7.7 Hz, 1H), 5.78 (s, 1H), 5.48 (s, 1H), 1.93 (s, 3H).

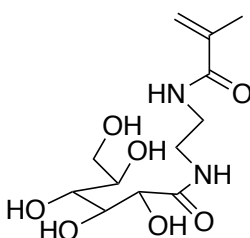
Synthesis of 2-aminoethyl methacrylamide hydrochloride (**AEMA**) (**2-10**) (Scheme 2-4):



**N-(2-Aminoethyl)-2-methylprop-2-enamide;hydrochloride (AEMA)<sup>14</sup>:** The title compound was synthesized according to the modified procedure from the previous report with slight modifications.<sup>14</sup> Ethylenediamine (EDA) (**2-9**) (10.0 g, 0.167 mol) was mixed with 85 mL isopropanol, followed by a dropwise addition of concentrated HCl (31 mL, 0.370 mol) at 0 °C. The suspension was filtered and washed with acetone to yield 20.0 g of ethylenediamine dihydrochloride (EDA · 2HCl) intermediate as a white solid in 91% yield. To a solution (**A**) of EDA · 2HCl (5.00 g, 38.0 mmol) and distilled water (25 mL), EDA (2.5 mL, 38.0 mmol) was added, and the reaction mixture was stirred for 30 min at room temperature. Then, the reaction was cooled to 0 °C and allowed to stabilize for 30 min. A small amount of hydroquinone (5 mg) was dissolved in a solution (**B**) of methanol (10 mL) and methacrylic anhydride (14 mL, 94.0 mmol). Solution **B** was added dropwise to solution **A** at a speed of 1–2 drop per second at 0 °C. After the addition, the reaction was warmed up to ambient temperature and stirred overnight. Then, the reaction mixture was cooled down to 0 °C, and concentrated HCl (7 mL) was added dropwise to the solution at 0 °C. After 30 min stirring, the reaction solution was concentrated in vacuo at 50 °C to obtain an oily crude mixture as a yellowish slurry. The crude was washed vigorously with acetone (6 × 200 mL) until a light-yellow, non-sticky precipitation formed. The suspension was filtered and dried to obtain a crude solid. Sequentially, the crude solid was dissolved into 200 mL isopropanol (containing 5.00 mg of hydroquinone), then heated up to 70 °C, and stirred for 20 min. The product

(AEMA) (2-10) was extracted by hot isopropanol, and the white residue (unreacted EDA · 2HCl) was filtered off. The filtrate was concentrated to about 50 mL in vacuo and put in the fridge (4 °C) for crystallization. Light-yellow crystals were formed and then collected by vacuum filtration after 24 h (5.93 g, 48%). All spectral data corresponded to the literature.<sup>14</sup> <sup>1</sup>H NMR (700 MHz, D<sub>2</sub>O) δ 5.81 (s, 1H), 5.55 (s, 1H), 3.62 (t, *J* = 6.0 Hz, 2H), 3.22 (t, *J* = 5.9 Hz, 1H), 1.98 (s, 1H).

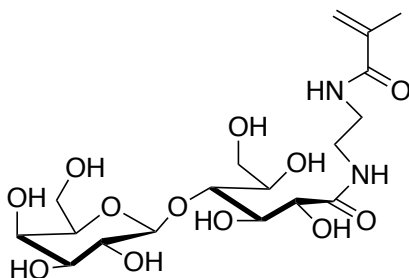
Synthesis of 2-gluconamidoethyl methacrylamide (GAEMA) (Scheme 2-4)<sup>15</sup>:



**2,3,4,5,6-Pentahydroxy-N-(2-methacrylamidoethyl)hexanamide (GAEMA)<sup>15</sup>:** The title compound was synthesized according to the previous report with slight modifications.<sup>15</sup> 2-Gluconolactone (8.00 g, 44.9 mmol) was dissolved first in methanol (300 mL). A solution of AEMA (2-10) (10.0 g, 60.8 mmol) and TEA (10.2 mL, 73.2 mmol) were added to it, and the reaction mixture was stirred overnight at room temperature. The precipitate formed gradually, and the crude product was filtered out and washed with isopropanol (3 × 100 mL) and acetone (3 × 100 mL) to give the white solid product GAEMA (11.0 g, 80%). All spectral data corresponded to the literature.<sup>15</sup>

<sup>1</sup>H NMR (500 MHz, D<sub>2</sub>O) δ 5.72 (s, 1H), 5.48 (s, 1H), 4.32 (d, *J* = 3.5 Hz, 1H), 4.10 (app t, *J* = 2.9 Hz, 1H), 3.84 (d, *J* = 12.7 Hz, 1H), 3.77 (d, *J* = 3.1 Hz, 2H), 3.71–3.64 (m, 1H), 3.52–3.39 (comp m, 4H), 1.94 (s, 3H).

Synthesis of 2-lactobionaidoethyl methacrylamide (LAEMA) (Scheme 2-4)<sup>16</sup>:



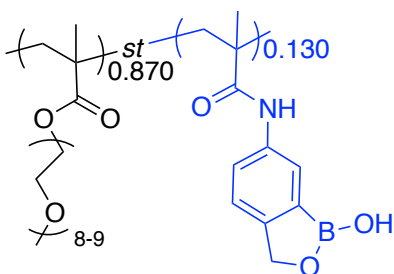
**2,3,5,6-Tetrahydroxy-N-(2-methacrylamidoethyl)-4-(((2S,3R,4S,5R,6R)-3,4,5-trihydroxy-6-(hydroxymethyl)tetrahydro-2H-pyran-2-yl)oxy)hexanamide:**

The title compound was synthesized according to the previous report, with slight modifications.<sup>16</sup> Firstly, commercially available lactobionic acid (5.08 g, 14.2 mmol) was spread to the wall of a 250-mL round bottom flask. Methanol (125 mL) was added to the flask, followed by vigorous shaking to prevent aggregation of sugar. TFA (~5 mL) was added to the solution, and the reaction was stirred at 60 °C overnight. Then, the methanol was removed completely in vacuo until the lactobionolactone crude turned foamy and a crispy white solid was observed. Another 50 mL of methanol was added to dissolve the white solid completely with vigorous shaking, followed by an addition of 2 mL TFA and solvent evaporation as described before. The processes of adding methanol, TFA, and then solvent evaporation were repeated three times to ensure the complete conversion of lactobionic acid to lactobionolactone. Afterwards, the freshly prepared and completely dried lactobionolactone (5.00 g, 14.2 mmol) was dissolved in distilled water (5 mL) in 50 wt%. **AEMA (2-10)** (3.00 g, 17.0 mmol) and TEA (2.66 mL, 18.4 mmol) were mixed in the reaction solution. The reaction mixture was stirred in darkness at room temperature for 1 to 5 days until a white precipitation formed. The suspension was filtered, and the solid was washed with acetone (2 × 100 mL) to obtain a pale white product **LAEMA** in high purity (3.65 g, 55%). All spectral data corresponded to the literature.<sup>16</sup>

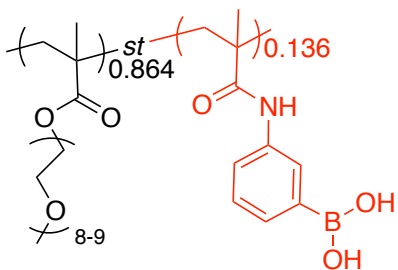
<sup>1</sup>H NMR (498 MHz, D<sub>2</sub>O) δ 5.73 (s, 1H), 5.49 (s, 1H), 4.59 (d, *J* = 7.8 Hz, 1H), 4.43 (d, *J* = 2.6 Hz, 1H), 4.22 (dd, *J* = 4.1, 2.7 Hz, 1H), 4.04–3.42 (comp m, 15H), 1.96 (s, 3H).

### 2.5.2.2 Synthesis of polymers

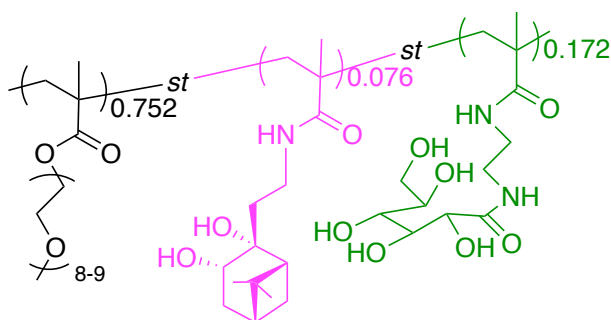
General procedures for polymerizations (Scheme 2-6): Various statistical polymers with different ratios of components were synthesized via free radical polymerization. Briefly, monomers were dissolved in a solution of methanol/H<sub>2</sub>O in a 25-mL reaction tube or a suitable round bottom flask. A solution of ACVA (initiator, 0.005 mol%) was dissolved in 1 mL of methanol and added to the reaction mixture to target the degree of polymerization (DP) of 200. Then, the reaction vessel was sealed with a septum, and the neck was wrapped carefully with Parafilm, followed by degassing for 45 min with nitrogen. The reaction was carried out at 70 °C with constant stirring for 16 h, and then quenched in a dry-ice/acetone bath. The crude polymer solution was dialysed using Fisherbrand® dialysis tubing (MWCO 6,000–8,000) for 1 to 2 days, and the purified polymer solution was lyophilized for 2 days to yield pure polymers. **Notes:** For polymers, the integrated signals were used to calculate the composition. The numbers outside the brackets stand for the molar ratios of each component in the polymers, and the numbers are totaled as 1.



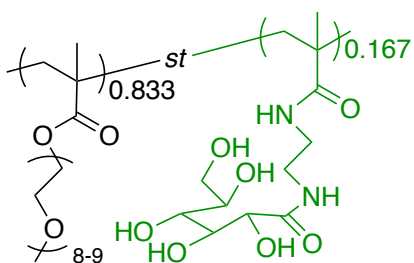
**Poly(PEGMA-*st*-MAAmBO) (PB):** Prepared from **PEGMA** (2.83 g, 5.66 mmol), **MAAmBO** (0.217 g, 1.00 mmol) and ACVA (9.30 mg, 0.0332 mmol) in a solvent of methanol (10 mL) and H<sub>2</sub>O (2 mL). 2.80 g polymer **PB'** was obtained as a yellowish sticky paste (92%).



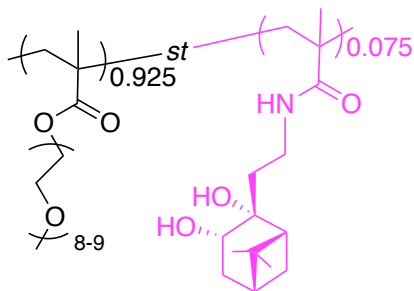
**Poly(PEGMA-*st*-MAPBA) (PB')**: Prepared from **PEGMA** (1.00 g, 2.00 mmol), **MAPBA** (72.3 mg, 0.353 mmol) and **ACVA** (3.29 mg, 0.0118 mmol) in a solvent of methanol (3.5 mL) and H<sub>2</sub>O (0.7 mL). 1.00 g polymer **PB'** was obtained as a yellowish sticky paste (93%).



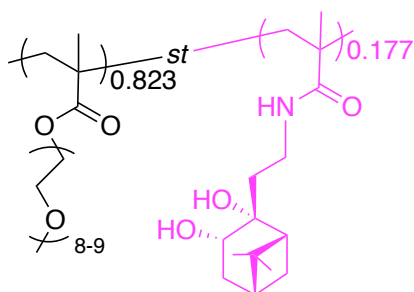
**Poly(PEGMA-*st*-nopoldiol-*st*-GAEMA) (PNG)**: Prepared from **PEGMA** (1.96 g, 3.93 mmol), **nopoldiol** (0.150 g, 0.562 mmol), **GAEMA** (0.344 g, 1.12 mmol) and **ACVA** (7.86 mg, 0.0281 mmol) in a solvent of methanol (18 mL) and H<sub>2</sub>O (18 mL). 2.20 g polymer **PNG** was obtained as a white sticky paste (88%).



**Poly(PEGMA-*st*-GAEMA) (PG)**: Prepared from **PEGMA** (0.653 g, 1.31 mmol), **GAEMA** (0.1 g, 0.325 mmol) and **ACVA** (2.24 mg, 0.00800 mmol) in a solvent of methanol (5 mL) and H<sub>2</sub>O (5 mL). 0.611 g polymer **PG** was obtained as a white sticky paste (81%).



**Poly(PEGMA-*st*-nopoldiol) (PN):** Prepared from **PEGMA** (0.420 g, 0.840 mmol), **nopoldiol** (25 mg, 0.0936 mmol) and **ACVA** (1.31 mg, 0.00468 mmol) in a solvent of methanol (4 mL) and H<sub>2</sub>O (4 mL). 0.39 g polymer **PN** was obtained as a white sticky paste (89%).



**Poly(PEGMA-*st*-nopoldiol) (PN'):** Prepared from **PEGMA** (0.653 g, 1.31 mmol), **nopoldiol** (86.7 mg, 0.325 mmol) and **ACVA** (2.26 mg, 0.00807 mmol) in a solvent of methanol (5 mL) and H<sub>2</sub>O (5 mL). 0.63 g polymer **PN'** was obtained as a white sticky paste (85%).

### 2.5.3 Fabrication of Hydrogels

Prior to hydrogel formation, **polymer 1** and **polymer 2** (Table 2-6) were dissolved in pH 7.4 PBS buffer at 10 wt/v% concentration. Then, equal volumes of these two polymer solutions were mixed in a microcentrifuge tube or a glass vial, followed by a gentle swirling or vortex. The hydrogels were formed quickly between a few seconds to 9 min, depending on the hydrogel type.

### 2.5.4 Monomeric Binding Studies via NMR

#### 2.5.4.1 NMR studies

The binding study of monomer **MAAmBO** and diols was investigated by <sup>1</sup>H NMR and <sup>11</sup>B NMR in 0.05 M D<sub>2</sub>O potassium phosphate buffer:ACN-*d*<sub>3</sub> (65:35 w%). Prior to mixing with

ACN-*d*<sub>3</sub>, the pD values (read directly from pH meter) of the D<sub>2</sub>O potassium phosphate buffer were adjusted to 8.1, 7.0, 4.8, and 1.1 by adding DCl and NaOD, which were equal to the desired pH values of 8.5, 7.4, 5.2, and 1.5 according to the equation:

$$\text{pD} = \text{pH meter reading} + 0.40 \quad (2)$$

where the ‘pH meter reading’ was obtained with an apparatus standardized to read pH in H<sub>2</sub>O solution.<sup>36</sup> The prepared NMR solvent with the same pH value was used to dissolve **MAAmBO** and a diol compound to investigate their benzoxaborolate formation at a preset pH condition. For example, 20 mM of **MAAmBO** and **nopoldiol** were prepared independently in the abovementioned NMR solvent (pH 7.4) and mixed in an NMR tube with a 1:1 volume ratio to obtain a mixture of 10 mM of each compound. The NMR tube was shaken, and the NMR spectra were obtained 5–7 h after mixing to ensure that the equilibrium was obtained.

**Table 2-11.** Calculation method of conversion% to benzoxaborolate.

<b>Diols</b>	<b>Calculation of conversion% to benzoxaborolate</b>	<b>NMR spectra page No.</b>
<b>nopoldiol</b>	$\frac{\text{integration of -CH}_2\text{- (4.58–4.69 ppm)}}{\text{integration of -CH}_2\text{- (4.92–4.98 ppm) + integration of -CH}_2\text{- (4.58–4.69 ppm)}} \times 100$	159–162
<b>nopoldiol<sup>a</sup></b>	$\frac{\text{integration of Ar-H (7.80 ~ 7.82 ppm)}}{\text{integration of Ar-H (7.80 ~ 7.82 ppm) + integration of Ar-H (7.73 ~ 7.75 ppm)}} \times 100$	162–165
<b>LAEMA<sup>b</sup></b>	$\frac{\frac{\text{integration of Ar-H (7.07–7.81 ppm)}}{3} - \frac{\text{integration of -CH}_2\text{- (4.93–4.97 ppm)}}{2}}{\frac{\text{integration of Ar-H (7.07–7.81 ppm)}}{3}} \times 100$	165–167

<b>GAEMA</b>	$\frac{\text{integration of -CH}_2\text{- (4.61-4.65 ppm)}}{\text{integration of -CH}_2\text{- (4.94-4.97 ppm)+integration of -CH}_2\text{- (4.61-4.65 ppm)}} \times 100$	168–170
<b>D-glucose</b>	$\frac{\text{integration of -CH}_2\text{- (4.59 ppm)}}{\text{integration of -CH}_2\text{- (4.90-4.97 ppm)+integration of -CH}_2\text{- (4.59 ppm)}} \times 100$	170–172
<b>D-fructose</b>	$\frac{\text{integration of -CH}_2\text{- (4.60-4.64 ppm)}}{\text{integration of -CH}_2\text{- (4.92-4.97 ppm)+integration of -CH}_2\text{- (4.60-4.64 ppm)}} \times 100$	173–175
<b>catechol</b>	$\frac{\text{integration of -CH}_2\text{- (4.75 ppm)}}{\text{integration of -CH}_2\text{- (4.92-4.97 ppm)+integration of -CH}_2\text{- (4.75 ppm)}} \times 100$	175–177
<b>capecitabine</b>	$\frac{\text{integration of -CH}_2\text{- (4.62 ppm)}}{\text{integration of -CH}_2\text{- (4.92-4.97 ppm)+integration of -CH}_2\text{- (4.62 ppm)}} \times 100$	178–180

<sup>a</sup>Calculation of conversion to nopoldiol-boronate from 3-methylacrylamido phenylboronic acid (**MAPBA**) and **nopoldiol**, where **Ar-H** stands for one proton on the aromatic ring of **MAPBA**, and **Ar-H** stands for one proton on the newly formed nopoldiol-boronate aromatic ring. <sup>b</sup>Due to the unclear signals of the benzoxaborolate **-CH<sub>2</sub>-**, the calculation method was changed as shown.

#### 2.5.4.2 ESI-MS studies

ESI-MS tests were carried out to confirm the formation of nopoldiol-benzoxaborolate at pH 7.4 and 1.5 (Figure 2-11). **Nopoldiol** and **MAAmBO** were dissolved and mixed in pH 7.4 or pH 1.5 buffer in a concentration of 10 mM (each compound), and the solutions were allowed to stabilize for 10 min before dilution. Then, acetonitrile was used to dilute the stock solution to reach a final concentration of 0.1 mM (each compound). The solutions were subjected for ESI-MS tests immediately after preparation. The nopoldiol-benzoxaborolate peaks with mass of 465.2 *m/z* were captured in the negative mode in both cases, indicating the success formation of the benzoxaborolate. **Notes:** To detect the signal of the neutral nopoldiol-benzoxaborolate **2** under negative mode, the molecule may lose a proton of a hydroxyl group to show a signal of  $[M - H]^-$  at 465.2 *m/z*.

## 2.5.5 Rheological Measurements of Hydrogels

All of the rheological measurements, including gelation time determination, oscillatory frequency sweeps, oscillatory strain sweeps, and step-strain tests were measured by AR-G2 rheometer (TA Instruments) with a 20-mm 2.008° cone plate geometry at 25 °C.<sup>37</sup>

### 2.5.5.1 Gelation time determination

The procedure for gelation time measurements was performed as described in the previous report.<sup>38</sup> Briefly, the complementary two polymers (**polymer 1** and **polymer 2** described in Table 2-6) were dissolved in PBS 7.4 buffer in 10 w/v% concentration. Then, 0.2 mL of **polymer 1** solution was spread onto the parallel plates of the rheometer, followed by the uniform addition of 0.2 mL of **polymer 2** solution to the surface of **polymer 1** solution. The modulus change was monitored at a constant frequency of 1 Hz and a strain of 1.0%, and the gelation time was defined as the time that the storage modulus ( $G'$ ) surpasses the storage modulus ( $G''$ ).

### 2.5.5.2 Dynamic oscillatory frequency sweeps

To compare the mechanical properties, oscillatory frequency sweeps of SN and DCN hydrogels that formed at pH 7.4 were tested from 0.1 rad/s to 100 rad/s with a constant strain of 1%. Furthermore, DCN hydrogels that formed at pH 7.4 to 1.5 were tested using the same methods. Samples were prepared according to the description in Section 2.5.3 by using pH buffers, and samples were allowed to stabilize for 18 h under ambient temperature before testing.

### 2.5.5.3 Oscillatory strain sweeps and step-strain tests

To investigate the self-healing properties of the DCN hydrogels, **PBNG** at pH values from 8.5 to 1.5, 10 w/v% hydrogel **PBNG** were prepared according to the description in Section 2.5.3 and allowed to stabilize for 18 h at room temperature. Then, the gels were immersed completely in pH buffers (pH 8.5, 7.4, 5.2, and 1.5) for 24 h. Oscillatory strain amplitude sweeps from 0.1% to 1000% at a constant frequency (1 Hz) were tested to determine the critical strain of gel failure. Afterwards, step strain tests were carried out by applying a large strain (a strain higher than the critical strain) and a small strain (1%) cyclically to the gel; the

gel networks were disrupted under the large strain for ~60 s and recovered under the small strain (1%) for another ~60 s. The processes were repeated for two cycles under the same conditions. (Note: 10 w/v% **PBN** was used for testing the self-healing property without the immersion process.)

## 2.5.6 Stability Studies of Hydrogels

**General Methods:** To evaluate the stability/degradation behavior of hydrogels, 10 w/v% of hydrogels were prepared as described in Section 2.5.3. The hydrogels were prepared in microcentrifuge tubes and allowed to incubate for 16 h at 37 °C to achieve complete cross-linking. Then, the hydrogels were weighed, followed by an addition of 1 mL of either H<sub>2</sub>O<sub>2</sub>, polyol solutions (mixture of 30 mM glucose and 15 mM fructose) or pH buffers on top of the gels. The solutions were refreshed every three days, and the stability/degradation of the hydrogels was monitored by measuring the weight remaining after a preset interval, according to the equation:

$$\text{Weight remaining}\% = \frac{W_t}{W_i} \times 100 \quad (3)$$

where  $W_t$  refers to the final weight and  $W_i$  represent initial weight. Three samples were tested for each test.

### 2.5.6.1 Monomeric ROS-responsive degradation studies via NMR

Benzoxaborole **2-2** and **nopoldiol** were dissolved separately in the abovementioned NMR solvent of D<sub>2</sub>O potassium phosphate buffer (pH 7.4):ACN-*d*<sub>3</sub> (65:35 w%) to obtain the stock solutions with a concentration of 20 mM. Then, 0.2 mL of each solution and 0.4 mL of NMR solvent were mixed in the NMR tubes to reach the final concentration of 5 mM (each compound), and the NMR tubes were allowed to sit for 10 min. Sequentially, 8 μL of 0, 100, 500, and 1000 mM H<sub>2</sub>O<sub>2</sub> solutions were added to the NMR tubes to obtain the compound mixtures with 0, 1, 5, and 10 mM of H<sub>2</sub>O<sub>2</sub>, respectively. <sup>1</sup>H NMR was used to monitor the oxidation/degradation process after 20 and 45 min (Scheme 2-7, Figure 2-23, and Figure 2-24). The conversion% to benzoxaborolate **2-16** was calculated according to the equation:

$$\text{Conversion\% to benzoxaborole } \mathbf{2-16} = \frac{\text{integration of } \mathbf{d} (\sim 5.50 \text{ ppm})}{\text{integration of peak } \mathbf{b+d+e} (5.60\text{--}5.50 \text{ ppm})} \times 100 \quad (4)$$

where the calculations are based on monitoring the more deshielded proton on the terminal alkene. Detailed spectra are shown on page 181–185.

### 2.5.6.2 Stability study of nopoldiol-benzoxaborolate against polyols via NMR

A solution of 10 mM of **MAAmBO** and **nopoldiol** in D<sub>2</sub>O potassium phosphate buffer/ACN-*d*<sub>3</sub> (65:35 wt%) was prepared as described in the previous monomeric binding NMR study. The mixtures were mixed immediately with either D-glucose or D-fructose to obtain a final concentration of 15 mM or 30 mM, respectively. The **MAAmBO/nopoldiol/D-glucose** and **MAAmBO/nopoldiol/D-fructose** solutions were incubated for 16 h before NMR analysis. The previous calculation method (Table 2-11) was not applicable for this study as the rest of the free **MAAmBO** would bind with sugars and effect the integration of **-CH<sub>2</sub>-**; the conversion to benzoxaborolate for this study was calculated according to the equation:

$$\text{Conversion\% to nopoldiol-benzoxaborolate for polyols competition study} = \frac{\text{integration of signal at } 5.21\text{--}5.22 \text{ ppm}}{\text{integration of signal at } 5.33 \text{ ppm} + \text{integration of signal at } 5.21\text{--}5.22 \text{ ppm}} \times 100 \quad (5)$$

where the 5.33 ppm and 5.21–5.22 ppm peaks represent one proton on the free **nopoldiol** (terminal alkene) and one proton on the nopoldiol-benzoxaborolate (terminal alkene on **nopoldiol** side), respectively.

### 2.5.7 pH-Responsive drug release

The pH-responsive drug releasing of Dox-loaded hydrogel **PBNG** was carried out using the following method. Polymer **PNG** was dissolved with PBS 7.4 at a concentration of 10 wt/v%, and 0.45 mg Dox was dissolved in 150 μL of distilled water. Then, 15 mg of polymer **PB** was dispersed in the Dox solution to obtain a solution of 10 wt/v% **PB** with 3 mg/mL of Dox. The **PB/Dox** solution was mixed with 150 μL of prepared 10 wt/v% **PNG** polymer solution in a microcentrifuge tube, followed by gentle stirring to form Dox-load **PBNG** (0.45 mg Dox/gel).

The gelation occurred quickly, within seconds, and the hydrogels were allowed to stabilize for 18 h under ambient temperature. Afterwards, the hydrogels were transferred carefully to dialysis tubes (MWCO 6,000–8,000) and sealed with cotton thread to avoid the impact of leached polymers on absorption. Encapsulation efficiency was considered 100% because of the homogenous and fast encapsulation process. Then, 10 mL of buffer solutions with pH values of 7.4, 5.2, and 1.5 were added in 25 mL vials, and the hydrogels were immersed in the solutions completely. The vials were incubated in a thermostatic shaker (37 °C, 120 rpm) to mimic the body conditions. 1 mL of releasing media were withdrawn at certain time intervals, followed by additions of 1 mL fresh buffer solutions. 100 μL of releasing media were added to a standard 96-well plate, and the release rate of Dox was monitored by UV absorbance testing at 485 nm. 0.045 mg/mL (0.0776 mM) of Dox was normalized as 100% of cumulative release, and a calibration curve was prepared accordingly (Figure 2-30). Three hydrogels for each pH condition were tested independently.

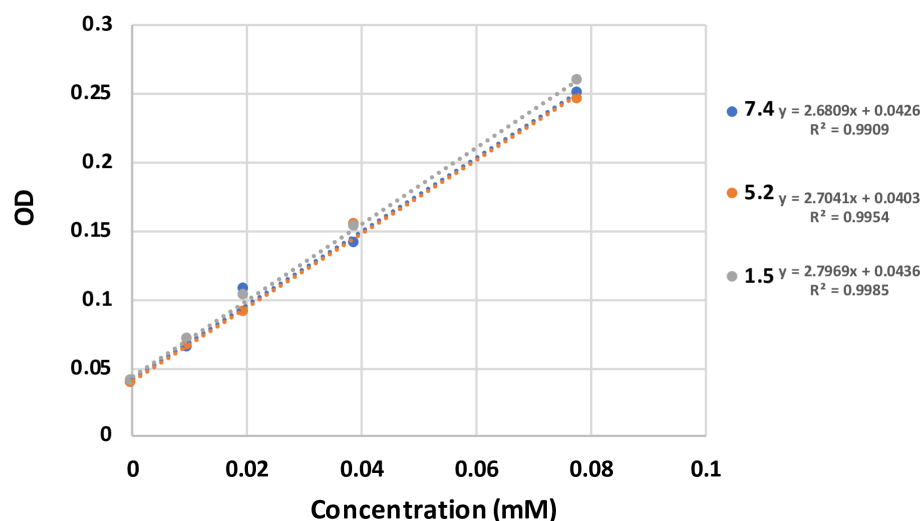


**Figure 2-30.** Calibration curve of Dox at pH 7.4, 5.2, and 1.5.

### 2.5.8 Cytotoxicity Tests of Polymers and Hydrogels

**Polymers:** Standard MTT assays were conducted to evaluate the toxicity of polymer **PB** and **PNG**. Briefly, HeLa cells were seeded in 96-well microplates with a cell density  $1 \times 10^4$  cells per well in 100 μL of high glucose DMEM culture media (including 10% FBS, 1% penicillin/streptomycin and 1% sodium pyruvate). After 24 h of incubation at 37 °C with a

balanced air humidity and 5% CO<sub>2</sub>, the culture medium was replaced with 200 μL of polymer solution with the desired concentration, and all of the polymer solutions were sterilized by filtering through 0.22-μm filter tips. The cells were incubated for another 24 h, followed by the addition of MTT solution (20 μL, 5 mg/mL). After 4 h of incubation, the culture media were aspirated, and 100 μL of DMSO/isopropanol (1:1 volume ratio) solution was used to dissolve the crystal formazan. Absorbance at 570 nm was measured by UV-vis, and the O.D. values, that are proportional to the numbers of living cells, were converted to cell viabilities.

**Hydrogel extracts:** This test was performed according to the previous report, with slight changes.<sup>23</sup> Polymer **PB** and **PNG** were dissolved in DMEM cell culture media in 10 wt/v%. The polymer solutions were sterilized by filtering through 0.22-μm filter tips. Then, 0.5 mL of each solution were mixed in a vial to form a hydrogel. The gelation occurred quickly, in seconds, and the hydrogel was allowed to stabilize for 2 h. Afterwards, the hydrogel was cut into two pieces, and the weights were measured. DMEM of 10- and 40-times hydrogel weights were added to a 6-well cell culture plate, and the hydrogels were immersed in the media and incubated for 24 h and 48 h, respectively. The hydrogel extracts were withdrawn and utilized to culture HeLa cells according to the same protocol described earlier.

### 2.5.9 3D Cell Encapsulation

This experiment was carried out according to the reported methods with slight changes.<sup>23</sup> HeLa cells were chosen as an example of 3D cell encapsulation, and the optimal DCN hydrogel **PBNG** was used for this application. Firstly, **PB** and **PNG** were dissolved in DMEM with a concentration of 10 wt/v% and sterilized by filtering through 0.22-μm filter tips. Then, the desired number of cells were taken and centrifuged to the bottom of a centrifuge tube; the final cell density in the formed hydrogels was  $2.5 \times 10^6$  cell/mL. **PB** polymer solution was added to the centrifuge tube and gently pipetted to mix with the cells. Afterwards, the same volume of **PB**/cells suspension and **PNG** solution were mixed on the surface of 35-mm glass bottom dishes. The gelation occurred rapidly, and the cells were encapsulated homogeneously inside the hydrogel network. After 10 min of incubation, 2 mL of DMEM were added to the dishes, and the cells were incubated for 24 h and 48 h. Before the cell imaging, the DMEM were withdrawn, and the hydrogels were washed twice with sterilized PBS solution. A solution of LIVE/DEAD<sup>TM</sup> Cell Imaging Kit was added to the dishes, and the cells were

incubated for 15 min for cell staining. CLSM 710 Meta confocal laser scanning microscope (Carl Zeiss, Jena, Germany) was used to visualize the cells, and the live/dead controls were shown in Figure 2-31. Cell viability of encapsulated cells were quantified by Imaris Image Analysis Software (n = 4).

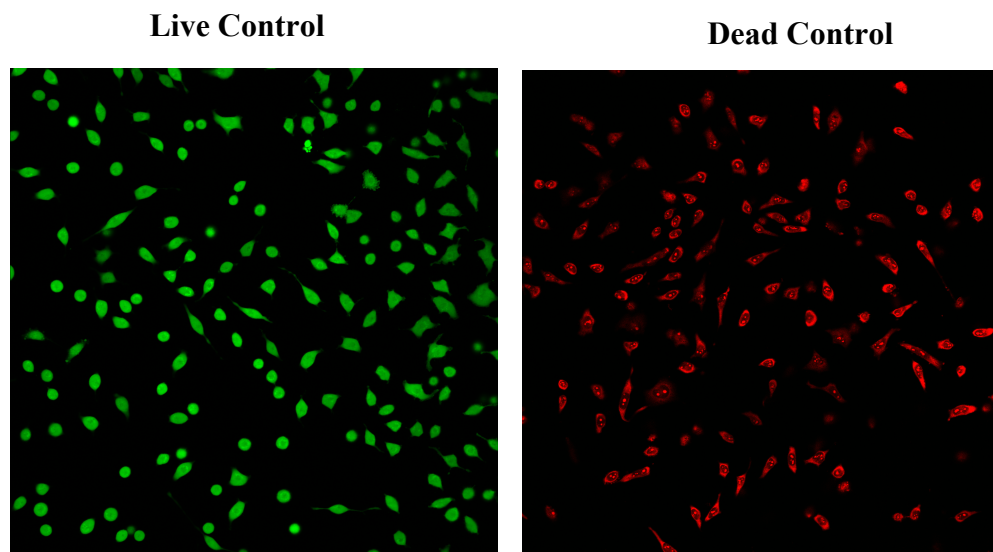


**Figure 2-31.** Live and dead control images of HeLa cells cultured on cell culture plate.

## References

- (1) Toh, W. S.; Loh, X. J., *Mater. Sci. Eng. C* **2014**, *45*, 690–697.
- (2) Wang, W.; Narain, R.; Zeng, H., *Front Chem* **2018**, *6*, 497.
- (3) Akgun, B.; Hall, D. G., *Angew. Chem. Int. Ed.* **2016**, *55*, 3909–3913.
- (4) Akgun, B.; Li, C.; Hao, Y.; Lambkin, G.; Derda, R.; Hall, D. G., *J. Am. Chem. Soc.* **2017**, *139*, 14285–14291.
- (5) Yang, Y.; Ding, X.; Urban, M. W., *Prog. Polym. Sci.* **2015**, *49–50*, 34–59.
- (6) Rizwan, M.; Yahya, R.; Hassan, A.; Yar, M.; Azzahari, A.; Selvanathan, V.; Sonsudin, F.; Abouloula, C., *Polymers* **2017**, *9*, 137.
- (7) Schmaljohann, D., *Adv. Drug Deliv. Rev* **2006**, *58*, 1655–1670.
- (8) Kunihiro, K.; Dumais, L.; Lafitte, G.; Varvier, E.; Tomas, L.; Harris, C. S., *Adv. Synth. Catal.* **2018**, *360*, 2757–2761.
- (9) Fu, Z.; He, J.; Tong, A.; Xie, Y.; Wei, Y., *Synthesis* **2013**, *45*, 2843–2852.
- (10) Samaniego Lopez, C.; Hebe Martínez, J.; Uhrig, M. L.; Coluccio Leskow, F.; Spagnuolo, C. C., *Chem. Eur. J* **2018**, *24*, 6344–6348.
- (11) Schumacher, S.; Grüneberger, F.; Katterle, M.; Hettrich, C.; Hall, D. G.; Scheller, F. W.; Gajovic-Eichelmann, N., *Polymer* **2011**, *52*, 2485–2491.

- (12) Adamczyk-Woźniak, A.; Cyrański, M. K.; Jakubczyk, M.; Klimentowska, P.; Koll, A.; Kołodziejczak, J.; Pojmaj, G.; Żubrowska, A.; Żukowska, G. Z.; Sporzyński, A., *J. Phys. Chem. A* **2010**, *114*, 2324–2330.
- (13) Bałczewski, P.; Bachowska, B.; Białas, T.; Biczak, R.; Wiczorek, W. M.; Balińska, A., *J. Agric. Food Chem.* **2007**, *55*, 1881–1892.
- (14) Deng, Z.; Bouchékif, H.; Babooram, K.; Housni, A.; Choytun, N.; Narain, R., *J. Polym. Sci. A* **2008**, *46*, 4984–4996.
- (15) Deng, Z.; Ahmed, M.; Narain, R., *J. Polym. Sci. A* **2009**, *47*, 614–627.
- (16) Deng, Z.; Li, S.; Jiang, X.; Narain, R., *Macromolecules* **2009**, *42*, 6393–6405.
- (17) Alterio, V.; Cadoni, R.; Esposito, D.; Vullo, D.; Di Fiore, A.; Monti, S. M.; Caporale, A.; Ruvo, M.; Sechi, M.; Dumy, P., *ChemComm* **2016**, *52*, 11983–11986.
- (18) Li, J.; Ma, L.; Li, X.; Lu, C.; Liu, H., *Ind. Eng. Chem. Res.* **2005**, *44*, 5478–5482.
- (19) Kotsuchibashi, Y.; Agustin, R. V. C.; Lu, J.-Y.; Hall, D. G.; Narain, R., *ACS Macro Lett.* **2013**, *2*, 260–264.
- (20) Warneke, J.; Wang, Z.; Zeller, M.; Leibfritz, D.; Plaumann, M.; Azov, V. A., *Tetrahedron* **2014**, *70*, 6515–6521.
- (21) Gibas, I.; Janik, H., *Chem. Chem. Technol.* **2010**, *4*, 297–304.
- (22) Yang, T.; Long, H.; Malkoch, M.; Kristofer Gamstedt, E.; Berglund, L.; Hult, A., *J. Polym. Sci. A* **2011**, *49*, 4044–4054.
- (23) Chen, Y.; Diaz-Dussan, D.; Wu, D.; Wang, W.; Peng, Y.-Y.; Asha, A. B.; Hall, D. G.; Ishihara, K.; Narain, R., *ACS Macro Lett.* **2018**, *7*, 904–908.
- (24) Ishihara, K.; Mu, M.; Konno, T.; Inoue, Y.; Fukazawa, K., *J. Biomater. Sci. Polym. Ed* **2017**, *28*, 884–899.
- (25) Abraham, G. A.; de Queiroz, A. A. A.; Román, J. S., *Biomaterials* **2001**, *22*, 1971–1985.
- (26) Dowlut, M.; Hall, D. G., *J. Am. Chem. Soc.* **2006**, *128*, 4226–4227.
- (27) Bérubé, M.; Dowlut, M.; Hall, D. G., *J. Org. Chem.* **2008**, *73*, 6471–6479.
- (28) Matteson, D. S.; Man, H.-W., *J. Org. Chem.* **1996**, *61*, 6047–6051.
- (29) Diaz-Dussan, D.; Nakagawa, Y.; Peng, Y.-Y.; C, L. V. S.; Ebara, M.; Kumar, P.; Narain, R., *ACS Macro Lett.* **2017**, *6*, 768–774.
- (30) Peng, Y.-Y.; Diaz-Dussan, D.; Kumar, P.; Narain, R., *Biomacromolecules* **2018**, *19*, 4052–4058.
- (31) Peng, Y.-Y.; Diaz-Dussan, D.; Kumar, P.; Narain, R., *Bioconjugate Chem.* **2018**, *30*, 405–412.
- (32) Vshyvenko, S.; Clapson, M. L.; Suzuki, I.; Hall, D. G., *ACS Medicinal Chemistry Letters* **2016**, *7*, 1097–1101.
- (33) Mo, R.; Gu, Z., *Mater. Today* **2016**, *19*, 274–283.
- (34) Lee, K. Y.; Mooney, D. J., *Chem. Rev.* **2001**, *101*, 1869–1880.
- (35) Wang, Y.; Zhang, X.; Mu, J.; Li, C., *New J. Chem.* **2013**, *37*, 796–803.
- (36) Glasoe, P. K.; Long, F., *J. Phys. Chem. A* **1960**, *64*, 188–190.
- (37) Chen, Y.; Wang, W.; Wu, D.; Nagao, M.; Hall, D. G.; Thundat, T.; Narain, R., *Biomacromolecules* **2018**, *19*, 596–605.
- (38) Zhang, Y.; Fu, C.; Li, Y.; Wang, K.; Wang, X.; Wei, Y.; Tao, L., *Polym. Chem* **2017**, *8*, 537–544.

# Chapter 3

## Benzoxaborole-based Nanogel as a Stable and Stimuli-Sensitive Nanocarrier Towards pH and Oxidation-Responsive Cancer Drug Delivery

### 3.1 Introduction

Capecitabine (CAPE) (Figure 3-1) is an orally administered fluoropyrimidine carbamate chemotherapy medication classified as an antimetabolite.<sup>1-2</sup> It is used to treat breast, colon, gastric, gastroesophageal, and colorectal cancers.<sup>3</sup> Research has shown that CAPE can be absorbed quickly through the gastrointestinal wall and then metabolized to 5-fluorouracil (5-FU). Subsequently, 5-FU participates in blocking the function of thymidylate synthases, thus inhibiting DNA production and mitigating cancer cell proliferation.<sup>4</sup> CAPE, as an important anti-cancer drug, is embodied in the World Health Organization's List of Essential Medicines, which recognizes the most effective and safe medicines that are essential to health care systems.<sup>5</sup> Nevertheless, anti-cancer treatments with this medicine require a high therapeutic dose (2.5 g/m<sup>2</sup>), and the rapid gastrointestinal tract absorption limits the half-life of this medicine to 0.55–0.89 h.<sup>6</sup> Furthermore, the high hydrophilicity of CAPE gives rise to a water solubility as high as 26 mg/mL;<sup>7</sup> this causes poor cellular uptake of the drug and a decrease in its efficacy.<sup>6</sup> Hence, it is crucial to develop a stimuli-responsive drug carrier that could encapsulate this medicine, prolong its lifetime, and maintain the appropriate drug concentration in the bloodstream.

There are two significant challenges for the encapsulation of CAPE in nanocarriers. Firstly, owing to the high hydrophilicity of this drug, the traditional encapsulation pathway of utilizing the hydrophobic interactions between the drug molecules and the hydrophobic core of the nanoparticles is not efficient.<sup>7</sup> Secondly, CAPE is a neutral molecule with an isoelectric point of only about 2.43 (negative).<sup>6</sup> Therefore, encapsulation through electrostatic interactions is not entirely feasible owing to its weak attraction to cationic polymers.<sup>8</sup>

### 3.1.1 Attempts at Encapsulating Capecitabine (CAPE) into Nanoparticles Through Covalent Bonds

Enormous research efforts have been devoted to developing more stable nanocarriers for the encapsulation and delivery of CAPE. To this end, one of the best ways of encapsulating neutral and hydrophilic drugs is to conjugate them to the nanocarriers through covalent bonds.<sup>8-10</sup> As shown in Figure 3-1, CAPE contains a ribose (1,2-cis diol) moiety in its chemical structure, which allows it to bind with boronic acids to form the corresponding cyclic arylboronic esters.

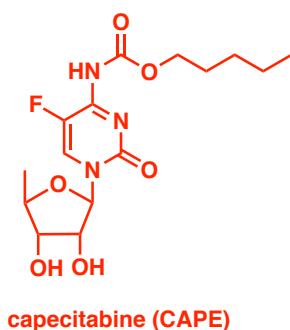
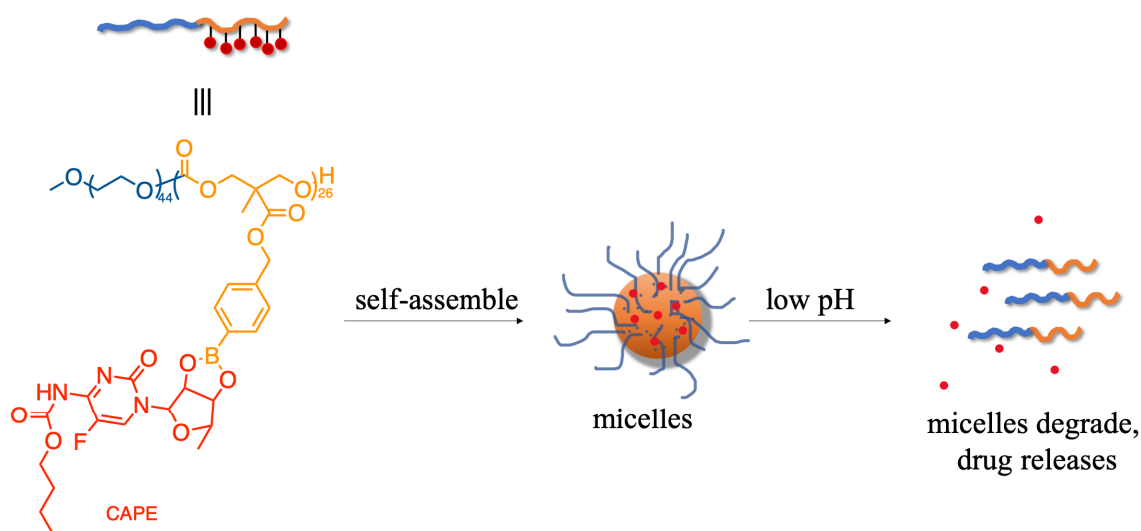


**Figure 3-1.** Chemical structure of capecitabine.

Some research groups have exploited the strategy of arylboronic ester formation to improve the encapsulation efficiency and the stability of the resulting nanoparticles. For example, Herrera-Alonso and co-workers used micelles with a phenylboronic acid (PBA) core to conjugate with CAPE, albeit with moderate drug loading efficiency (Figure 3-2, a).<sup>3</sup> Shi and co-workers developed an iminoboronate-based micelle that involves an intermolecular coordination between 2-formylphenylboronic acid and the pendent primary amines on polylysine (PLys). The resulting iminoboronate affords a strong binding with CAPE, and the resulting complex is also sensitive to glutathione (GSH) and low pH conditions due to the labile iminoboronate moieties (Figure 3-2, b).<sup>8</sup>

Both examples incorporate micelles as drug carriers, where the micellation depends highly on the critical micelle concentration (CMC). In other words, at a polymer

**(a) Herrera-Alonso and co-workers, PBA-CAPE micelles<sup>3</sup>**



**(b) Shi and co-workers, iminoboronate-based micelles<sup>8</sup>**

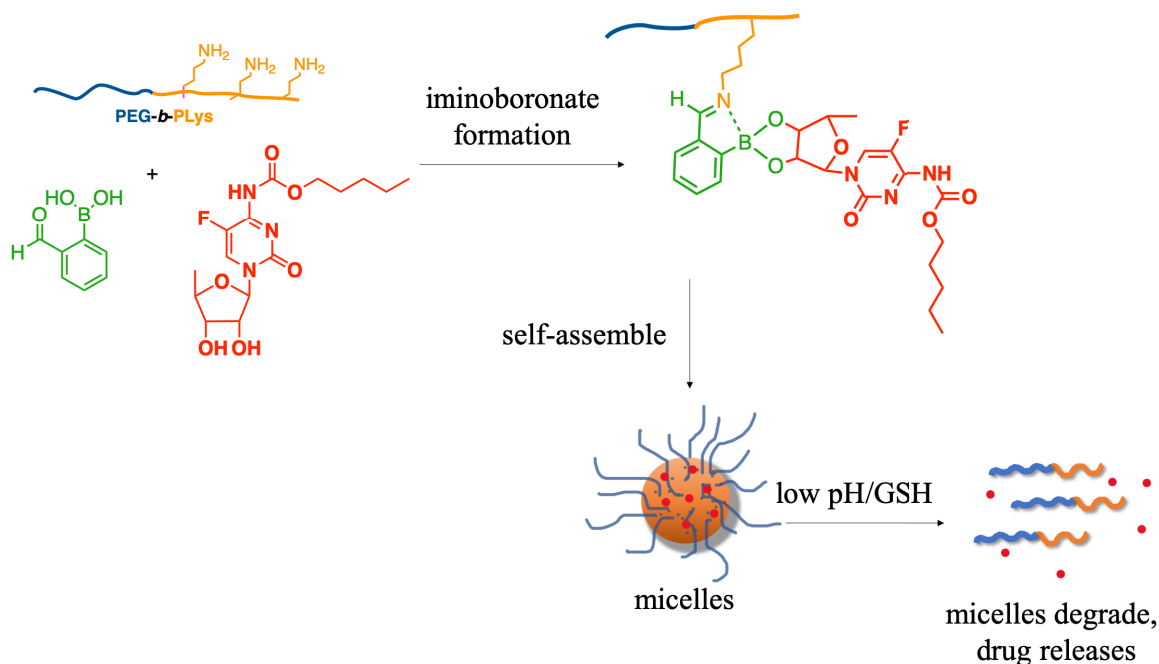


**Figure 3-2.** Reported methods for covalent bond-mediated polymer–drug conjugates to form nanoparticles.

concentration that is lower than the CMC, the polymers cannot self-assemble into stable micelles for the encapsulation of drugs (described later in Figure 3-4). Furthermore, as discussed in Section 1.1.5.1, conventional arylboronic acids with a high  $pK_a$  value (8–9) are not able to form stable arylboronic esters with 1,2-cis diols under physiological conditions.

Therefore, the resulting polymer–drug conjugates are unstable, and they ultimately would hamper the lifetime of the nanocarrier during the administration. As a result, a nanoparticle that could afford a more efficient CAPE encapsulation to form a more stable nanocarrier under physiological conditions is highly desirable.

## 3.2 Objective

In this work, we aim to develop a stable nanocarrier for the encapsulation of CAPE. Nanogel, a type of nano-sized hydrogel, is constructed from 3D cross-linked networks and shows excellent stability.<sup>11</sup> Like micelles, drug molecules can be conjugated on the nanogel polymer matrices through covalent bonds, thus effectively enhancing the drug loading capacity.<sup>11</sup> Nopoldiol, a rigid cyclic 1,2-cis diol, has been shown to bind benzoxaborole tightly with high stability (Chapter 2). Herein, the nopoldiol-benzoxaborolate cross-links (Figure 3-3) are introduced in the nanogel system to afford a stable and stimuli-responsive network. In addition, the proportion of benzoxaborole moieties is designed to be higher than that of nopoldiol units. Therefore, the extra benzoxaborole moieties are expected to conjugate CAPE by forming stable benzoxaborolate covalent bonds under physiological conditions. The resulting nanocarriers are designed to be dual-responsive to pH and ROS (e.g., H<sub>2</sub>O<sub>2</sub>) for the release of the encapsulated drugs on demand.

In addition, a long-linker benzoxaborole-based monomer (**LB**) is designed to improve the hydrophilicity of the resulting nanoparticles for better compatibility with the hydrophilic drug (CAPE). Both the **LB**-containing nanoparticle and the nanogel were assessed via drug releasing tests for a better understanding of the drug encapsulation and releasing mechanism.

## 3.3 Results and Discussion

### 3.3.1 Design of Nanogels

To develop a suitable nanocarrier for CAPE encapsulation, **polymer A** and **polymer B** were designed as polymer precursors for the fabrication of nanoparticles (Figure 3-3). Specifically, **polymer A** contains sufficient benzoxaborole moieties to bind nopoldiol units in **polymer B** and the CAPE molecules. **Polymer B** is composed only of a small amount of nopoldiol in an

attempt to build cross-links with benzoxaborole, while leaving room for benzoxaborole–CAPE binding. It is proposed that the two polymers with pendent benzoxaborole and nopoldiol units are expected to cross-link efficiently to form nanogels. By mixing CAPE with the precursor solutions, the drug can be conjugated in the polymeric matrices through the formation of covalent bonds between the benzoxaborole moieties and the 1,2-cis diol in CAPE.

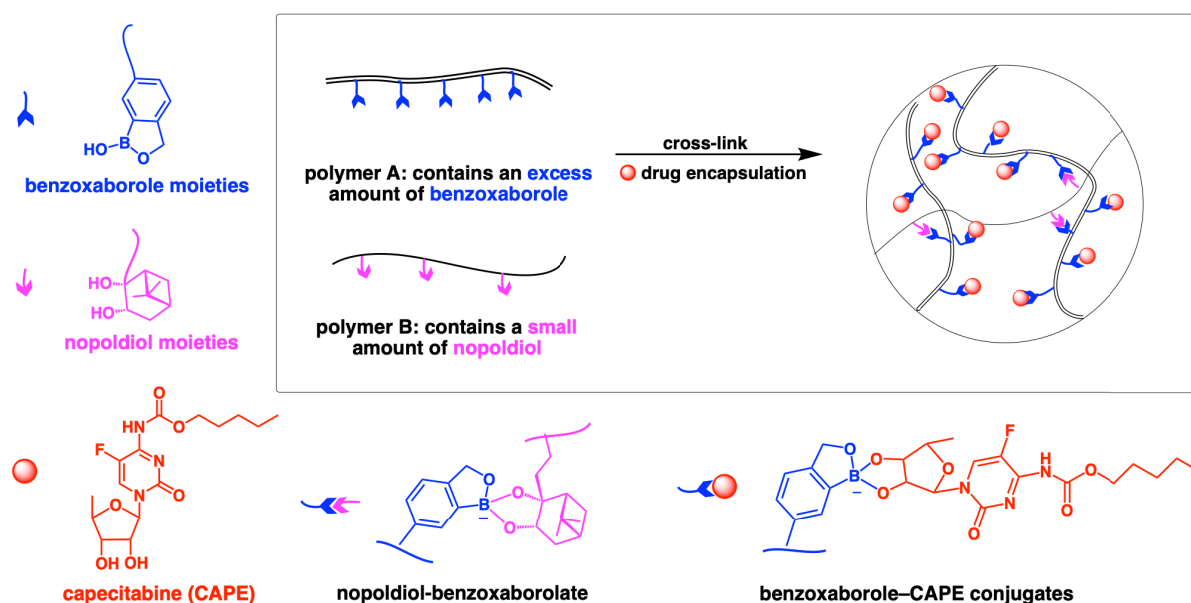


**Figure 3-3.** Graphic illustration of the design and preparation of benzoxaborolate-based CAPE nanocarriers.

Compared to the two methods for CAPE encapsulation reported previously (Figure 3-2), our system is advantageous for two reasons:

- 1) Unlike micelles, which require a polymer concentration higher than their CMC value to form stable self-assemblies, the nanogel formation is independent of the polymer concentration; it could contribute to a prolonged lifetime of nanoparticles in biological systems (Figure 3-4).
- 2) Due to its lower pKa compared to phenylboronic acid, benzoxaborole as the binding partner for drug molecules could enhance the stability of the newly formed polymer–drug covalent bonds (Chapter 1). Therefore, the resulting nanogels are expected to possess an improved drug encapsulation efficiency and a more sustainable drug release profile.

As described in Chapter 1.2, compared to normal cells, the cancer microenvironment of tumors typically exhibits a lower pH, an elevated ROS level, an increased sialic acid concentration, and a higher glutathione (GSH) level. Therefore, the drug-containing nanogels are expected to exhibit stimuli-responsive drug release that targets cancerous cells.

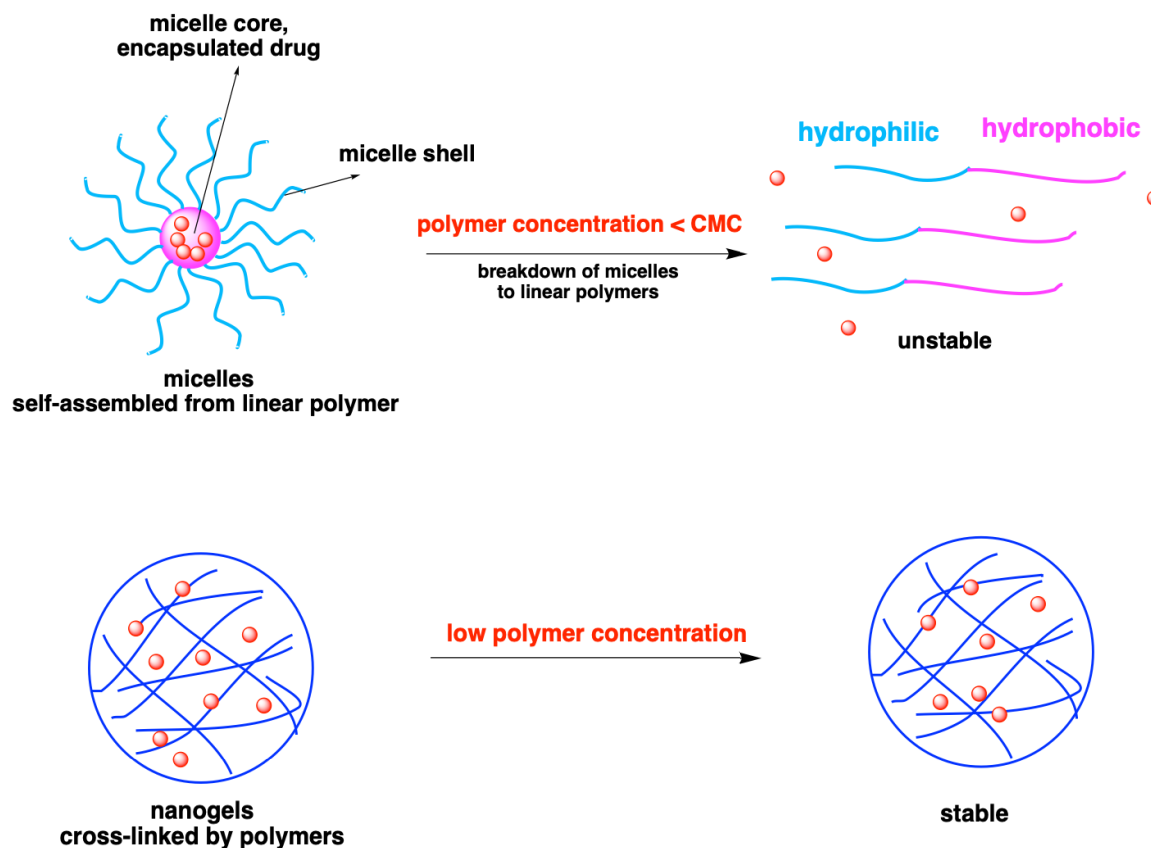


**Figure 3-4.** Comparison of stability of micelles and nanogels upon dilution.

Shown in Figure 3-5 are two possible pathways to trigger the drug release. In pathway 1, the nopoldiol-benzoxaborolate units can degrade partially at low pH (details are shown in Chapter 2), which could result in slight nanogel swelling/degradation due to the decreased cross-link density. More importantly, the low pH conditions in a tumor environment can cause cleavage of all the acid-sensitive benzoxaborole–CAPE conjugates, thus releasing the drug. In pathway 2, the overproduced ROS could oxidize either the nopoldiol- or CAPE-benzoxaborolate to 2-hydroxybenzyl alcohol, followed by the release of free nopoldiol or CAPE, respectively, in the process (details are shown in Chapter 2). Moreover, it is notable that the pendent benzoxaborole moieties could bind the overexpressed sialic acids on the

cancerous cell membrane, thus helping the uptake of this nanomedicine through receptor-mediated endocytosis (Chapter 1).

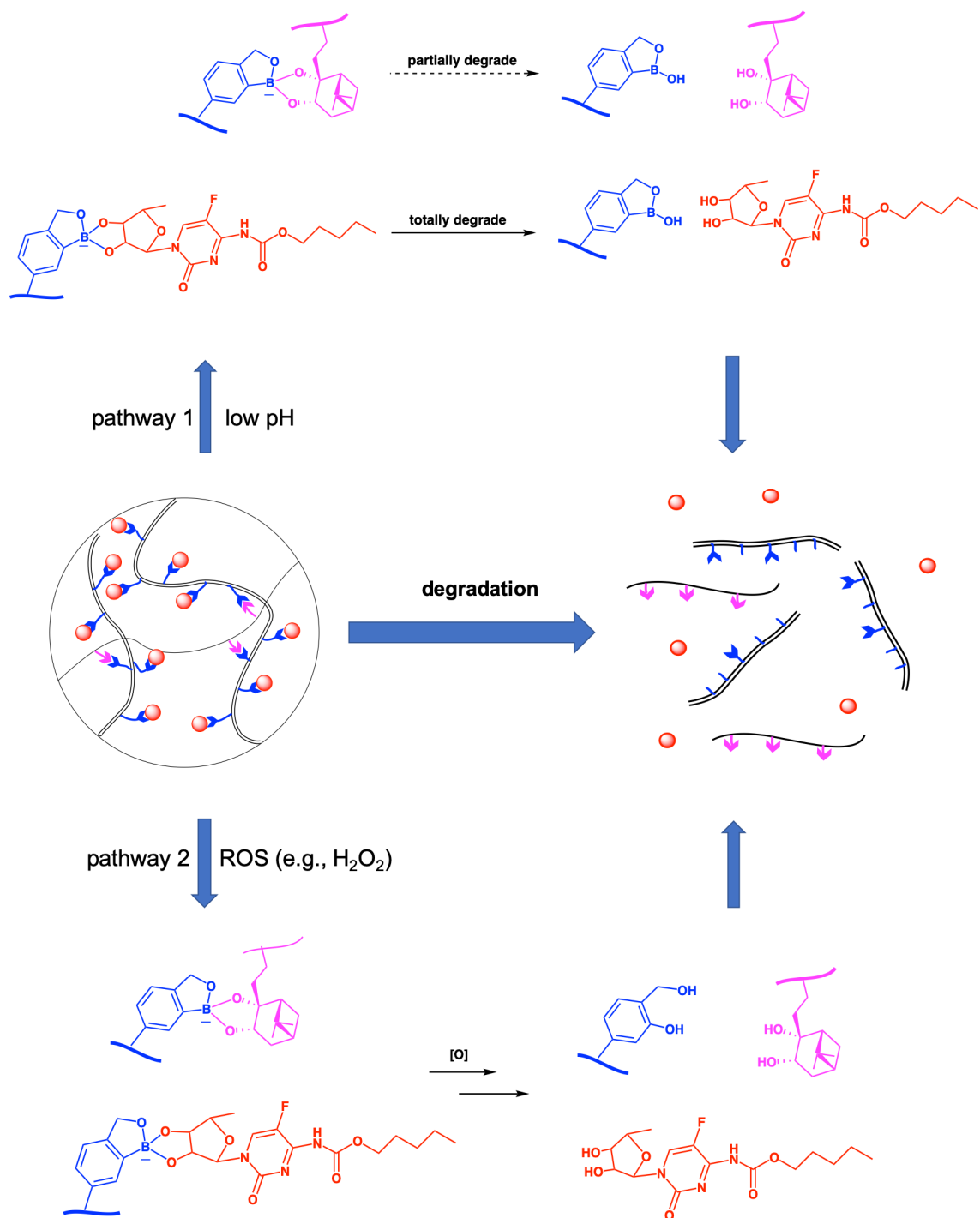


**Figure 3-5.** Proposed pathways of pH and ROS dual-responsive degradation of nanogels.

### 3.3.1.1 Design and synthesis of monomers

The nopoldiol-based monomer, (1*R*)-(-)-nopoldiol-methacrylamido-diol (**nopoldiol**), was synthesized using the same method described in Chapter 2 (Scheme 2-3). Here, the choice of the benzoxaborole-based monomer should include the following considerations:

- 1) The **MAAmBO** monomer that has been applied in the hydrogel project (Chapter 2) is too hydrophobic. For this nanogel project, a significant proportion of benzoxaborole moieties is required to conjugate as much CAPE as possible. However, the dominating hydrophobic character in the polymer could cause an undesirable polymer aggregation, thus limiting the contact surface area of polymers with drug molecules and inhibiting their bindings.
- 2) Due to its short length, the **MAAmBO** may be sterically hindered by other moieties on the backbone and prevent their approach to CAPE.

To address this problem, a new benzoxaborole-based monomer with a longer linker, 2-(2-(2-methacrylamidoethoxy)ethoxy)-benzoxaborole (**LB**), was designed (Figure 3-6). An ethylene glycol type spacer was inserted in the **LB** molecule to increase the molecule hydrophilicity and length. The **LB** with a long-linker was expected to afford a more compact ‘brush’-like polymer with more flexible arms and a higher contact area for better polymer–drug conjugation.

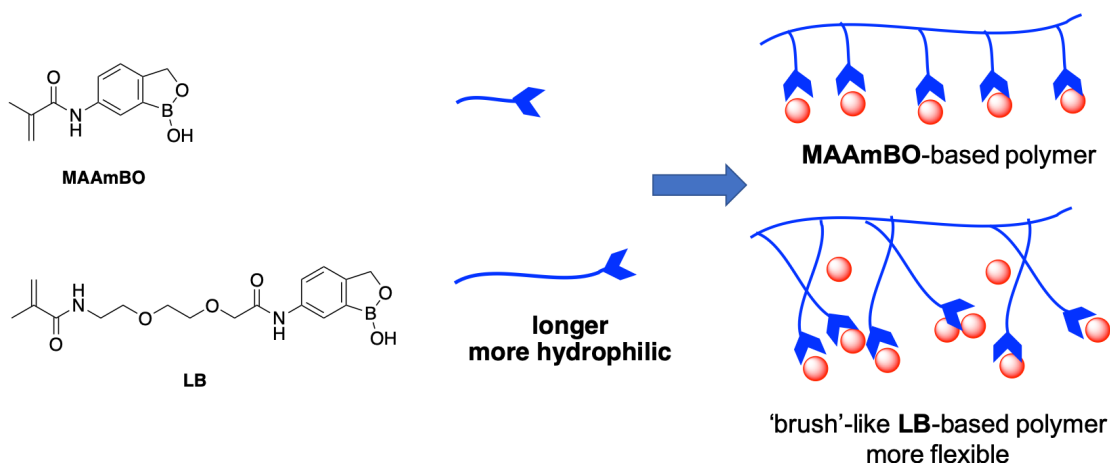
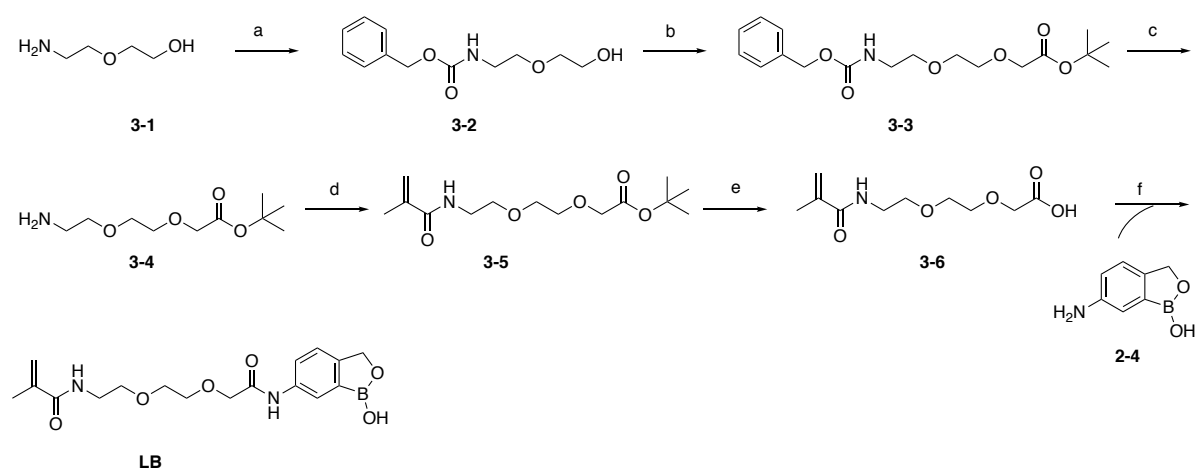


**Figure 3-6.** Structures of **MAAmBO** and **LB** and a graphic illustration of **MAAmBO**- and **LB**-based polymer–drug conjugation.

Monomer **LB** was synthesized as shown in Scheme 3-1, where the first three steps for making *tert*-butyl 2-(2-(2-aminoethoxy)ethoxy)acetate (**3-4**) followed a previous report with slight modifications.<sup>12</sup> Then, compound **3-4** underwent an acylation reaction with methacrylic anhydride to give *tert*-butyl 2-(2-(2-methacrylamidoethoxy)ethoxy)acetate (**3-5**). Next, the *tert*-butyl group on **3-5** was cleaved with trifluoroacetic acid (TFA) to obtain compound 2-(2-(2-methacrylamidoethoxy)ethoxy)acetic acid (**3-6**). Lastly, **3-6** was reacted with aminobenzoxaborole **2-4** through an amide coupling reaction to form the desired long-linker monomer **LB**.

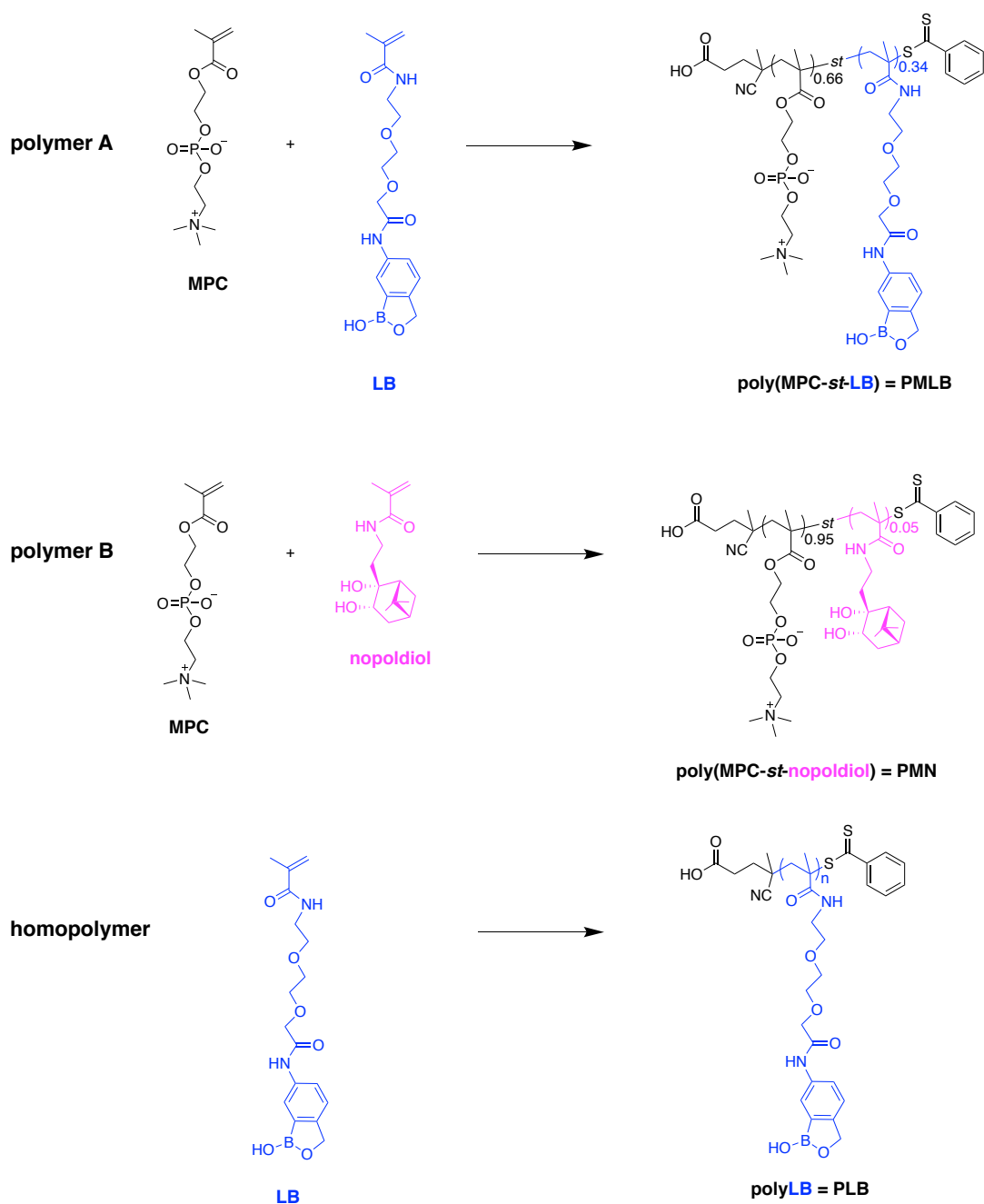


**Scheme 3-1.** Synthesis of monomer 2-(2-(2-methacrylamidoethoxy)ethoxy)-benzoxaborole (**LB**). Reaction conditions: (a) benzyl chloroformate, TEA, DCM, 0 °C for 2 h, then r.t., overnight, quantitative yield. (b) *tert*-butyl bromoacetate, potassium *tert*-butoxide, THF, 0 °C for 2 h, then r.t., overnight, 50–59% yield, (c) Pd/C, H<sub>2</sub>, MeOH, r.t., 1.5 h, quantitative yield, (d) methacrylic anhydride, TEA, MeOH, 0 °C for 2 h, then r.t., overnight, 92–94% yield, (e) TFA, MeOH, 0 °C for 2 h, then r.t., overnight, quantitative yield, (f) HATU, TEA, DCM, r.t. 41–50% yield.

### 3.3.1.2 Design and synthesis of polymers

As described earlier in Figure 3-3, **polymer A** was expected to contain as many benzoxaborole moieties as possible, and **polymer B** should only comprise a small amount of nopoldiol moieties to afford the desired level of cross-linking with **LB** to form nanogels. However, in **polymer A**, the hydrophilicity of the polymer needs to be ensured to avoid polymer aggregations and to prevent poor compatibility between the polymer and the hydrophilic drug, CAPE. **MPC**, a zwitterionic monomer, was chosen as the backbone component due to its hydrophilicity and its well-established biocompatibility.<sup>13</sup> As shown in Scheme 3-2, **polymer A** was designed with a statistical copolymer with monomer **MPC** and **LB**, where the final

polymer of poly(MPC-*st*-LB) (PMLB) contains 34 mol% of LB moieties. Polymer B was synthesized with monomer MPC and **nopoldiol** to produce poly(MPC-*st*-nopoldiol) (PMN), where **nopoldiol** moieties only represent 5 mol% in composition.



**Scheme 3-2.** Synthesis of polymers **PMLB** and **PMN**. Reaction conditions: 4-cyanopentanoic acid dithiobenzoate (CTP), 4,4'-azobis(4-cyanovaleric acid) (ACVA), MeOH, 70 °C, 24 h; 50%, 61%, 4.6% yield for polymer A, B, and homopolymer, respectively. Numbers indicate proportions of each component in the statistical polymers (normalized to 1).

In addition, a homopolymer of **LB**, **PLB**, also was synthesized for a control study to investigate its behavior in drug encapsulation/release compared to nanogels, where the homopolymer is defined as using only one component in the polymer structure. All the polymers were synthesized through reversible addition–fragmentation chain-transfer (RAFT) polymerization with a designed degree of polymerization (DP) of 200.

### 3.3.2 Nanogel Preparation and Drug Release Methodology

Detailed experimental procedures of both nanoparticles and nanogels will be explained case by case along with the results because the conditions of experiments vary according to the optimization process.

General methods for nanogel preparations (Figure 3-7): **polymer A (PMLB)** was dispensed in a pH 7.4 buffer solution with a desired concentration. Then, a CAPE solution was mixed with the **polymer A** solution and incubated for 30 min to allow conjugation of the linear **PMLB** with CAPE. Next, this **PMLB**–CAPE mixture and a **polymer B (PMN)** solution were added dropwise to another vessel slowly with vigorous stirring. Nanogels were formed as the complementary groups cross-linked, encapsulating the drug molecules, and then the nanogel solution was allowed to stabilize for 1 h at room temperature.

General methods for nanogel drug release experiments (Figure 3-7): 1 mL of nanogel solution was added to a dialysis tube with a MWCO (molecular-weight cutoff) of 6,000–8,000 Da and sealed with cotton thread. Then, the dialysis tube was immersed in 20 mL of release media (buffers with various pH values or 10 mM H<sub>2</sub>O<sub>2</sub> solution). The pores on the dialysis tubing prevent the leaking of nanogels/polymers to the release media, while allowing small molecules (CAPE) to disperse freely. After preset intervals, 1 mL of release media was taken out for UV absorption tests, and 1 mL of fresh media was added. The cumulative drug release percent was calculated based on the UV absorption at wavelength of 295 nm.

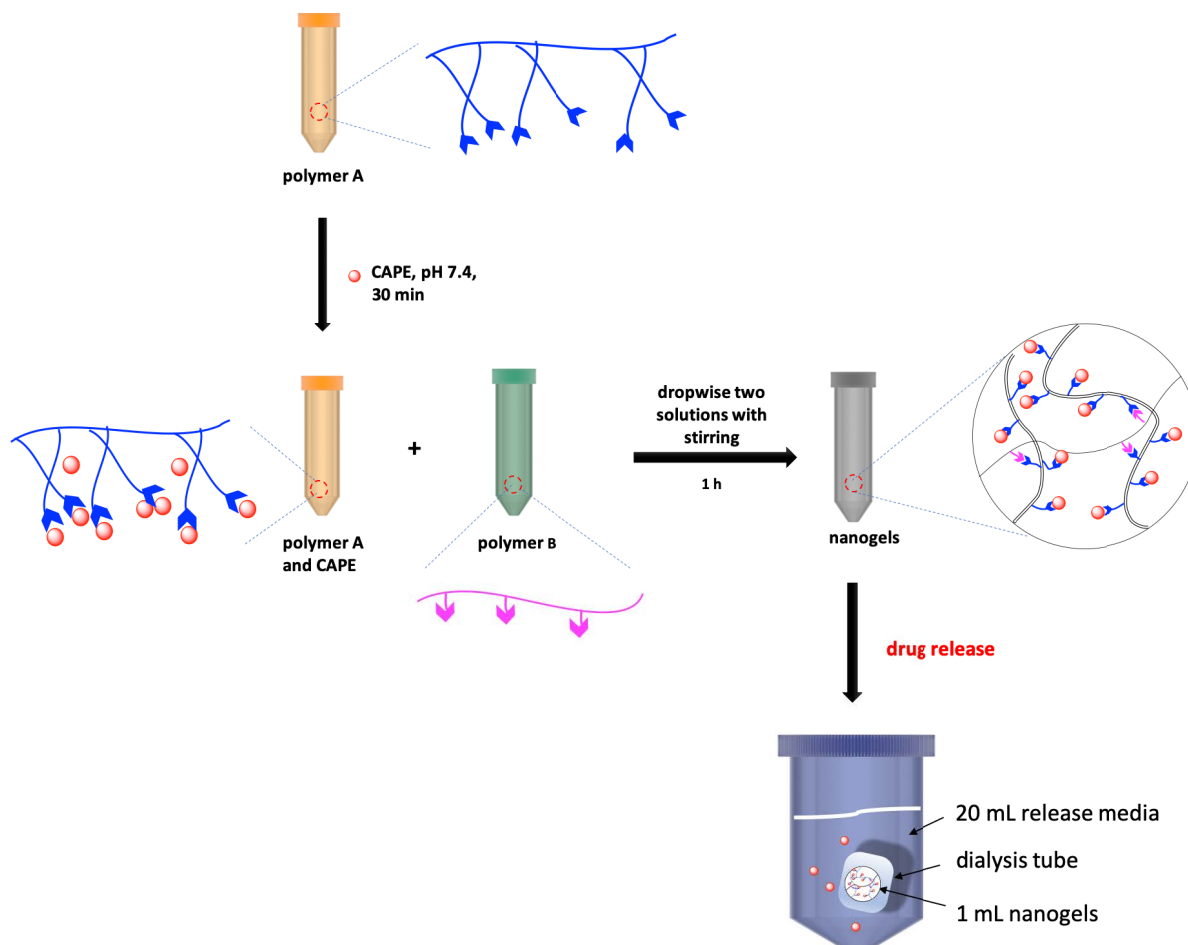


**Figure 3-7.** Graphical representation of nanogel preparations and nanogel drug release methods.

### 3.3.3 Attempts at Using LB-based Nanoparticles for CAPE Drug Delivery

#### 3.3.3.1 Homopolymer-based nanoparticles

The first attempt in this project was to use only the LB monomer to form homopolymers PLB. It is notable that the short monomer MAAmBO cannot form a stable micelle in aqueous solution owing to its hydrophobicity. Therefore, we expected the LB monomer to form a homopolymer-based micelle due to its amphiphilic properties, which could have potential use in future applications.

Unfortunately, the polymerization reaction of the homopolymer **PLB** was not very successful as it only gave a 4.6% yield. The low yield probably resulted from the undesired reaction conditions and reagent ratios. The **PLB** was found to aggregate to nanoparticles at neutral pH, and the nanoparticles were not stable enough; they aggregated and precipitated

eventually after 24 h. The SEM imaging confirmed the morphologies of these nanoparticles as spheres (Figure 3-8).

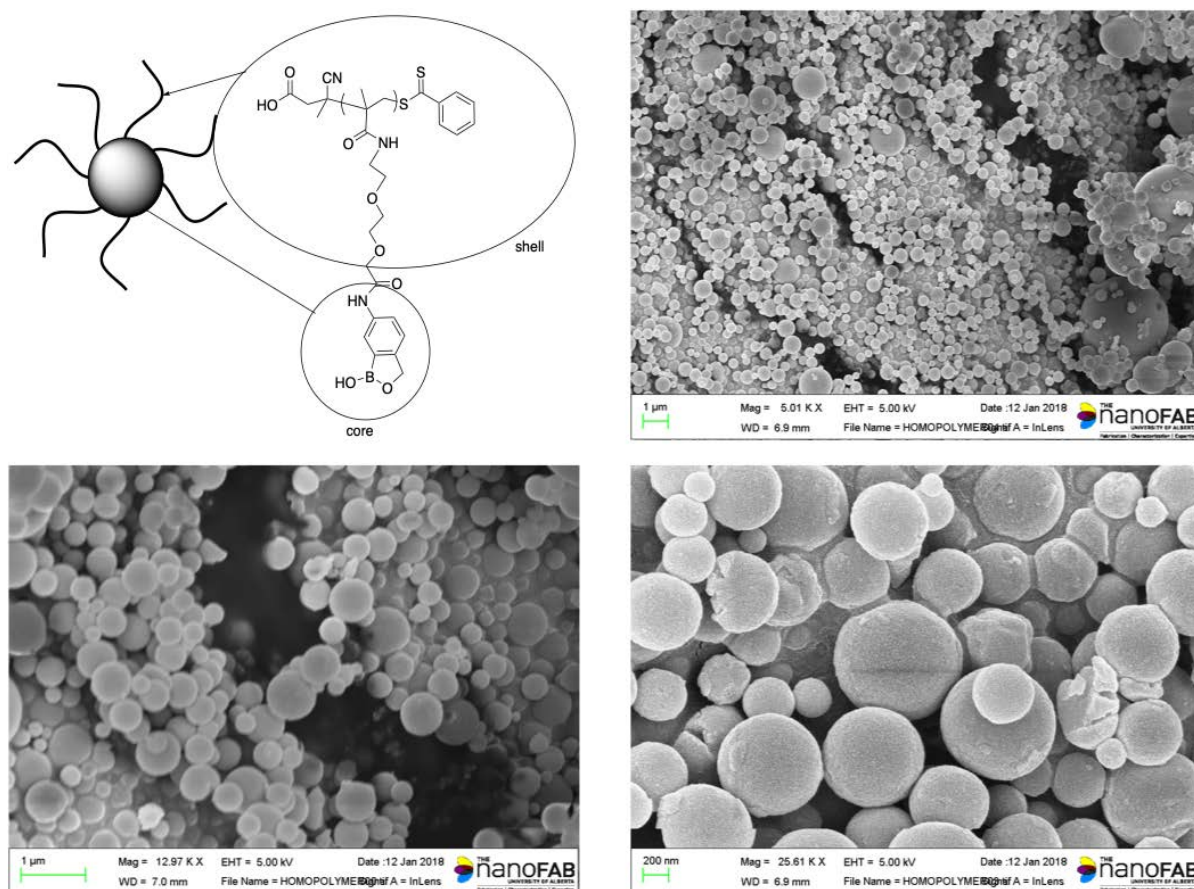


**Figure 3-8.** Proposed structure (micelles) and SEM images of homopolymer-based nanoparticles from **PLB**.

Encouraged by the abovementioned observations, we set out to try the drug encapsulation trials with this nanoparticle by using a nanoprecipitation method. Specifically, 10 mg **PLB** were dissolved in 0.5 mL of organic solvent, THF, where the nanoparticles were degraded into linear polymers. Then, a solution of 10 mg of CAPE in 0.5 mL MeOH was combined with the **PLB** solution to allow polymer–drug conjugations and was stabilized for 1 h. Next, the 1 mL mixture of **PLB** and CAPE was added dropwise to 9 mL of PBS pH 7.4, where the linear and soluble polymer–drug conjugate (in THF) suddenly self-assemble to spherical nanoparticles under neutral aqueous conditions. The drug-encapsulated nanoparticles were allowed to stabilize for 1 h, and the drug release method was the same as described earlier in

Section 3.3.2. Table 3-1 lists the incubation and drug release conditions for **PLB**-based homopolymer nanoparticles.

**Table 3-1.** Incubation and drug release conditions for **PLB**-based homopolymer nanoparticles.

Description: <b>PLB</b> -based homopolymer nanoparticles	
Incubation conditions (nanoprecipitation)	Release media
THF to 7.4 PBS, 10 mg/mL drug	pH 9.6
	pH 7.4
	pH 5.2

As shown in Figure 3-9, at pH 7.4 and 5.2, the drug release profiles were nearly identical, where ~60% of the encapsulated CAPE was released after 5.6 h. In contrast, CAPE was released rapidly at a higher pH of 9.6, where ~55% of CAPE was released within 1 h and released completely after 5.5 h. This result is surprising because we expected an acid-triggered drug release profile. The possible rationalization for this phenomenon could be due to base-triggered morphological changes, where the hydrophobic benzoxaborole moieties in the nanoparticle were ionized under basic conditions. Therefore, the cores became hydrophilic due to their ionic nature, and the CAPE was released rapidly along with the disruption of the aggregate.

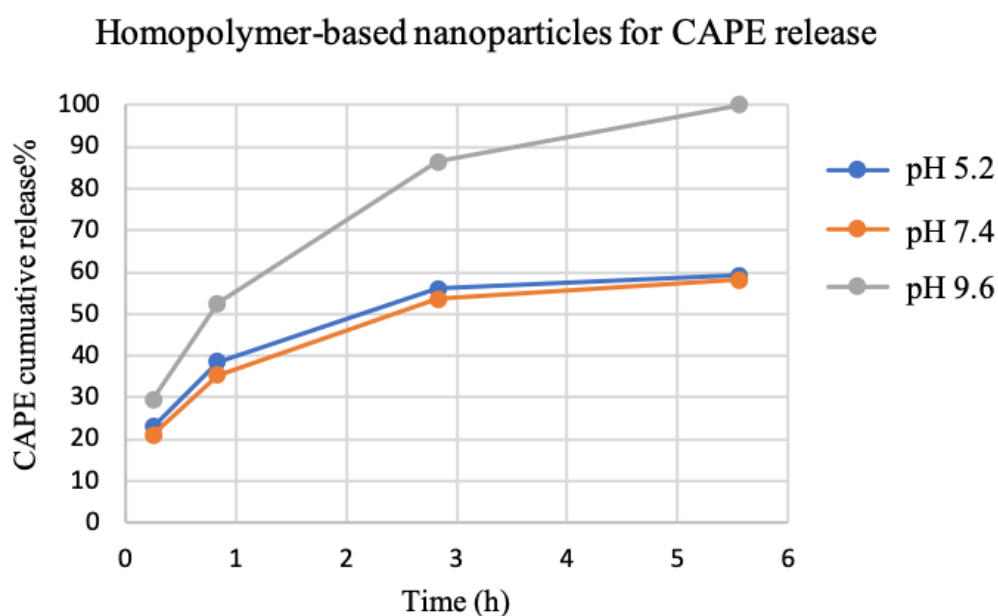


**Figure 3-9.** CAPE cumulative release profiles using homopolymer-based nanoparticles (**PLB**).

Overall, these results indicated that the drug molecules were more likely to be encapsulated physically in the nanoparticles. There was possibly some drug conjugated to benzoxaborole; however, the resulting benzoxaborolates may not be tight enough to hold the CAPE while experiencing the nanoparticle morphological changes and exposure to dilute aqueous conditions. Therefore, the homopolymer nanoparticle was found unsuitable for this particular application.

### 3.3.3.2 Copolymer-based nanoparticles

To investigate the influence of polymer types for nanoparticle-based CAPE drug release, polymer **PMLB** was tested next. Because **PMLB** is insoluble in THF due to its zwitterionic nature, nanoprecipitation did not work. Therefore, 10 mg of **PMLB** were dissolved in 1 mL of CAPE solution (1 mg/mL drug in PBS 7.4), followed by incubation for 1 h (Table 3-2). The drug release experiment followed the same procedure as described earlier in Section 3.3.2. Three types of release media, pH 7.4 buffer, pH 5.2 buffer, and pH 7.4 + H<sub>2</sub>O<sub>2</sub> 10 mM buffer, were used for testing the acid- and H<sub>2</sub>O<sub>2</sub>-responsiveness of this nanoparticle.

Figure 3-10 shows the CAPE releasing profiles using **PMLB**-based copolymer nanoparticles. Unlike the homopolymer nanoparticles, this copolymer-based nanoparticle shows a dramatic acid-triggered drug release with pH 5.2 release media, where nearly all the CAPE released after 3.5 h. The same trend was found when adding 10 mM H<sub>2</sub>O<sub>2</sub>, which indicates the oxidative degradation of nanogel cross-links and the polymer–drug conjugates.

**Table 3-2.** Incubation and drug release conditions for **PMLB**-based copolymer nanoparticles.

Description: <b>PMLB</b> -based copolymer nanoparticles	
Incubation conditions	Release media
7.4 PBS, 1 mg/mL drug	pH 7.4
	pH 5.2
	pH 7.4 + H <sub>2</sub> O <sub>2</sub> 10 mM

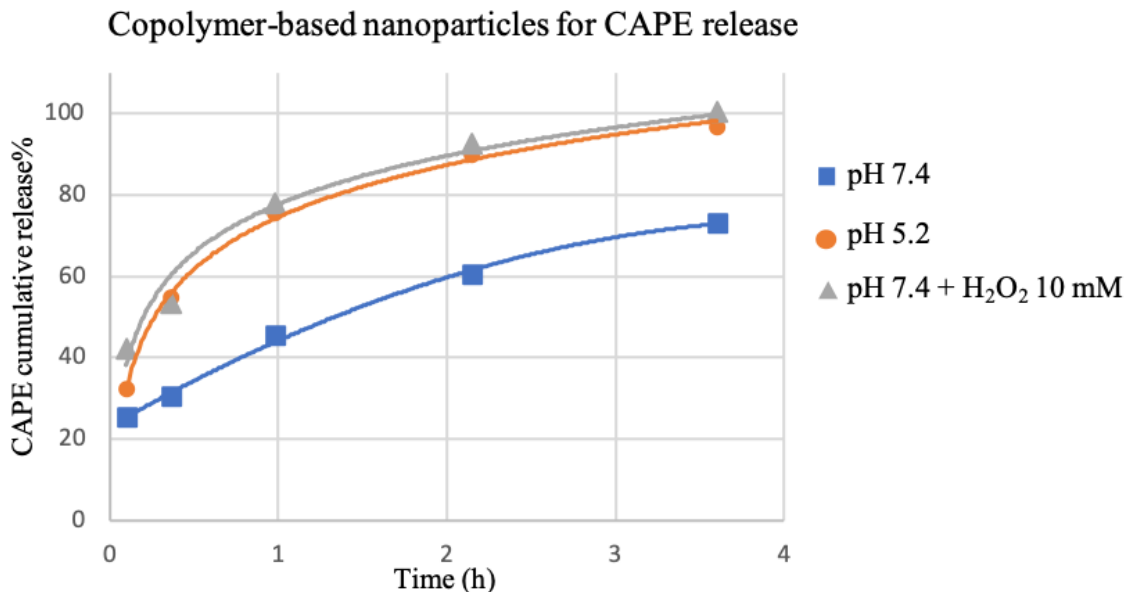


**Figure 3-10.** CAPE cumulative release profiles using copolymer-based nanoparticles (**PMLB**).

Overall, the copolymer-based nanoparticle was able to meet our objectives of developing an acid- and H<sub>2</sub>O<sub>2</sub>-sensitive drug carrier. However, a more stable nanogel is still more desirable for the purpose of a sustainable drug release, as discussed in Section 3.3.

### 3.3.4 Attempts at Using PMLB–PMN Nanogels for CAPE Drug Delivery

#### 3.3.4.1 PMLB–PMN nanogel with 1:1 weight ratio

The nanogels formed by **PMLB** and **PMN** in a 1:1 weight ratio were tested first for drug encapsulation and drug release. The experiment was performed as described in Figure 3-7, where **PMLB** was incubated with CAPE for 30 min, followed by mixing with **PMN** solution with vigorous stirring. This **PMLB–PMN** nanogel was freeze-dried and then visualized by SEM imaging. As shown in Figure 3-11, these nanogels exhibit a spherical morphology, as expected, with a diameter of around 200–400 nm.

Table 3-3 lists the experimental conditions and Figure 3-12 demonstrates the CAPE release profiles. It is clear that both stimuli (acid and H<sub>2</sub>O<sub>2</sub>) could facilitate the drug releasing process; however, the differences among the neutral, acid, and H<sub>2</sub>O<sub>2</sub> conditions were not very significant (less than 10% difference).



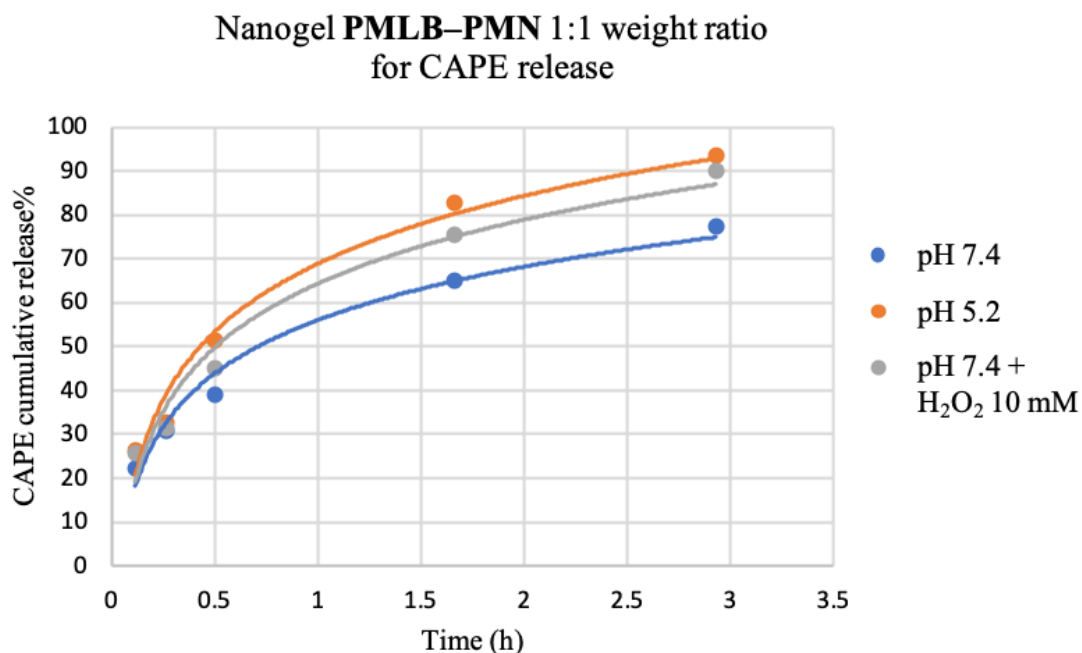


**Figure 3-12.** CAPE cumulative release profiles using **PMLB–PMN 1:1** weight ratio nanogels.

### 3.3.4.2 PMLB–PMN nanogel with various weight ratios

Due to the suspicions regarding suboptimal polymer proportions towards drug encapsulation, **PMLB–PMN** nanogels constructed with 3:1, 1:1, and 1:3 weight ratios were tested for their drug releasing properties (Table 3-4). The nanogel fabrication and drug release methods were the same as described in Section 3.3.3.1.

Figure 3-13 shows the drug releasing profiles, where, with a higher **PMN** weight ratio, the CAPE was released faster. The nanogels composed of 3:1 **PMLB:PMN** gave the best results with ~80% cumulative drug release after 4.5 h. These results support our assumption that a higher proportion of benzoxaborole-based polymer would provide more binding sites for CAPE, thus helping the drug encapsulation. In contrast, nanogels with three times higher concentration of **PMN** than **PMLB** have the least accessible binding sites, thus causing the fastest rate of drug release.

**Table 3-4.** Incubation conditions, polymer weight ratios, and drug release conditions for **PMLB–PMN** nanogels.

Description: <b>PMLB–PMN</b> nanogels with various weight ratios		
Incubation conditions	Weight ratios of <b>PMLB:PMN</b>	Release media
7.4 PBS, 1 mg/mL drug	3:1	pH 7.4
	1:1	pH 7.4
	1:3	pH 7.4

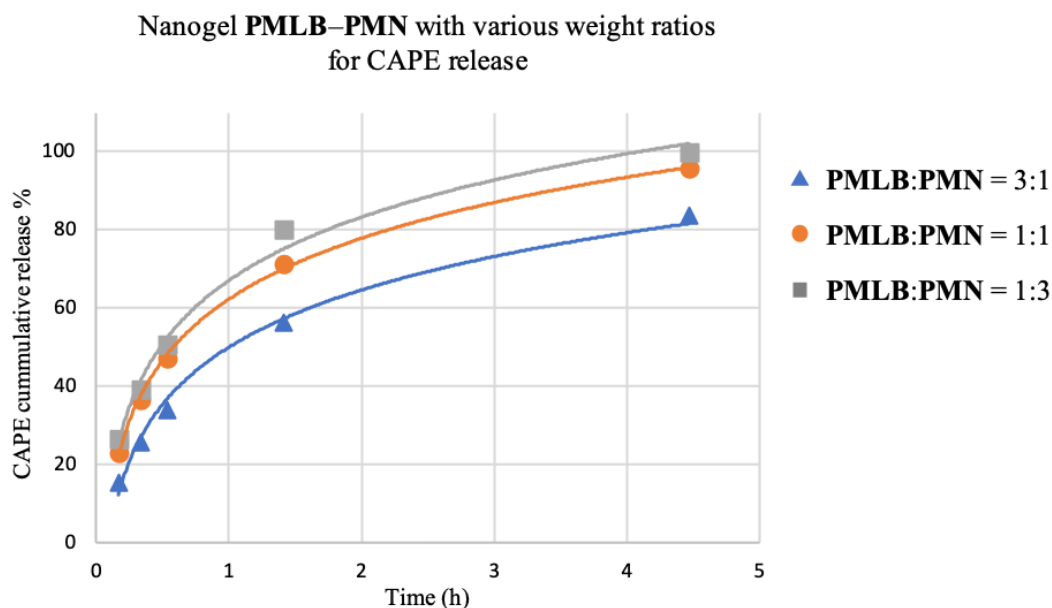


**Figure 3-13.** CAPE cumulative release profiles using **PMLB–PMN** nanogels with various weight ratios.

### 3.3.5 Polymer–Polymer and Polymer–CAPE Binding Studies via ARS Assays

Alizarin Red S (ARS) is a widely used compound for the detection of binding events between boronic acids and diols.<sup>14</sup> The ARS assay can evaluate the binding based on the changes in fluorescence intensity of emission qualitatively and quantitatively.<sup>14</sup> As described in Figure 3-14, the free ARS molecule has a low fluorescence; however, once it binds to arylboronic acids, the conjugated ARS molecule shows strong fluorescence. Sequentially, the addition of competing diols, such as CAPE or nopoldiol-containing polymers, can suppress the fluorescence intensity via transesterification by releasing the ARS-bound boronic acid, followed by the formation of benzoxaborole–CAPE and benzoxaborole–nopoldiol conjugates.

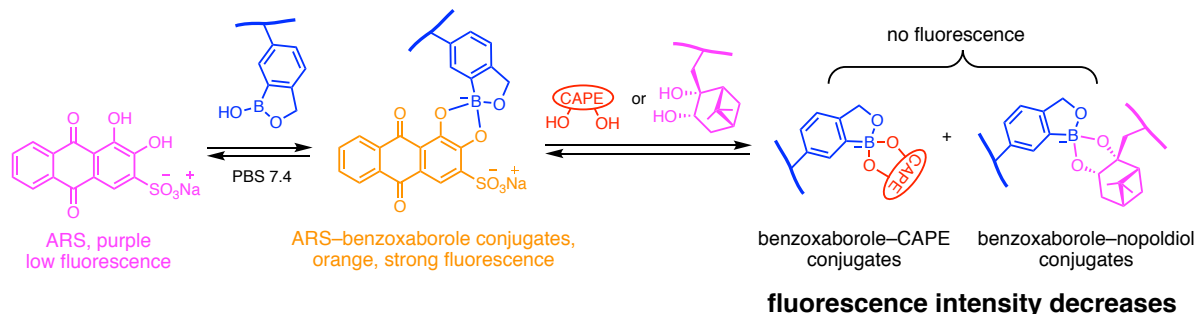


**Figure 3-14.** Demonstration of ARS assays for benzoxaborole–diol binding tests.

Figure 3-15 shows the fluorescence intensity profiles of polymer–polymer binding and polymer–drug binding. A pure ARS solution (control) showed a purple color and the lowest fluorescence intensity. By adding the benzoxaborole-containing polymer solution **PMLB**, the solution turned to light yellow with a dramatic increase of fluorescence intensity. Then, a **nopoldiol**-containing polymer, **PMN**, was added to the mixture of ARS and **PMLB**. As expected, the intensity was suppressed by about 20% due to the relatively low molar ratio of **nopoldiol** moieties in **PMN** compared to benzoxaborole moieties in **PMLB** ( $[\text{benzoxaborole}]:[\text{nopoldiol}] = 3.4:0.7$ ), and the solution color turned from light yellow to orange. To confirm that there were more benzoxaborole moieties available for binding, after the first polymer–polymer mixing, a solution of five times the original concentration of **PMN** ( $[\text{benzoxaborole}]:[\text{nopoldiol}] = 3.4:3.5$ ) was added to the mixture of ARS and **PMLB**. Unsurprisingly, the fluorescence intensity almost decreased to the level of ARS (control), and the solution color also turned to purple. These observations indicate a nearly complete replacement of ARS–benzoxaborole conjugates with benzoxaborole–nopoldiol conjugates and the highly efficient binding between the two polymers.

The binding between polymer **PMLB** and drug molecule CAPE was evaluated using the same method (Figure 3-15B). Because the binding affinity of benzoxaborole and CAPE is about two times lower than that of **nopoldiol** (at pH 7.4, Section 2.3.3) and the binding between polymer and drug is not as strong as polymer–polymer binding (cross-linked at multiple sites), adding even more than three times the molar ratio of CAPE ( $[\text{benzoxaborole}]:[\text{CAPE}] = 3.4:12$ ) only resulted in ~5% of fluorescence suppression, and doubling the original CAPE concentration ( $[\text{benzoxaborole}]:[\text{CAPE}] = 3.4:24$ ) only decreased the intensity by ~10%.

In summary, the binding between **PMLB** with **PMN/CAPE** was monitored quantitatively by ARS assays. **PMLB** binds tighter with **PMN** than with **CAPE**, and a higher concentration of competing reactants (**PMN** or **CAPE**) results in a stronger suppression in fluorescence intensity, demonstrating a more complete and effective binding.

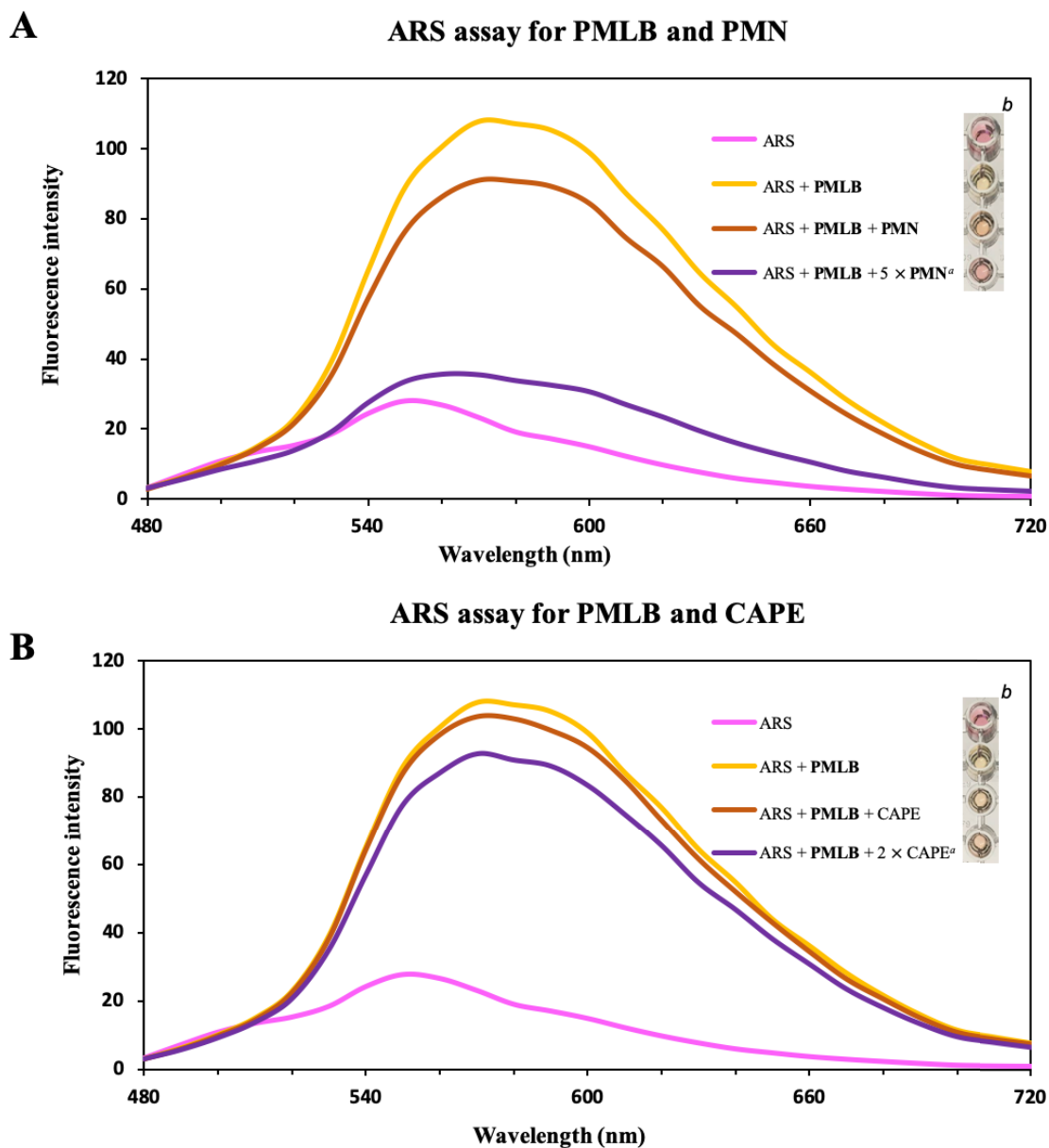


**Figure 3-15.** ARS assays for (A) binding between **PMLB** and **PMN** in concentration of  $[\text{ARS}]:[\text{benzoxaborole}]:[\text{nopoldiol}] = 1:3.4:0.7$  and  $1:3.4:3.5$ , (B) binding between **PMLB** and **CAPE** in concentration of  $[\text{ARS}]:[\text{benzoxaborole}]:[\text{CAPE}] = 1:3.4:12$  and  $1:3.4:24$ .  $[\text{ARS}] = 700 \mu\text{M}$ , PBS pH 7.4 buffer, excitation: 450 nm.

<sup>a</sup>n times of original concentration. <sup>b</sup>Color changes in corresponding wells.

### 3.4 Conclusions and Challenges

In this chapter, both benzoxaborole-containing nanoparticles and nanogels were applied for the controlled drug delivery of an anti-cancer drug, CAPE. The formations of the nanoparticles was confirmed by SEM imaging, and the binding between polymer–polymer and polymer–drug was measured with ARS displacement assays. A number of experiments on drug release at different pH buffers and H<sub>2</sub>O<sub>2</sub> solutions were performed. The results confirmed the pH- and ROS-responsiveness of this system, and the nanoparticles were able to release the drug over a few hours. Despite the success of responsive drug release, these results are preliminary, and there are still many limitations and challenges to address as part of this ongoing study:

- 1) The drug delivery system only releases the drug over ~3–5 h, which may not be long enough for clinical use.
- 2) The differences in the drug releasing rate between conditions of pH 7.4, pH 5.2, and 10 mM H<sub>2</sub>O<sub>2</sub> are not significant (Figure 3-12). Ideally, the nanoparticle should preserve the CAPE inside the nanocarrier at physiological pH with a minimum amount of drug leaking, and once exposed to a trigger such as a low pH and H<sub>2</sub>O<sub>2</sub>, it can release the cargos rapidly.
- 3) It is difficult to remove the unencapsulated drug before the drug releasing test, which makes it impossible to calculate the drug encapsulation efficiency (how much drug was encapsulated compared to the original amount). Not removing free drugs will result in a burst of drug release while performing the tests and cause an unpredictable variability in the final result, which will influence the assessment of a suitable nanocarrier.

There are two ways to remove the unencapsulated drug after the nanogel formation and drug encapsulation process. One method is to centrifuge the nanogel solution, discard the upper layer that contains free drug, and resuspend the nanogels in a fresh solution. Another method is to purify the nanogel solution (containing free drug) through dialysis. The free drugs can be removed through the pores on the dialysis membrane, and the nanogels would remain. However, both methods did not work satisfactorily with our system. Specifically, the high hydrophilicity/water solubility of nanogels prevents it from being centrifuged. Furthermore,

the dynamic benzoxaborole–CAPE bonds dissociate quickly upon dilution; therefore, the dialysis method also will remove most of the encapsulated CAPE, which is undesired.

Overall, this project has been only partially successful, and a more stable nanocarrier or a better drug encapsulation method needs to be developed for a more efficient, long-lasting, and stimuli-responsive drug delivery system.

## 3.5 Experimental

### 3.5.1 General Information

#### 3.5.1.1 Materials

All chemical reagents were used as received from their chemical supplier, unless specified otherwise. Alizarin Red S (ARS), hydroquinone, triethylamine (TEA), trifluoroacetic acid (TFA), 4,4'-azobis(4-cyanovaleric acid) (ACVA), capecitabine (CAPE), hydrogen peroxide (H<sub>2</sub>O<sub>2</sub>), potassium phosphate (KH<sub>2</sub>PO<sub>4</sub>), potassium phosphate dibasic (K<sub>2</sub>HPO<sub>4</sub>), acetic acid, potassium chloride (KCl), sodium chloride (NaCl), and all the organic solvents were purchased from Sigma-Aldrich. Palladium, 10% on activated carbon, and potassium *t*-butoxide, were obtained from Strem. Methacrylic anhydride and benzyl chloroformate were purchased from Alfa Aesar, and *tert*-butyl bromoacetate, 98% was purchased from Matrix Scientific. HATU was purchased from Combi-Blocks. 4-Cyanopentanoic acid dithiobenzoate (CTP) were synthesized according to a previous report.<sup>15</sup> Detailed synthesis and characterizations of **nopoldiol** monomer and amino-benzoxaborole (**2-4**) were shown in Chapter 2 (Scheme 2-2 and 2-3).

#### 3.5.1.2 Characterization and instrumentation

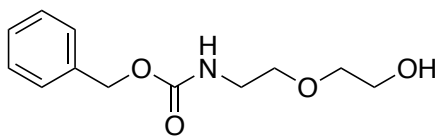
NMR spectra were recorded on INOVA-400, INOVA-500 or INOVA-700 MHz instruments. The residual solvent protons, DMSO-*d*<sub>6</sub> (2.50 ppm) and D<sub>2</sub>O (4.79 ppm), were used as internal standards, and the carbon signal (<sup>13</sup>C) of DMSO-*d*<sub>6</sub> (39.52 ppm) was used as an internal standard. MestReNova software was used to analyze all of the NMR data. The following abbreviations are used in reporting NMR data: s, singlet; d, doublet; t, triplet; q, quartet; dd, doublet of doublets; m, multiplet. High-resolution mass spectra (HRMS) using electrospray ionization (ESI) were recorded by the University of Alberta Mass Spectrometry Services

Laboratory. Fluorescence intensity was measured by SpectraMax<sup>®</sup> i3x. Scanning Electron Microscopy (Zeiss Sigma FESEM, nanoFAB, University of Alberta) was used to characterize freeze-dried nanoparticles.

### 3.5.2 Chemical Synthesis and Analytical Data

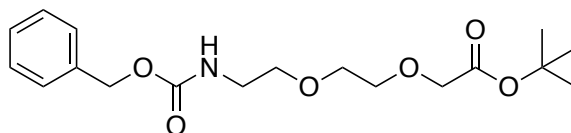
#### 3.5.2.1 Synthesis of monomer

Synthesis of 2-(2-(2-methacrylamidoethoxy)ethoxy)-benzoxaborole (LB) (Scheme 3-1):



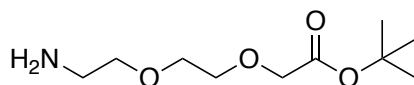
Benzyl 2-(2-hydroxyethoxy)ethylcarbamate (3-2)<sup>12</sup>: The title compound was synthesized according to a previous report with slight modifications.<sup>12</sup> 2-(2-Aminoethoxy)ethanol (3-1) (10.7 g, 0.102 mol) was dissolved in 80 mL of DCM in a single-neck round bottom flask. TEA (10.3 g, 0.102 mol) was added to the solution, and the reaction flask was cooled to 0 °C with an ice bath. Then, a solution of benzyl chloroformate (20.8 g, 0.122 mol) in 50 mL DCM was added slowly to the reaction mixture with an additional funnel at a rate of ~1 drop per second. The reaction mixture was stirred for 2 h at 0 °C, then brought to ambient temperature and stirred overnight. The reaction mixture was washed with saturated NaHCO<sub>3</sub> solution (80 mL), and the aqueous layer was extracted with DCM (3 × 100 mL). The organic layers were combined, dried with Na<sub>2</sub>SO<sub>4</sub>, filtered, and concentrated in vacuo. A colorless oil was obtained in quantitative yield (24.5 g). The product was used directly in the next step without further purifications. All spectral data corresponded to the literature.<sup>12</sup>

<sup>1</sup>H NMR (498 MHz, DMSO-*d*<sub>6</sub>) δ 7.39–7.32 (m, 4H), 7.32–7.28 (m, 1H), 7.28–7.24 (m, 1H), 5.01 (s, 2H), 4.56 (t, *J* = 6.1 Hz, 1H), 3.48 (q, *J* = 5.2 Hz, 2H), 3.41 (q, *J* = 5.2, 4.4 Hz, 4H), 3.15 (q, *J* = 5.9 Hz, 2H).



***N*-(Benzyloxycarbonyl)-2-(2-(2-aminoethoxy)ethoxy)acetate *tert*-butyl ester (3-3)**<sup>12</sup>: The title compound was synthesized according to a previous report with slight modifications.<sup>12</sup> Compound **3-2** (12.4 g, 52.0 mmol) was dissolved in 200 mL THF in a single-neck round bottom flask and was cooled to 0 °C with an ice bath. A solution of potassium *tert*-butoxide (6.16 g, 55.0 mmol) in 50 mL THF was added to the reaction mixture, and the mixture was stirred for 30 min at 0 °C. Then, *tert*-butyl bromoacetate (24.4 g, 125 mmol) was added, and the reaction mixture was stirred at 0 °C for 3 h, brought to ambient temperature, and stirred overnight. Next, 50 mL distilled water were added to the reaction mixture, followed by evaporation to discard organic solvents. The residue was extracted with EtOAc (3 × 100 mL), and the organic layers were combined, dried with Na<sub>2</sub>SO<sub>4</sub>, filtered, and concentrated in vacuo. The crude product was purified by flash chromatography (hexanes to EtOAc 9:1 to 0:1) A colorless liquid (10.8 g, 59%) was obtained as the product **3-3**. All spectral data corresponded to the literature.<sup>12</sup>

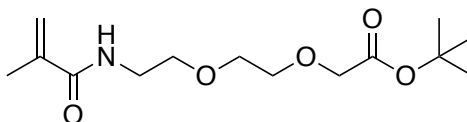
<sup>1</sup>H NMR (400 MHz, DMSO-*d*<sub>6</sub>) δ 7.39–7.32 (m, 4H), 7.32–7.28 (m, 1H), 7.28–7.23 (m, 1H), 5.01 (s, 2H), 3.97 (s, 2H), 3.59–3.48 (m, 4H), 3.41 (t, *J* = 6.0 Hz, 2H), 3.14 (q, *J* = 6.0 Hz, 2H), 1.41 (s, 9H).



***tert*-Butyl 2-(2-(2-aminoethoxy)ethoxy)acetate (3-4)**<sup>12</sup>: The title compound was synthesized according to a previous report with slight modifications.<sup>12</sup> Compound **3-3** (18.5 g, 52.5 mmol) was dissolved in 80 mL of MeOH in a single-neck round bottom flask. An adapter with both a vacuum and a nitrogen inlet was connected on the flask. The reaction mixture was evacuated by vacuum for 1 min and then purged with nitrogen. These steps were repeated three times, followed by addition of 10% Pd/C (1 mg) to the reaction solution. Then, the degassing and purging processes were repeated for another three times, and the nitrogen was replaced with a hydrogen balloon. The reaction mixture was stirred overnight, and the hydrogen was removed by vacuum. The mixture was filtered through celite, and the filtrate was concentrated

in vacuo to obtain pure product **3-4** in quantitative yield (12.2 g). The product was used directly for the next step without further purification. All spectral data corresponded to the literature.<sup>12</sup>

<sup>1</sup>H NMR (400 MHz, DMSO-*d*<sub>6</sub>) δ 3.98 (s, 2H), 3.60–3.55 (m, 2H), 3.53–3.49 (m, 2H), 3.35 (t, *J* = 5.8 Hz, 3H), 2.64 (d, *J* = 11.6 Hz, 2H), 1.42 (s, 9H).



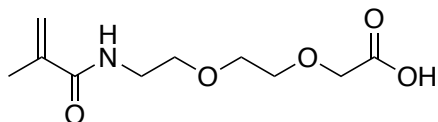
**tert-Butyl 2-(2-(2-methacrylamidoethoxy)ethoxy)acetate (3-5):** Compound **3-4** (11.4 g, 48.9 mmol) was dissolved in 100 mL MeOH in a single-neck round bottom flask. 10 mg of hydroquinone were added to the solution to prevent self-polymerization of the methacrylates during the reaction. Then, TEA (4.9 g, 48.5 mmol) was added to the reaction mixture, and the reaction was cooled to 0 °C with an ice bath. Methacrylic anhydride (8.72 g, 56.6 mmol) was added slowly to the reaction using a syringe pump with a speed of 1 mL/h. The reaction mixture was stirred at 0 °C for 3 h, brought to ambient temperature, and stirred overnight. Next, the solvent was evaporated, the residue was washed with 80 mL distilled water, and extracted with EtOAc (3 × 100 mL). The organic layers were combined, dried over Na<sub>2</sub>SO<sub>4</sub>, filtered, and concentrated in vacuo. The crude product was purified by flash chromatography (hexanes to EtOAc 9:1 to 0:1). The combined fractions were evaporated carefully by a rotovap without any heat (ideally 0 °C), and a colorless liquid (12.9 g, 44.9 mmol) was obtained as the product **3-5** (92%).

<sup>1</sup>H NMR (500 MHz, DMSO-*d*<sub>6</sub>) δ 7.90 (t, *J* = 5.1 Hz, 1H), 5.64 (s, 1H), 5.33–5.31 (m, 1H), 3.98 (s, 2H), 3.59–3.55 (m, 2H), 3.54–3.51 (m, 2H), 3.45 (t, *J* = 6.1 Hz, 2H), 3.26 (q, *J* = 6.0 Hz, 2H), 1.84 (s, 3H), 1.42 (s, 9H).

<sup>13</sup>C NMR (126 MHz, DMSO-*d*<sub>6</sub>) δ 169.3, 167.4, 139.8, 118.9, 80.6, 69.7, 69.4, 68.7, 68.0, 38.7, 27.7, 18.5.

IR (cast film, cm<sup>-1</sup>): 3348, 2978, 2930, 2872, 1747, 1662, 1624, 1530, 1147, 1124.

HRMS (ESI) for [M+Na]<sup>+</sup> C<sub>14</sub>H<sub>25</sub>NNaO<sub>5</sub>: calcd.310.1625; found 310.1623.



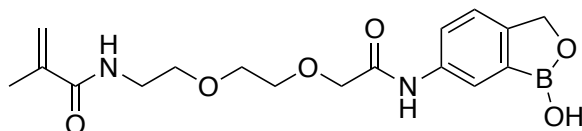
**2-(2-(2-Methacrylamidoethoxy)ethoxy)acetic acid (3-6):** Compound **3-5** (12.8 g, 44.6 mmol) was mixed with 20 mL DCM in a single-neck round bottom flask at 0 °C. TFA (5 mL, 65.3 mmol) was added to the reaction mixture, and the mixture was stirred for 3 h at 0 °C. Then, the reaction mixture was evaporated under vacuum to give product **3-6** with quantitative yield. The product was used directly for the next step without further purification.

<sup>1</sup>H NMR (500 MHz, DMSO-*d*<sub>6</sub>) δ 7.89 (s, 1H), 5.64 (s, 1H), 5.30 (s, 1H), 4.01 (d, *J* = 1.0 Hz, 2H), 3.58 (dd, *J* = 5.6, 3.2 Hz, 2H), 3.52 (dd, *J* = 5.8, 3.2 Hz, 2H), 3.45 (t, *J* = 6.1 Hz, 2H), 3.26 (q, *J* = 6.0 Hz, 2H), 1.84 (s, 3H).

<sup>13</sup>C NMR (126 MHz, DMSO-*d*<sub>6</sub>) δ 171.5, 167.4, 139.8, 118.9, 69.7, 69.4, 68.7, 67.5, 38.7, 18.5.

IR (cast film, cm<sup>-1</sup>): 3361, 2925, 2876, 2546, 1762, 1651, 1593, 1168.

HRMS (ESI) for (M-H)<sup>-</sup> C<sub>10</sub>H<sub>16</sub>NO<sub>5</sub>: calcd. 230.1034; found 230.1033.



**2-(2-(2-Methacrylamidoethoxy)ethoxy)-benzoxaborole (LB):** Compound **3-6** (10.5 g, 45.5 mmol) was mixed in 60 mL DCM, followed by an addition of TEA (7.00 g, 69.3 mmol). Then, HATU (17.3 g, 45.5 mmol) was added to the reaction mixture, and the solution was stirred for 1 h. Next, amino-benzoxaborole (**2-4**) (6.5 g, 43.2 mmol) was added to the reaction mixture, and the reaction mixture was stirred overnight under ambient conditions. Then, the reaction was partitioned between 1 M HCl solution (80 mL) and DCM (80 mL) three times. The organic layers were combined, dried over Na<sub>2</sub>SO<sub>4</sub>, filtered, and concentrated in vacuo. The crude product was purified by flash chromatography using EtOAc: DCM: MeOH 1:1:0 to 1:1:0.05. A yellow sticky oil was obtained as the product **3-6** (6.40 g, 17.7 mmol) in 41% yield.

<sup>1</sup>H NMR (400 MHz, DMSO-*d*<sub>6</sub>) δ 9.64 (s, 1H), 9.21 (s, 1H), 8.05 (d, *J* = 1.8 Hz, 1H), 7.94 (t, *J* = 5.8 Hz, 1H), 7.63 (dd, *J* = 8.2, 2.0 Hz, 1H), 7.36–7.32 (dd, *J* = 8.0, 2.6 Hz, 1H), 5.65 (dt, *J*

= 1.4, 0.9 Hz, 1H), 5.31 (p,  $J = 1.5$  Hz, 1H), 4.94 (s, 2H), 4.09 (s, 2H), 3.70–3.60 (m, 4H), 3.51 (t,  $J = 6.2$  Hz, 2H), 3.31–3.27 (m, 2H), 1.83 (dd,  $J = 1.5, 0.9$  Hz, 3H).

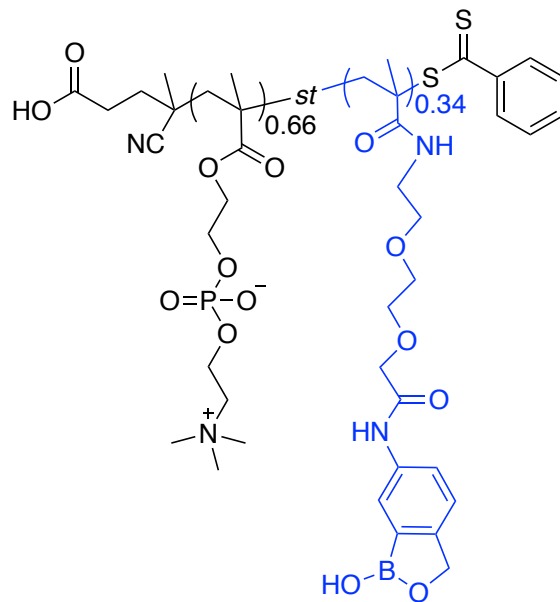
$^{13}\text{C}$  NMR (126 MHz, DMSO- $d_6$ )  $\delta$  168.13, 167.61, 149.09, 139.82, 137.10, 122.87, 121.58, 121.48, 119.07, 70.32, 70.24, 69.68, 69.36, 68.83, 18.59.

IR (cast film,  $\text{cm}^{-1}$ ): 3317, 2926, 2877, 1657, 1613, 1536, 1106.

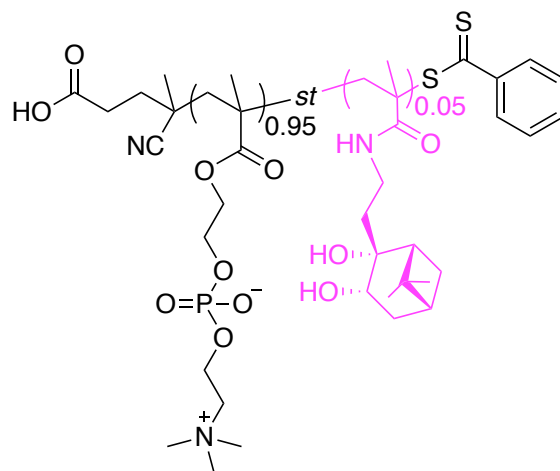
HRMS (ESI) for  $[\text{M-H}]^- \text{C}_{17}\text{H}_{23}\text{BN}_2\text{O}_6$ : calcd. 361.1576; found 361.1576.

### 3.5.2.2 Synthesis of polymers

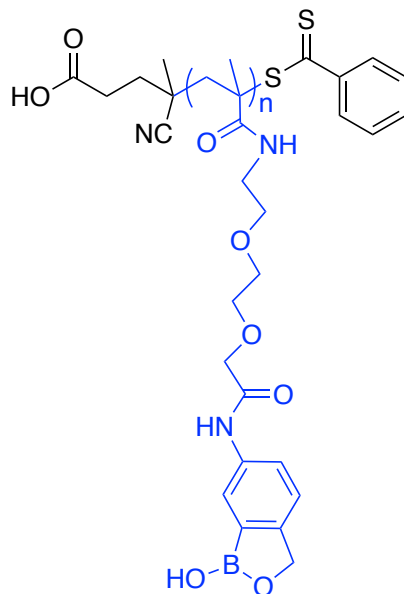
General procedures for polymerizations (Scheme 3-2): The homopolymer **PLB** and various statistical polymers (**PMLB** and **PMN**) with different ratios of components were synthesized via RAFT polymerization. Monomers were dissolved in a solution of methanol/ $\text{H}_2\text{O}$  or DMF in a 25-mL reaction tube or a suitable round bottom flask. A solution of CTP (chain transfer agent, 0.0050 mol%) and ACVA (initiator, 0.0017 mol%) was dissolved in 1 mL of methanol and added to the reaction mixture to target the degree of polymerization (DP) of 200. Then, the reaction vessel was sealed with a septum, and the neck was wrapped carefully with Parafilm, followed by degassing for 45 min with nitrogen. The reaction was performed at 70 °C with constant stirring for 16 h and then quenched in a dry-ice/acetone bath. The crude polymer solution was dialyzed using Fisherbrand<sup>®</sup> dialysis tubing (MWCO 6,000–8,000) for 1 to 2 days, and the purified polymer solution was lyophilized for 2 days to yield pure polymers. The integration of  $^1\text{H}$  NMR signals were used to calculate the composition of polymers. The numbers outside the brackets represent the molar ratios of each component in the polymers, and the numbers are totaled as 1.



**Poly(MPC-*st*-LB) (PMLB):** Prepared from **MPC** (0.414 g, 1.41 mmol), **LB** (0.509 g, 1.41 mmol), **CTP** (3.93 mg, 0.0140 mmol), and **ACVA** (1.3 mg, 0.00464 mmol) in a solvent of methanol (5 mL) and H<sub>2</sub>O (5 mL). A quantity of 0.467 g of polymer **PMLB** was obtained as a yellow sticky oil (50%).



**Poly(MPC-*st*-nopoldiol) (PMN):** Prepared from **MPC** (1.09 g, 3.70 mmol), **LB** (0.052 g, 0.195 mmol), **CTP** (5.45 mg, 0.0195 mmol), and **ACVA** (1.82 mg, 0.00650 mmol) in a solvent of methanol (5 mL) and H<sub>2</sub>O (5 mL). A quantity of 0.7 g of polymer **PMLB** was obtained as a transparent sticky oil (61%).



**PolyLB (PLB):** Prepared from **LB** (0.775 g, 2.14 mmol), CTP (3 mg, 0.0107 mmol), and ACVA (1.00 mg, 0.00357 mmol) in a solvent of 5 mL DMF. A quantity of 0.036 g of polymer **PLB** was obtained as a yellow sticky oil (4.6%).

### 3.5.3 ARS Assays

To a standard 96-well plate, ARS, **PMLB**, **PMN**, and CAPE were dissolved in pH 7.4 PBS buffer and added to the wells to reach the designed final concentrations shown in Table 3-5. Fluorescence intensity was measured by SpectraMax® i3x with an excitation of 450 nm. The measurements were performed 10 min after the mixing of different solutions.

**Table 3-5.** Design of ARS assays for (A) binding between **PMLB** and **PMN**, and (B) **PMLB** and CAPE.

A	Concentration (mM)			
	Well 1	Well 2	Well 3	Well 4
ARS	0.70	0.70	0.70	0.70
Benzoxaborole moieties (in PMLB) <sup>a</sup>	–	2.38	2.38	2.38
Nopoldiol moieties (in PMN) <sup>a</sup>	–	–	0.49	2.45
Description <sup>b</sup>	ARS	ARS + PMLB	ARS + PMLB + PMN	ARS + PMLB + 5 × PMN

B	Concentration (mM)			
	Well 1	Well 2	Well 3	Well 4
ARS	0.70	0.70	0.70	0.70
Benzoxaborole moieties (in PMLB) <sup>a</sup>	–	2.38	2.38	2.38
CAPE	–	–	8.4	16.8
Description <sup>b</sup>	ARS	ARS + PMLB	ARS + PMLB + CAPE	ARS + PMLB + 2 × CAPE

<sup>a</sup>Concentrations of benzoxaborole and nopoldiol moieties in the polymer were calculated based on the molar ratio of each component. <sup>b</sup>Corresponding to the legend in Figure 3-15.

## References

- (1) Caudle, K. E.; Thorn, C. F.; Klein, T. E.; Swen, J. J.; McLeod, H. L.; Diasio, R. B.; Schwab, M., *Clin. Pharmacol. Ther.* **2013**, *94*, 640-645.
- (2) Smith, A. D.; Datta, S. P.; Smith, G. H., *Oxford dictionary of biochemistry and molecular biology*. Oxford University Press: **1997**.
- (3) Deshayes, S.; Cabral, H.; Ishii, T.; Miura, Y.; Kobayashi, S.; Yamashita, T.; Matsumoto, A.; Miyahara, Y.; Nishiyama, N.; Kataoka, K., *J. Am. Chem. Soc.* **2013**, *135*, 15501-15507.
- (4) Van Cutsem, E.; Hoff, P. M.; Harper, P.; Bukowski, R. M.; Cunningham, D.; Dufour, P.; Graeven, U.; Lokich, J.; Madajewicz, S.; Maroun, J. A.; Marshall, J. L.; Mitchell, E. P.; Perez-Manga, G.; Rougier, P.; Schmiegel, W.; Schoelmerich, J.; Sobrero, A.; Schilsky, R. L., *Br. J. Cancer* **2004**, *90*, 1190-1197.
- (5) Organization, W. H., *Geneva: WHO* **2015**.
- (6) Ghadiri, M.; Vasheghani - Farahani, E.; Atyabi, F.; Kobarfard, F.; Mohamadyar - Toupkanlou, F.; Hosseinkhani, H., *J. Biomed. Mater. Res. A* **2017**, *105*, 2851-2864.
- (7) Aguirre-Chagala, Y. E.; Santos, J. L.; Huang, Y.; Herrera-Alonso, M., *ACS Macro Lett.* **2014**, *3*, 1249-1253.
- (8) Ma, R.; Zhang, C.; Liu, Y.; Li, C.; Xu, Y.; Li, B.; Zhang, Y.; An, Y.; Shi, L., *RSC Adv.* **2017**, *7*, 21328-21335.
- (9) Senevirathne, S. A.; Washington, K. E.; Biewer, M. C.; Stefan, M. C., *J. Mater. Chem. B* **2016**, *4*, 360-370.
- (10) Larson, N.; Ghandehari, H., *Chem. Mater.* **2012**, *24*, 840-853.
- (11) Vinogradov, S. V.; Bronich, T. K.; Kabanov, A. V., *Adv. Drug Deliv. Rev.* **2002**, *54*, 135-147.
- (12) Kohl, F.; Schmitz, J.; Furtmann, N.; Schulz-Fincke, A.-C.; Mertens, M. D.; Küppers, J.; Benkhoff, M.; Tobiasch, E.; Bartz, U.; Bajorath, J., *Org. Biomol. Chem* **2015**, *13*, 10310-10323.
- (13) Ukawa, M.; Akita, H.; Masuda, T.; Hayashi, Y.; Konno, T.; Ishihara, K.; Harashima, H., *Biomaterials* **2010**, *31*, 6355-6362.
- (14) Springsteen, G.; Wang, B., Alizarin Red S. *ChemComm* **2001**, 1608-1609.
- (15) Mitsukami, Y.; Donovan, M. S.; Lowe, A. B.; McCormick, C. L., *Macromolecules* **2001**, *34*, 2248-2256.

# Chapter 4

## Thesis Conclusions and Future Perspectives

### 4.1 Thesis Conclusions

Over the past few decades, ‘smart’ biomaterials (hydrogels, nanoparticles, etc.) that can respond to environmental stimuli, such as temperature, pH, and chemicals (glucose, GSH, ROS etc.) have been studied extensively for applications in wound dressing, targeted anti-cancer drug delivery, cell encapsulation, and tissue engineering.<sup>1-3</sup> Undoubtedly, the tremendous advancements of these biomaterials could not have been achieved without polymer and organic chemistry research.<sup>1,4</sup> The choice of cross-links, that is, the use of an appropriate chemical ligation reaction between polymer chains, is essential for the achievement of an ideal biomaterial towards specific biomedical applications. This thesis describes the use of a nopoldiol-benzoxaborolate condensation reaction in the preparation of both hydrogels and nanogels. The incorporation of this cross-linking chemistry into biomaterial synthesis was expected to provide rigid and stimuli-responsive cross-links for the formation of a stable polymer-based 3D network, thus improving the properties of the resulting biomaterials. To the best of my knowledge, there have been no studies on the use of nopoldiol-benzoxaborolate cross-links for the preparation of hydrogel/nanogel prior to this study. The unique hydrolytic stability, acid-resistant property, oxidative degradability, and bioorthogonality (towards endogenous polyols) of the nopoldiol-benzoxaborolate enable this new variant of boronic ester-containing cross-links to be a more suitable candidate for the preparation of in situ forming click hydrogels (Chapter 2) and drug-encapsulated nanogels (Chapter 3).

In Chapter 2, I described a dual-cure network (DCN) system for the preparation of a self-healing, in situ forming, and bioorthogonal hydrogel that is hydrolytically stable and acid-resistant. The design was based on the combination of rigid nopoldiol-benzoxaborolate cross-links and dynamic sugar-benzoxaborolate cross-links, where the rigid segment could stabilize the gel network even under extreme pH conditions or in polyol solutions, and the dynamic

segment could maintain the self-healing and pH-responsive properties of the hydrogel. The results show that the incorporation of nopoldiol-benzoxaborolate bioorthogonal click chemistry could accelerate the gelation process greatly, by ~10 times compared to that without **nopoldiol**. The resulting DCN hydrogel exhibits promising self-healing properties at an exceptionally wide range of pH (8.5–1.5) and can maintain its integrity for ~20 days under acidic pH (5.2 and 1.5) conditions; these are unique and promising features in the family of boronic acid-containing hydrogels. Finally, the pH-controlled drug release capability and biocompatibility of the optimal hydrogel **PBNG** were evaluated by the encapsulation/release of doxorubicin (Dox) and 3D cell encapsulation of HeLa cells, respectively. Overall, this project was highly successful and provides ample opportunity for future investigations and applications.

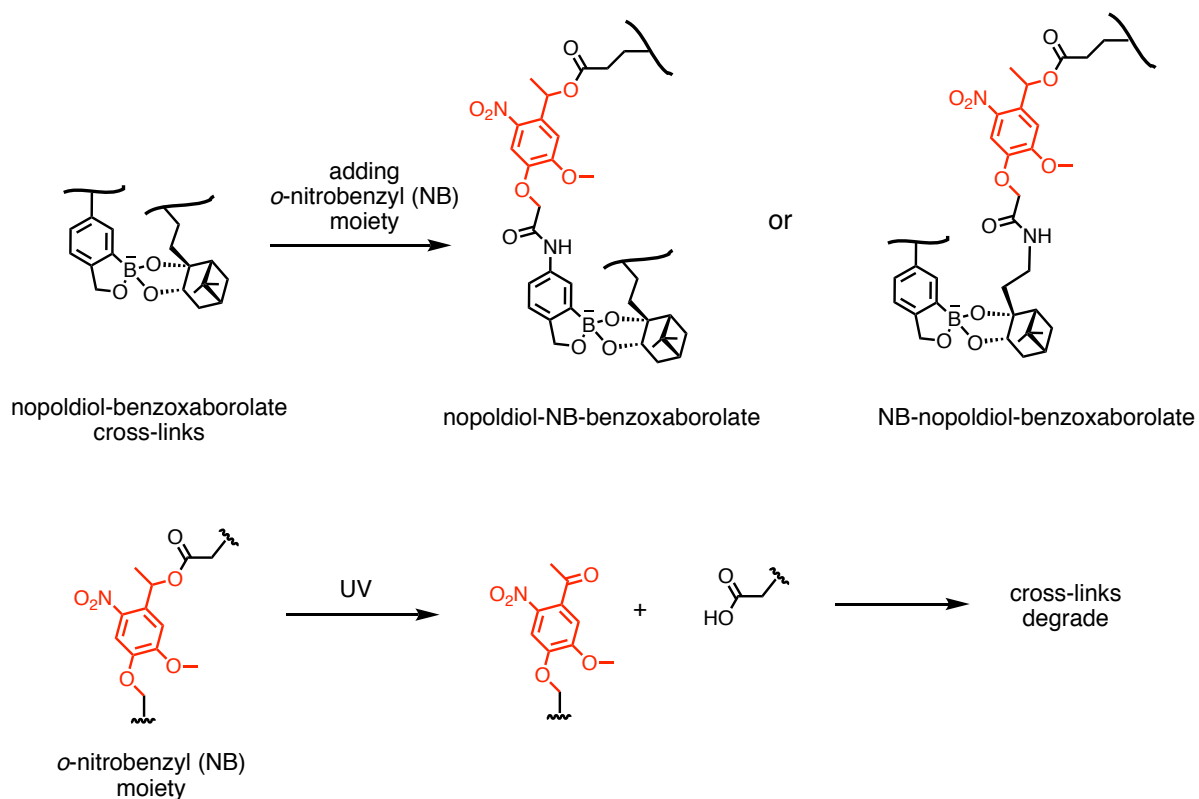
In Chapter 3, a novel nanogel system for the encapsulation of a diol-containing anti-cancer drug, capecitabine (CAPE) was described. Nano-sized 3D networks with ROS- and pH-responsiveness were developed with nopoldiol-benzoxaborolate serving as cross-links. A novel long-linker benzoxaborole-containing monomer **LB** was designed and synthesized to conjugate covalently with CAPE through arylboronic ester formation. Moreover, the improved hydrophilicity of this **LB** component was expected to be more compatible with the hydrophilic drug molecule, CAPE. This design also aimed to overcome current problems with the delivery of CAPE such as low drug carrier stability and poor binding affinity between arylboronic acids and CAPE. The results show that the optimal nanogel was able to release ~80% of CAPE over a period of 4.5 h in PBS pH 7.4 at room temperature, and a slight acceleration of drug release was found in acidic pH of 5.2 and in the presence of 10 mM H<sub>2</sub>O<sub>2</sub> in solution. However, there is still much room for improvement, including prolonged drug releasing time, higher sensitivity towards triggers, and a way to remove unencapsulated drugs for a more accurate calculation of drug encapsulation efficiency (c.f., Section 3.4).

## 4.2 Future Perspectives

### 4.2.1 Fast Hydrogel Degradation

It is important for hydrogels to be capable of degrading on demand to release cells for retrieval in applications such as cell expansion, drug screening, toxicological screening, and as models

for tissue engineering.<sup>5</sup> In Chapter 2, we demonstrated an efficient and benign bioorthogonal click reaction for the homogenous encapsulation of drug molecules and cells. However, the nopoldiol-benzoxaborolate cross-links are not readily degradable under mild physiological conditions. The only way to degrade this hydrogel rapidly is by adding oxidants such as H<sub>2</sub>O<sub>2</sub>, which would cause severe damage to cells and surrounding tissues. An alternative strategy to achieve the fast hydrogel degradation would consist in installing a light-sensitive linkage in the cross-links (Scheme 4-1), in which a *o*-nitrobenzyl (NB) moiety could be inserted either on the benzoxaborole or nopoldiol side of the nopoldiol-benzoxaborole cross-link. The NB could undergo rapid degradation under UV light and dissociate the cross-links. It is also true that the use of UV is not ideal for many biomedical applications, especially for cell encapsulation. A less harmful trigger that can induce a fast bond cleavage would be of great interest for the purposes of on demand hydrogel degradation.



**Scheme 4-1.** Proposed modification of nopoldiol-benzoxaborolate cross-links with UV-sensitive *o*-nitrobenzyl (NB) moiety.

## 4.2.2 Encapsulation of Hydrophilic and Neutral Drugs with Nanoparticles

Encapsulation of hydrophilic and neutral drugs in drug carriers is well known to be difficult because of the ease of drug diffusion in aqueous solution and the weak interaction between drug molecules and polymer matrices (Section 3.1). In Chapter 3, the development of a nanogel system composed of nopoldiol-benzoxaborolate cross-links and polymer–drug covalent conjugations was described for the encapsulation and release of CAPE. Despite the partial success of this system in controlled drug release, there are many unaddressed challenges remaining in this project, such as a short drug releasing time, insignificant differences in drug releasing rate under physiological conditions and with triggers (low pH and H<sub>2</sub>O<sub>2</sub>), and hardship in removing unencapsulated drugs (Section 3.4). One method to improve the encapsulation process would be to look for a better binding partner with CAPE to enhance the stability of the polymer–drug conjugates. An arylboronic acid with higher binding affinity with ribose (1,2-cis diol) would be ideal for this purpose. Furthermore, fine-tuning of the backbone components and the proportions of each component would be critical for the nanogel performance. For example, instead of using MPC as the backbone, PEG, DMA, or thermo-sensitive building blocks could be worth exploring.

The extension of studies presented in this thesis mentioned above constitute only a small glimpse of the vast potential of benzoxaborole and nopoldiol click chemistry in biomaterials. It is my hope that the information and future perspectives conveyed in this thesis will encourage the future development of boronic acid/ester-containing biomaterials and lead into a new era.

## References

- (1) Ebara, M.; Kotsuchibashi, Y.; Narain, R.; Idota, N.; Kim, Y.-J.; Hoffman, J. M.; Uto, K.; Aoyagi, T., *Smart biomaterials*. Springer: **2014**.
- (2) Medina, S. H., Schneider, J. P. **2017**, *Chemical Ligations in the Design of Hydrogel Materials. In Chemoselective and Bioorthogonal Ligation Reactions* (eds W. R. Algar, P. E. Dawson and I. L. Medintz).
- (3) Mo, R.; Gu, Z., *Mater. Today* **2016**, *19*, 274-283.
- (4) Buwalda, S. J.; Boere, K. W. M.; Dijkstra, P. J.; Feijen, J.; Vermonden, T.; Hennink, W. E., *J. Control. Release* **2014**, *190*, 254-273.
- (5) Truong, V. X.; Tsang, K. M.; Simon, G. P.; Boyd, R. L.; Evans, R. A.; Thissen, H.; Forsythe, J. S., *Biomacromolecules* **2015**, *16*, 2246-2253.

# Bibliography

- (1) Vert, M., *Prog. Polym. Sci.* **2007**, *32*, 755–761.
- (2) Gibas, I.; Janik, H., *Chem. Chem. Technol.* **2010**, *4*, 297–304.
- (3) Rizwan, M.; Yahya, R.; Hassan, A.; Yar, M.; Azzahari, A.; Selvanathan, V.; Sonsudin, F.; Abouloula, C., *Polymers* **2017**, *9*, 137.
- (4) Bemmelen, J., *Z Anorg Chem* **1894**, *5*, 466.
- (5) Wichterle, O.; LÍM, D., *Nature* **1960**, *185*, 117–118.
- (6) Buwalda, S. J.; Boere, K. W. M.; Dijkstra, P. J.; Feijen, J.; Vermonden, T.; Hennink, W. E., *J. Control. Release* **2014**, *190*, 254–273.
- (7) King, P. A.; Ward, J. A., *I. J. Polym. Sci. A* **1970**, *8*, 253–262.
- (8) Stafford, J. W., *Die Makromol. Chemie* **1970**, *134*, 57–69.
- (9) Nalbandian, R. M.; Henry, R. L.; Wilks, H. S., *J. of Biomed. Mater. Res.* **1972**, *6*, 583–590.
- (10) Kopecek, J., *J. Polym. Sci. A* **2009**, *47*, 5929–5946.
- (11) Otake, K.; Inomata, H.; Konno, M.; Saito, S., *Macromolecules* **1990**, *23*, 283–289.
- (12) Inomata, H.; Goto, S.; Saito, S., *Macromolecules* **1990**, *23*, 4887–4888.
- (13) Liang-chang, D.; Qi, Y.; Hoffman, A. S., *J. Control. Release* **1992**, *19*, 171–177.
- (14) Sawhney, A. S.; Pathak, C. P.; Hubbell, J. A., *Macromolecules* **1993**, *26*, 581–587.
- (15) Chujo, Y.; Sada, K.; Saegusa, T., *Macromolecules* **1993**, *26*, 6320–6323.
- (16) Chujo, Y.; Sada, K.; Saegusa, T., *Macromolecules* **1993**, *26*, 6315–6319.
- (17) Li, J.; Harada, A.; Kamachi, M., *Polym. J.* **1994**, *26*, 1019.
- (18) Cascone, M. G.; Sim, B.; Sandra, D., *Biomaterials* **1995**, *16*, 569–574.
- (19) Jeong, B.; Bae, Y. H.; Lee, D. S.; Kim, S. W., *Nature* **1997**, *388*, 860.
- (20) Petka, W. A.; Harden, J. L.; McGrath, K. P.; Wirtz, D.; Tirrell, D. A., *Science* **1998**, *281*, 389.
- (21) de Jong, S. J.; De Smedt, S. C.; Wahls, M. W. C.; Demeester, J.; Kettenes-van den Bosch, J. J.; Hennink, W. E., *Macromolecules* **2000**, *33*, 3680–3686.
- (22) Bertin, A., *Macromol. Chem. Phys.* **2012**, *213*, 2329–2352.
- (23) Dinerman, A. A.; Cappello, J.; Ghandehari, H.; Hoag, S. W., *Biomaterials* **2002**, *23*, 4203–4210.
- (24) Madan, M.; Bajaj, A.; Lewis, S.; Udupa, N.; Baig, J., *Indian J. Pharm. Sci* **2009**, *71*, 242.
- (25) Dimatteo, R.; Darling, N. J.; Segura, T., *Adv. Drug Deliv. Rev* **2018**, *127*, 167–184.
- (26) Elisseeff, J.; Anseth, K.; Sims, D.; McIntosh, W.; Randolph, M.; Langer, R., *Proc. Natl. Acad. Sci. U.S.A.* **1999**, *96*, 3104.
- (27) Yang, B.; Zhang, Y.; Zhang, X.; Tao, L.; Li, S.; Wei, Y., *Polym. Chem* **2012**, *3*, 3235–3238.
- (28) Choi, B.; Loh, X. J.; Tan, A.; Loh, C. K.; Ye, E.; Joo, M. K.; Jeong, B., *In In-Situ Gelling Polymers* **2015**, pp 5–35.
- (29) Seliktar, D., *Science* **2012**, *336*, 1124–1128.

- (30) Yang, J.-A.; Yeom, J.; Hwang, B. W.; Hoffman, A. S.; Hahn, S. K., *Prog. Polym. Sci.* **2014**, *39*, 1973–1986.
- (31) Yu, L.; Ding, J., *Chem. Soc. Rev.* **2008**, *37*, 1473–1481.
- (32) Tibbitt, M. W.; Anseth, K. S., *Biotechnol. Bioeng.* **2009**, *103*, 655–663.
- (33) Lee, K. Y.; Mooney, D. J., *Chem. Rev.* **2001**, *101*, 1869–1880.
- (34) Heskins, M.; Guillet, J. E., *J Macromol. Sci. A* **1968**, *2*, 1441–1455.
- (35) Qiu, Y.; Park, K., *Adv. Drug Deliv. Rev* **2012**, *64*, 49–60.
- (36) Ci, T.; Chen, L.; Yu, L.; Ding, J., *Sci. Rep.* **2014**, *4*, 5473.
- (37) Lutz, J.-F.; Akdemir, Ö.; Hoth, A., *J. Am. Chem. Soc.* **2006**, *128*, 13046–13047.
- (38) Schmaljohann, D., *Adv. Drug Deliv. Rev* **2006**, *58*, 1655–1670.
- (39) Kocak, G.; Tuncer, C.; Bütün, V., *Polym. Chem* **2017**, *8*, 144–176.
- (40) Salem, A. K.; Rose, F. R. A. J.; Oreffo, R. O. C.; Yang, X.; Davies, M. C.; Mitchell, J. R.; Roberts, C. J.; Stolnik-Trenkic, S.; Tandler, S. J. B.; Williams, P. M.; Shakesheff, K. M., *Adv. Mater.* **2003**, *15*, 210–213.
- (41) Foo, C. T. W. P.; Lee, J. S.; Mulyasmita, W.; Parisi-Amon, A.; Heilshorn, S. C., *Proc. Natl. Acad. Sci. U.S.A.* **2009**, *106*, 22067–22072.
- (42) Miyata, T.; Asami, N.; Uragami, T., *J. Polym. Sci. B* **2009**, *47*, 2144–2157.
- (43) Um, S. H.; Lee, J. B.; Park, N.; Kwon, S. Y.; Umbach, C. C.; Luo, D., *Nat. Mater.* **2006**, *5*, 797.
- (44) Li, J.; Loh, X. J., *Adv. Drug Deliv. Rev* **2008**, *60*, 1000–1017.
- (45) Hoffman, A. S., *Adv. Drug Deliv. Rev* **2012**, *64*, 18–23.
- (46) Ding, X.; Wang, Y., *J. Mater. Chem. B* **2017**, *5*, 887–906.
- (47) Blasco, E.; Wegener, M.; Barner-Kowollik, C., *Adv. Mater.* **2017**, *29*, 1604005.
- (48) Odian, G., *Principles of polymerization*. John Wiley & Sons: **2004**.
- (49) Hoyle, C. E.; Bowman, C. N., *Angew. Chem. Int. Ed.* **2010**, *49*, 1540–1573.
- (50) Nair, D. P.; Podgorski, M.; Chatani, S.; Gong, T.; Xi, W.; Fenoli, C. R.; Bowman, C. N., *Chem. Mater.* **2013**, *26*, 724–744.
- (51) Lowe, A. B., *Polym. Chem* **2014**, *5*, 4820–4870.
- (52) Morgan, C.; Magnotta, F.; Ketley, A., *J. Polym. Sci. A* **1977**, *15*, 627–645.
- (53) Agard, N. J.; Prescher, J. A.; Bertozzi, C. R., *J. Am. Chem. Soc.* **2004**, *126*, 15046–15047.
- (54) Baskin, J. M.; Prescher, J. A.; Laughlin, S. T.; Agard, N. J.; Chang, P. V.; Miller, I. A.; Lo, A.; Codelli, J. A.; Bertozzi, C. R., *Proc. Natl. Acad. Sci. U.S.A.* **2007**, *104*, 16793–16797.
- (55) Blasco, E.; Wegener, M.; Barner-Kowollik, C., *Adv. Mater.* **2017**, *29*, 1604005.
- (56) Rydholm, A. E.; Bowman, C. N.; Anseth, K. S., *Biomaterials* **2005**, *26*, 4495–4506.
- (57) Hoyle, C. E.; Lowe, A. B.; Bowman, C. N., *Chem. Soc. Rev.* **2010**, *39*, 1355–1387.
- (58) Shih, H.; Lin, C.-C., *Biomacromolecules* **2012**, *13*, 2003–2012.
- (59) Rydholm, A. E.; Anseth, K. S.; Bowman, C. N., *Acta Biomater.* **2007**, *3*, 449–455.
- (60) Rydholm, A. E.; Reddy, S. K.; Anseth, K. S.; Bowman, C. N., *Polymer* **2007**, *48*, 4589–4600.
- (61) Dong, D.; Li, J.; Cui, M.; Wang, J.; Zhou, Y.; Luo, L.; Wei, Y.; Ye, L.; Sun, H.; Yao, F., *ACS Appl. Mater. Interfaces* **2016**, *8*, 4442–4455.

- (62) Macdougall, L. J.; Truong, V. X.; Dove, A. P., *ACS Macro Lett.* **2017**, *6*, 93–97.
- (63) Saito, H.; Hoffman, A. S.; Ogawa, H. I., *J. Bioact. Compat. Polym.* **2007**, *22*, 589–601.
- (64) Wang, T.; Turhan, M.; Gunasekaran, S., *Polym. Int.* **2004**, *53*, 911–918.
- (65) Tan, H.; Chu, C. R.; Payne, K. A.; Marra, K. G., *Biomaterials* **2009**, *30*, 2499–2506.
- (66) Truong, V. X.; Tsang, K. M.; Simon, G. P.; Boyd, R. L.; Evans, R. A.; Thissen, H.; Forsythe, J. S., *Biomacromolecules* **2015**, *16*, 2246–2253.
- (67) Hodgson, S. M.; McNelles, S. A.; Abdullahu, L.; Marozas, I. A.; Anseth, K. S.; Adronov, A., *Biomacromolecules* **2017**, *18*, 4054–4059.
- (68) Hodgson, S. M.; Bakaic, E.; Stewart, S. A.; Hoare, T.; Adronov, A., *Biomacromolecules* **2016**, *17*, 1093–1100.
- (69) Xu, J.; Filion, T. M.; Prifti, F.; Song, J., *Chem. Asian J.* **2011**, *6*, 2730–2737.
- (70) Yu, F.; Cao, X.; Li, Y.; Zeng, L.; Zhu, J.; Wang, G.; Chen, X., *Polym. Chem.* **2014**, *5*, 5116–5123.
- (71) García-Astrain, C.; Gandini, A.; Peña, C.; Algar, I.; Eceiza, A.; Corcuera, M.; Gabilondo, N., *RSC Adv.* **2014**, *4*, 35578–35587.
- (72) Truong, V. X.; Ablett, M. P.; Richardson, S. M.; Hoyland, J. A.; Dove, A. P., *J. Am. Chem. Soc.* **2015**, *137*, 1618–1622.
- (73) Alge, D. L.; Azagarsamy, M. A.; Donohue, D. F.; Anseth, K. S., *Biomacromolecules* **2013**, *14*, 949–953.
- (74) Lang, K.; Chin, J. W., *ACS Chem. Biol.* **2014**, *9*, 16–20.
- (75) Patterson, D. M.; Nazarova, L. A.; Prescher, J. A., *ACS Chem. Biol.* **2014**, *9*, 592–605.
- (76) Taylor, D. L.; in het Panhuis, M., *Adv. Mater.* **2016**, *28*, 9060–9093.
- (77) Diba, M.; Spaans, S.; Ning, K.; Ippel, B. D.; Yang, F.; Loomans, B.; Dankers, P. Y.; Leeuwenburgh, S. C., *Adv. Mater. Interfaces* **2018**, *5*, 1800118.
- (78) Shi, Y.-g.; Wang, J.-w.; Li, H.; Hu, G.-f.; Li, X.; Møllerup, S. K.; Wang, N.; Peng, T.; Wang, S., *Chem. Sci.* **2018**, *9*, 1902–1911.
- (79) Wei, Z.; Yang, J. H.; Zhou, J.; Xu, F.; Zrínyi, M.; Dussault, P. H.; Osada, Y.; Chen, Y. M., *Chem. Soc. Rev.* **2014**, *43*, 8114–8131.
- (80) Zou, W.; Dong, J.; Luo, Y.; Zhao, Q.; Xie, T., *Adv. Mater.* **2017**, *29*, 1606100.
- (81) Shu, X. Z.; Liu, Y.; Luo, Y.; Roberts, M. C.; Prestwich, G. D., *Biomacromolecules* **2002**, *3*, 1304–1311.
- (82) Shu, X. Z.; Liu, Y.; Palumbo, F.; Prestwich, G. D., *Biomaterials* **2003**, *24*, 3825–3834.
- (83) Wu, Z.; Zhang, X.; Zheng, C.; Li, C.; Zhang, S.; Dong, R.; Yu, D., *Eur. J. Pharm. Sci.* **2009**, *37*, 198–206.
- (84) Lei, Z. Q.; Xiang, H. P.; Yuan, Y. J.; Rong, M. Z.; Zhang, M. Q., *Chem. Mater.* **2014**, *26*, 2038–2046.
- (85) Kemp, M.; Go, Y.-M.; Jones, D. P., *Free Radic. Biol. Med.* **2008**, *44*, 921–937.
- (86) Wei, Z.; Yang, J. H.; Du, X. J.; Xu, F.; Zrínyi, M.; Osada, Y.; Li, F.; Chen, Y. M., *Macromol. Rapid Commun.* **2013**, *34*, 1464–1470.
- (87) Deng, C. C.; Brooks, W. L. A.; Abboud, K. A.; Sumerlin, B. S., *ACS Macro Lett.* **2015**, *4*, 220–224.
- (88) Roberts, M. C.; Hanson, M. C.; Massey, A. P.; Karren, E. A.; Kiser, P. F., *Adv. Mater.* **2007**, *19*, 2503–2507.

- (89) He, L.; Fullenkamp, D. E.; Rivera, J. G.; Messersmith, P. B., *ChemComm* **2011**, *47*, 7497–7499.
- (90) Medina, S. H., Schneider, J. P. **2017**, *Chemical Ligations in the Design of Hydrogel Materials. In Chemoselective and Bioorthogonal Ligation Reactions* (eds W. R. Algar, P. E. Dawson and I. L. Medintz).
- (91) Yan, J.; Springsteen, G.; Deeter, S.; Wang, B., *Tetrahedron* **2004**, *60*, 11205–11209.
- (92) Hoare, T. R.; Kohane, D. S., *Polymer* **2008**, *49*, 1993–2007.
- (93) Li, J.; Mooney, D. J., *Nat Rev Mater.* **2016**, *1*, 16071.
- (94) Nicodemus, G. D.; Bryant, S. J., *Tissue Eng Part B Rev* **2008**, *14*, 149–165.
- (95) Seliktar, D., *Science* **2012**, *336*, 1124.
- (96) Jiang, Y.; Chen, J.; Deng, C.; Suuronen, E. J.; Zhong, Z., *Biomaterials* **2014**, *35*, 4969–4985.
- (97) McKay, Craig S.; Finn, M. G., *Chem. Biol.* **2014**, *21*, 1075–1101.
- (98) Kolb, H. C.; Finn, M. G.; Sharpless, K. B., *Angew. Chem. Int. Ed.* **2001**, *40*, 2004–2021.
- (99) Fan, Y.; Deng, C.; Cheng, R.; Meng, F.; Zhong, Z., *Biomacromolecules* **2013**, *14*, 2814–2821.
- (100) Xu, J.; Feng, E.; Song, J., *J. Am. Chem. Soc.* **2014**, *136*, 4105–4108.
- (101) Ghanian, M. H.; Mirzadeh, H.; Baharvand, H., *Biomacromolecules* **2018**, *19*, 1646–1662.
- (102) Xu, Z.; Bratlie, K. M., *ACS Biomater. Sci. Eng.* **2018**, *4*, 2276–2291.
- (103) Guan, Y.; Zhang, Y., *Chem. Soc. Rev.* **2013**, *42*, 8106–8121.
- (104) Hall, Dennis G., 2<sup>nd</sup> Ed. *Boronic acids: preparation, applications in organic synthesis and medicine.* John Wiley & Sons, **2011**.
- (105) Li, Q.; Lü, C.; Liu, Z., *J. Chromatogr. A* **2013**, *1305*, 123–130.
- (106) Alexeev, V. L.; Das, S.; Finegold, D. N.; Asher, S. A., *Clin. Chem.* **2004**, *50*, 2353.
- (107) Liu, Y.; Ren, L.; Liu, Z., *ChemComm* **2011**, *47*, 5067–5069.
- (108) Wulff, G., *Pure Appl. Chem.* **1982**, *54*, 2093–2102.
- (109) Li, H.; Liu, Y.; Liu, J.; Liu, Z., *ChemComm* **2011**, *47*, 8169–8171.
- (110) Chen, Y.; Wang, W.; Wu, D.; Nagao, M.; Hall, D. G.; Thundat, T.; Narain, R., **2018**, *19*, 596–605.
- (111) Chen, Y.; Diaz-Dussan, D.; Wu, D.; Wang, W.; Peng, Y.-Y.; Asha, A. B.; Hall, D. G.; Ishihara, K.; Narain, R., *ACS Macro Lett.* **2018**, *7*, 904–908.
- (112) Wang, Y.; Li, L.; Kotsuchibashi, Y.; Vshyvenko, S.; Liu, Y.; Hall, D.; Zeng, H.; Narain, R., *ACS Biomater. Sci. Eng.* **2016**, *2*, 2315–2323.
- (113) Kotsuchibashi, Y.; Ebara, M.; Sato, T.; Wang, Y.; Rajender, R.; Hall, D. G.; Narain, R.; Aoyagi, T., *J. Phys. Chem. B* **2015**, *119*, 2323–2329.
- (114) Kotsuchibashi, Y.; Agustin, R. V. C.; Lu, J.-Y.; Hall, D. G.; Narain, R., *ACS Macro Lett.* **2013**, *2*, 260–264.
- (115) Diaz-Dussan, D.; Nakagawa, Y.; Peng, Y.-Y.; C, L. V. S.; Ebara, M.; Kumar, P.; Narain, R., *ACS Macro Lett.* **2017**, *6*, 768–774.
- (116) Alberti, K. G. M. M.; Zimmet, P. Z., *Diabet. Med.* **1998**, *15*, 539–553.
- (117) Shiino, D.; Murata, Y.; Kubo, A.; Kim, Y. J.; Kataoka, K.; Koyama, Y.; Kikuchi, A.; Yokoyama, M.; Sakurai, Y.; Okano, T., *J. Control Release* **1995**, *37*, 269–276.

- (118) Miyata, T.; Uragami, T.; Nakamae, K., *Adv. Drug Deliv. Rev* **2002**, *54*, 79–98.
- (119) Zhang, M.; Song, C.-C.; Su, S.; Du, F.-S.; Li, Z.-C., *ACS Appl. Mater. Interfaces* **2018**, *10*, 7798–7810.
- (120) Zhang, M.; Song, C.-C.; Du, F.-S.; Li, Z.-C., *ACS Appl. Mater. Interfaces* **2017**, *9*, 25905–25914.
- (121) van der Vliet, A.; Janssen-Heininger, Y. M., *J. Cell. Biochem.* **2014**, *115*, 427–435.
- (122) Hasirci, V.; Vrana, E.; Zorlutuna, P.; Ndreu, A.; Yilgor, P.; Basmanav, F. B.; Aydin, E., *J Biomater Sci Polym Ed* **2006**, *17*, 1241–1268.
- (123) Mo, R.; Gu, Z., *Mater. Today* **2016**, *19*, 274–283.
- (124) Chacko, R. T.; Ventura, J.; Zhuang, J.; Thayumanavan, S., *Adv. Drug Deliv. Rev* **2012**, *64*, 836–851.
- (125) Brigger, I.; Dubernet, C.; Couvreur, P., *Adv. Drug Deliv. Rev* **2012**, *64*, 24–36.
- (126) Huang, Y.; Gao, Y.; Chen, T.; Xu, Y.; Lu, W.; Yu, J.; Xiao, Y.; Liu, S., *ACS Biomater. Sci. Eng.* **2017**, *3*, 3364–3375.
- (127) Wang, J.; Zhang, Z.; Wang, X.; Wu, W.; Jiang, X., *J. Control. Release* **2013**, *168*, 1–9.
- (128) Zhang, T.; Chen, X.; Xiao, C.; Zhuang, X.; Chen, X., *Polym. Chem* **2017**, *8*, 6209–6216.
- (129) Li, J.; Dirisala, A.; Ge, Z.; Wang, Y.; Yin, W.; Ke, W.; Toh, K.; Xie, J.; Matsumoto, Y.; Anraku, Y., *Angew. Chem. Int. Ed.* **2017**, *56*, 14025–14030.
- (130) Qiu, F. Y.; Zhang, M.; Ji, R.; Du, F. S.; Li, Z. C., *Macromol. Rapid Commun* **2015**, *36*, 2012–2018.
- (131) Zhang, X.; Chen, B.; He, M.; Zhang, Y.; Peng, L.; Hu, B., *Analyst* **2016**, *141*, 1286–1293.
- (132) Deshayes, S.; Cabral, H.; Ishii, T.; Miura, Y.; Kobayashi, S.; Yamashita, T.; Matsumoto, A.; Miyahara, Y.; Nishiyama, N.; Kataoka, K., *J. Am. Chem. Soc.* **2013**, *135*, 15501–15507.
- (133) Canal, F.; Sanchis, J.; Vicent, M. J., *Curr. Opin. Biotechnol.* **2011**, *22*, 894–900.
- (134) Aguirre-Chagala, Y. E.; Santos, J. L.; Huang, Y.; Herrera-Alonso, M., *ACS Macro Lett.* **2014**, *3*, 1249–1253.
- (135) Lv, S.; Wu, Y.; Cai, K.; He, H.; Li, Y.; Lan, M.; Chen, X.; Cheng, J.; Yin, L., *J. Am. Chem. Soc.* **2018**, *140*, 1235–1238.
- (136) Toh, W. S.; Loh, X. J., *Mater. Sci. Eng. C.* **2014**, *45*, 690–697.
- (137) Wang, W.; Narain, R.; Zeng, H., *Front Chem* **2018**, *6*, 497.
- (138) Akgun, B.; Hall, D. G., *Angew. Chem. Int. Ed.* **2016**, *55*, 3909–3913.
- (139) Akgun, B.; Li, C.; Hao, Y.; Lambkin, G.; Derda, R.; Hall, D. G., *J. Am. Chem. Soc.* **2017**, *139*, 14285–14291.
- (140) Yang, Y.; Ding, X.; Urban, M. W., *Prog. Polym. Sci.* **2015**, *49–50*, 34–59.
- (141) Rizwan, M.; Yahya, R.; Hassan, A.; Yar, M.; Azzahari, A.; Selvanathan, V.; Sonsudin, F.; Abouloula, C., *Polymers* **2017**, *9*, 137.
- (142) Schmaljohann, D., *Adv. Drug Deliv. Rev* **2006**, *58*, 1655–1670.
- (143) Kunihiro, K.; Dumais, L.; Lafitte, G.; Varvier, E.; Tomas, L.; Harris, C. S., *Adv. Synth. Catal.* **2018**, *360*, 2757–2761.
- (144) Fu, Z.; He, J.; Tong, A.; Xie, Y.; Wei, Y., *Synthesis* **2013**, *45*, 2843–2852.

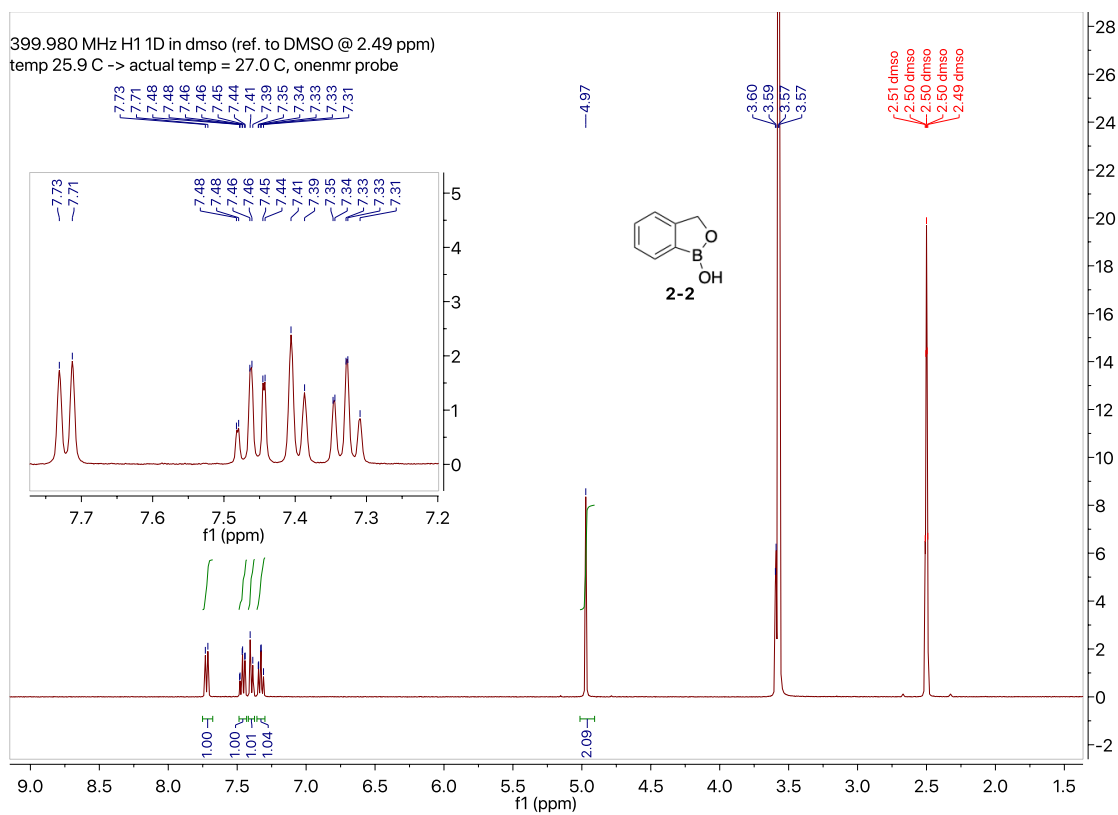
- (145) Samaniego Lopez, C.; Hebe Martínez, J.; Uhrig, M. L.; Coluccio Leskow, F.; Spagnuolo, C. C., *Chem. Eur. J* **2018**, *24*, 6344–6348.
- (146) Schumacher, S.; Grüneberger, F.; Katterle, M.; Hettrich, C.; Hall, D. G.; Scheller, F. W.; Gajovic-Eichelmann, N., *Polymer* **2011**, *52*, 2485–2491.
- (147) Adamczyk-Woźniak, A.; Cyrański, M. K.; Jakubczyk, M.; Klimentowska, P.; Koll, A.; Kołodziejczak, J.; Pojmaj, G.; Żubrowska, A.; Żukowska, G. Z.; Sporzyński, A., *J. Phys. Chem. A* **2010**, *114*, 2324–2330.
- (148) Bałczewski, P.; Bachowska, B.; Białas, T.; Biczak, R.; Wieczorek, W. M.; Balińska, A., *J. Agric. Food Chem.* **2007**, *55*, 1881–1892.
- (149) Deng, Z.; Bouchékif, H.; Babooram, K.; Housni, A.; Choytun, N.; Narain, R., *J. Polym. Sci. A* **2008**, *46*, 4984–4996.
- (150) Deng, Z.; Ahmed, M.; Narain, R., *J. Polym. Sci. A* **2009**, *47*, 614–627.
- (151) Deng, Z.; Li, S.; Jiang, X.; Narain, R., *Macromolecules* **2009**, *42*, 6393–6405.
- (152) Gibas, I.; Janik, H., *Chem. Chem. Technol.* **2010**, *4*, 297–304.
- (153) Yang, T.; Long, H.; Malkoch, M.; Kristofer Gamstedt, E.; Berglund, L.; Hult, A., *J. Polym. Sci. A* **2011**, *49*, 4044–4054.
- (154) Chen, Y.; Diaz-Dussan, D.; Wu, D.; Wang, W.; Peng, Y.-Y.; Asha, A. B.; Hall, D. G.; Ishihara, K.; Narain, R., *ACS Macro Lett.* **2018**, *7*, 904–908.
- (155) Ishihara, K.; Mu, M.; Konno, T.; Inoue, Y.; Fukazawa, K., *J. Biomater. Sci. Polym. Ed* **2017**, *28*, 884–899.
- (156) Abraham, G. A.; de Queiroz, A. A. A.; Román, J. S., *Biomaterials* **2001**, *22*, 1971–1985.
- (157) Dowlut, M.; Hall, D. G., *J. Am. Chem. Soc.* **2006**, *128*, 4226–4227.
- (158) Bérubé, M.; Dowlut, M.; Hall, D. G., *J. Org. Chem.* **2008**, *73*, 6471–6479.
- (159) Matteson, D. S.; Man, H.-W., *J. Org. Chem.* **1996**, *61*, 6047–6051.
- (160) Diaz-Dussan, D.; Nakagawa, Y.; Peng, Y.-Y.; C, L. V. S.; Ebara, M.; Kumar, P.; Narain, R., *ACS Macro Lett.* **2017**, *6*, 768–774.
- (161) Peng, Y.-Y.; Diaz-Dussan, D.; Kumar, P.; Narain, R., *Biomacromolecules* **2018**, *19*, 4052–4058.
- (162) Peng, Y.-Y.; Diaz-Dussan, D.; Kumar, P.; Narain, R., *Bioconjugate Chem.* **2018**, *30*, 405–412.
- (163) Vshyvenko, S.; Clapson, M. L.; Suzuki, I.; Hall, D. G., *ACS Medicinal Chemistry Letters* **2016**, *7*, 1097–1101.
- (164) Mo, R.; Gu, Z., *Mater. Today* **2016**, *19*, 274–283.
- (165) Lee, K. Y.; Mooney, D. J., *Chem. Rev.* **2001**, *101*, 1869–1880.
- (166) Wang, Y.; Zhang, X.; Mu, J.; Li, C., *New J. Chem.* **2013**, *37*, 796–803.
- (167) Glasoe, P. K.; Long, F., *J. Phys. Chem. A* **1960**, *64*, 188–190.
- (168) Chen, Y.; Wang, W.; Wu, D.; Nagao, M.; Hall, D. G.; Thundat, T.; Narain, R., *Biomacromolecules* **2018**, *19*, 596–605.
- (169) Zhang, Y.; Fu, C.; Li, Y.; Wang, K.; Wang, X.; Wei, Y.; Tao, L., *Polym. Chem* **2017**, *8*, 537–544.
- (170) Caudle, K. E.; Thorn, C. F.; Klein, T. E.; Swen, J. J.; McLeod, H. L.; Diasio, R. B.; Schwab, M., *Clin. Pharmacol. Ther.* **2013**, *94*, 640–645.

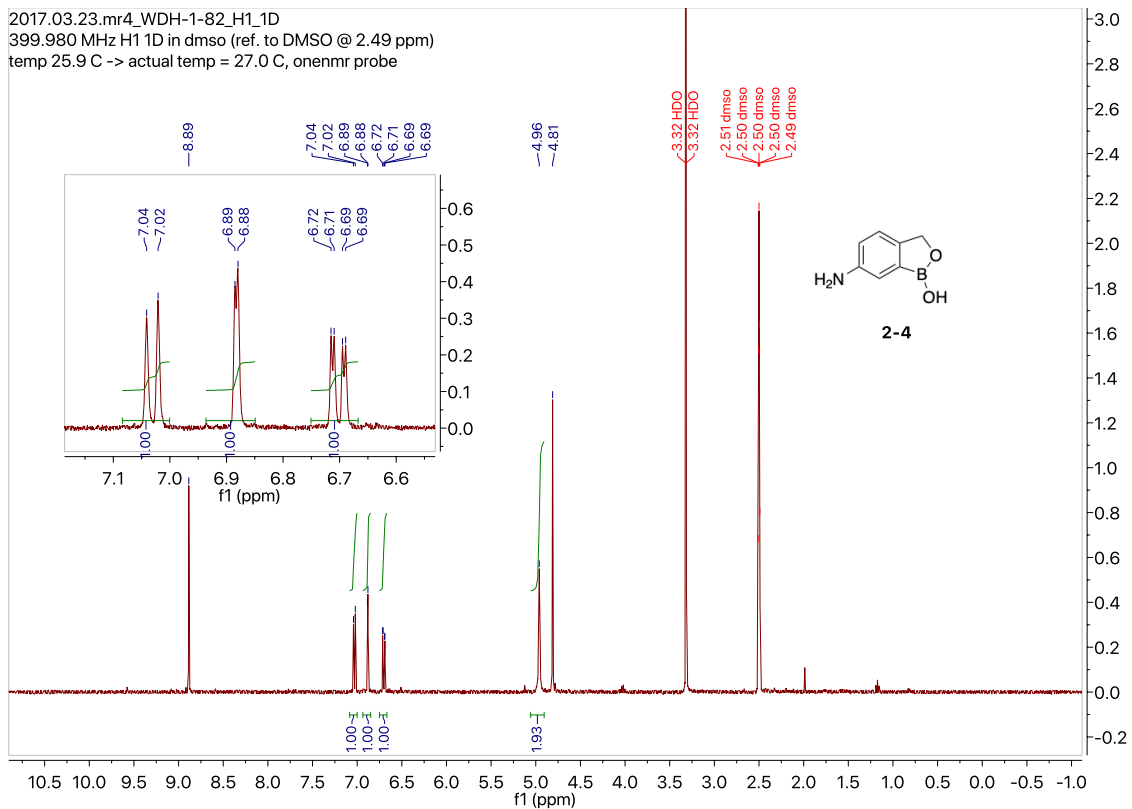
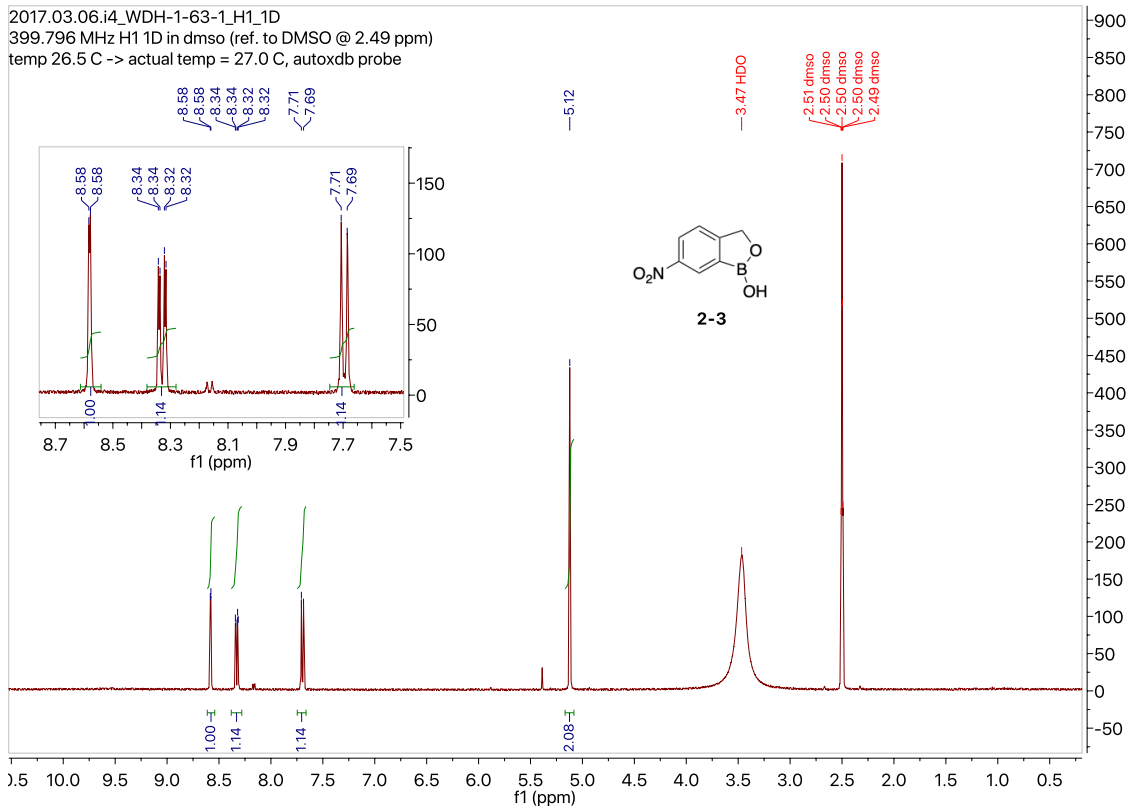
- (171) Smith, A. D.; Datta, S. P.; Smith, G. H., *Oxford dictionary of biochemistry and molecular biology*. Oxford University Press: **1997**.
- (172) Deshayes, S.; Cabral, H.; Ishii, T.; Miura, Y.; Kobayashi, S.; Yamashita, T.; Matsumoto, A.; Miyahara, Y.; Nishiyama, N.; Kataoka, K., *J. Am. Chem. Soc.* **2013**, *135*, 15501-15507.
- (173) Van Cutsem, E.; Hoff, P. M.; Harper, P.; Bukowski, R. M.; Cunningham, D.; Dufour, P.; Graeven, U.; Lokich, J.; Madajewicz, S.; Maroun, J. A.; Marshall, J. L.; Mitchell, E. P.; Perez-Manga, G.; Rougier, P.; Schmiegel, W.; Schoelmerich, J.; Sobrero, A.; Schilsky, R. L., *Br. J. Cancer* **2004**, *90*, 1190-1197.
- (174) Organization, W. H., *Geneva: WHO* **2015**.
- (175) Ghadiri, M.; Vasheghani - Farahani, E.; Atyabi, F.; Kobarfard, F.; Mohamadyar - Toupkanlou, F.; Hosseinkhani, H., *J. Biomed. Mater. Res. A* **2017**, *105*, 2851-2864.
- (176) Aguirre-Chagala, Y. E.; Santos, J. L.; Huang, Y.; Herrera-Alonso, M., *ACS Macro Lett.* **2014**, *3*, 1249-1253.
- (177) Ma, R.; Zhang, C.; Liu, Y.; Li, C.; Xu, Y.; Li, B.; Zhang, Y.; An, Y.; Shi, L., *RSC Adv.* **2017**, *7*, 21328-21335.
- (9) Senevirathne, S. A.; Washington, K. E.; Biewer, M. C.; Stefan, M. C., *J. Mater. Chem. B* **2016**, *4*, 360-370.
- (178) Larson, N.; Ghandehari, H., *Chem. Mater.* **2012**, *24*, 840-853.
- (179) Vinogradov, S. V.; Bronich, T. K.; Kabanov, A. V., *Adv. Drug Deliv. Rev.* **2002**, *54*, 135-147.
- (180) Kohl, F.; Schmitz, J.; Furtmann, N.; Schulz-Fincke, A.-C.; Mertens, M. D.; Küppers, J.; Benkhoff, M.; Tobiasch, E.; Bartz, U.; Bajorath, J., *Org. Biomol. Chem* **2015**, *13*, 10310-10323.
- (181) Ukawa, M.; Akita, H.; Masuda, T.; Hayashi, Y.; Konno, T.; Ishihara, K.; Harashima, H., *Biomaterials* **2010**, *31*, 6355-6362.
- (182) Springsteen, G.; Wang, B., Alizarin Red S. *ChemComm* **2001**, 1608-1609.
- (183) Mitsukami, Y.; Donovan, M. S.; Lowe, A. B.; McCormick, C. L., *Macromolecules* **2001**, *34*, 2248-2256.
- (184) Alterio, V.; Cadoni, R.; Esposito, D.; Vullo, D.; Di Fiore, A.; Monti, S. M.; Caporale, A.; Ruvo, M.; Sechi, M.; Dumy, P., *ChemComm* **2016**, *52*, 11983-11986.
- (185) Li, J.; Ma, L.; Li, X.; Lu, C.; Liu, H., *Ind. Eng. Chem. Res.* **2005**, *44*, 5478-5482.
- (186) Kotsuchibashi, Y.; Agustin, R. V. C.; Lu, J.-Y.; Hall, D. G.; Narain, R., *ACS Macro Lett.* **2013**, *2*, 260-264.
- (187) Warneke, J.; Wang, Z.; Zeller, M.; Leibfritz, D.; Plaumann, M.; Azov, V. A., *Tetrahedron* **2014**, *70*, 6515-6521.

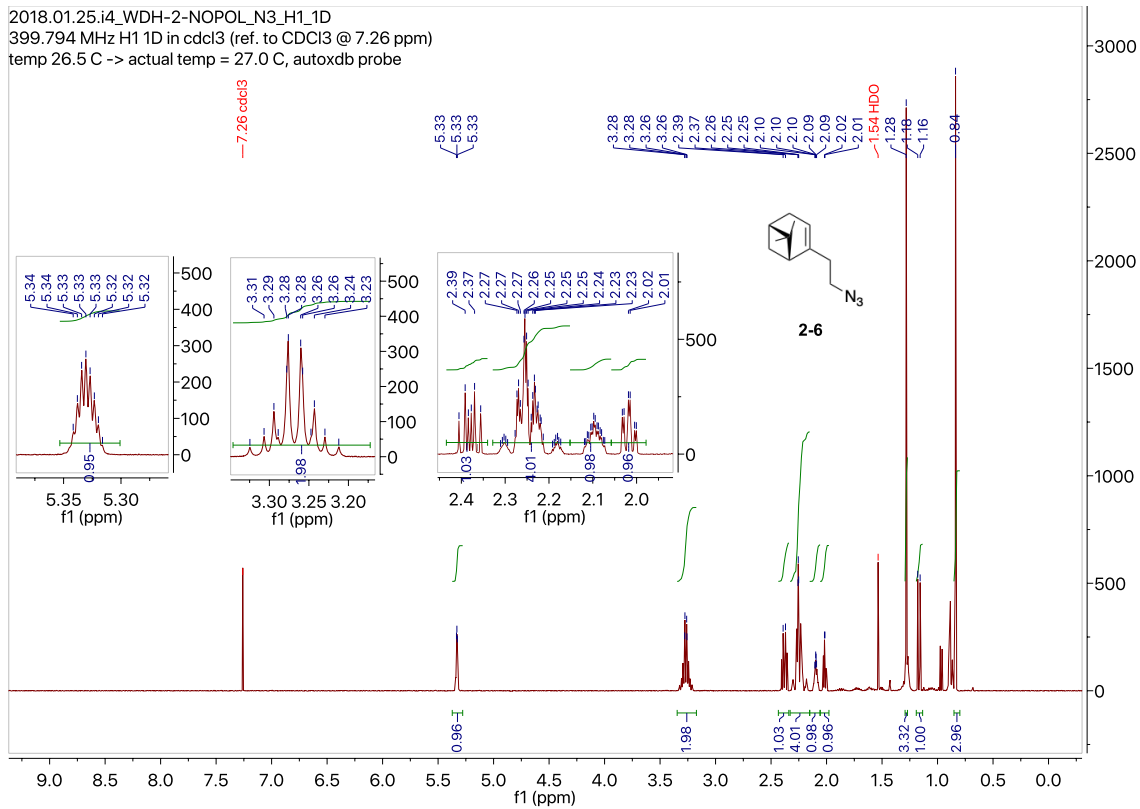
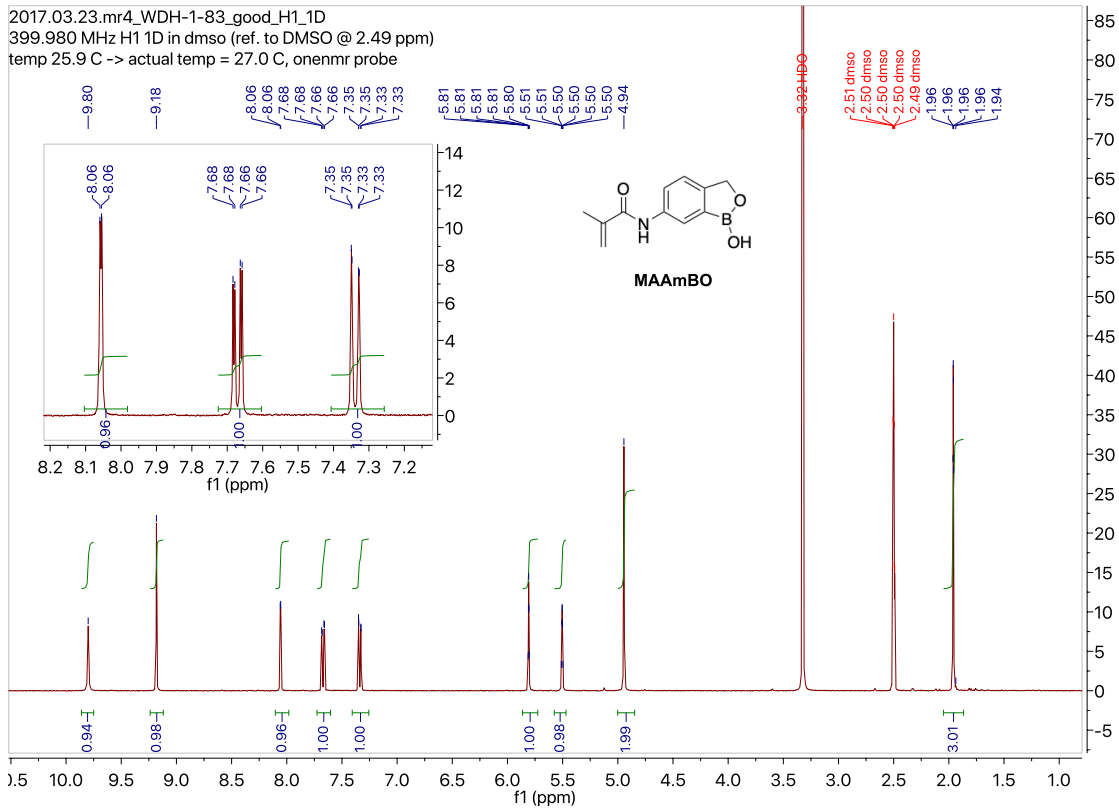
# Appendices

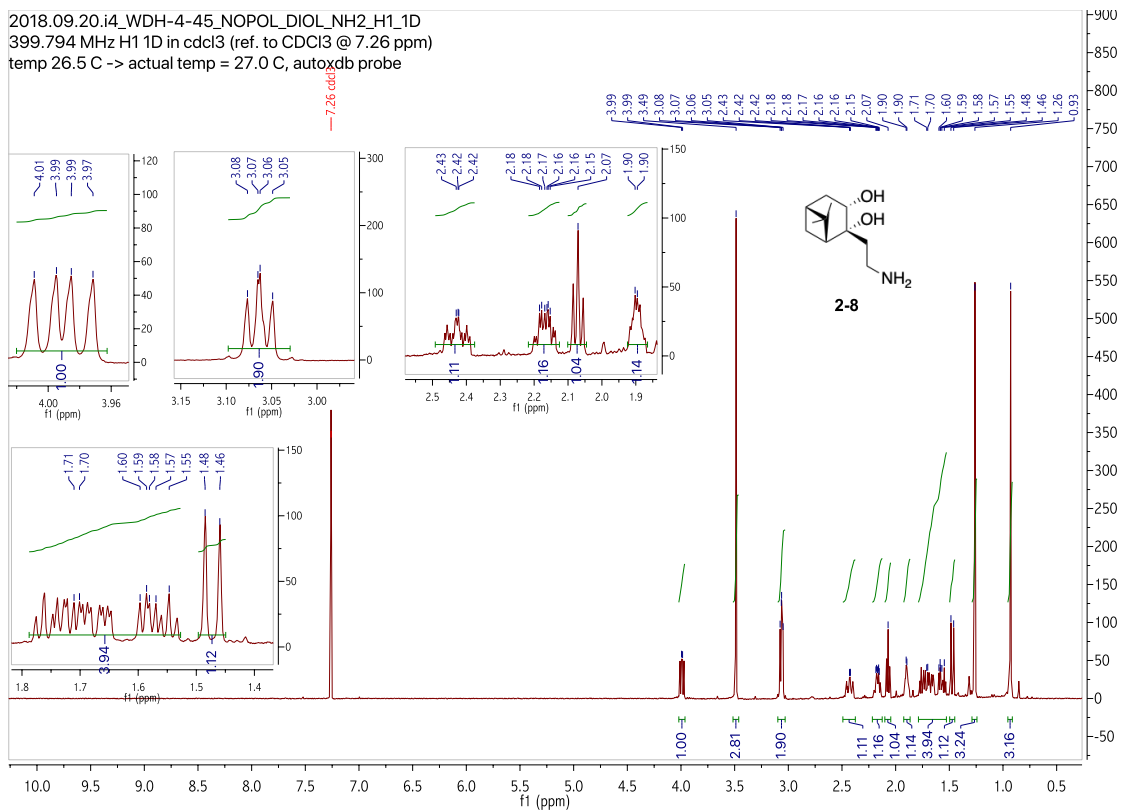
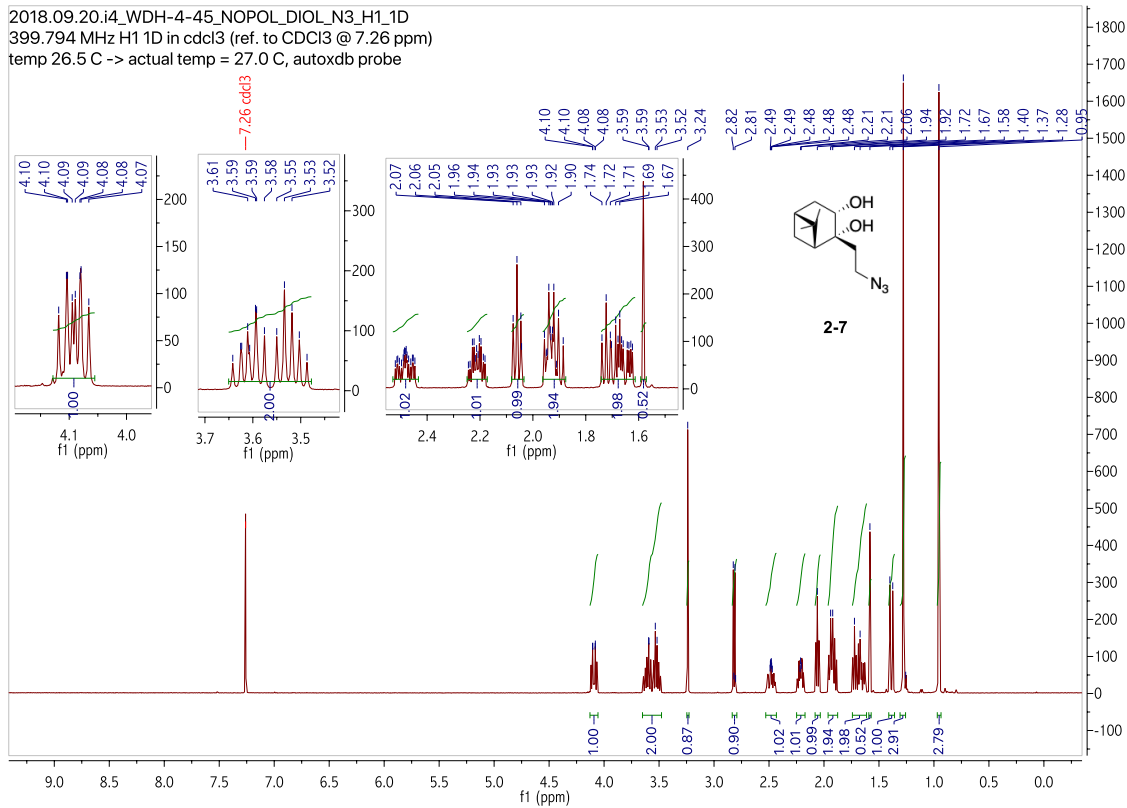
Appendix 1: Selected copies of NMR spectra of compounds, polymers, binding studies, and oxidative degradation studies found in Chapter 2.

## Compounds:

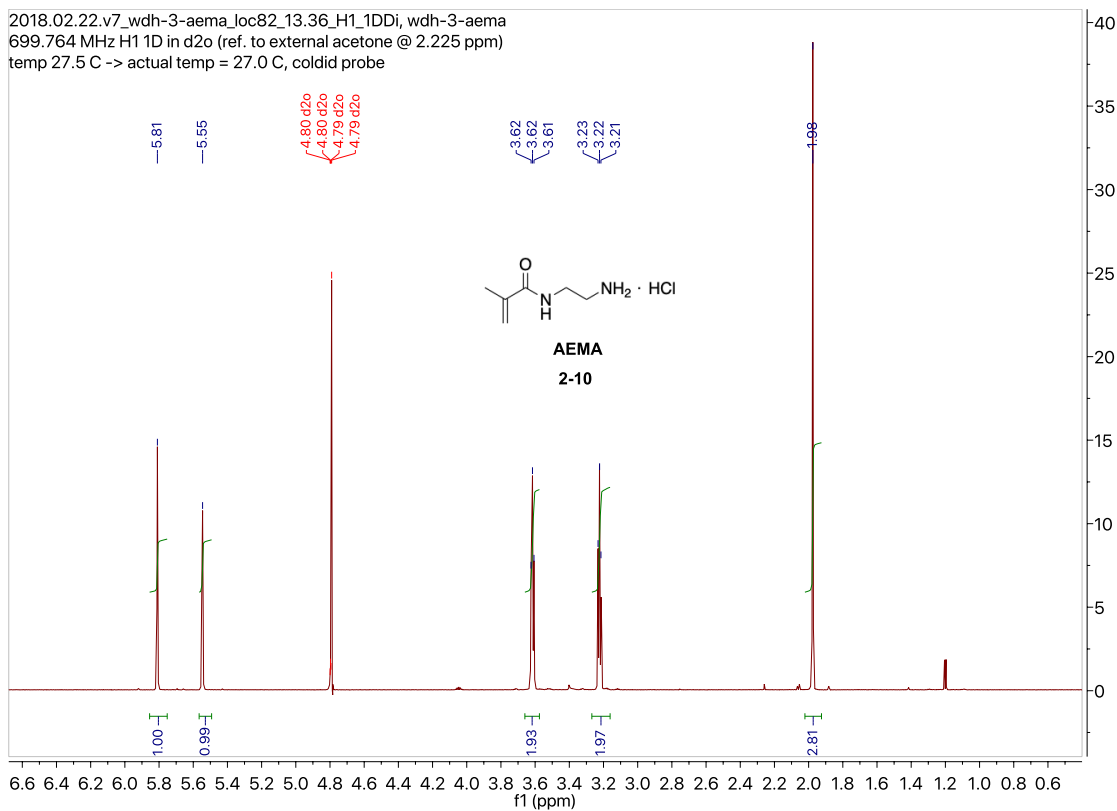
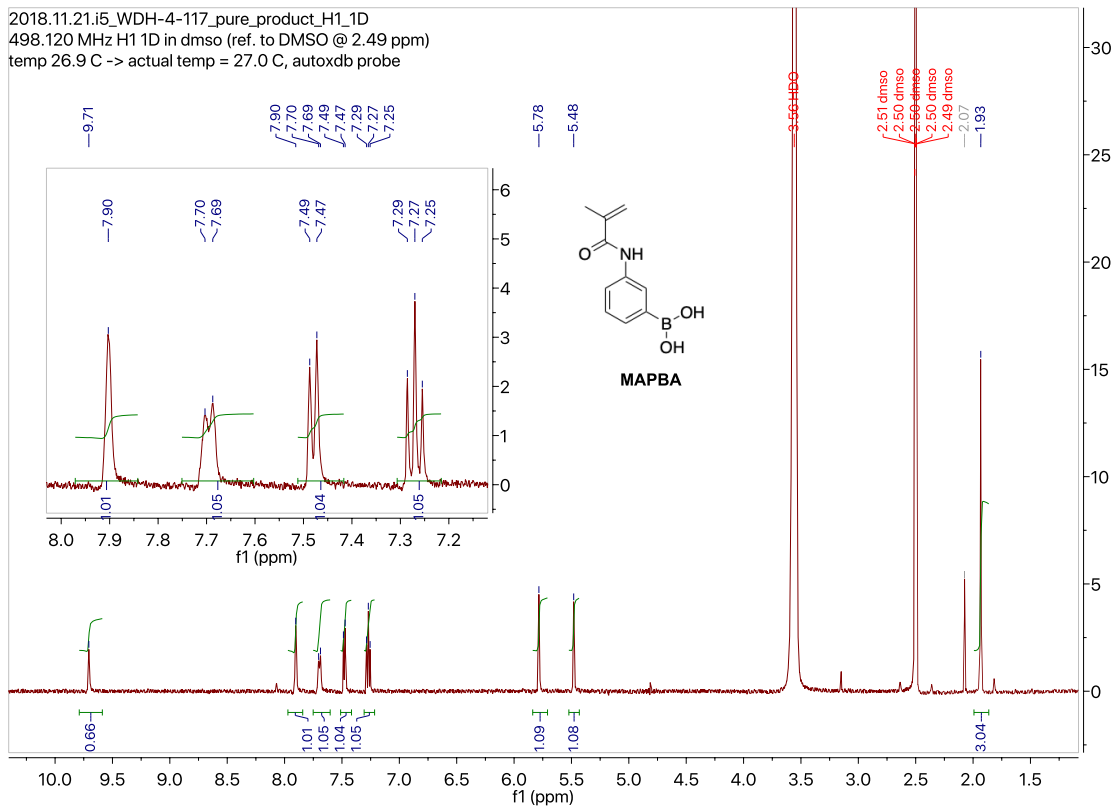


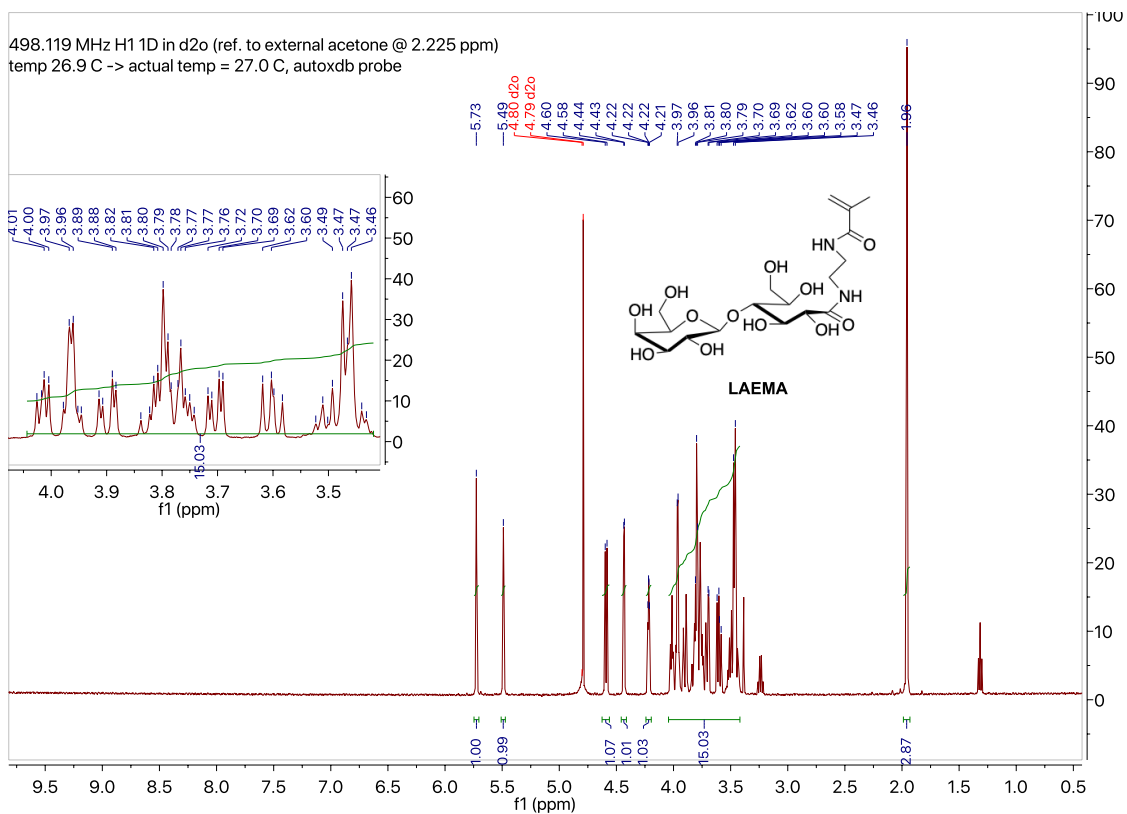
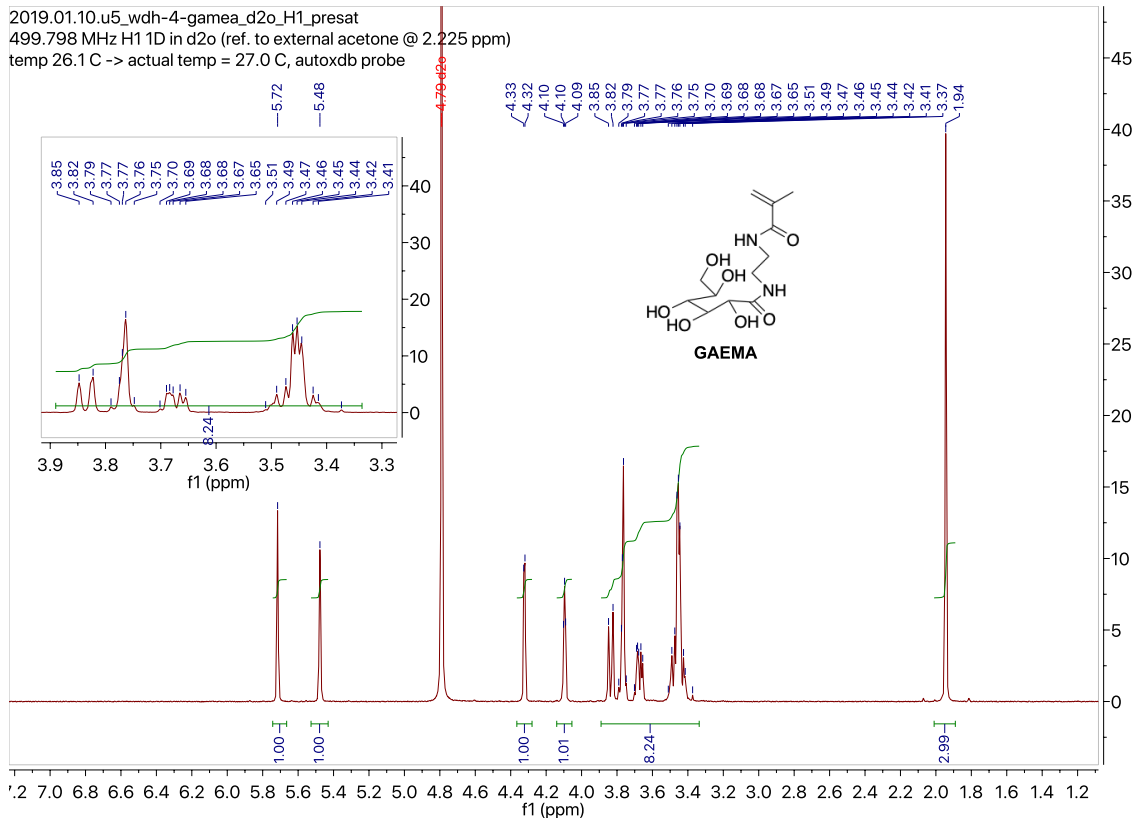




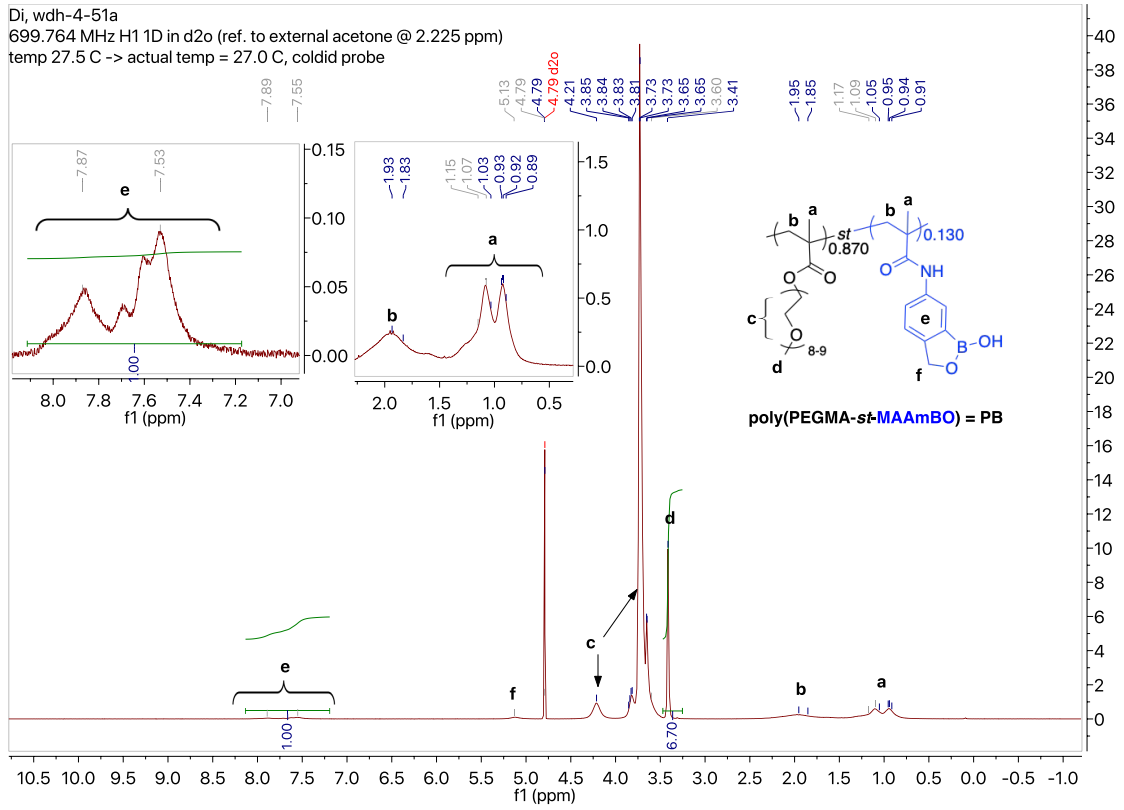


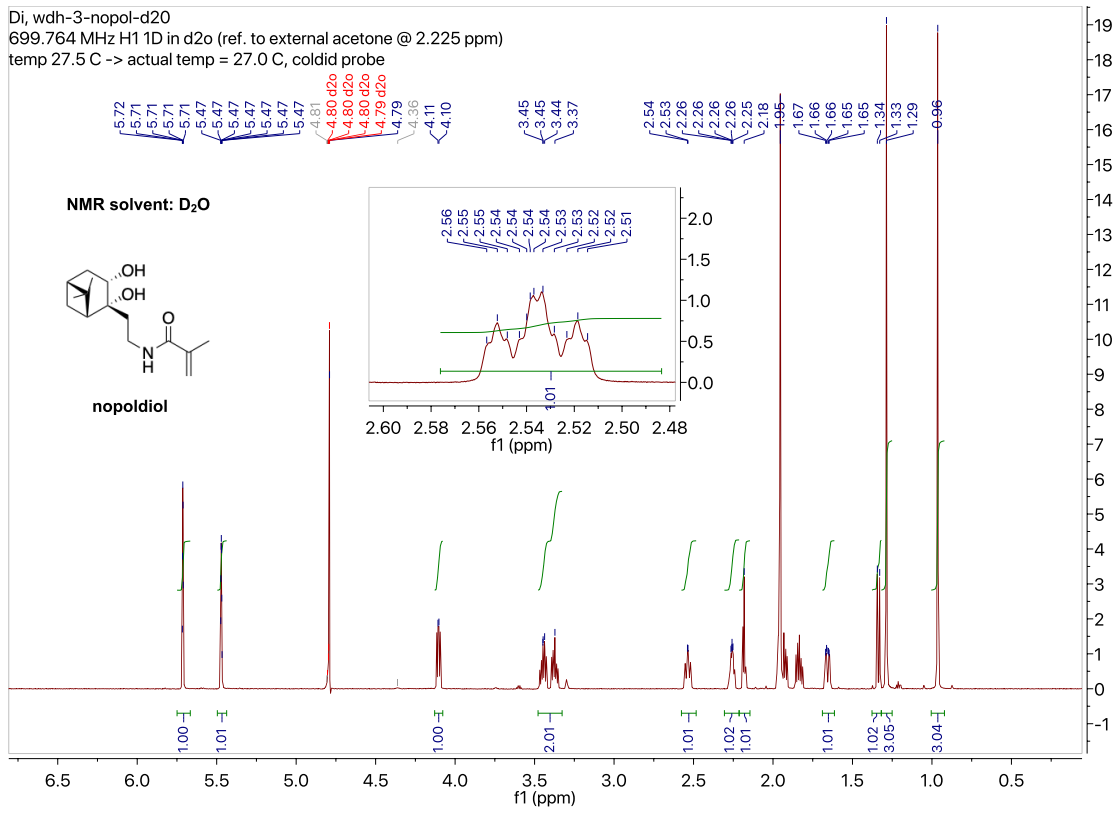
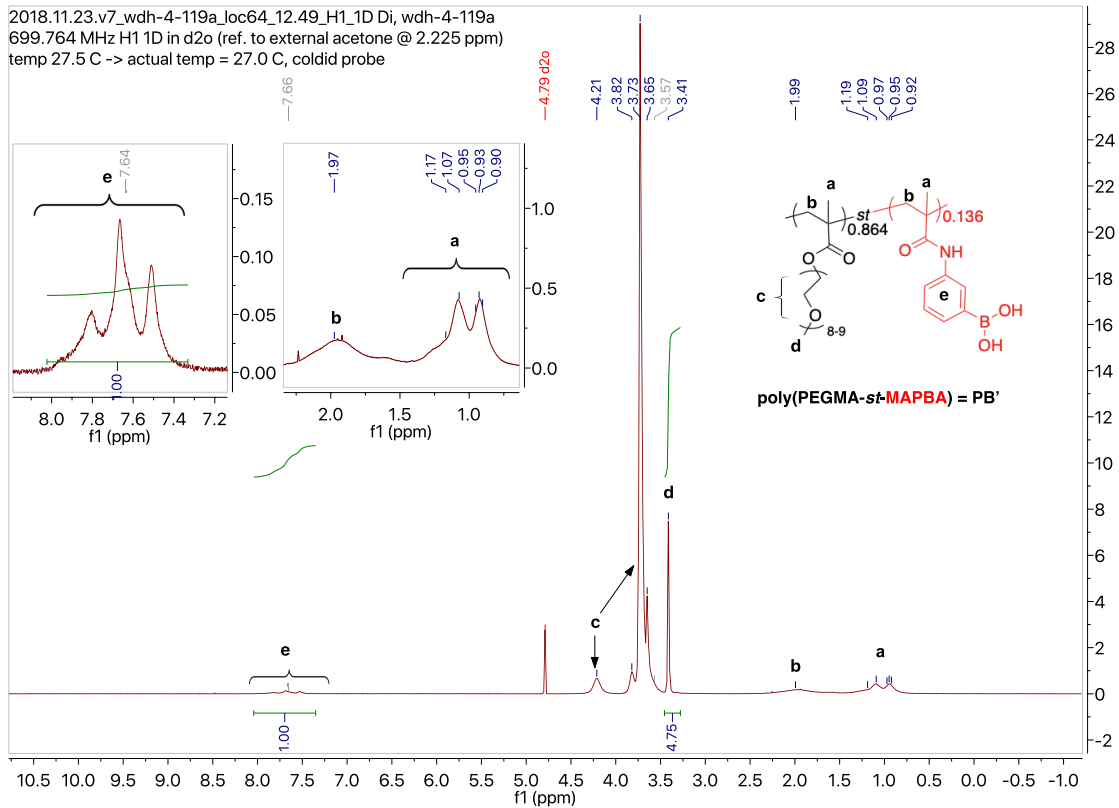


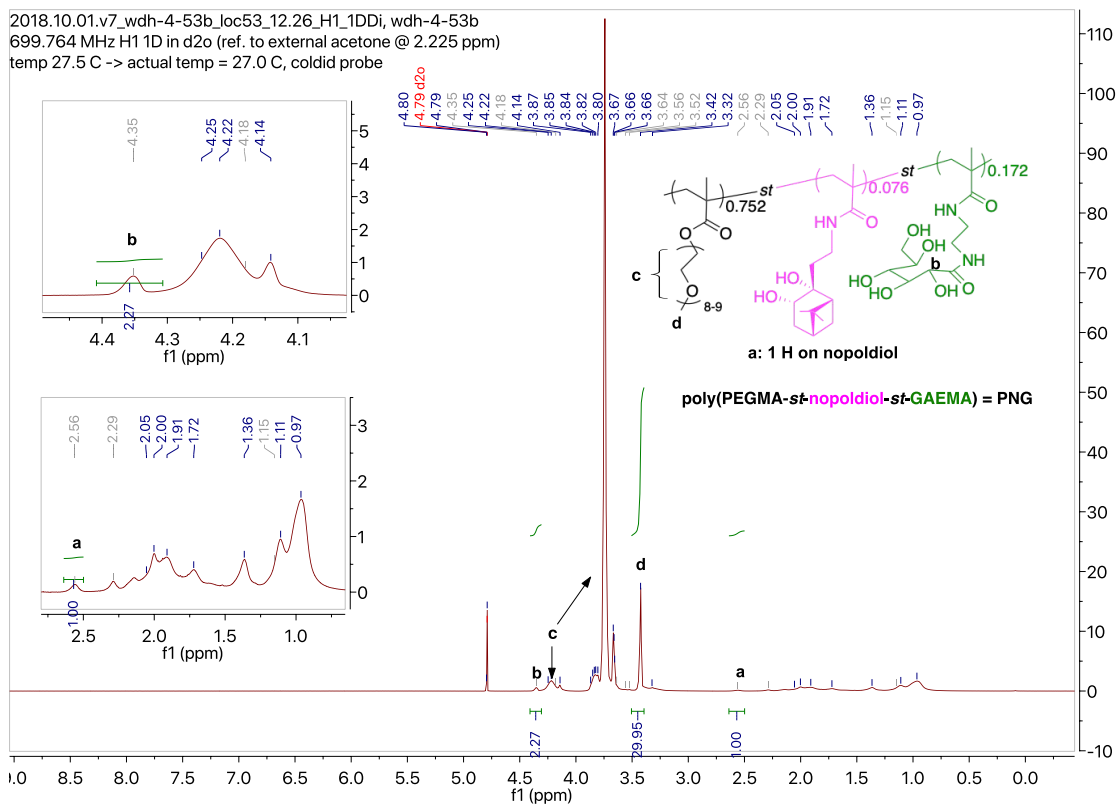




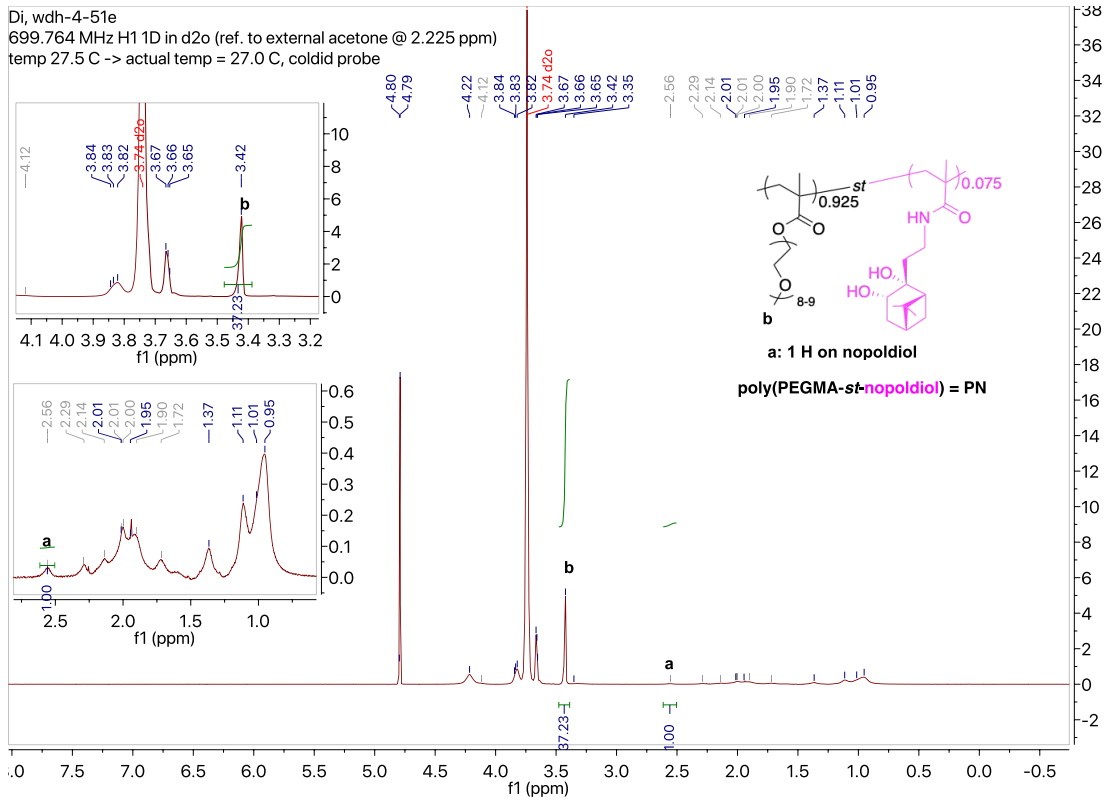
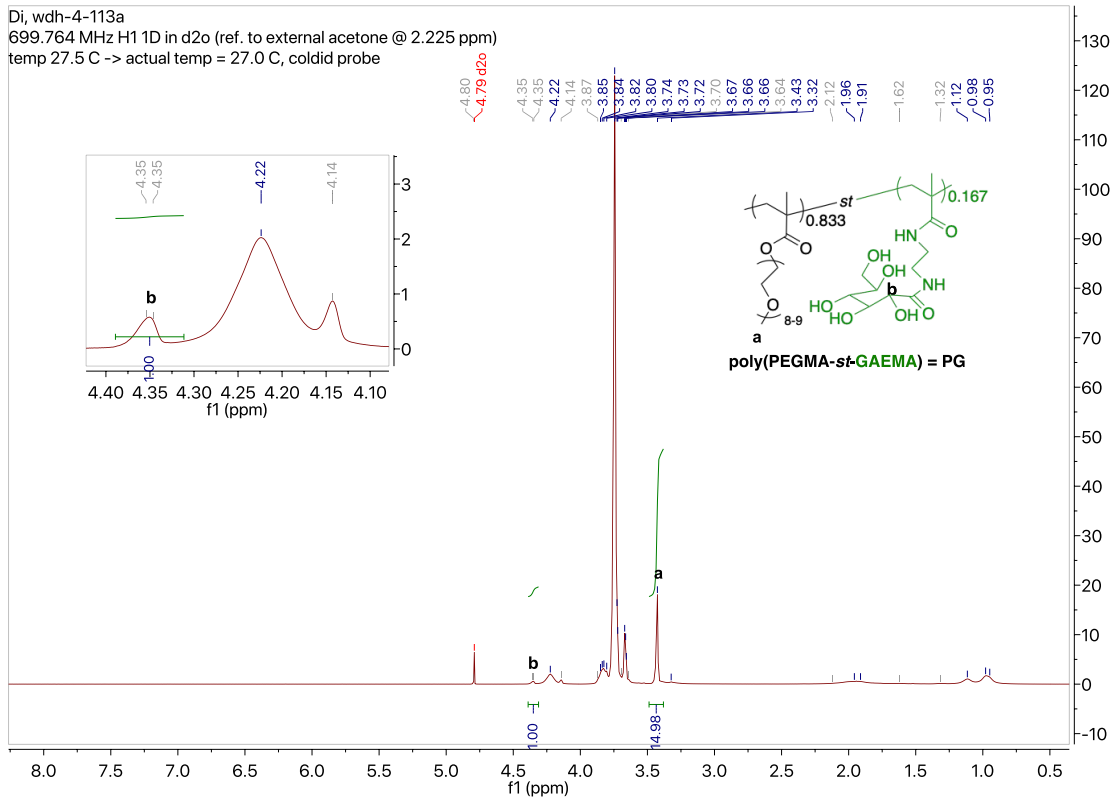
# Polymers:

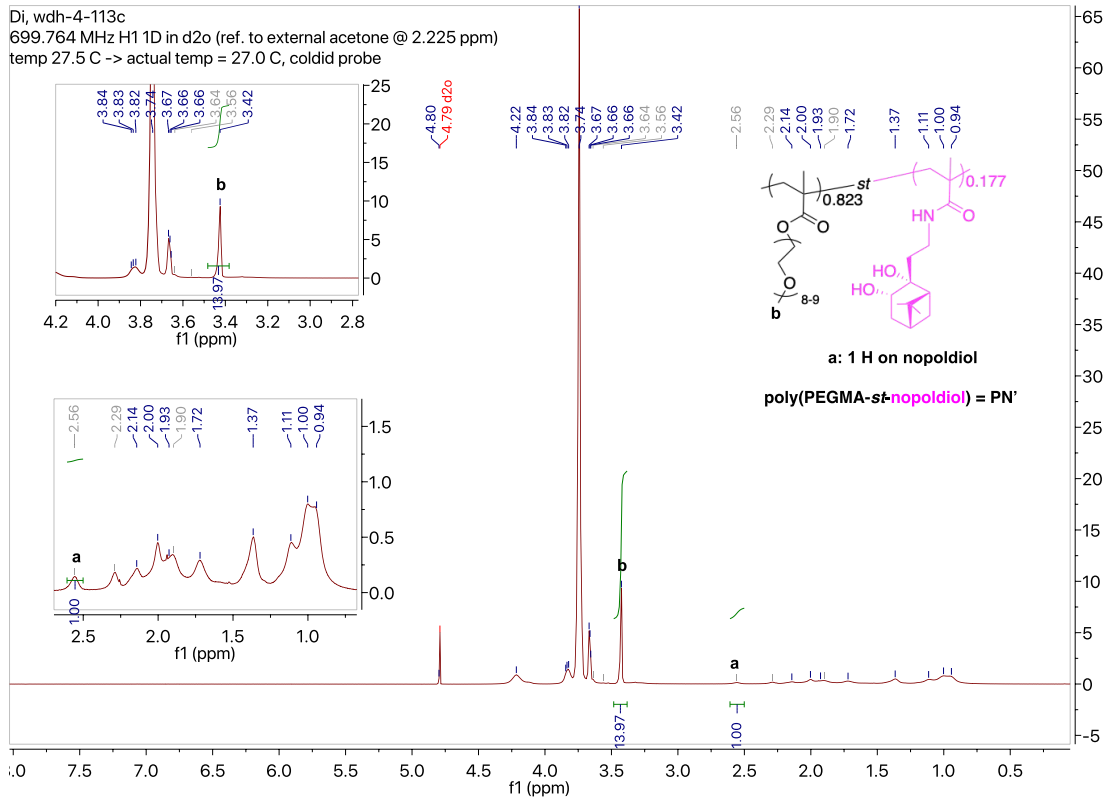






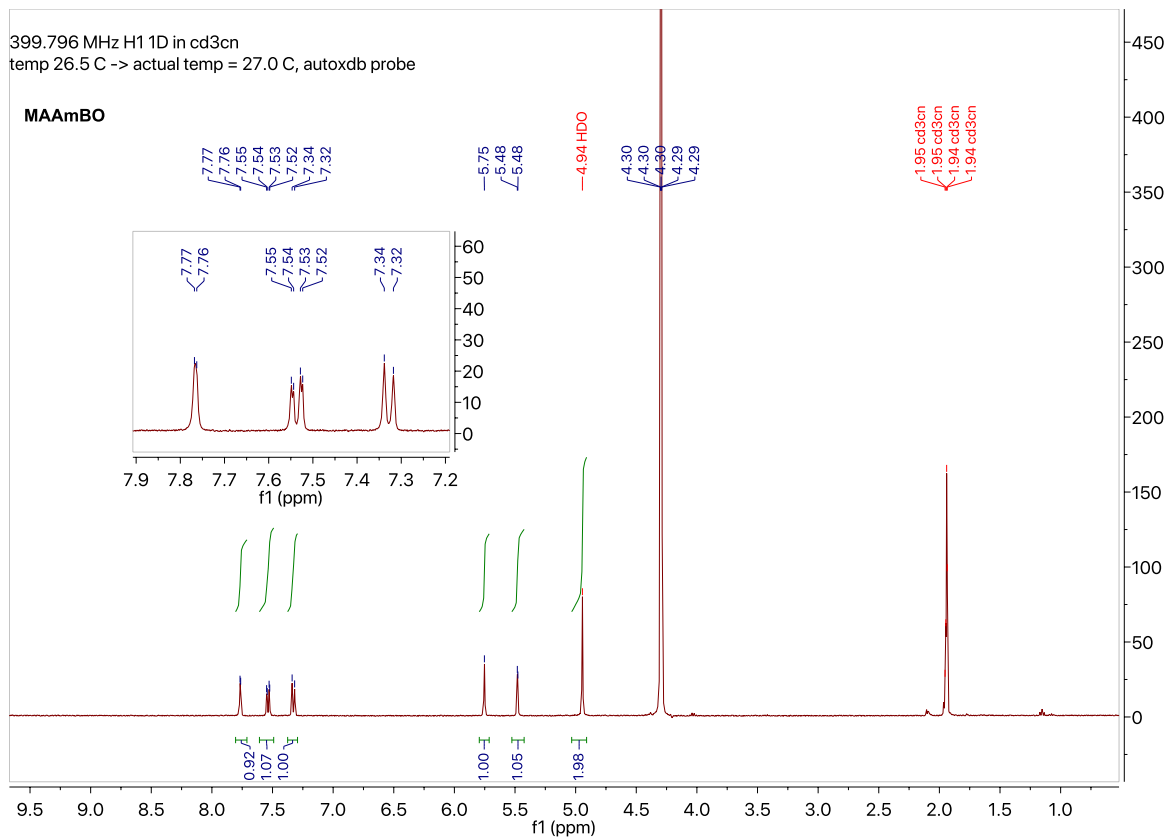
According to the  $^1\text{H}$  NMR spectrum of **nopoldiol** monomer in  $\text{D}_2\text{O}$ , the signal at 2.54 ppm represents 1 H on the molecule. Therefore, the signal at 2.56 ppm on the  $^1\text{H}$  NMR spectrum of polymer **PNG**, **PN**, and **PN'** was used to calculate the composition of **nopoldiol**.

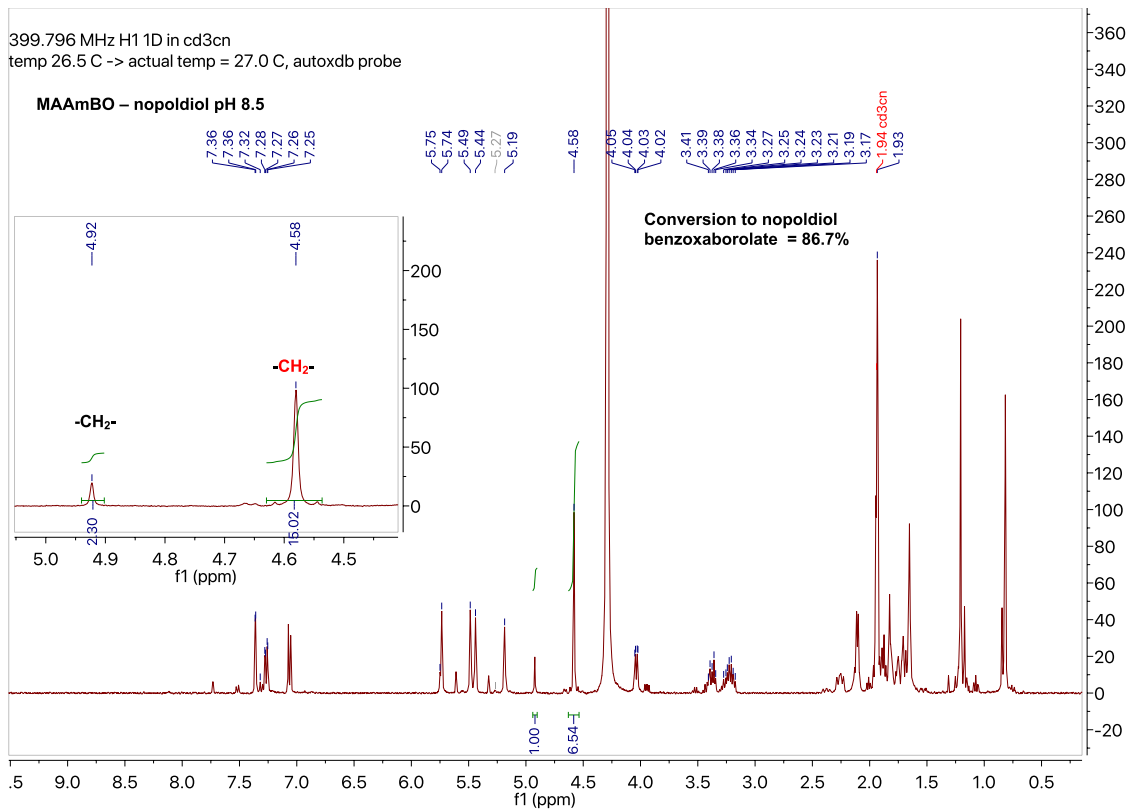
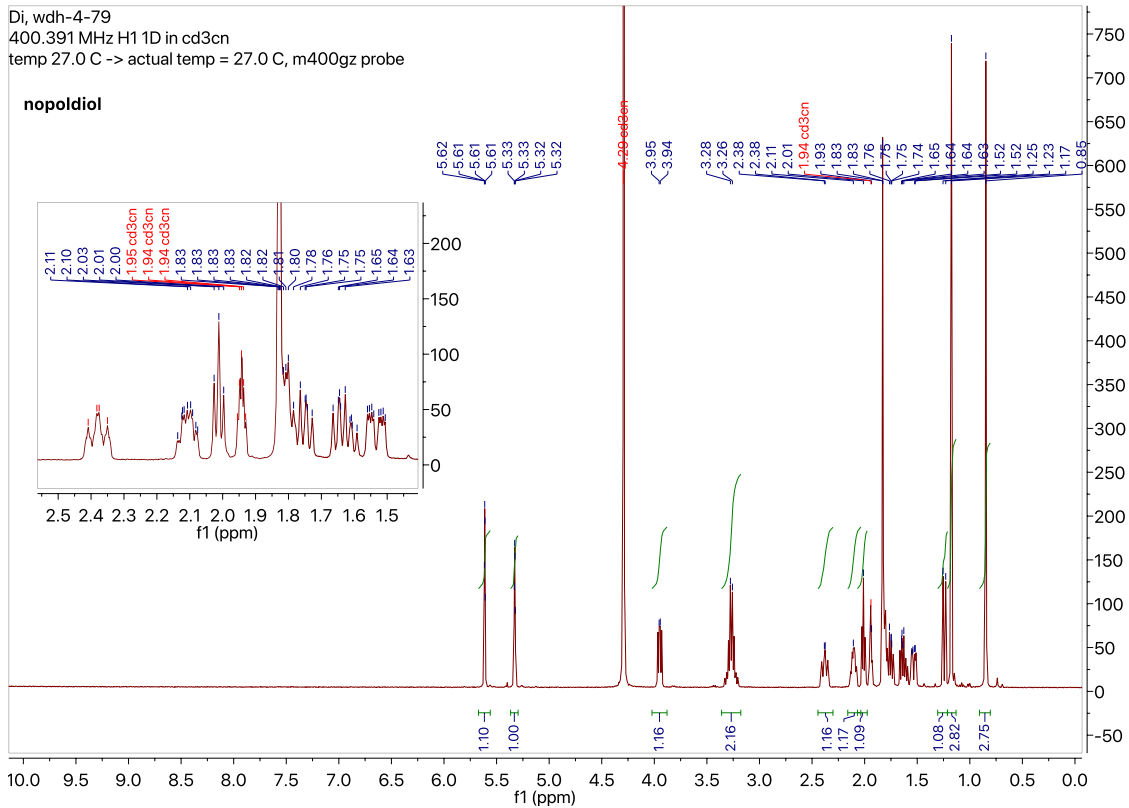


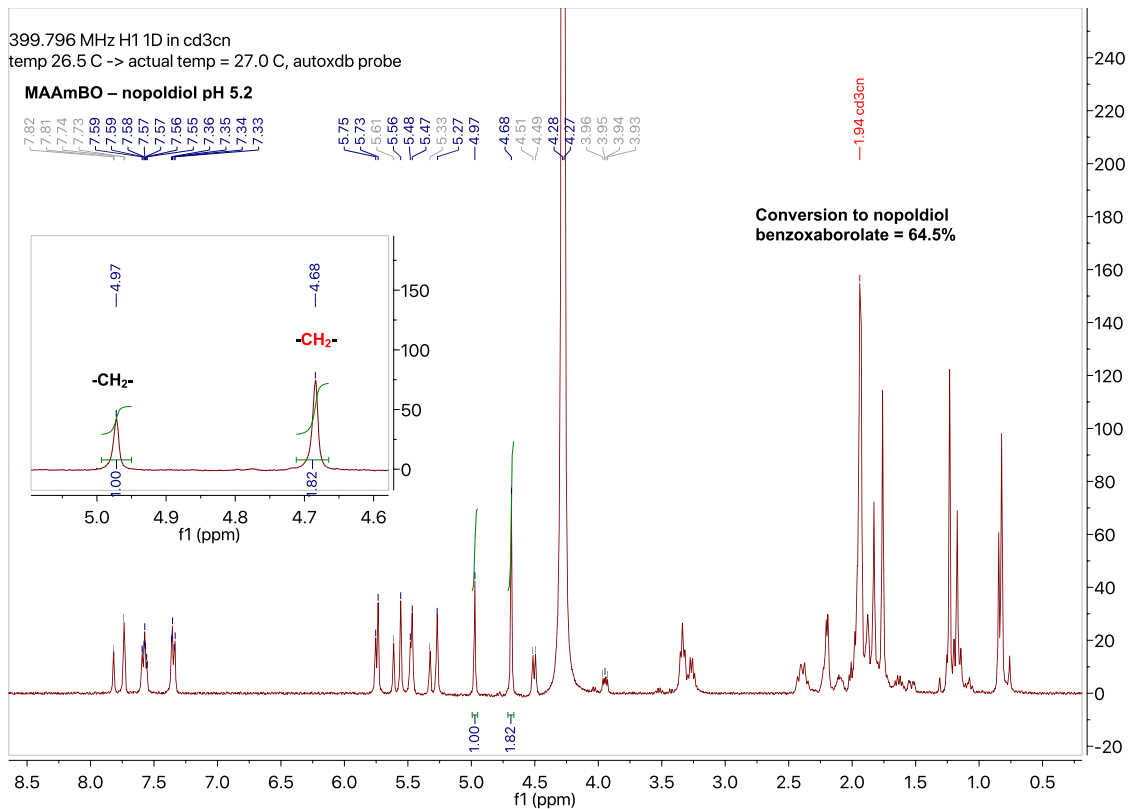
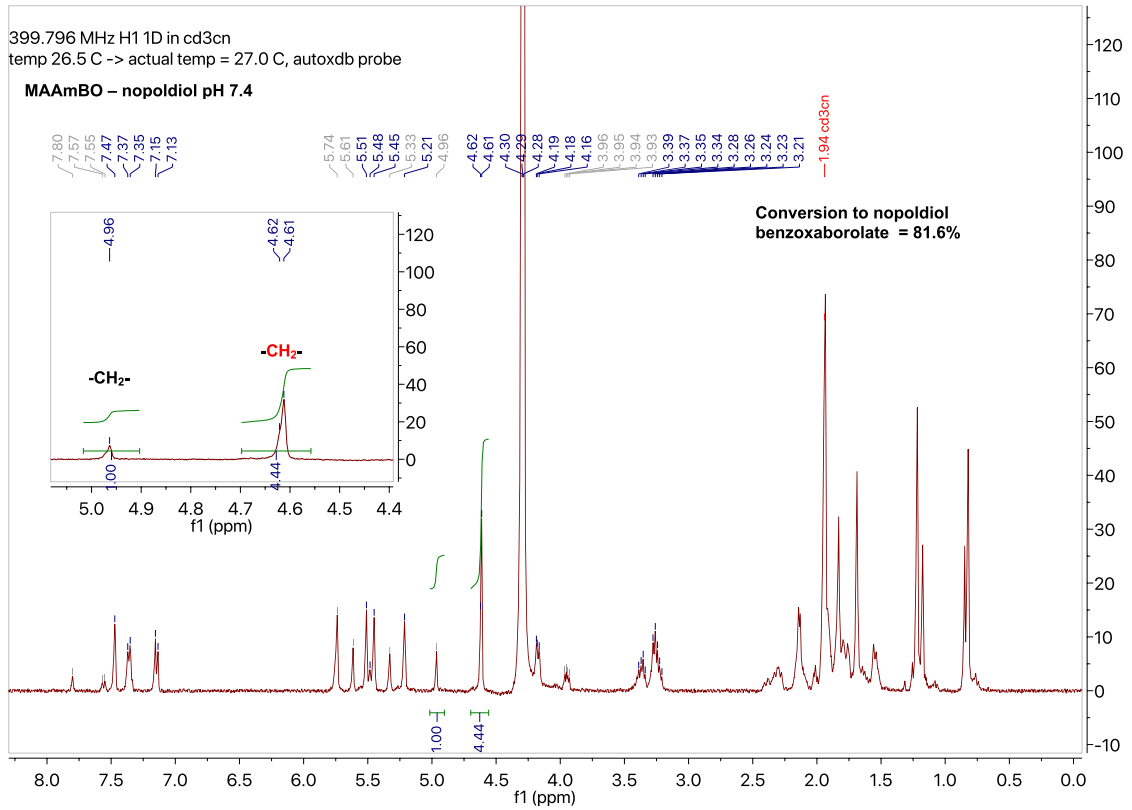


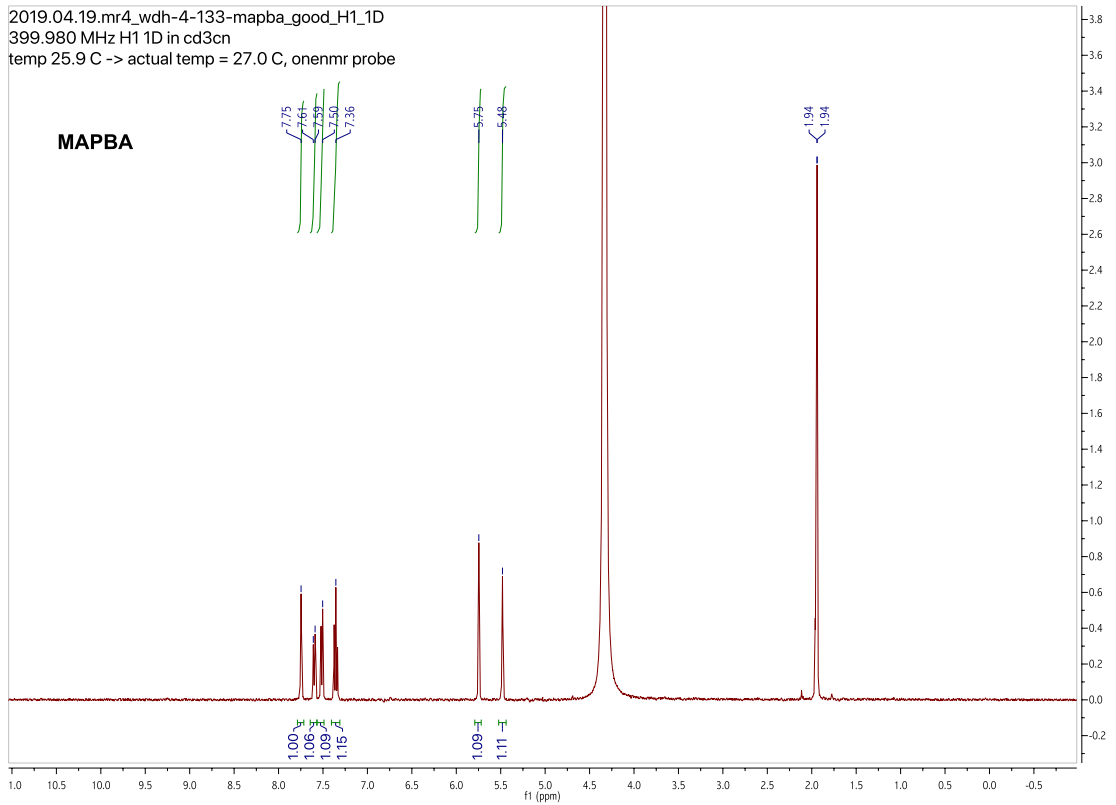
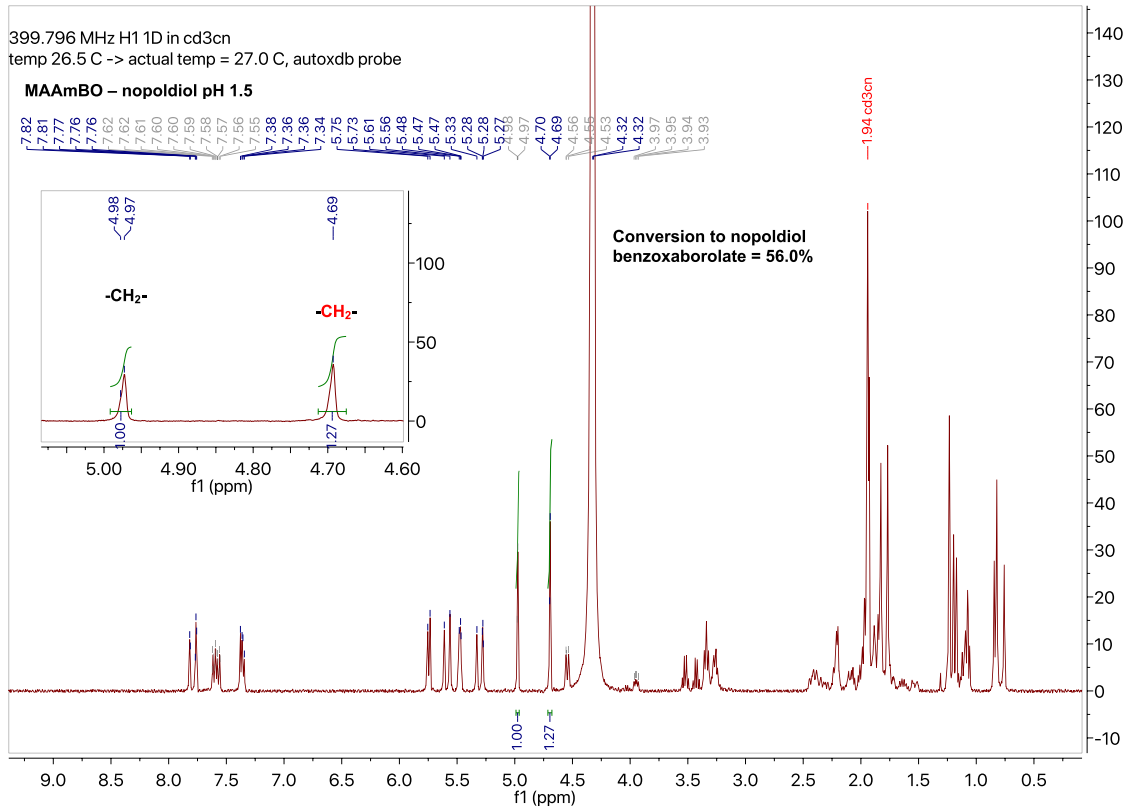
## Binding studies:

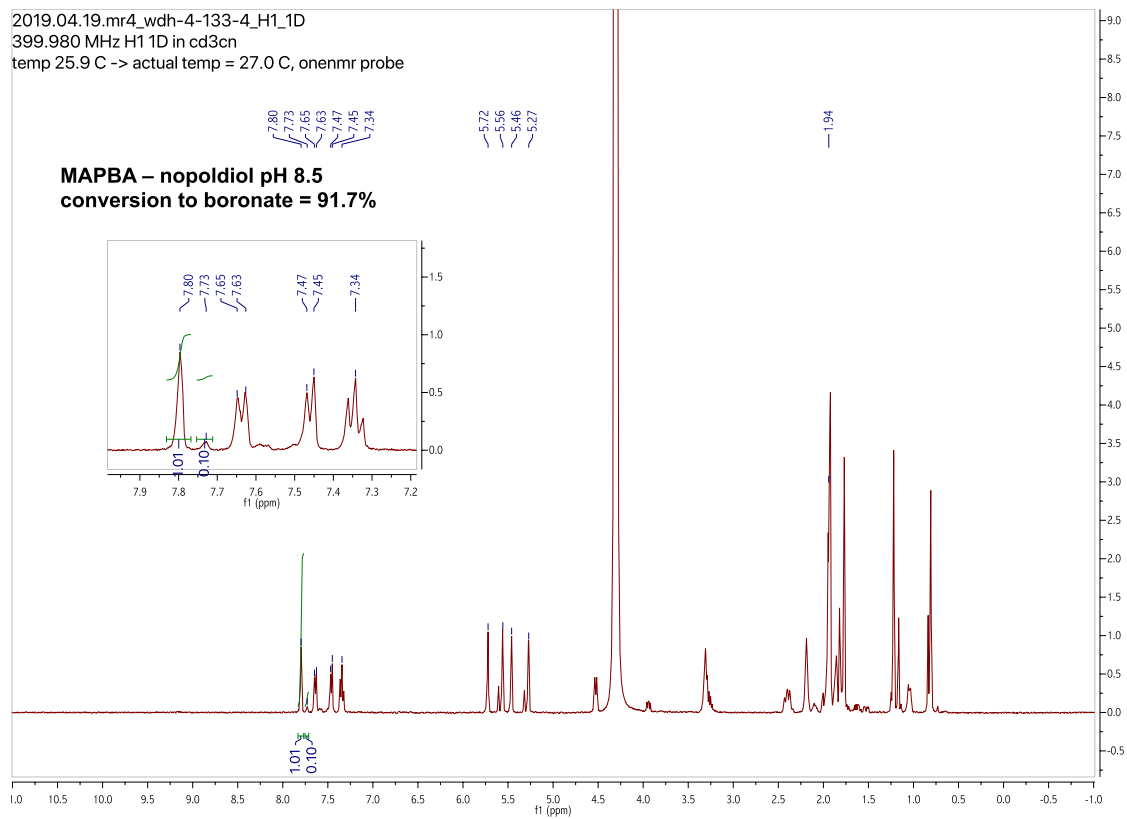
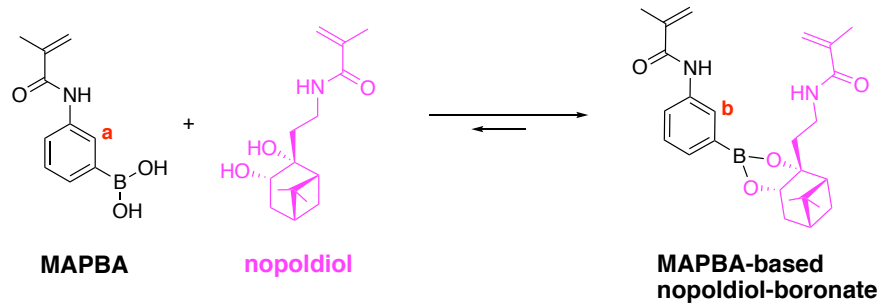
NMR solvent: D<sub>2</sub>O phosphate buffer:ACN-*d*<sub>3</sub> 65:35 w%, NMR was locked as ACN-*d*<sub>3</sub> while tuning.



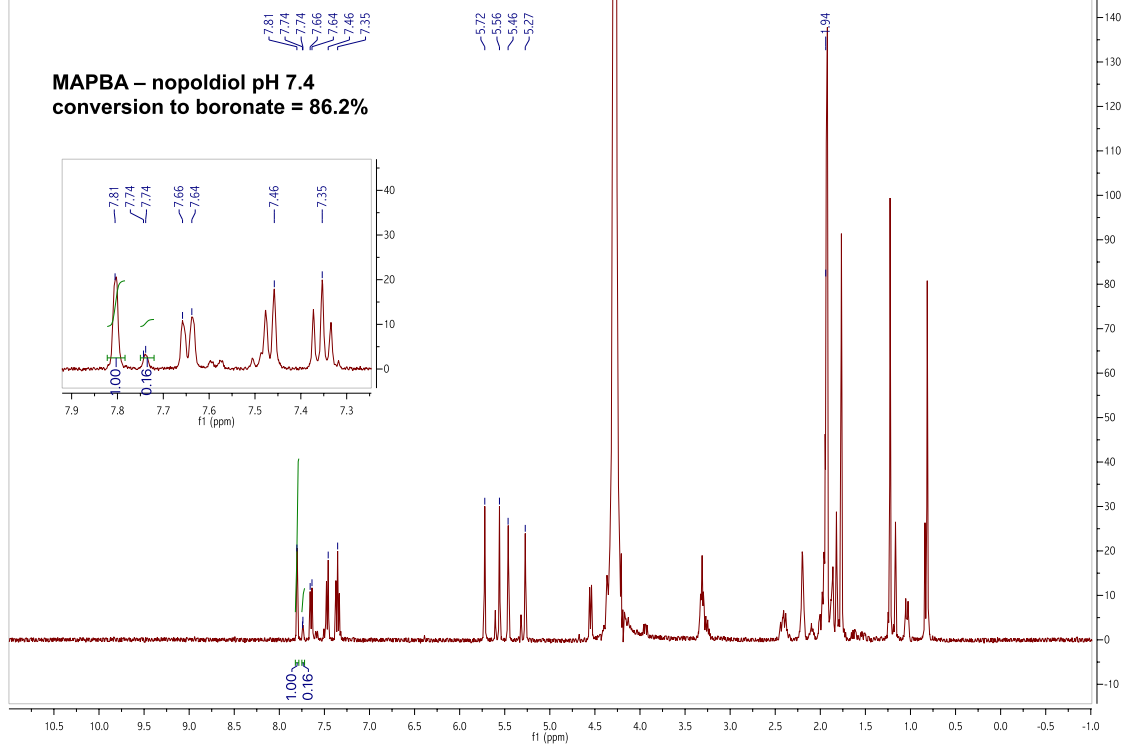




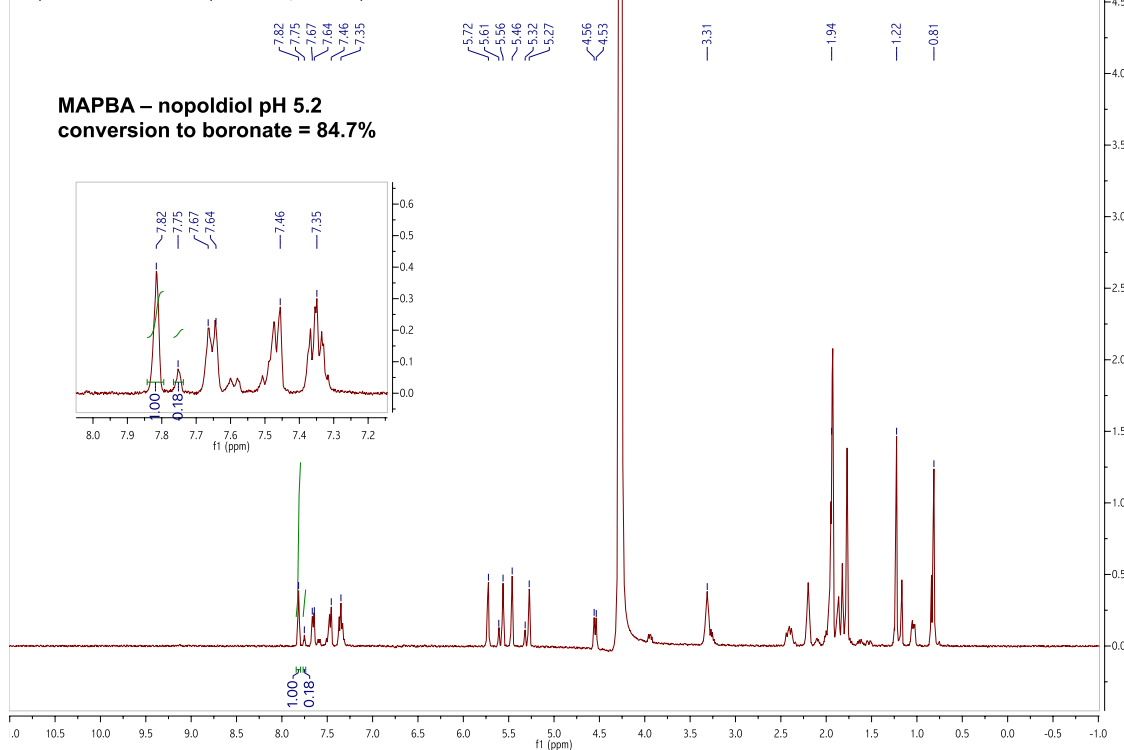


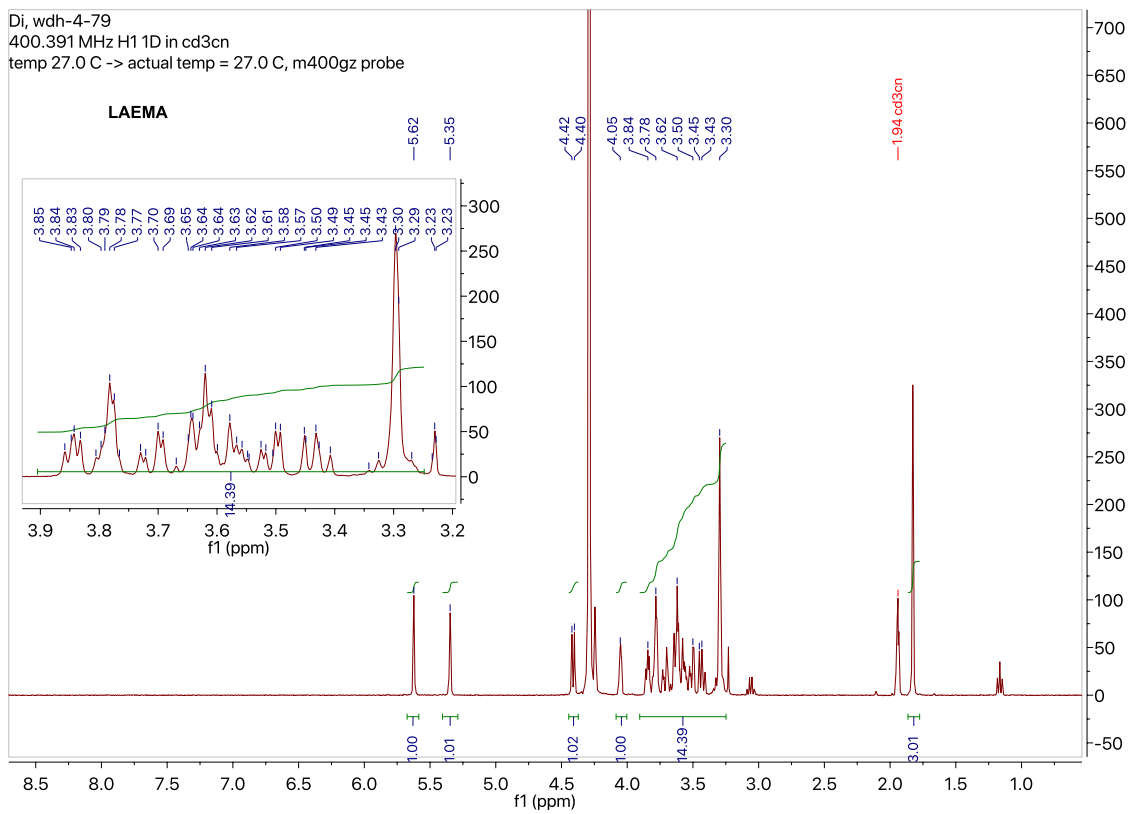
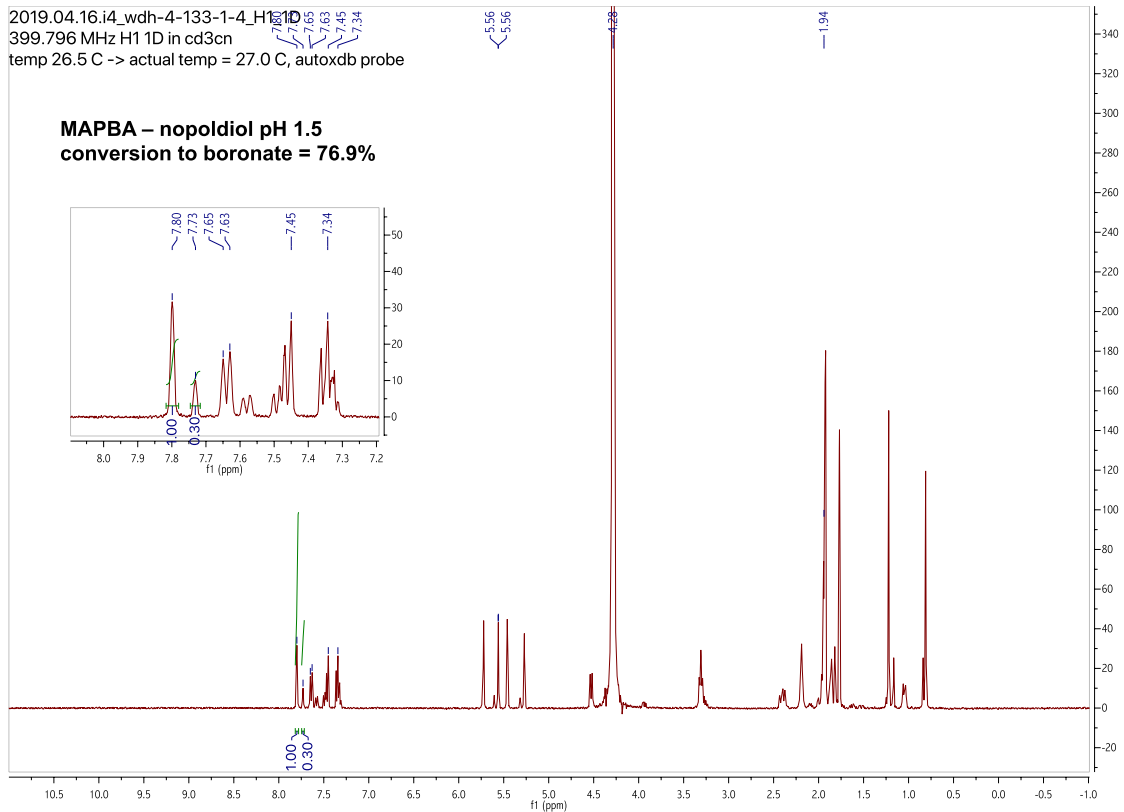


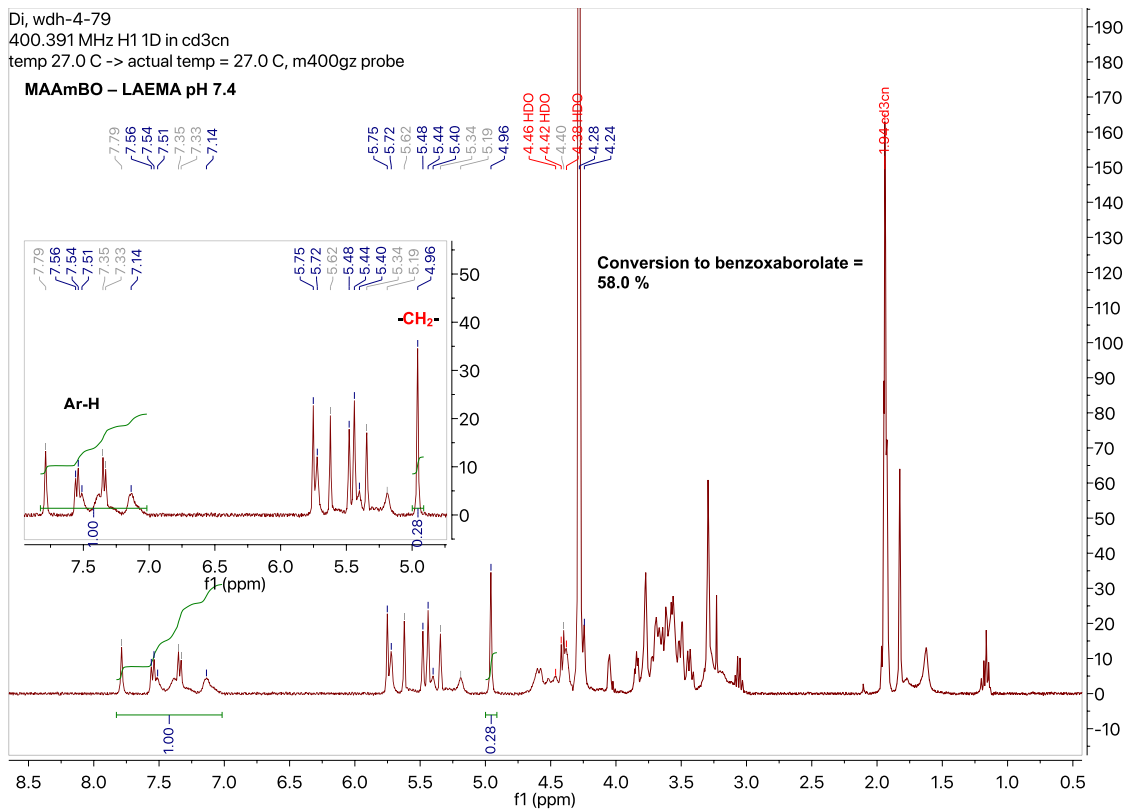
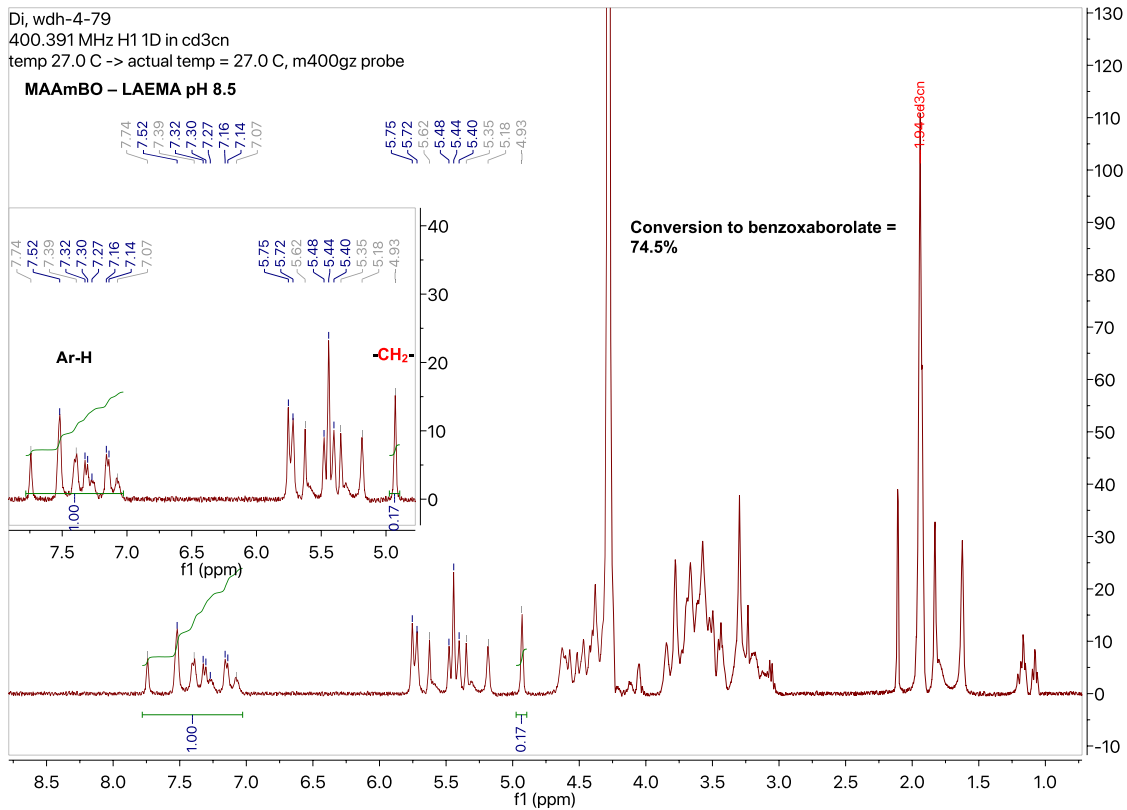
2019.04.16.i4\_wdh-4-133-1-3\_H1\_1D  
399.796 MHz H1 1D in cd3cn  
temp 26.5 C -> actual temp = 27.0 C, autotx probe

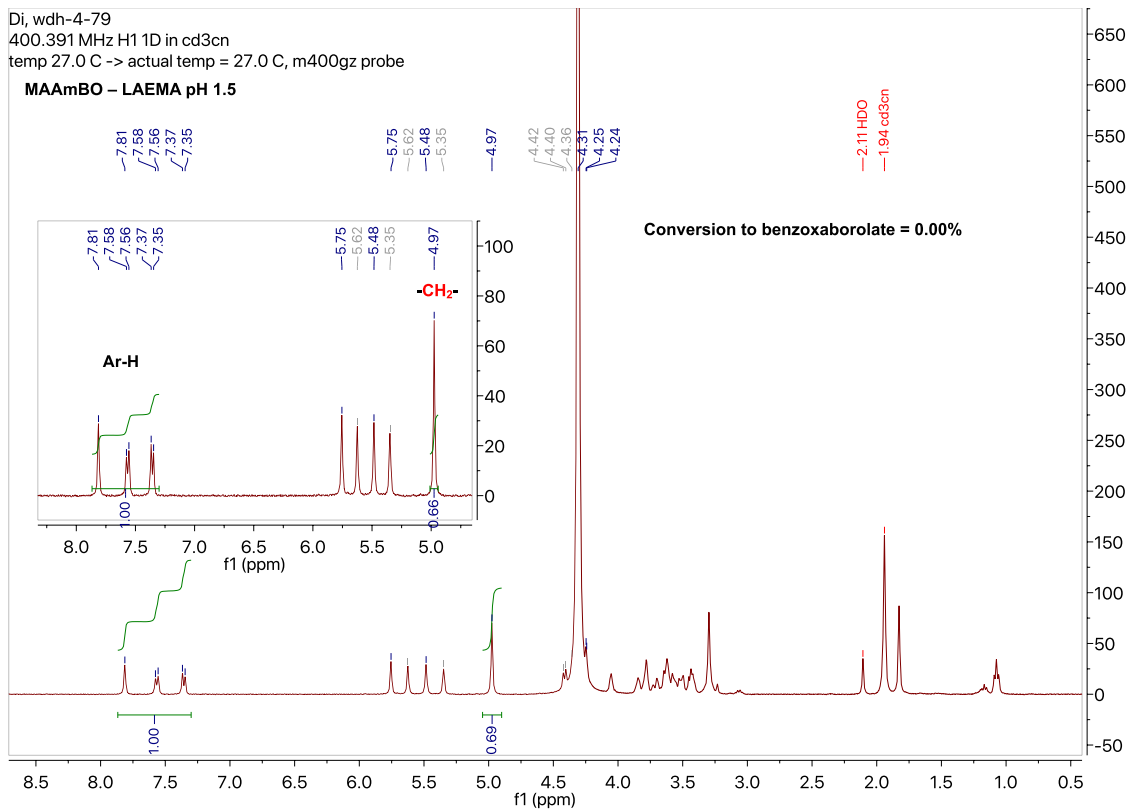
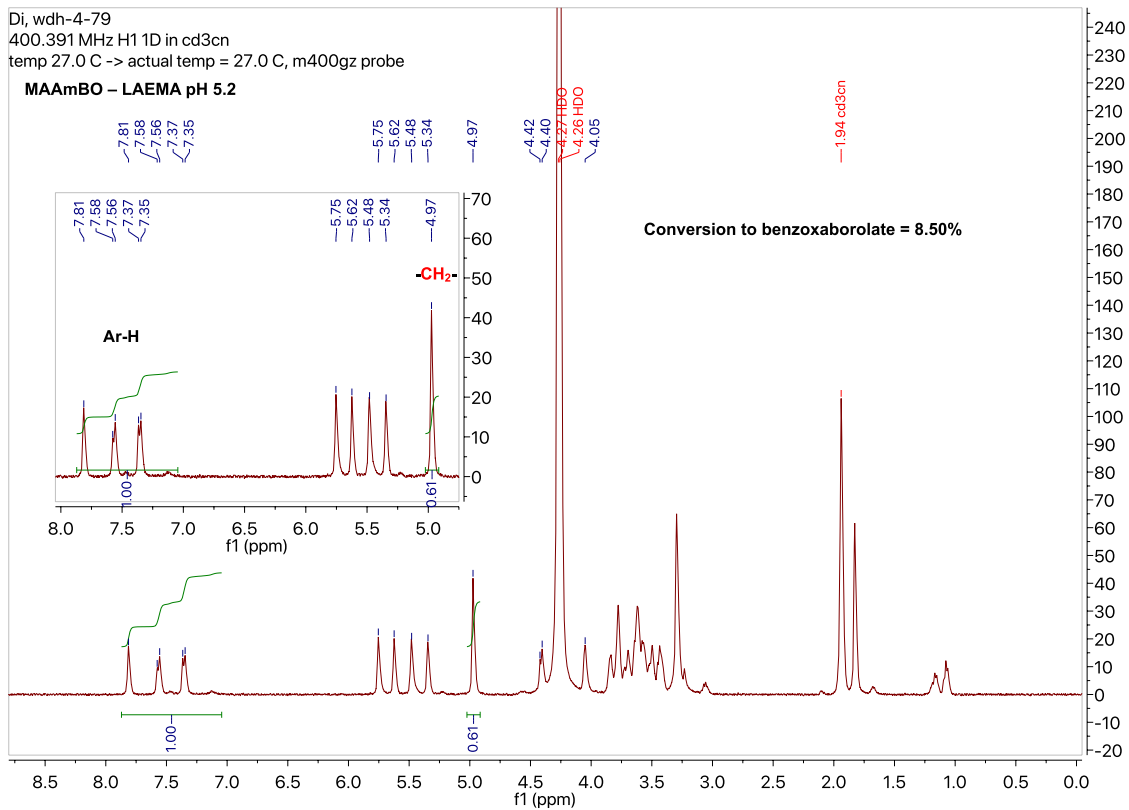


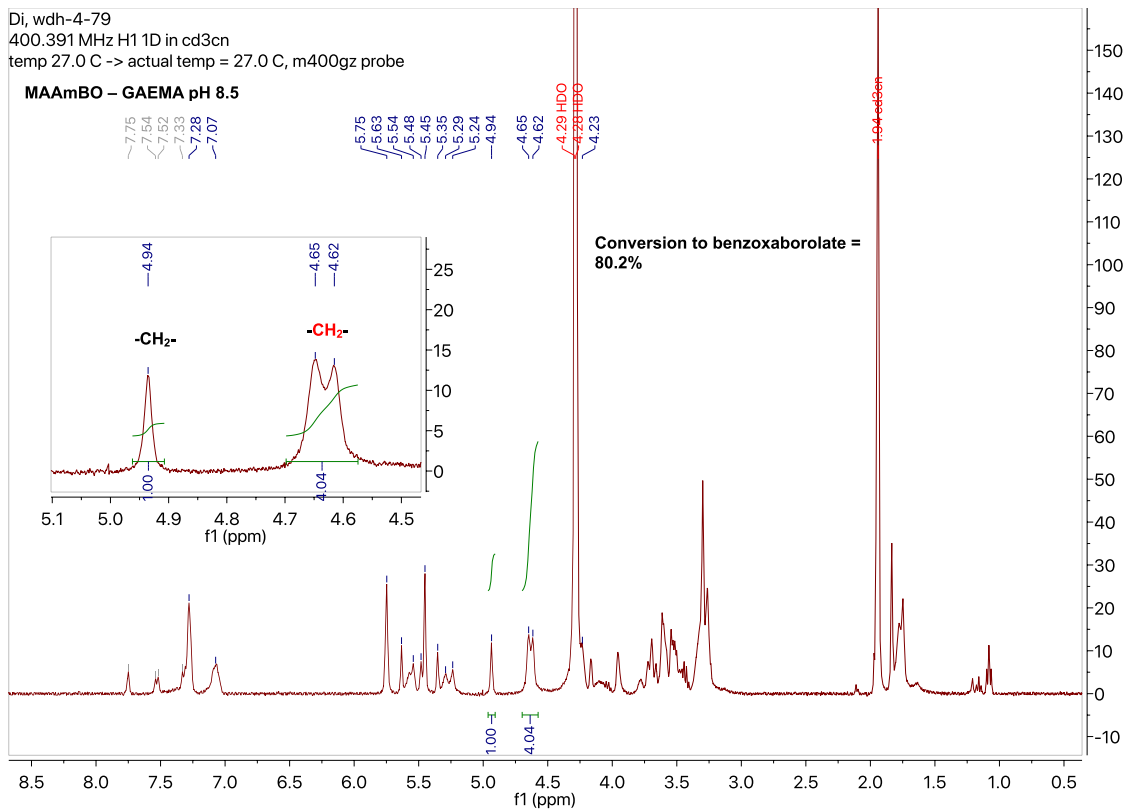
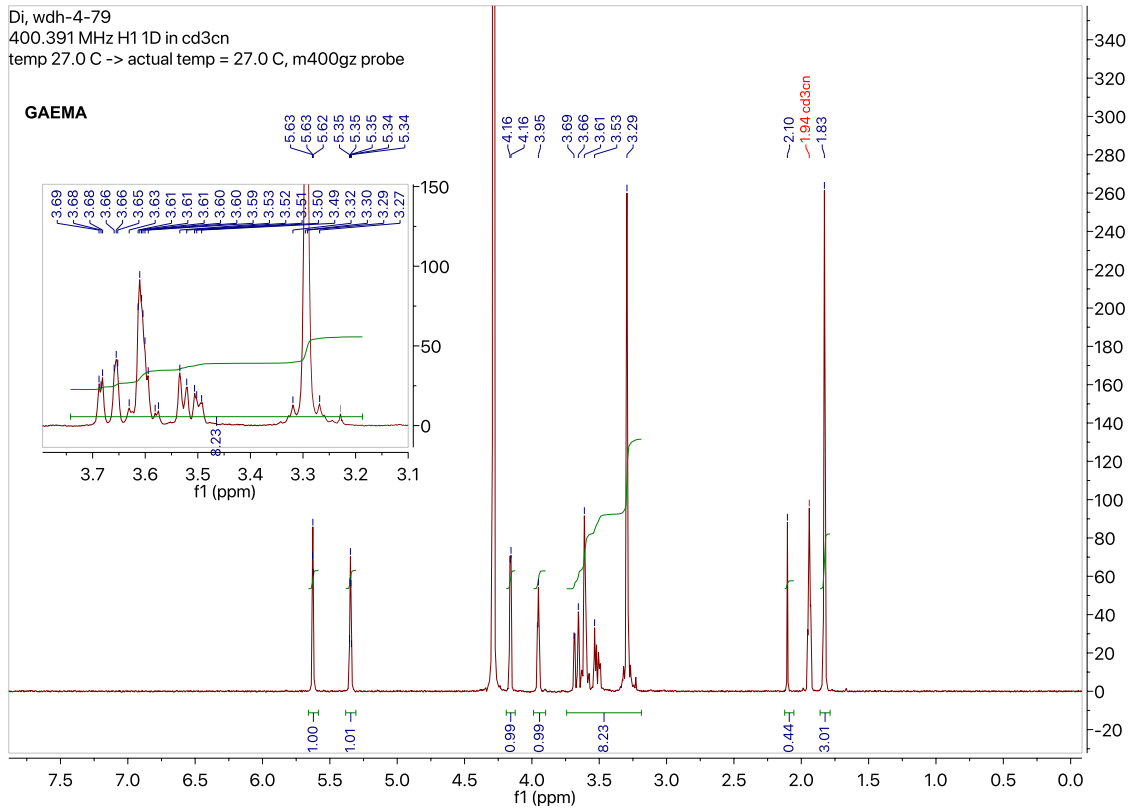
2019.04.19.mr4\_wdh-4-133-6\_H1\_1D  
399.980 MHz H1 1D in cd3cn  
temp 25.9 C -> actual temp = 27.0 C, onenmr probe

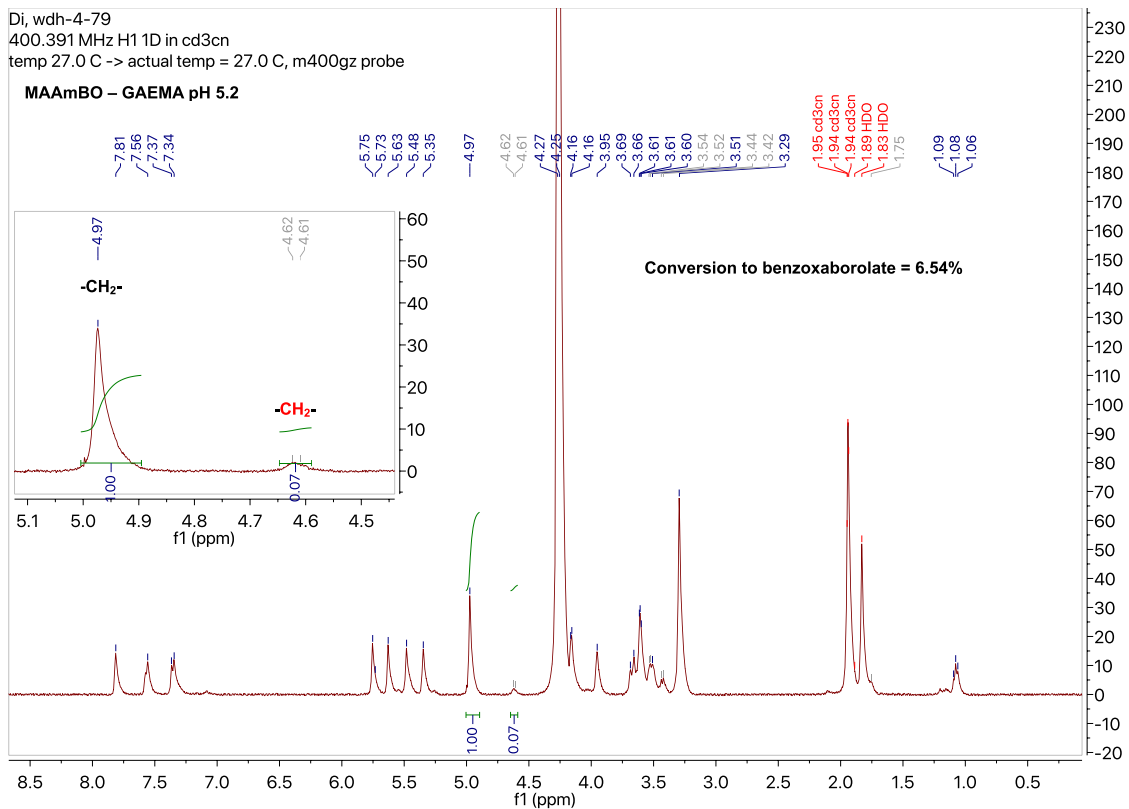
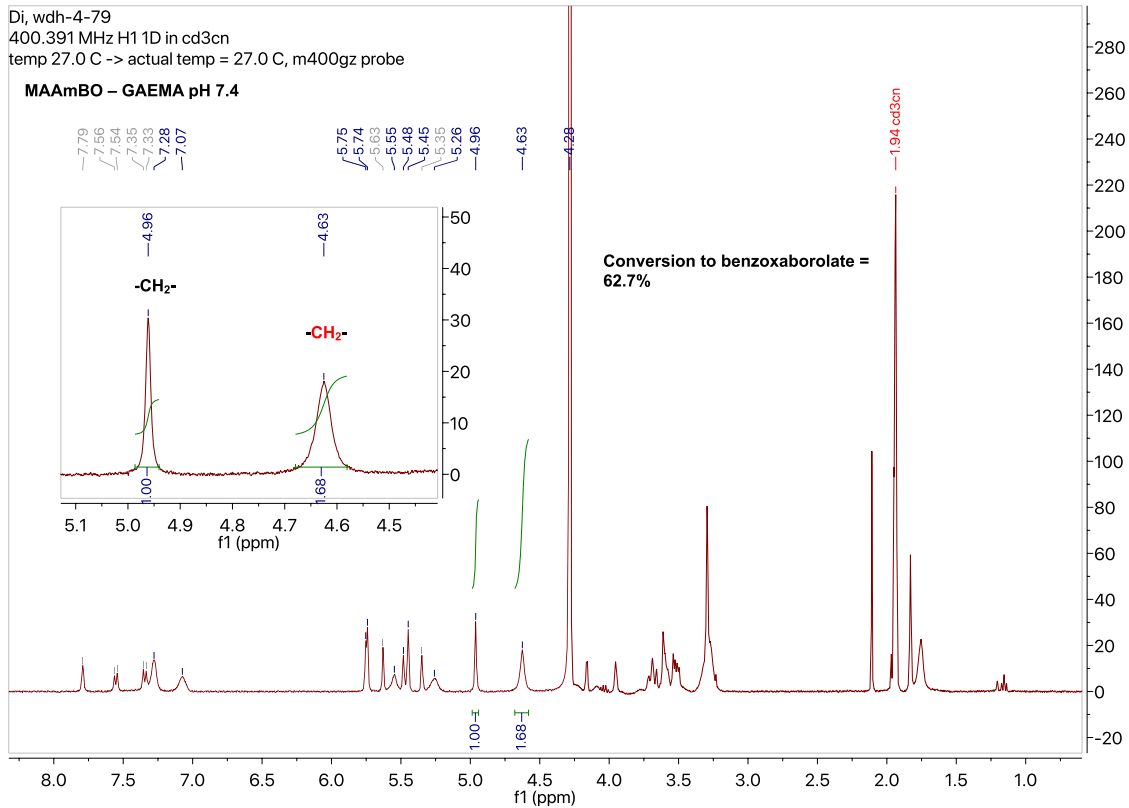


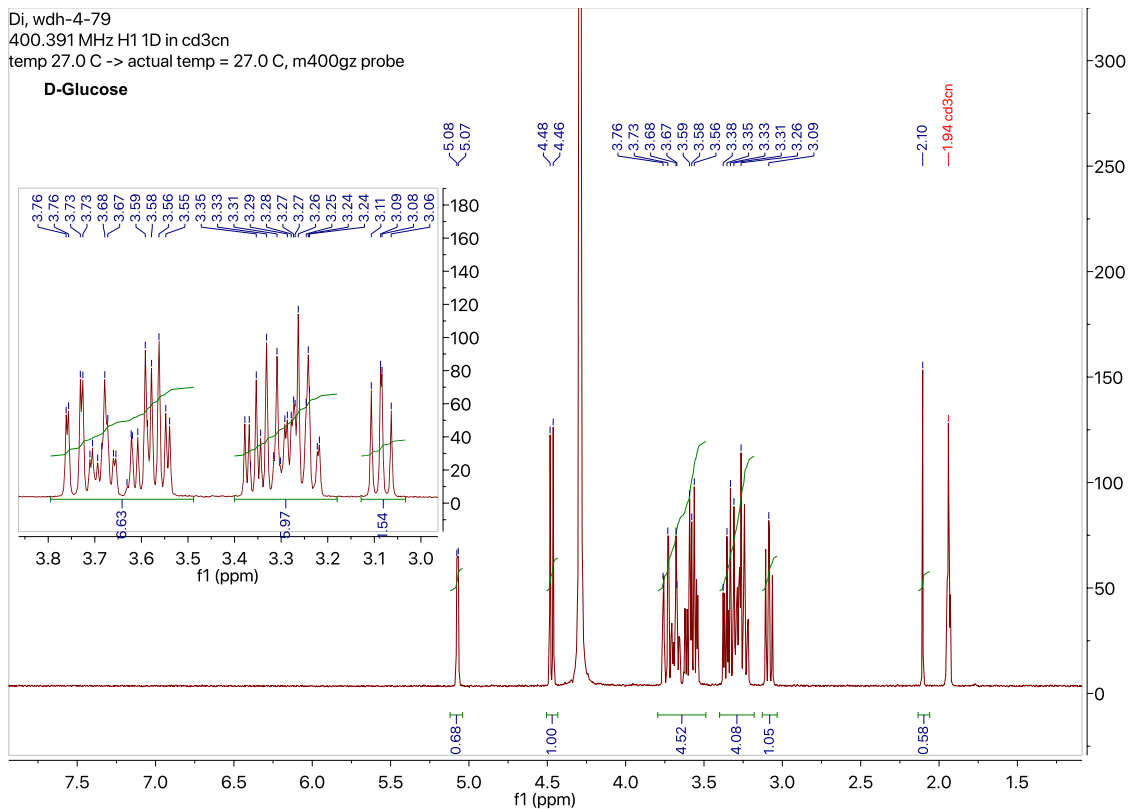
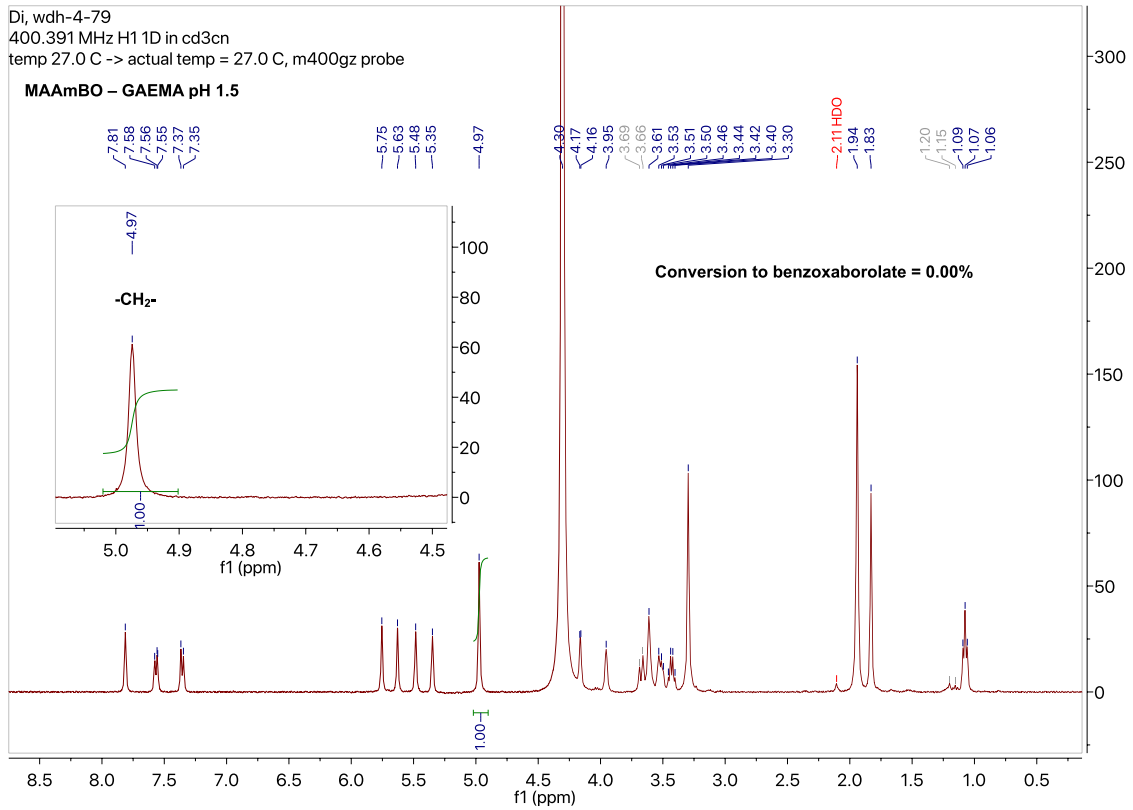


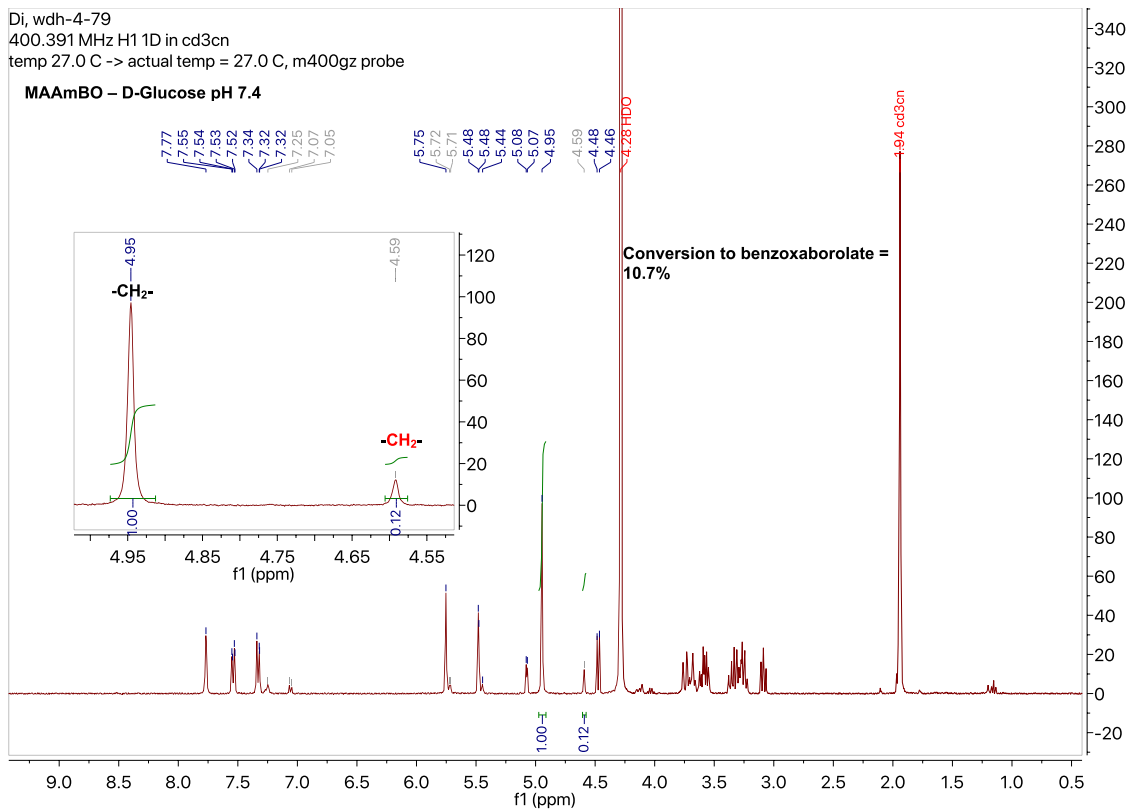
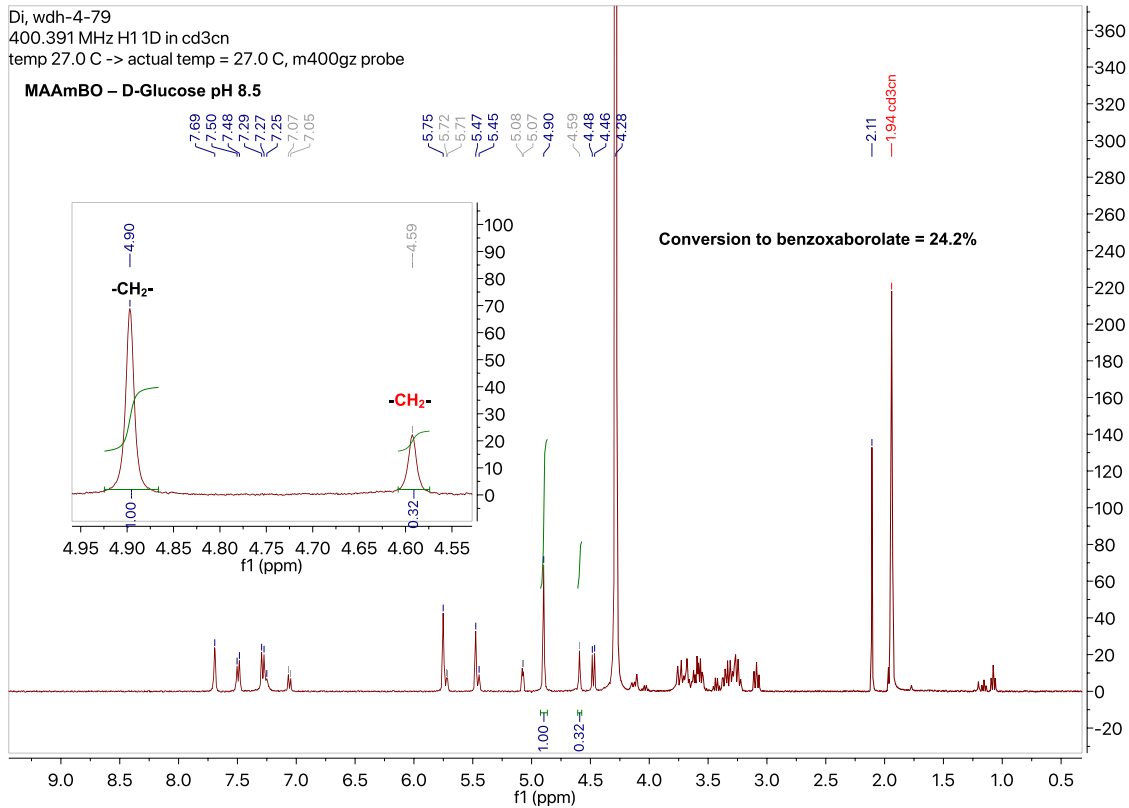


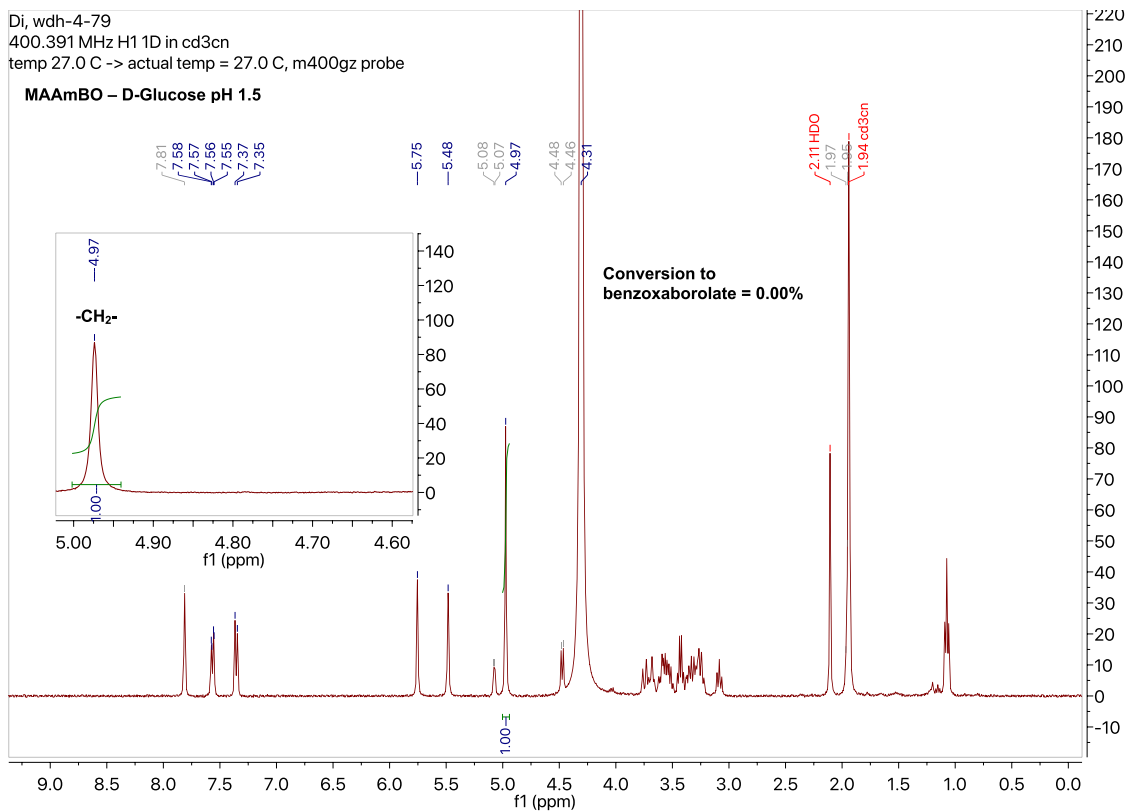
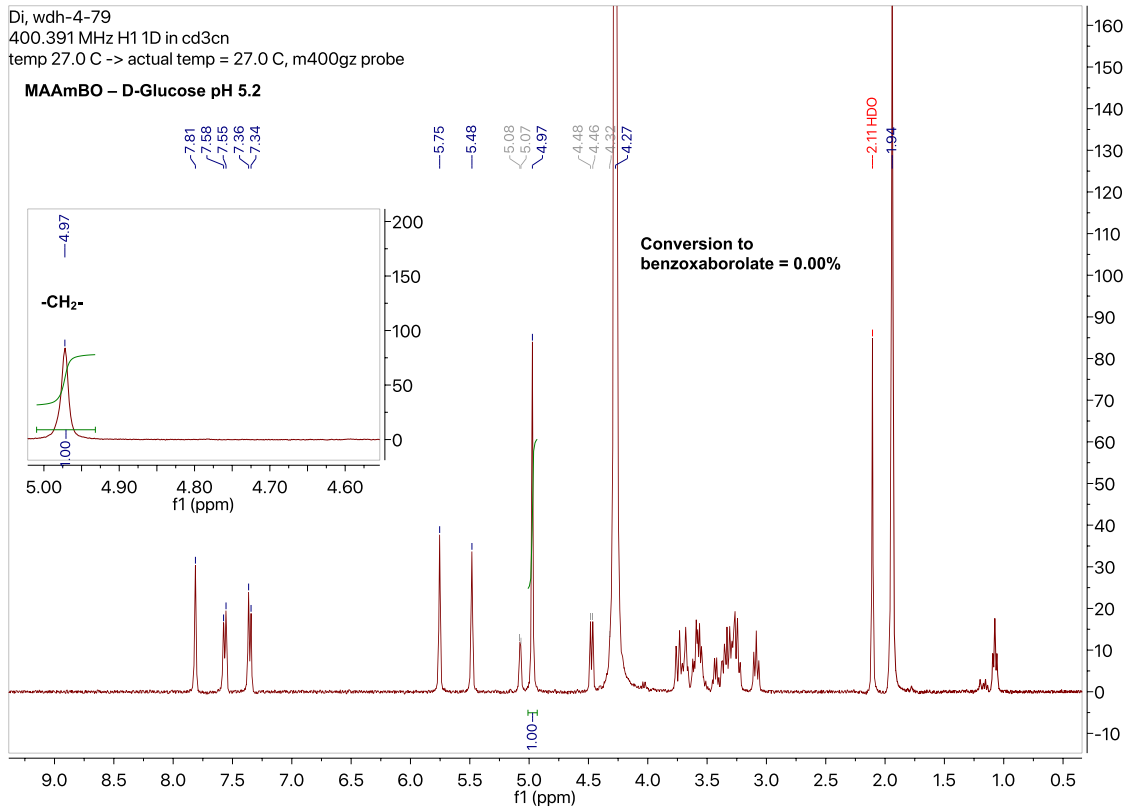


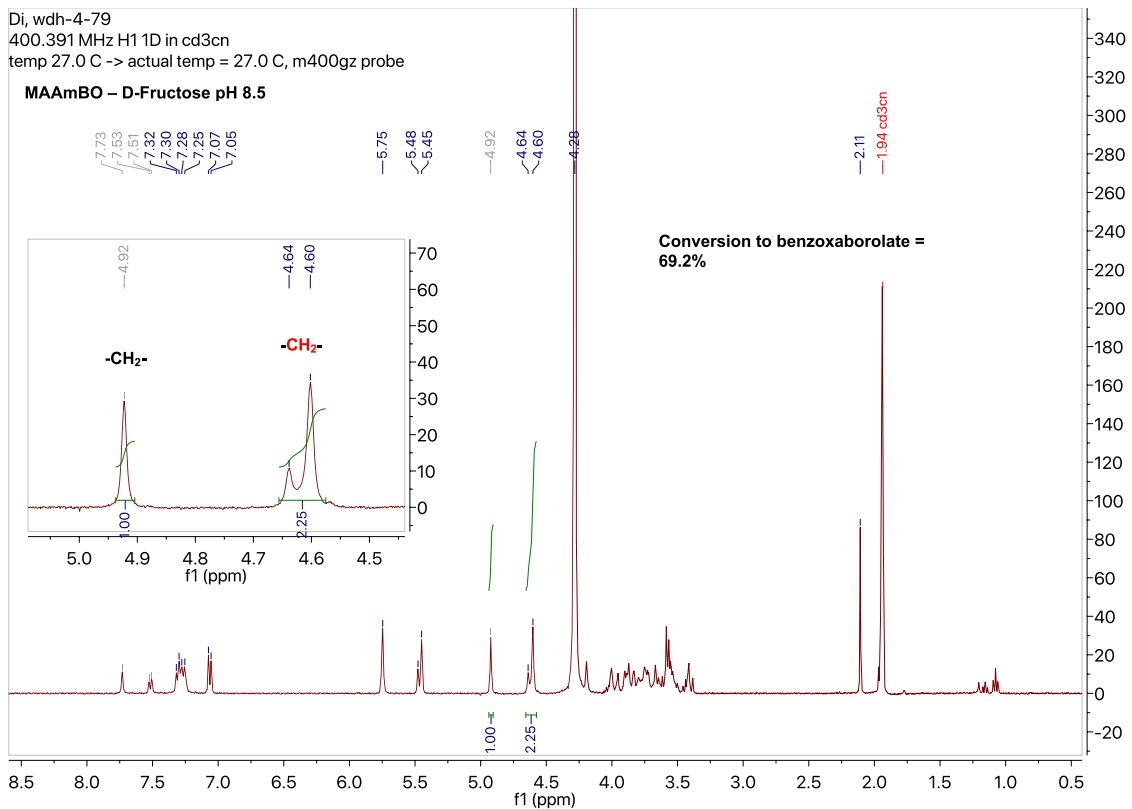
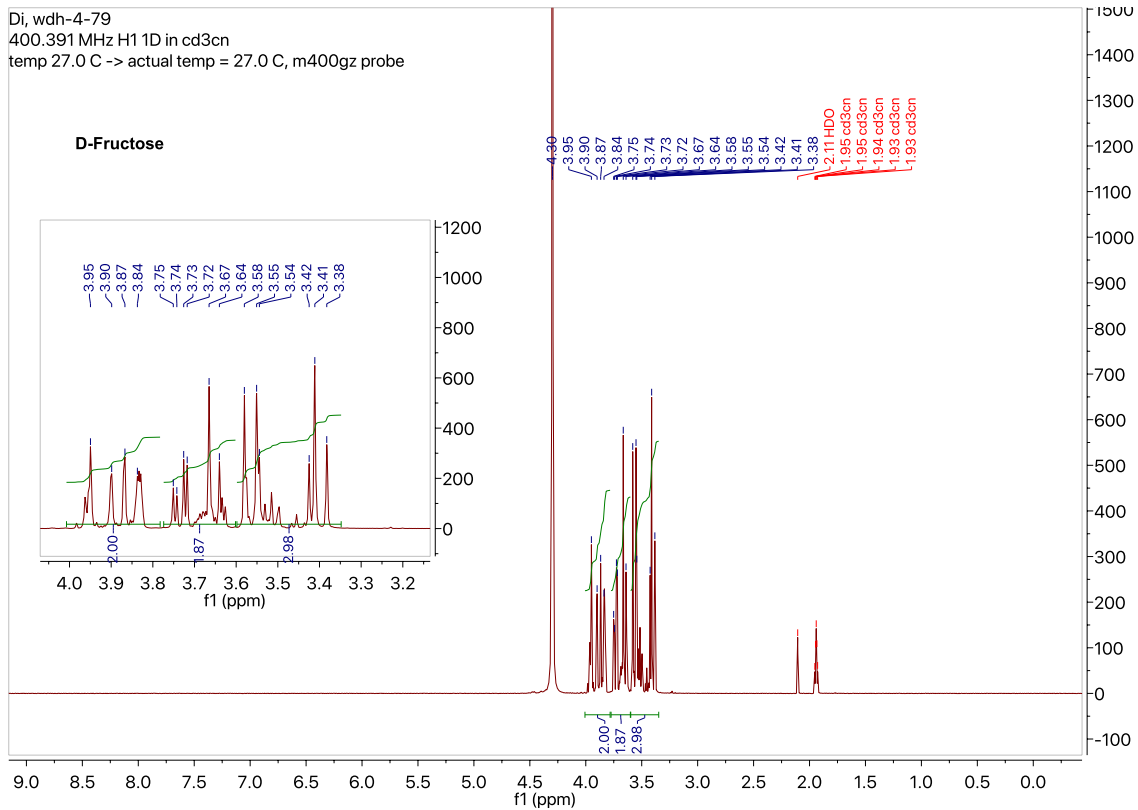


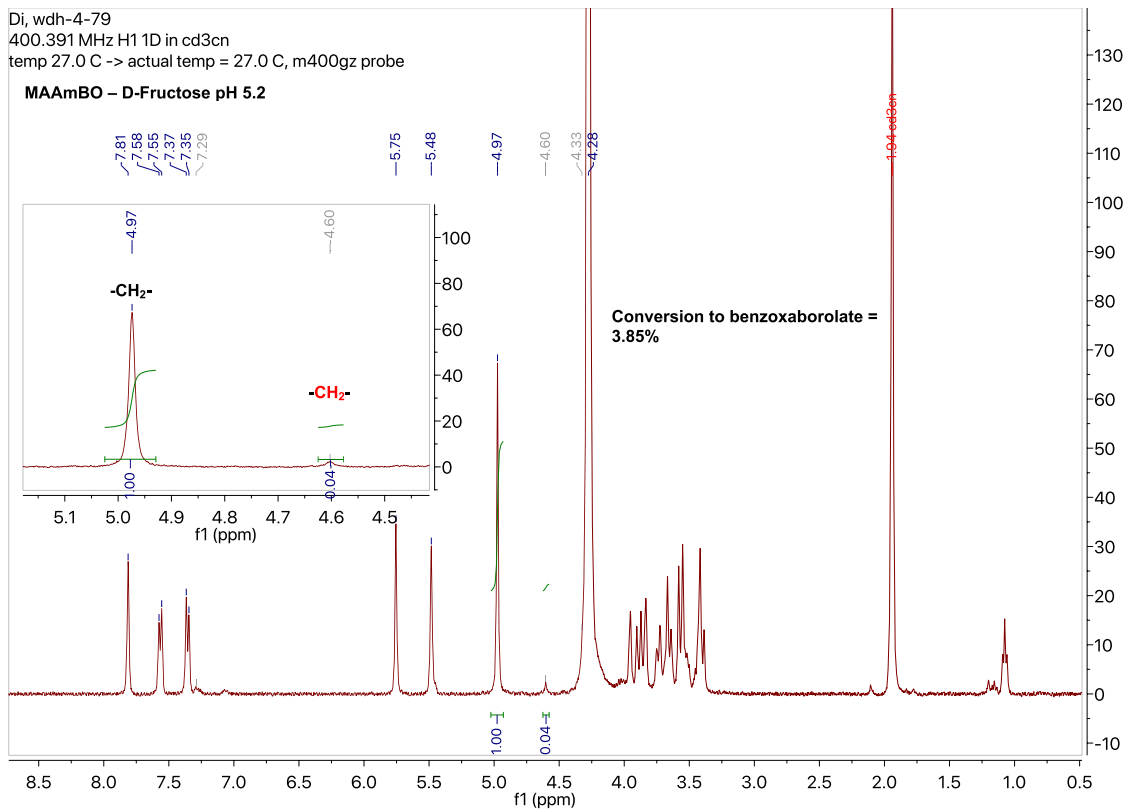
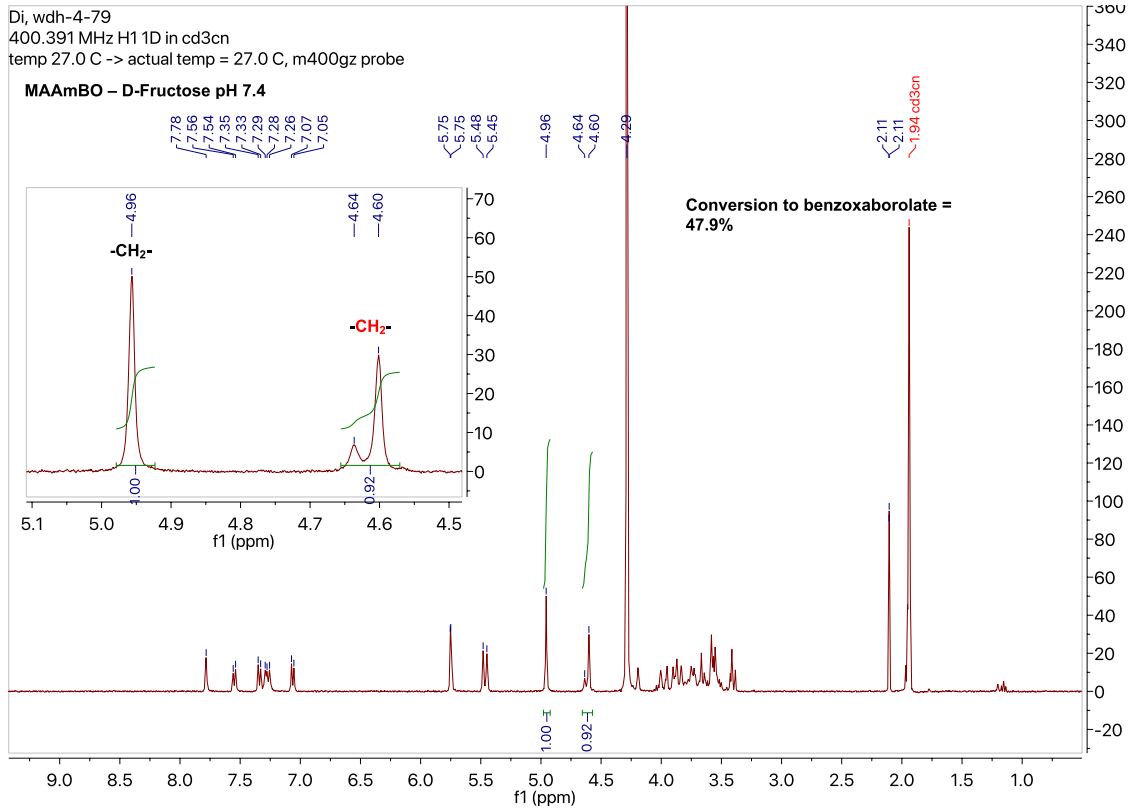


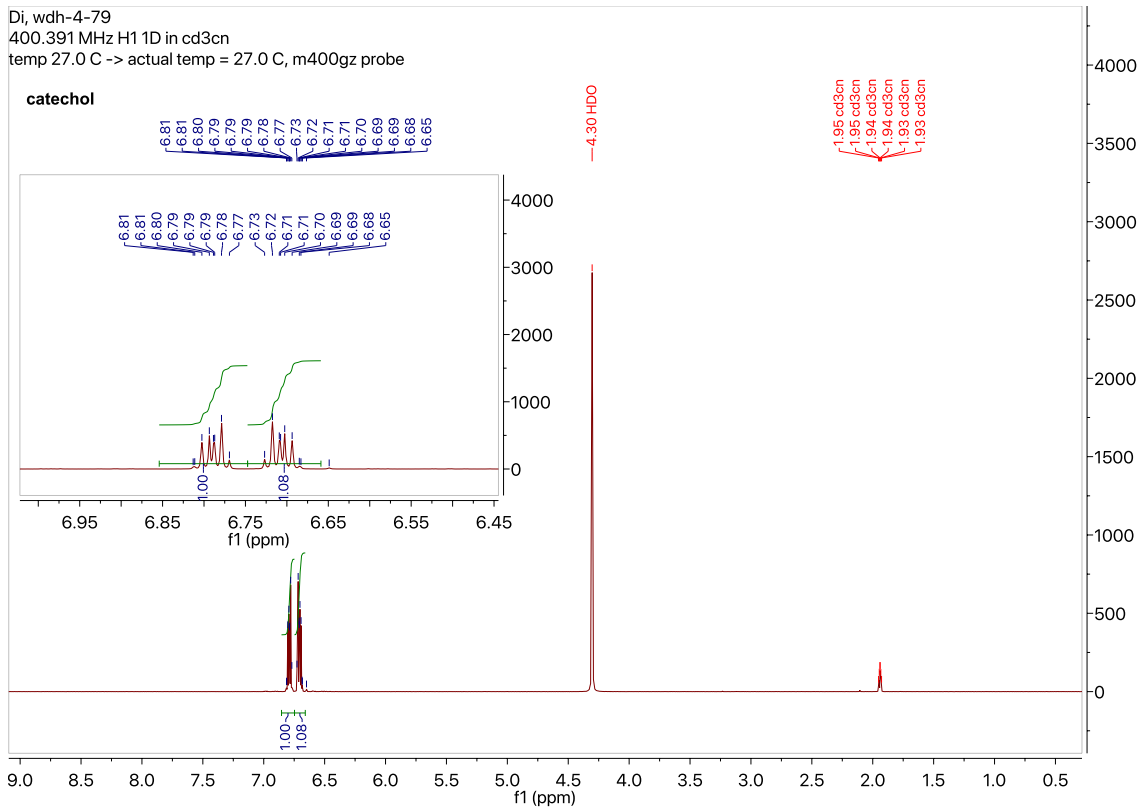
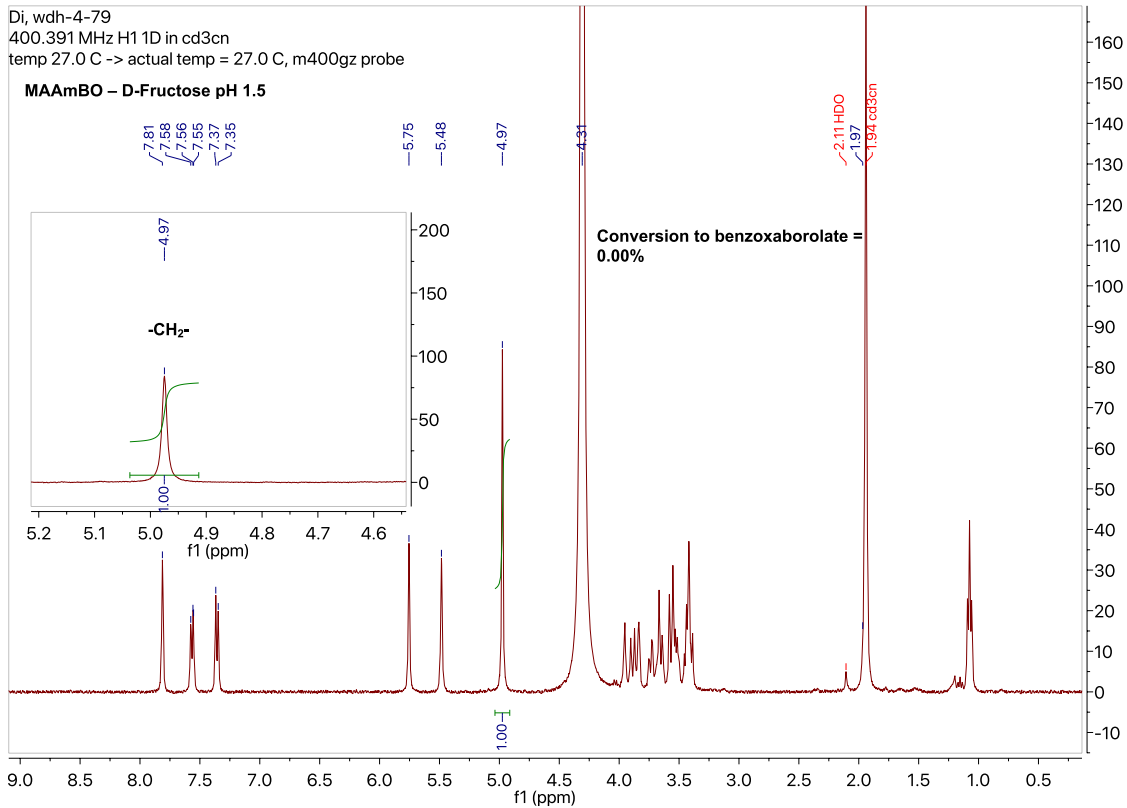


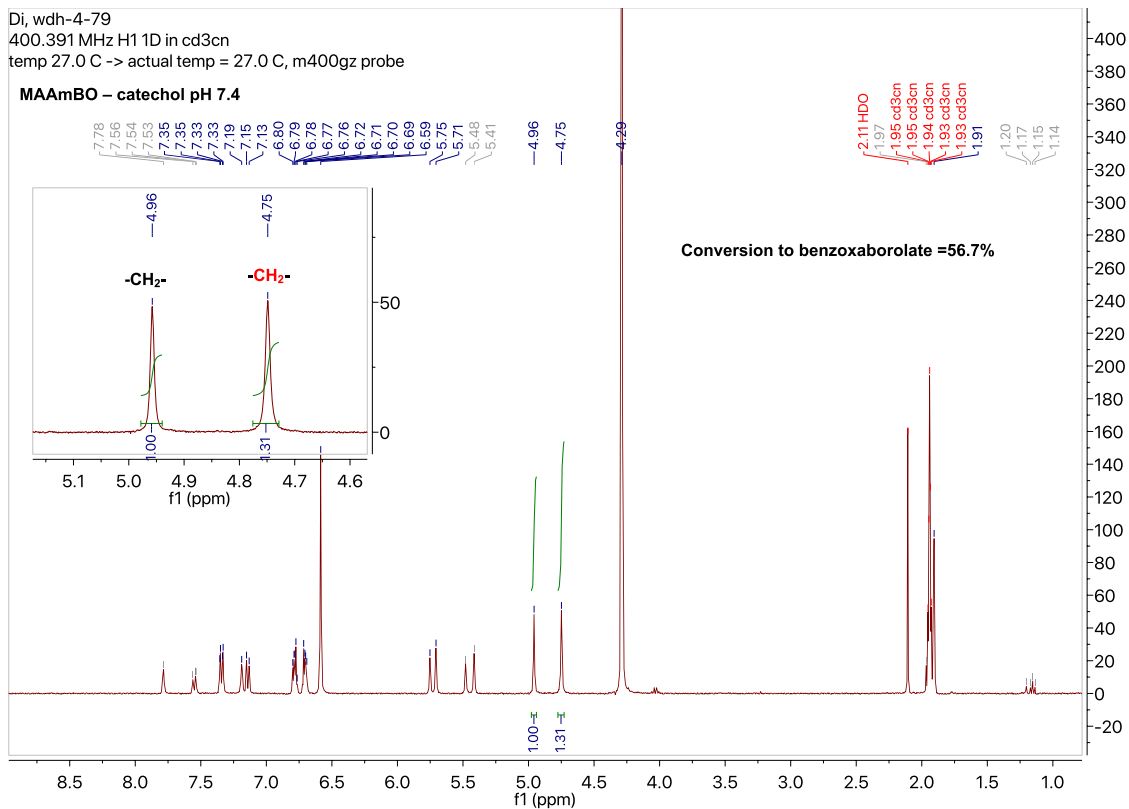
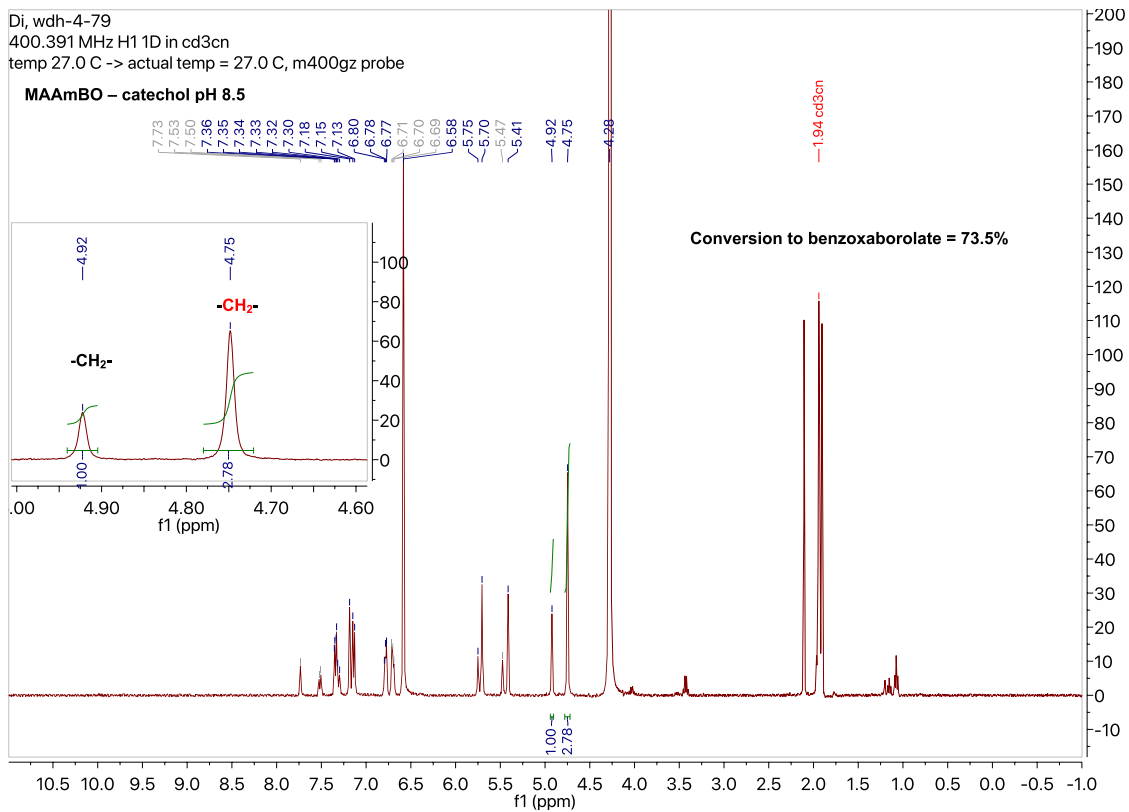


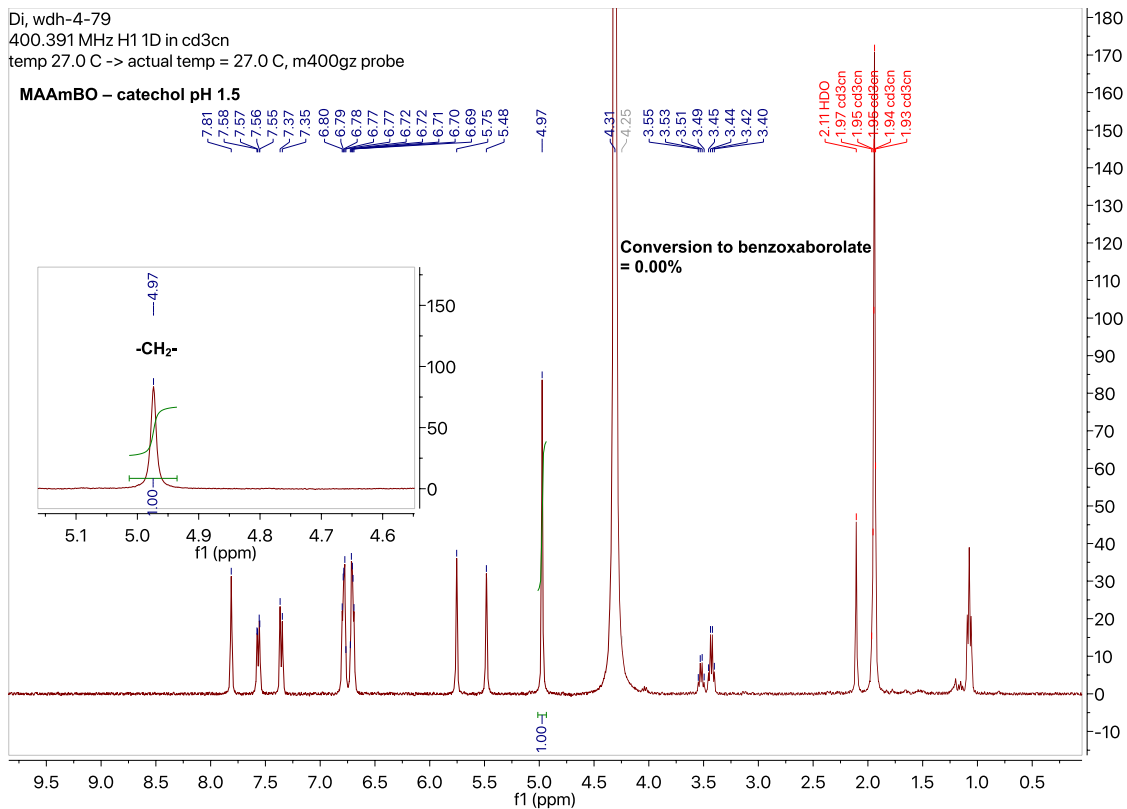
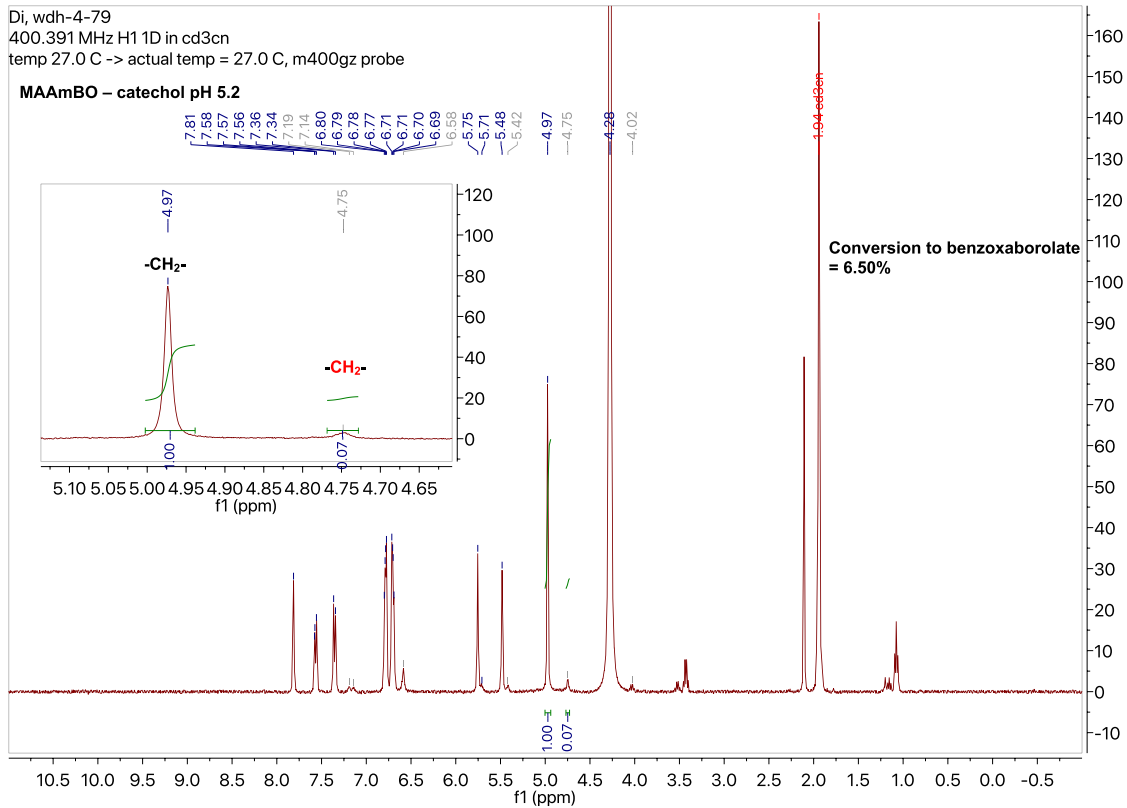


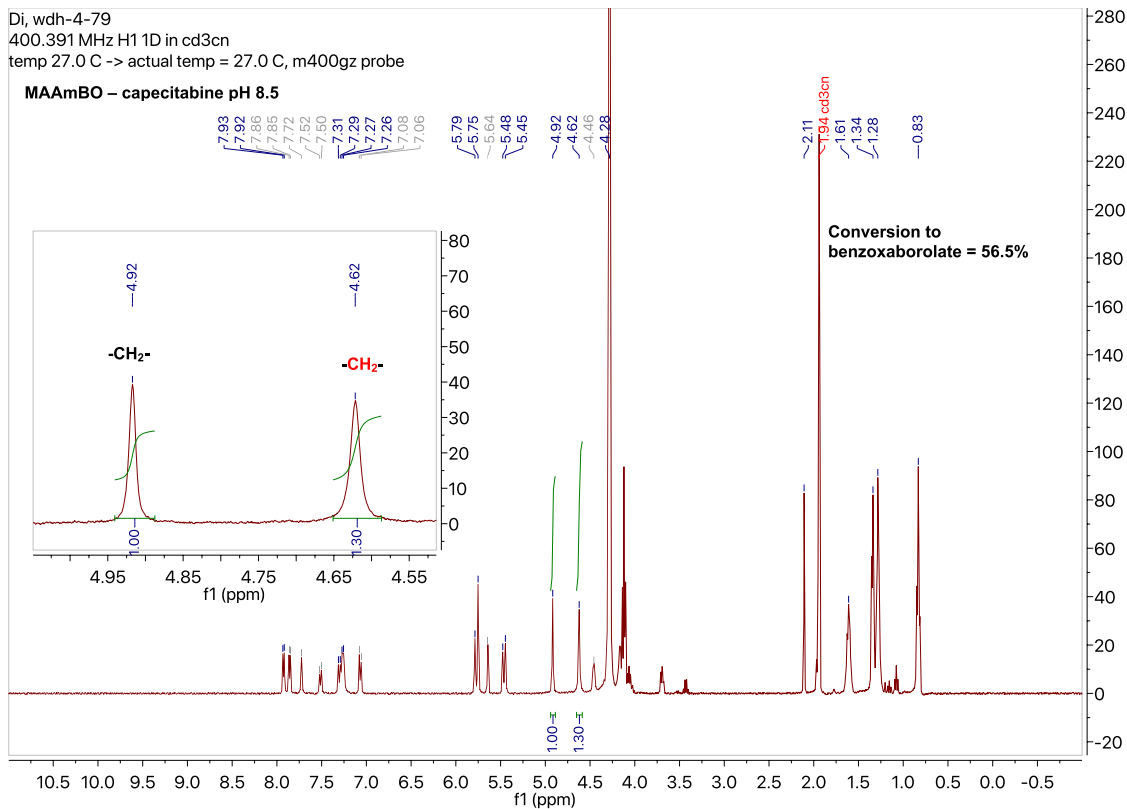
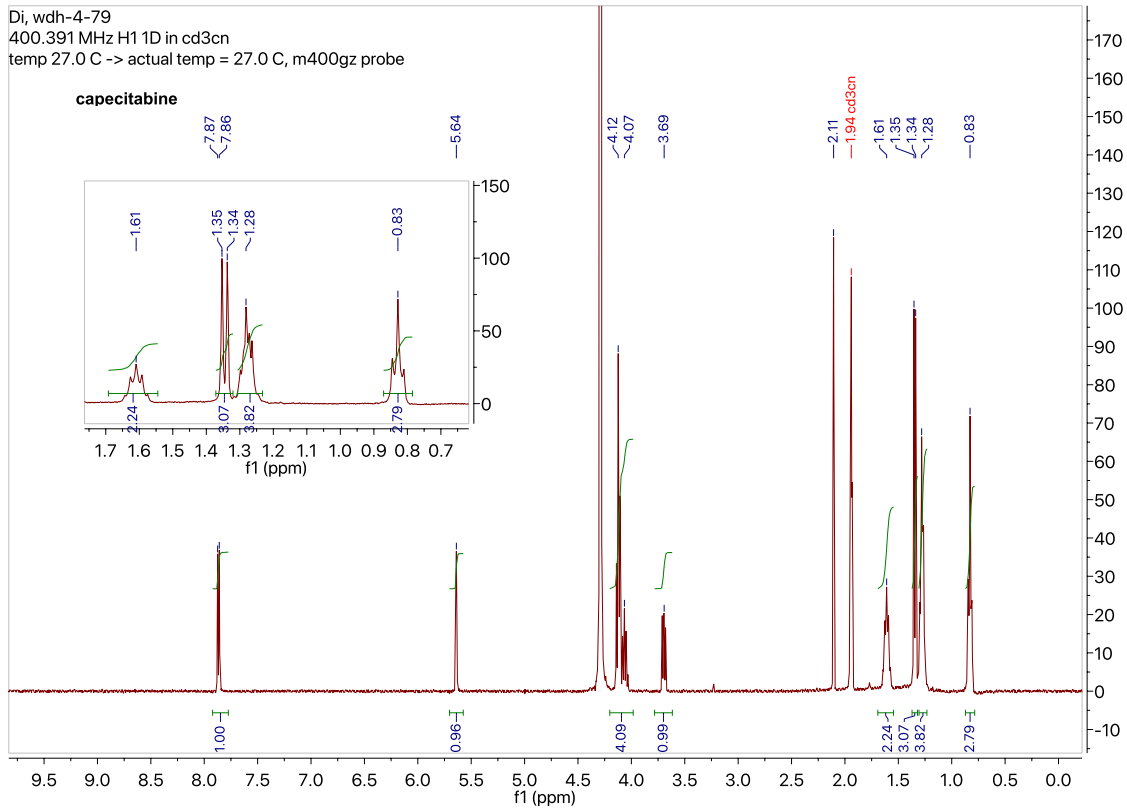


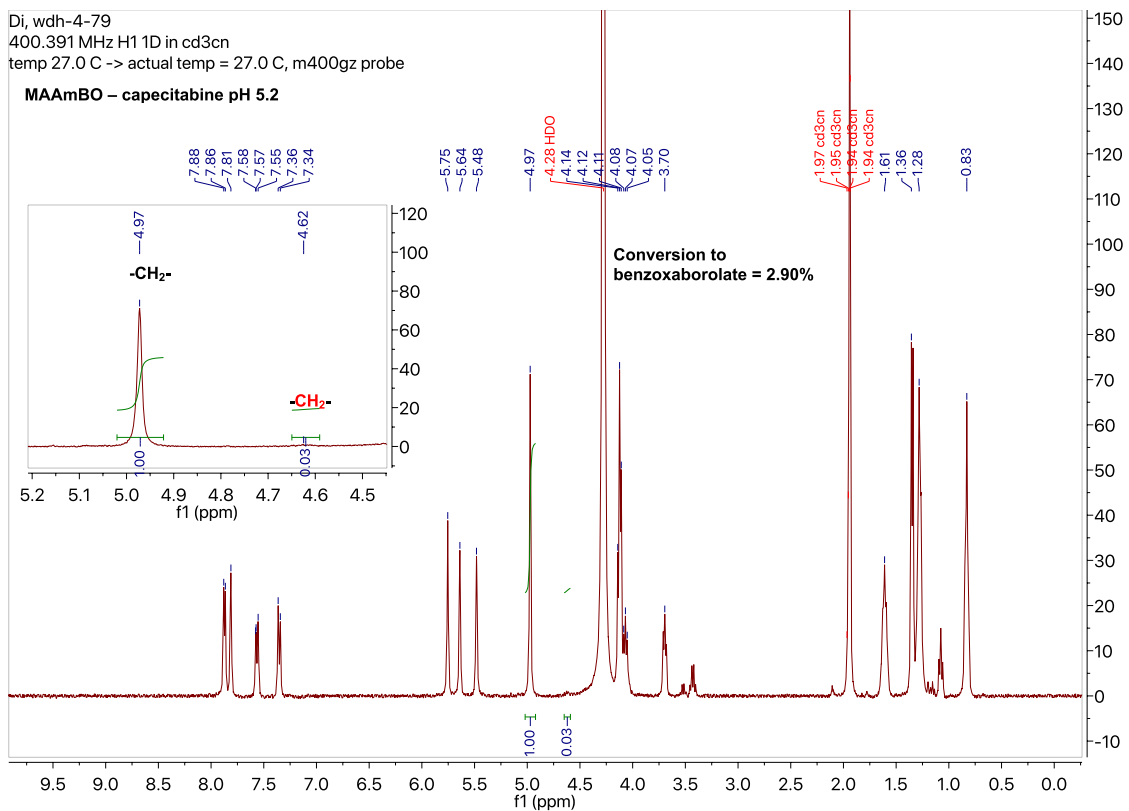
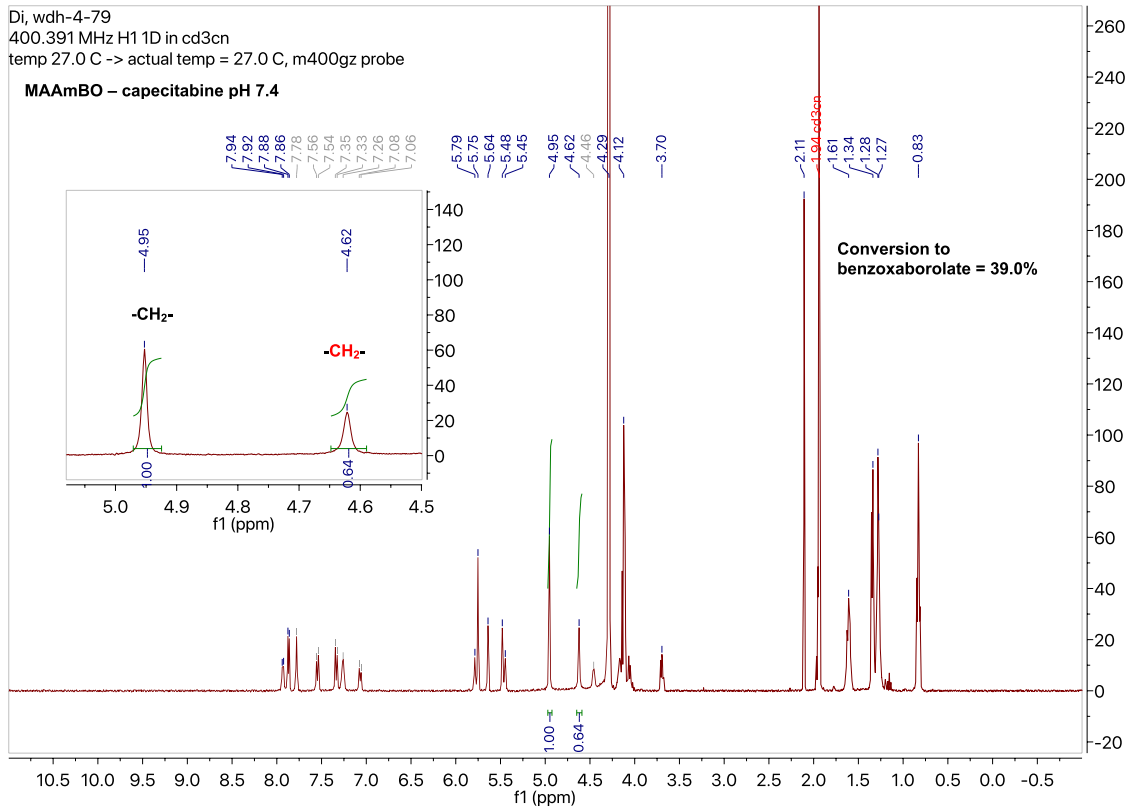


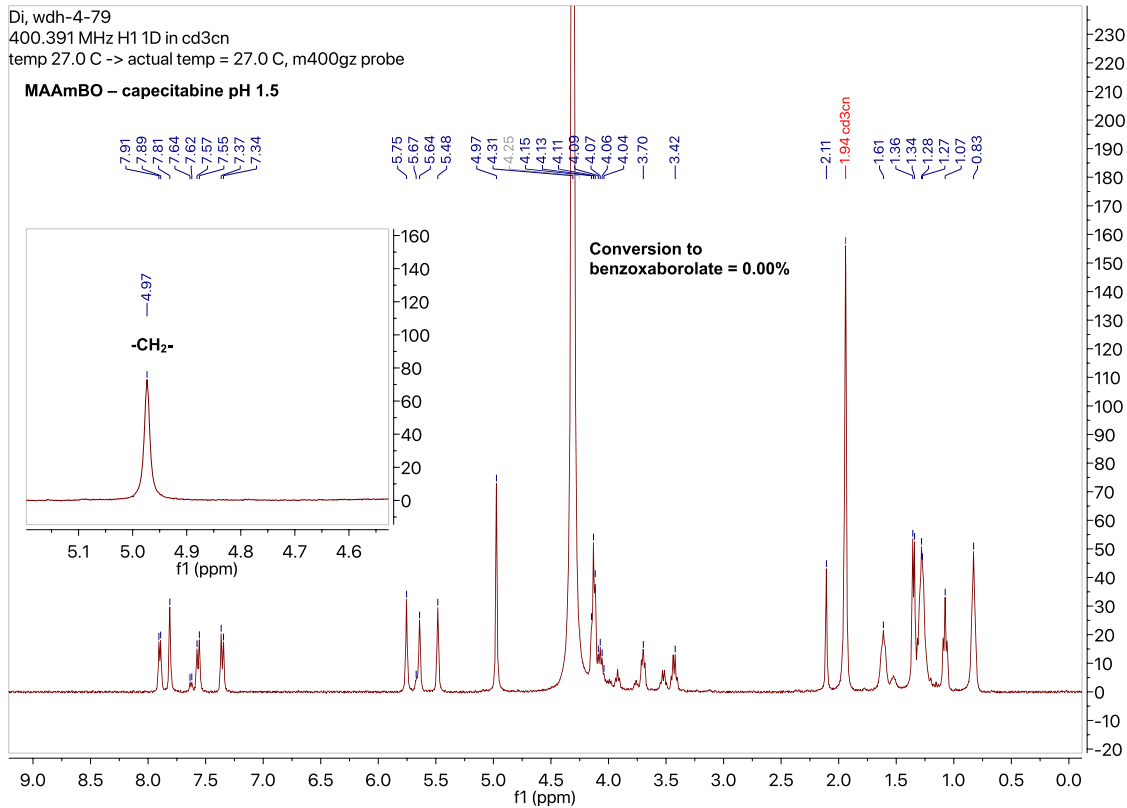






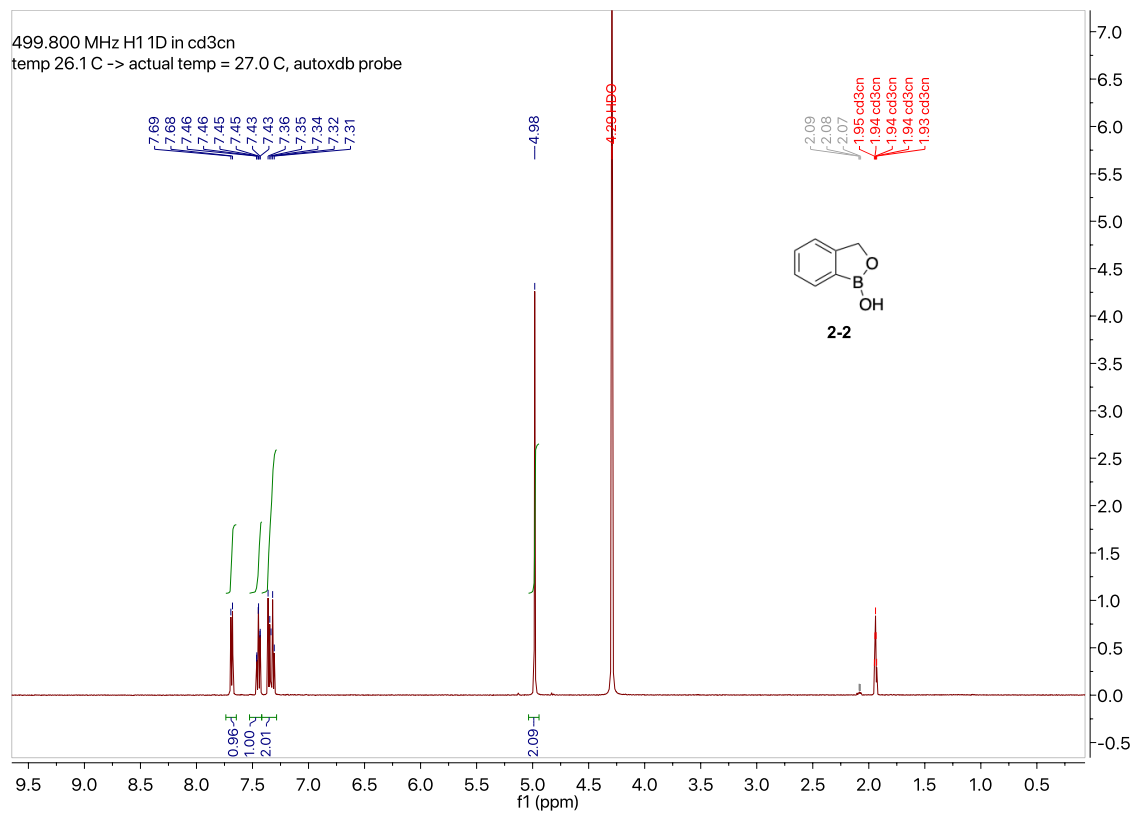


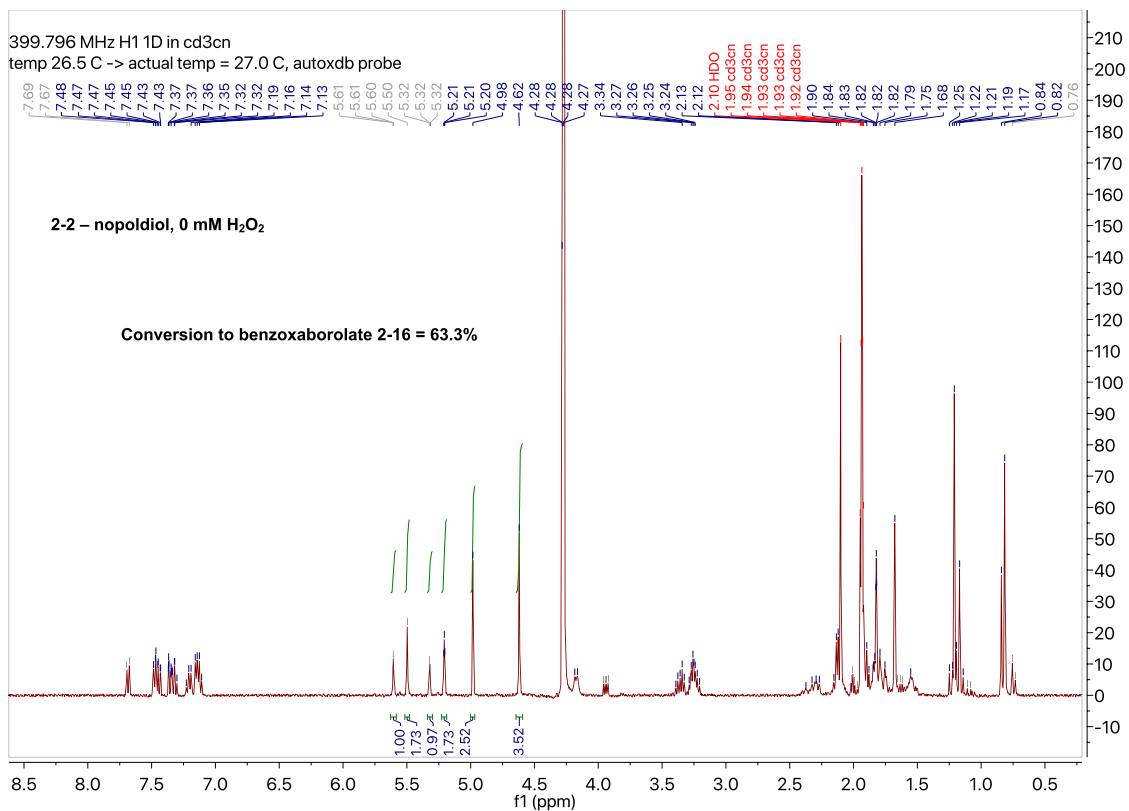
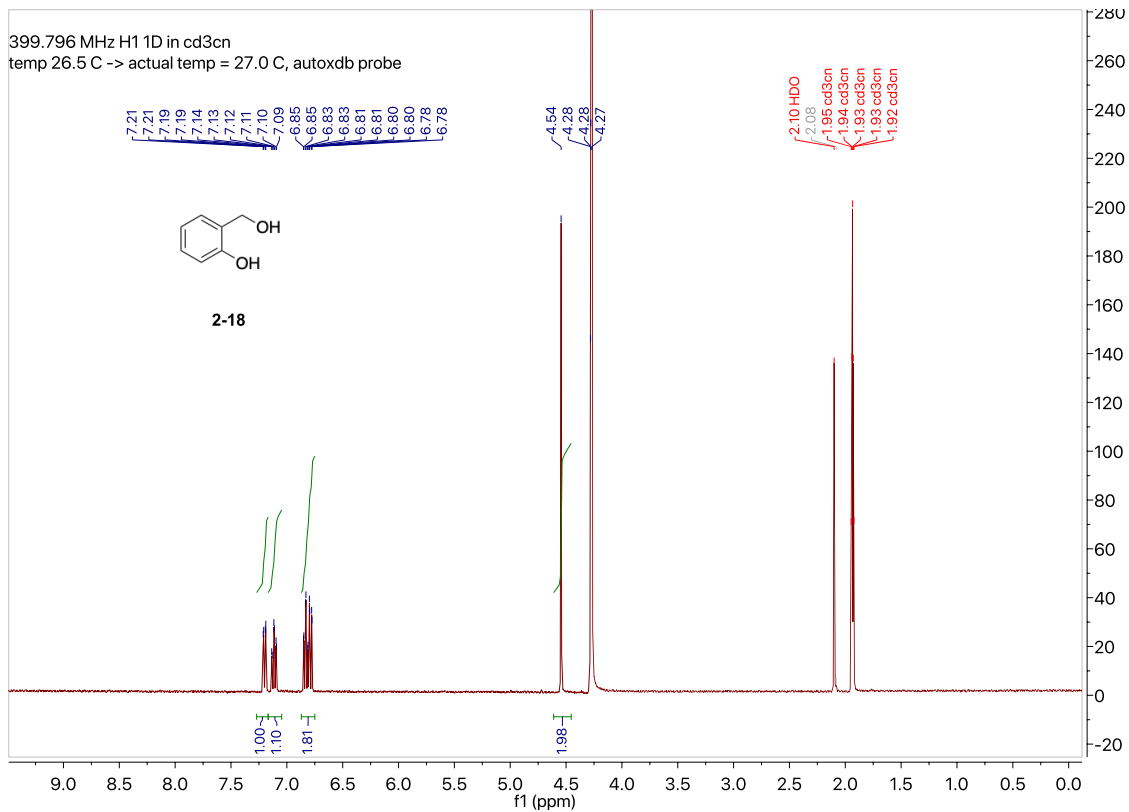


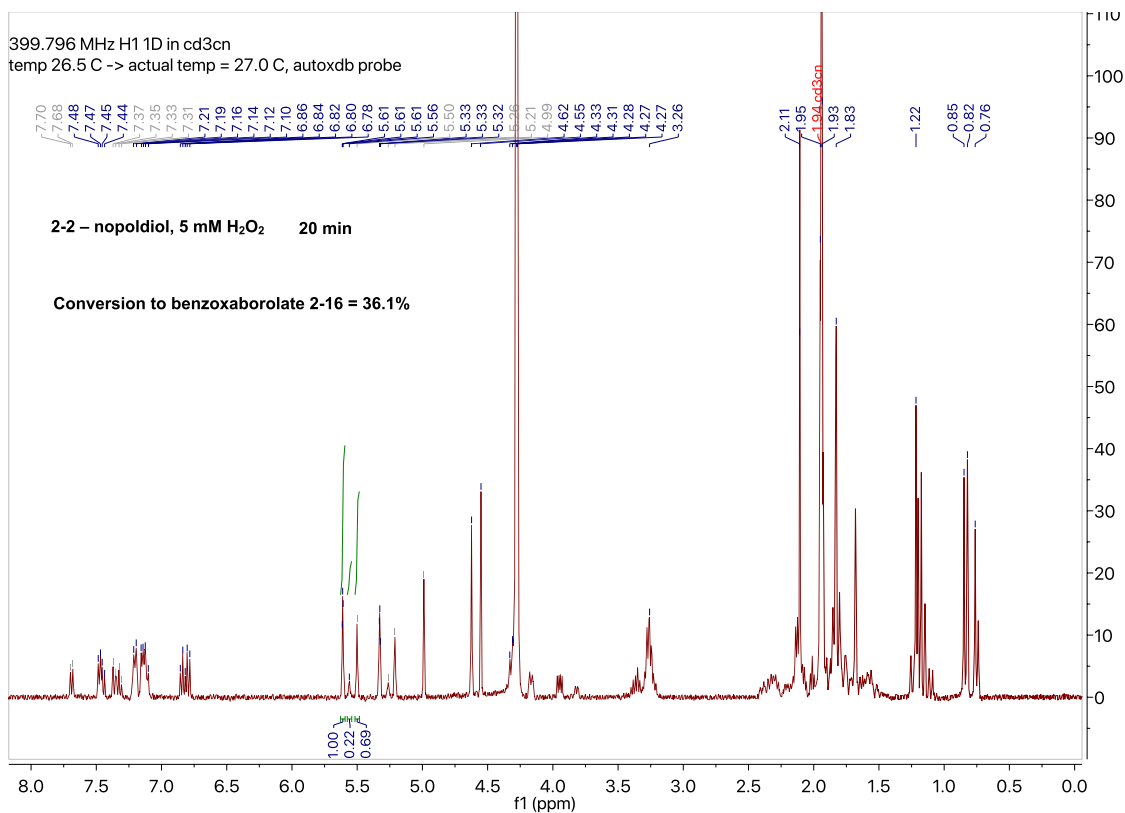
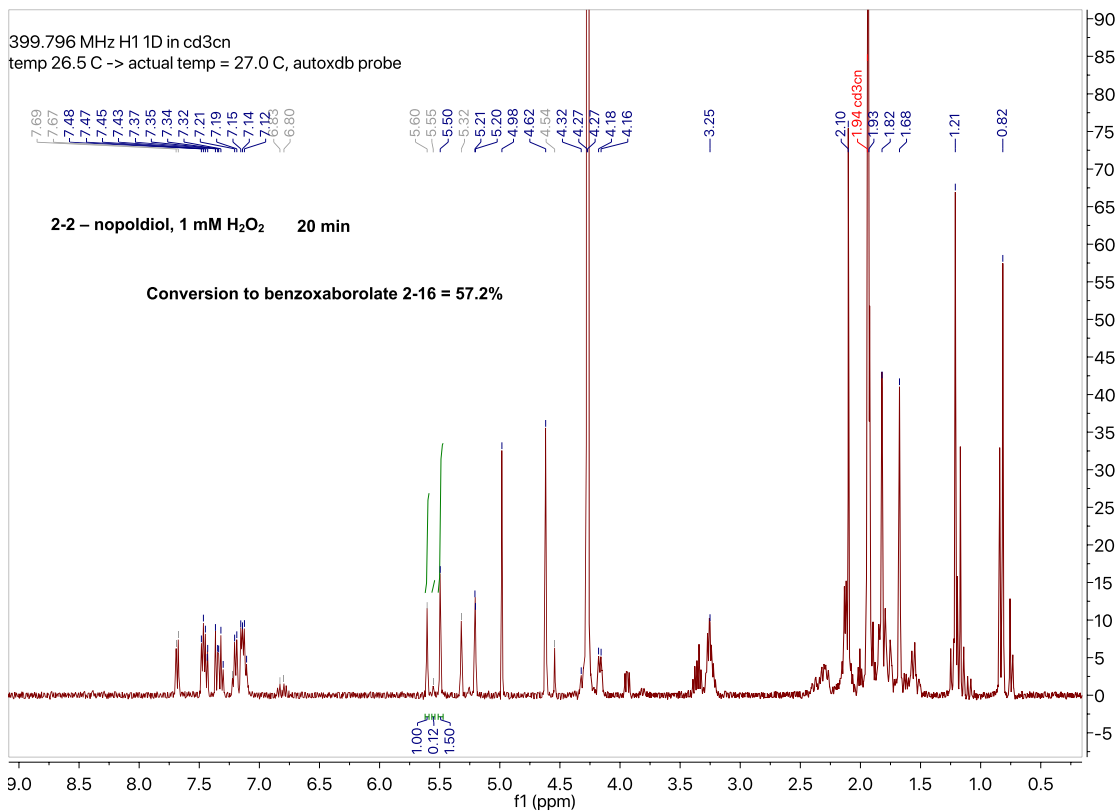


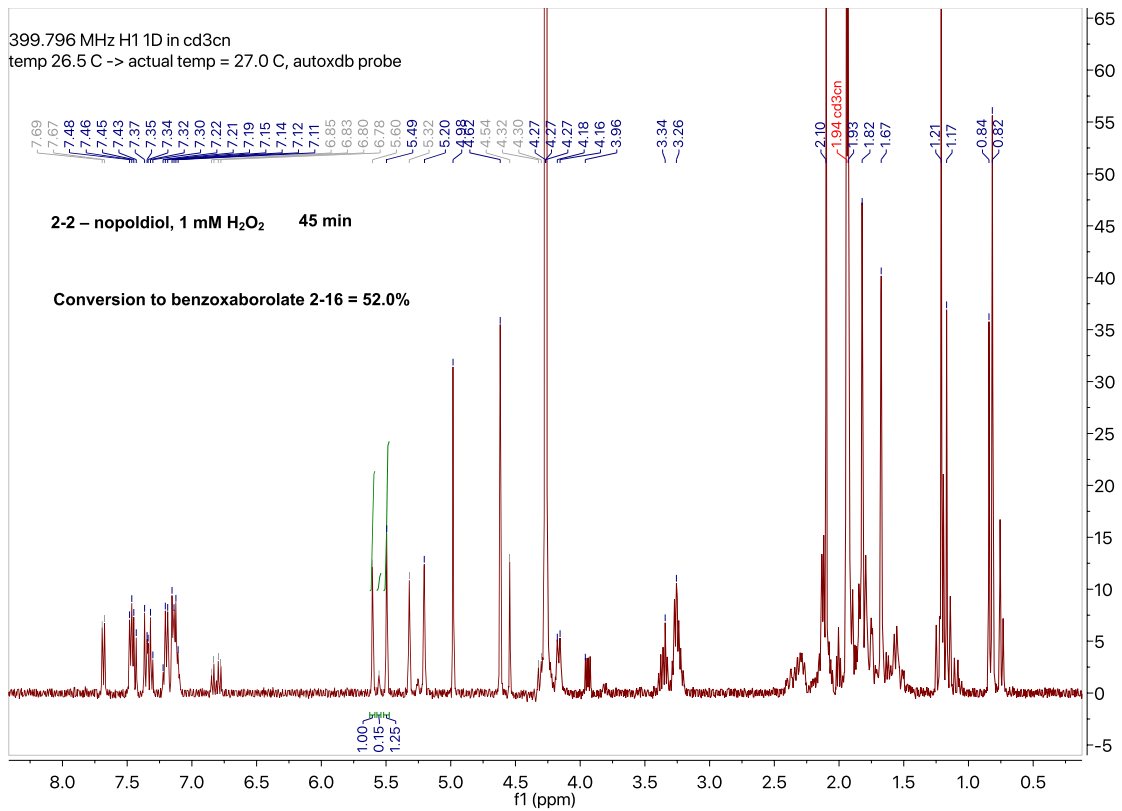
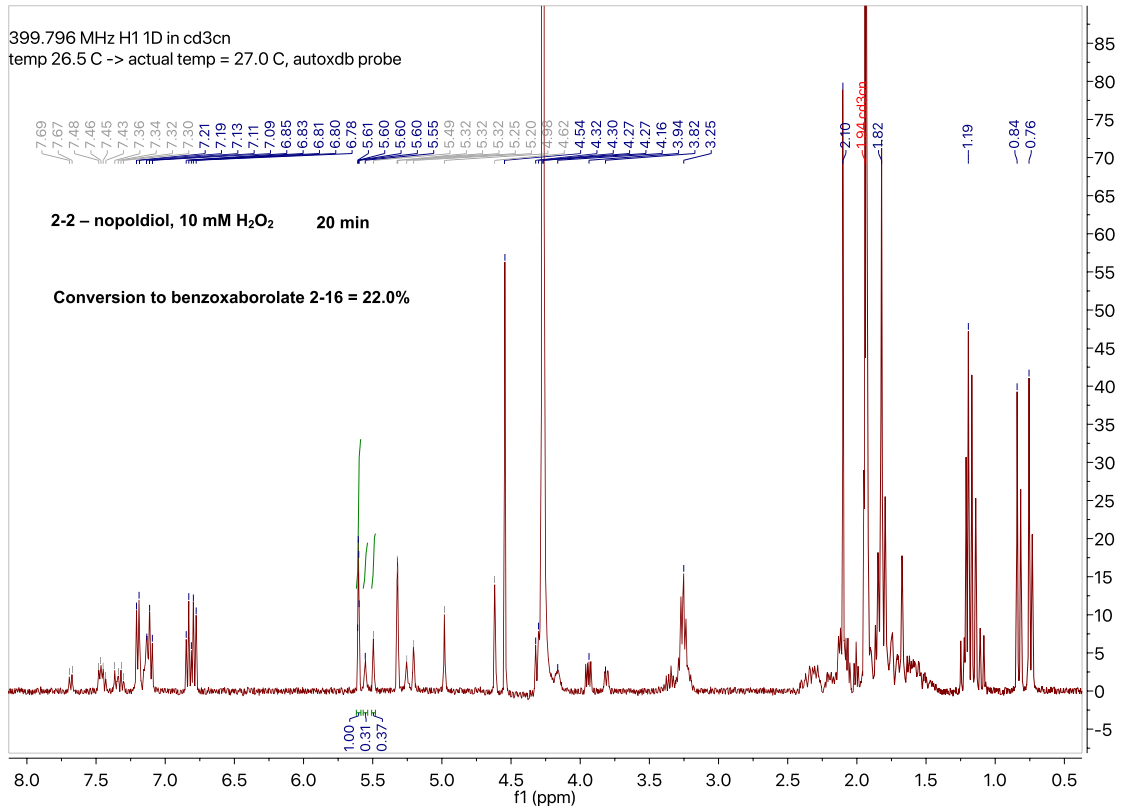
## Oxidative degradation studies:

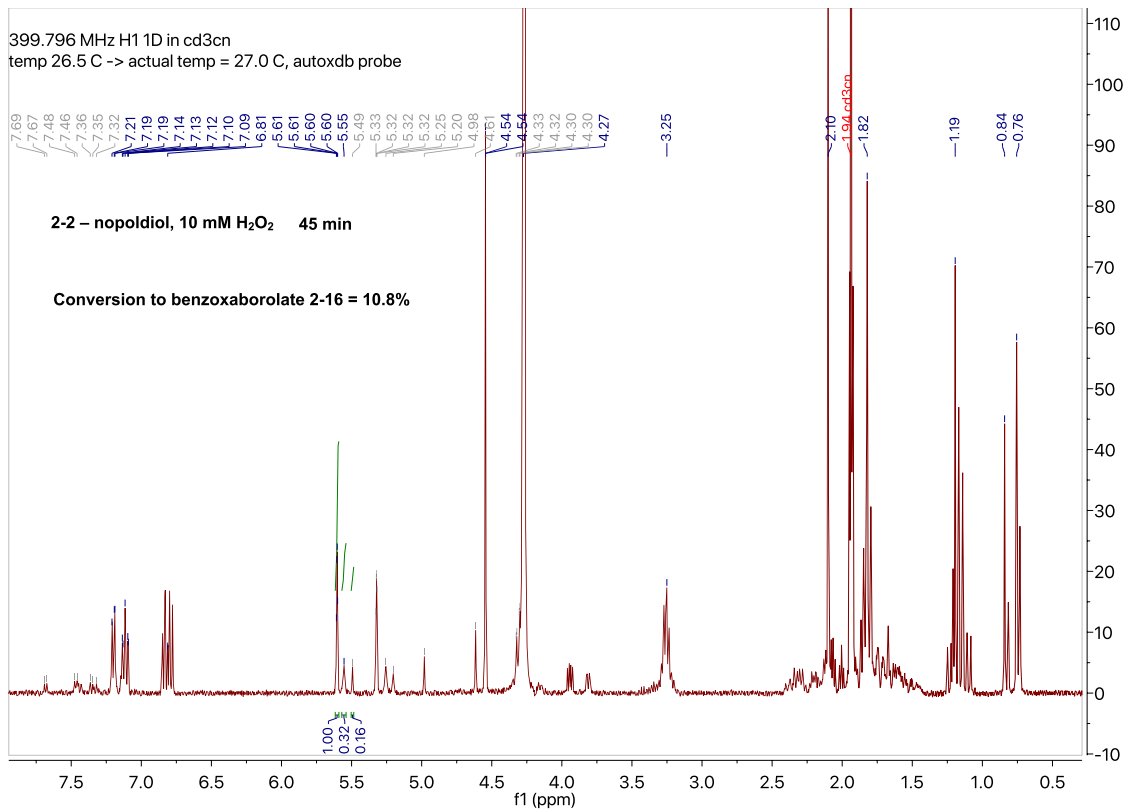
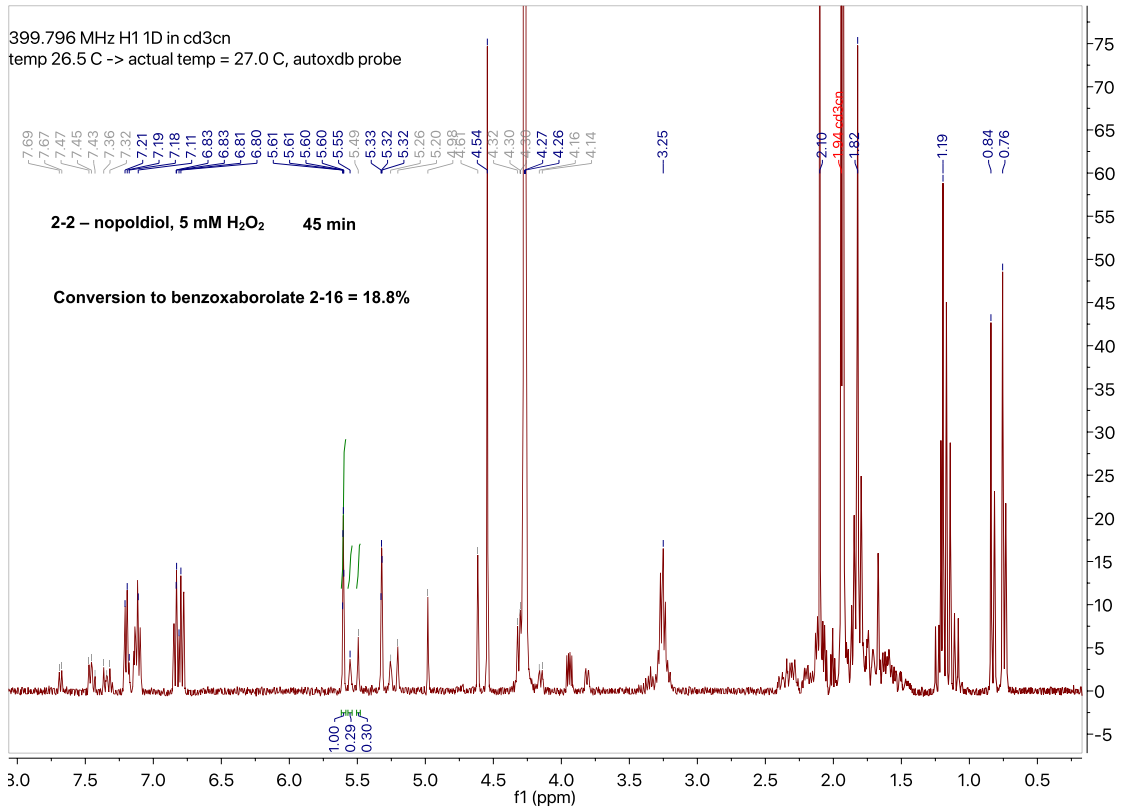
NMR solvent: D<sub>2</sub>O phosphate buffer:ACN-*d*<sub>3</sub> 65:35 w%, NMR was locked as ACN-*d*<sub>3</sub> while tuning.



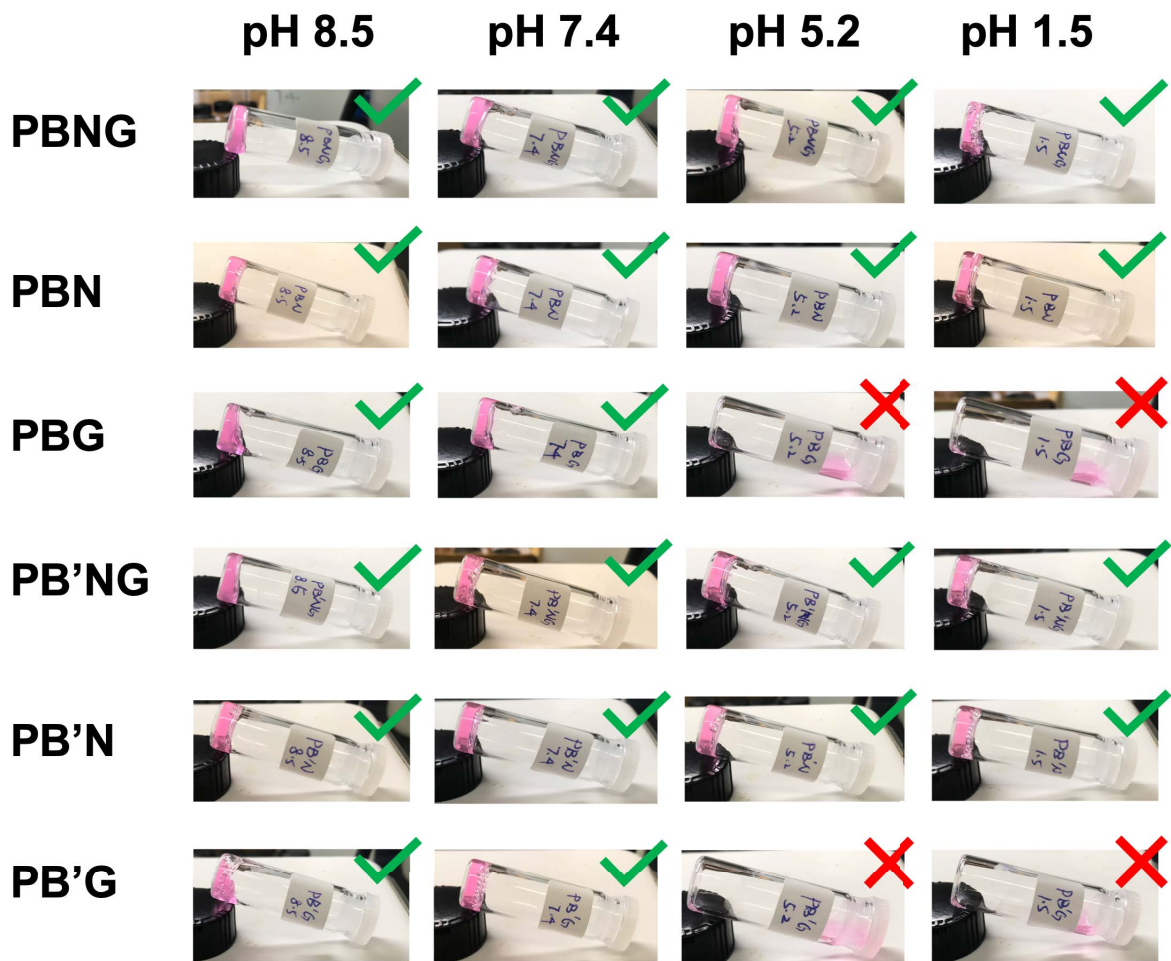








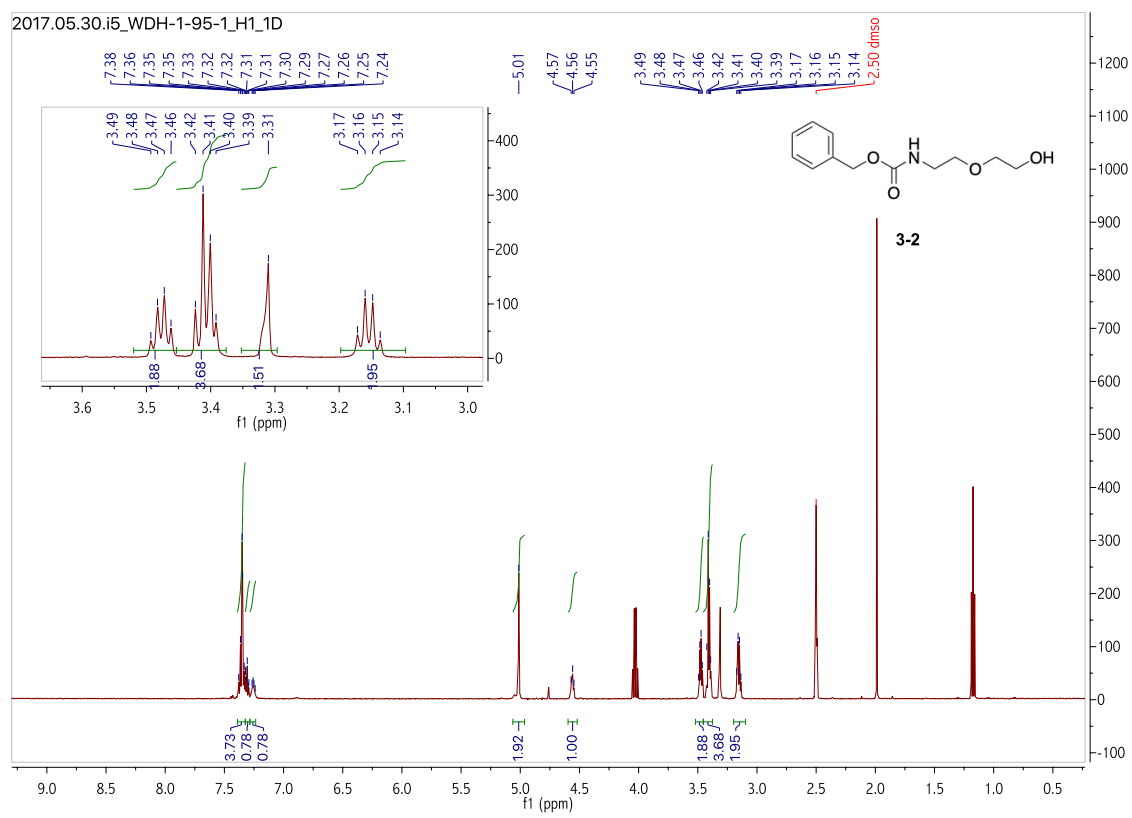
Pictures of hydrogel formations (stained by rhodamine B) from pH 8.5 to 1.5:

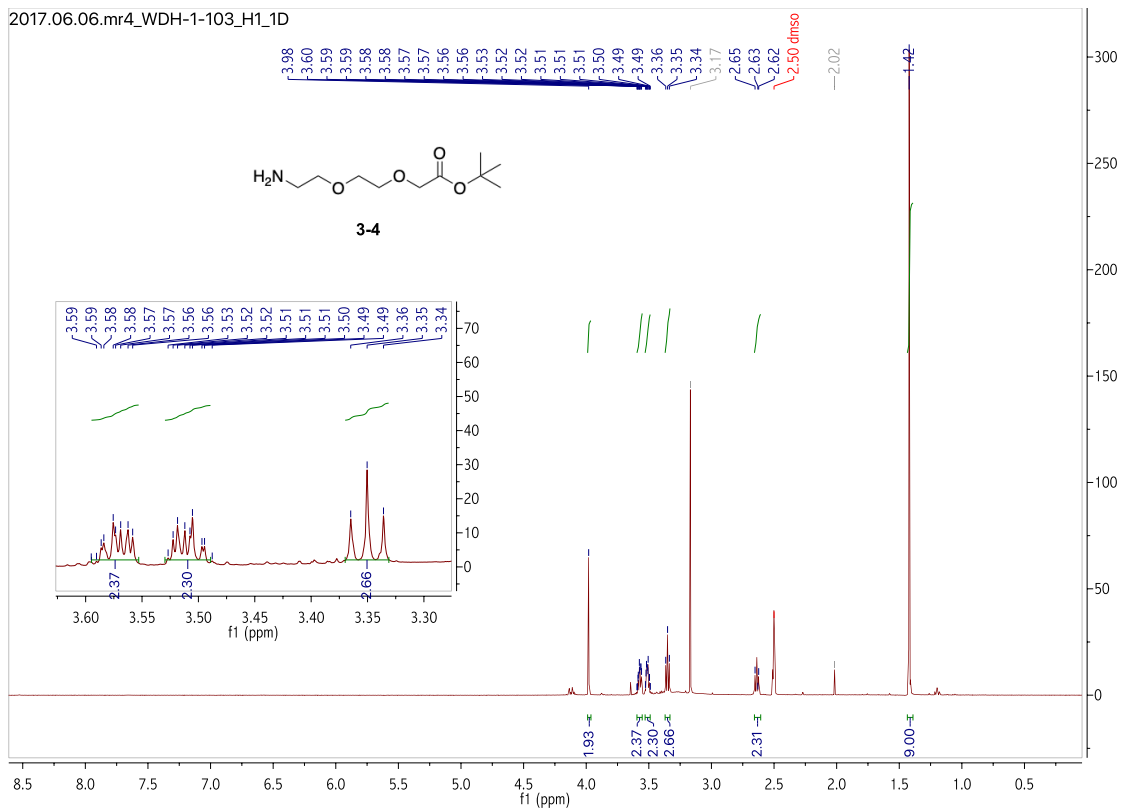
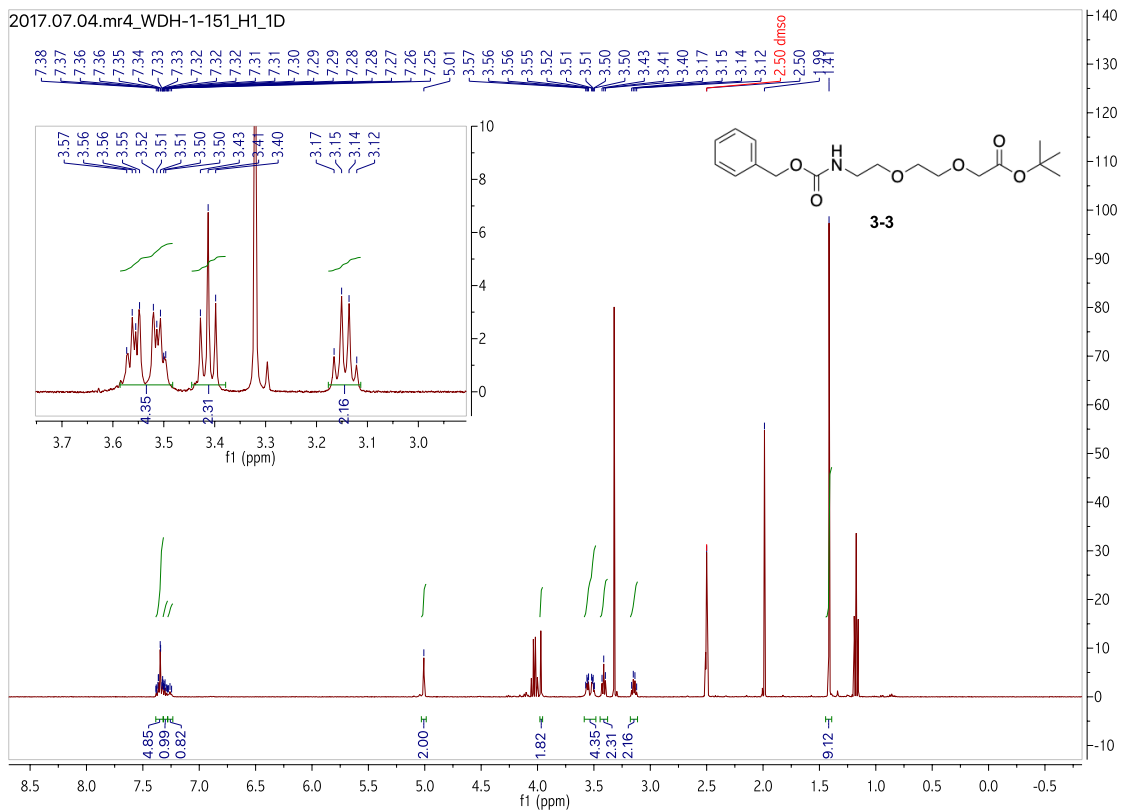


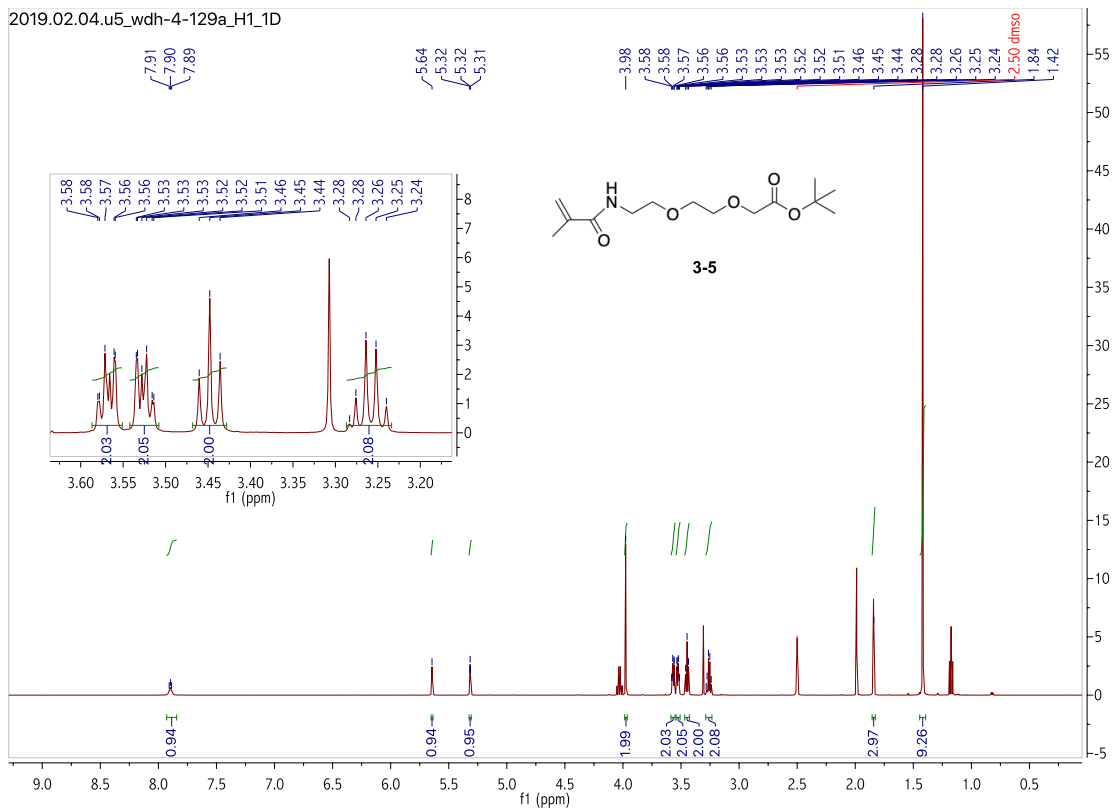
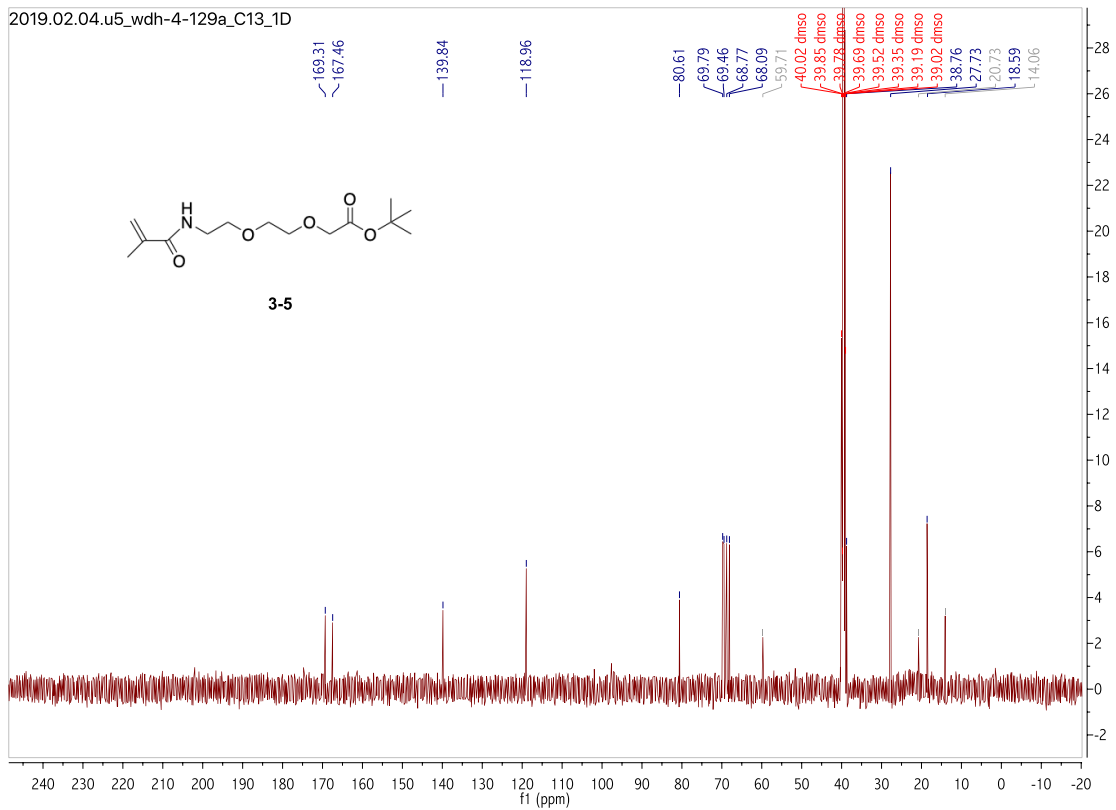
## Appendix 2: Selected copies of NMR spectra of compounds and polymers found in Chapter

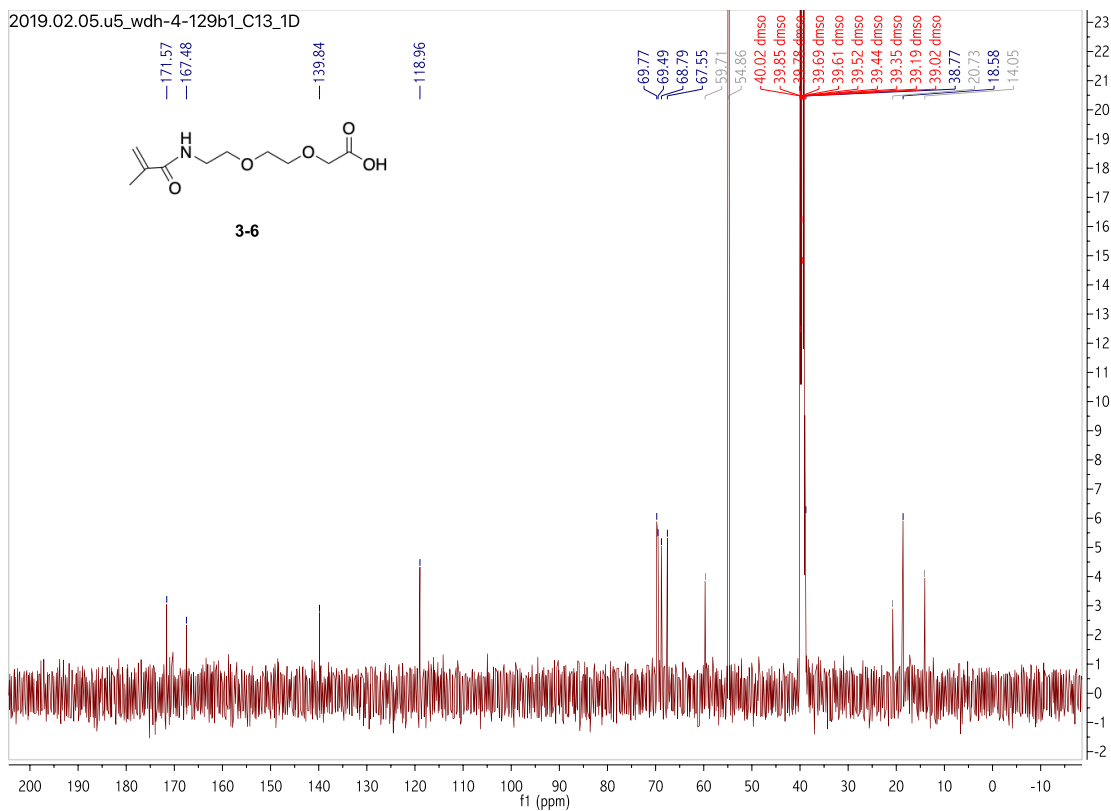
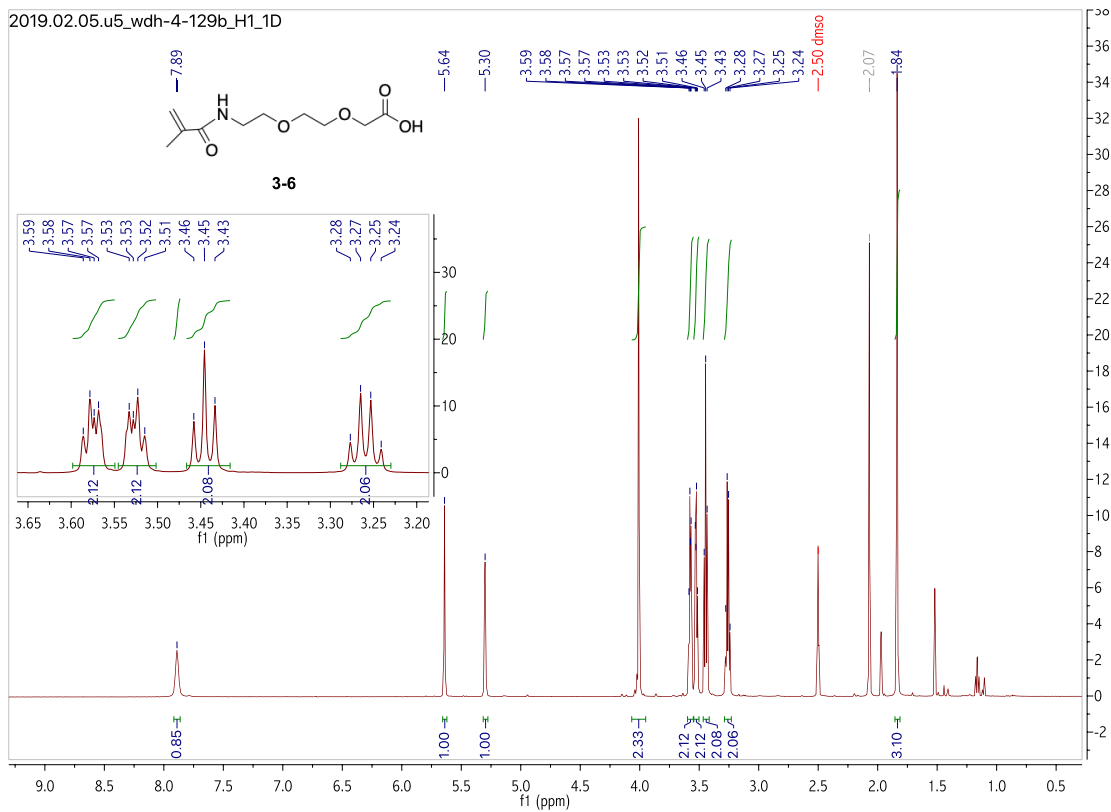
3.

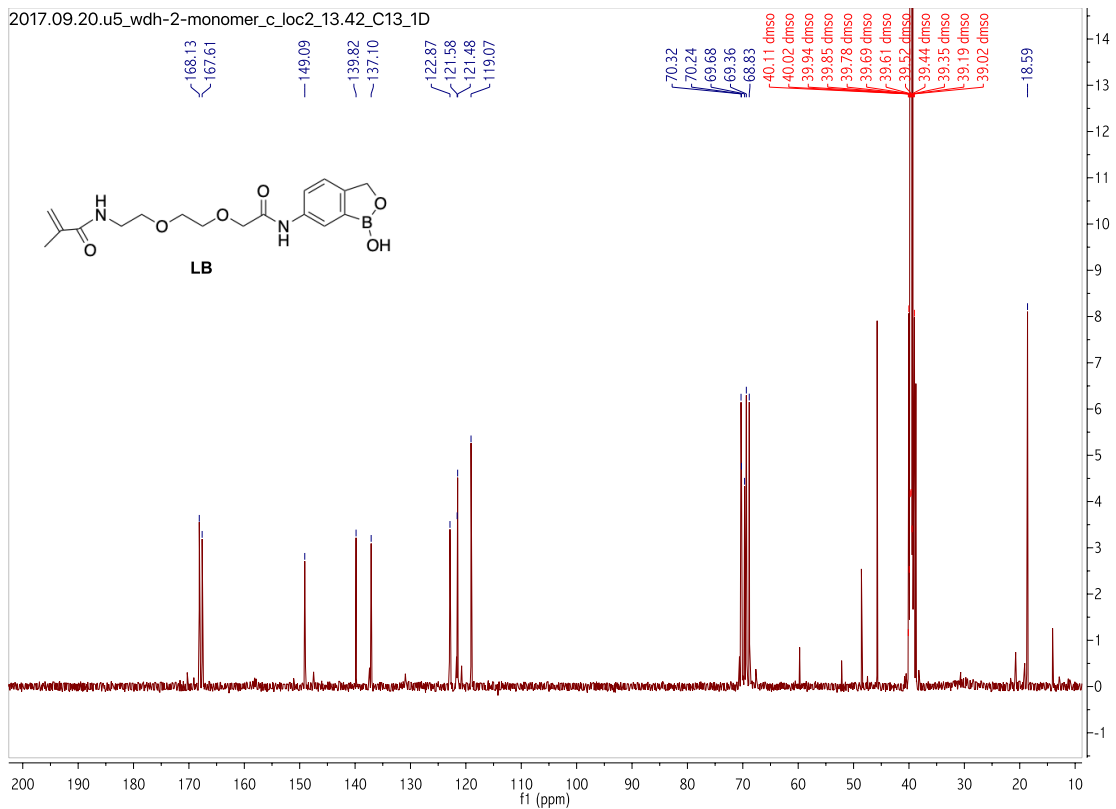
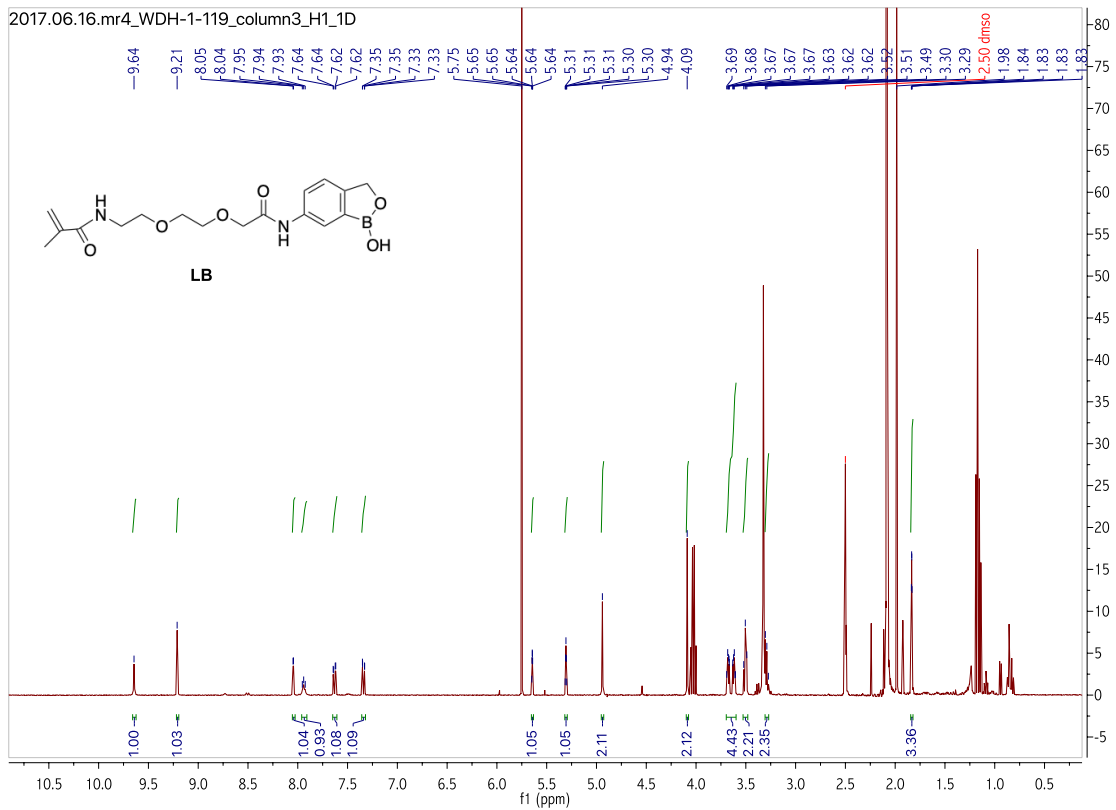
### Compounds:



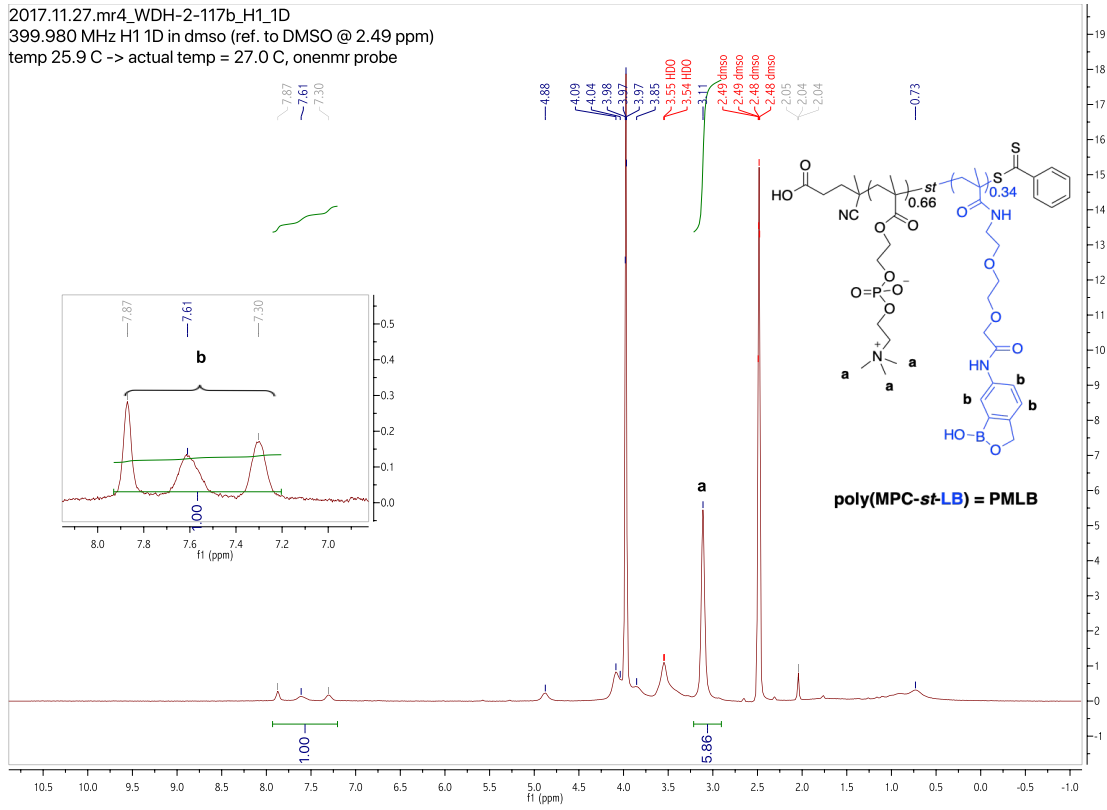


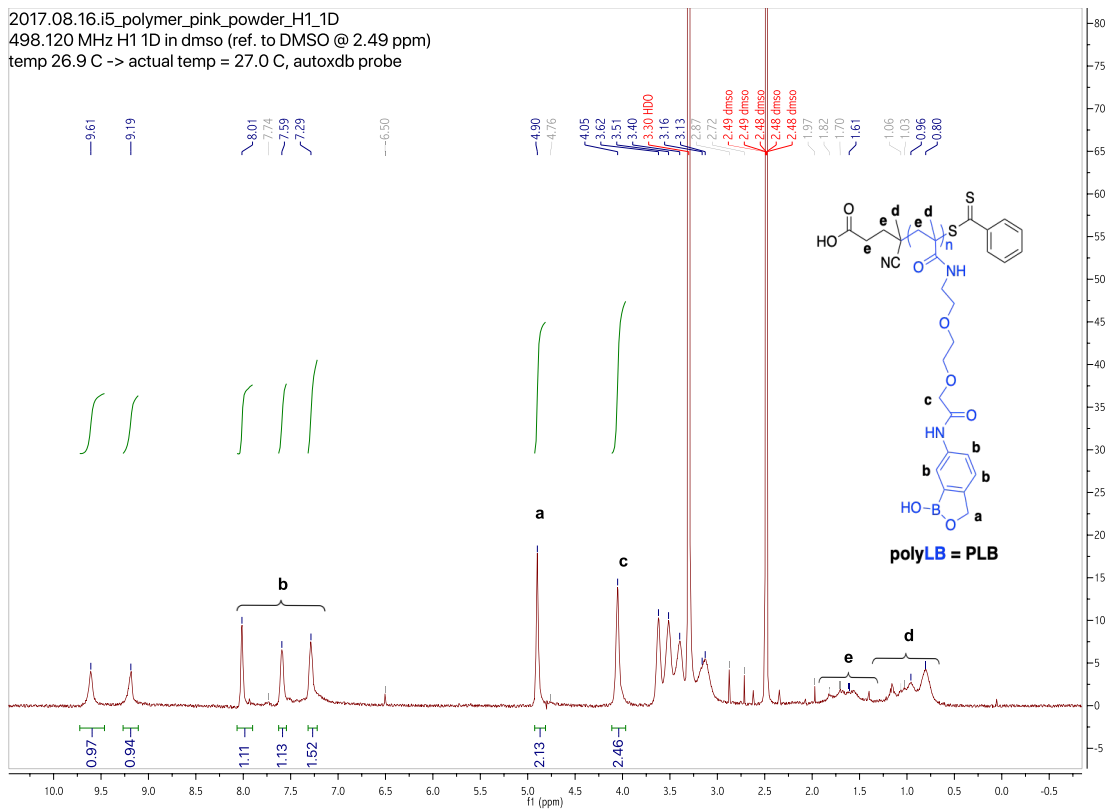
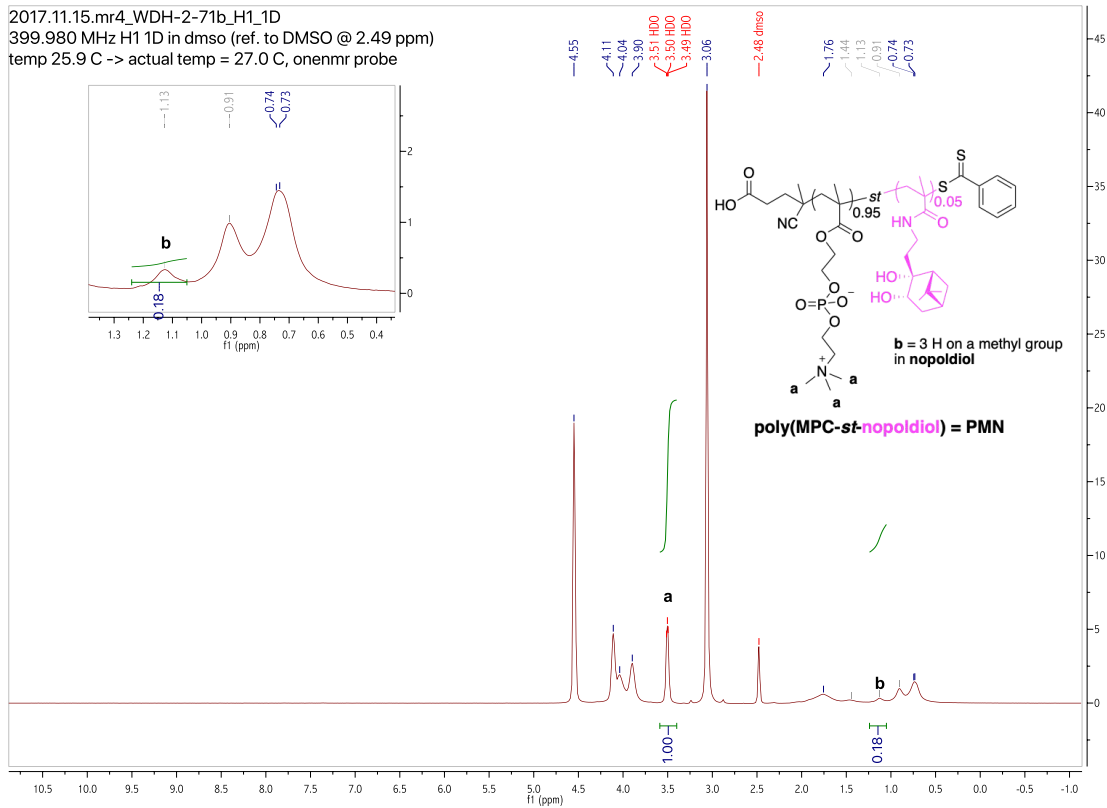






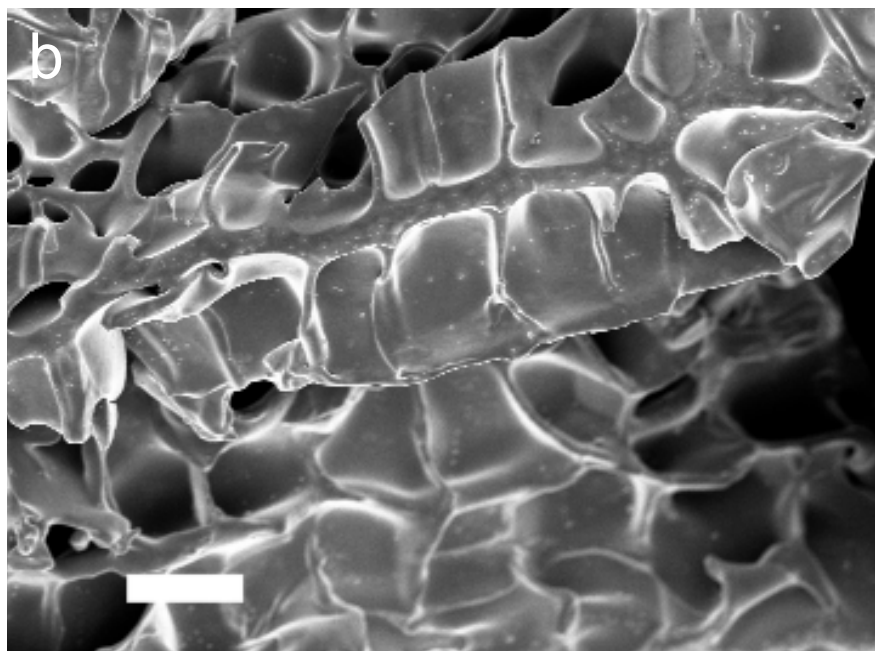
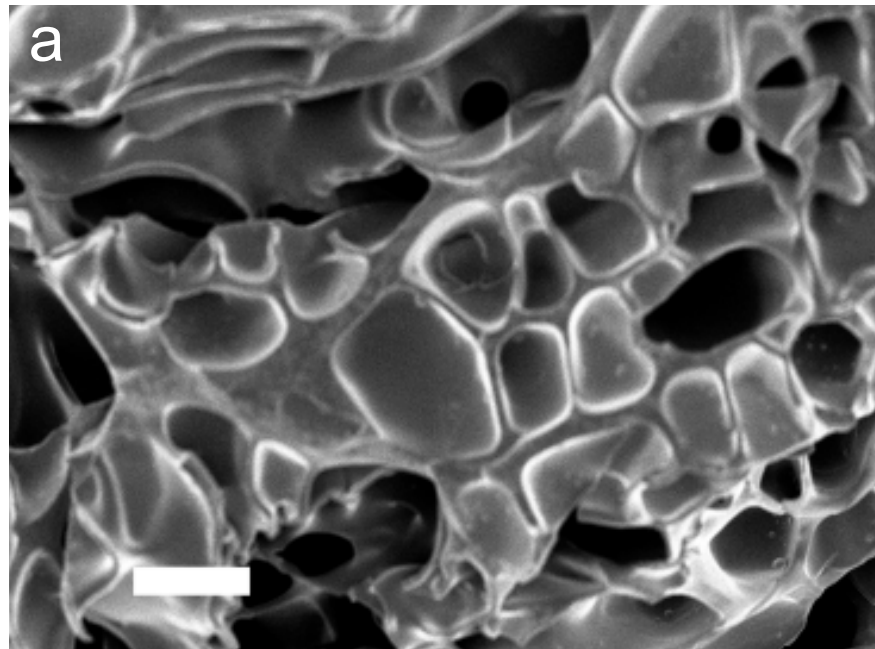
# Polymers:





Appendix 3: Enlarged SEM and CLSM images.

Figure 2-17:



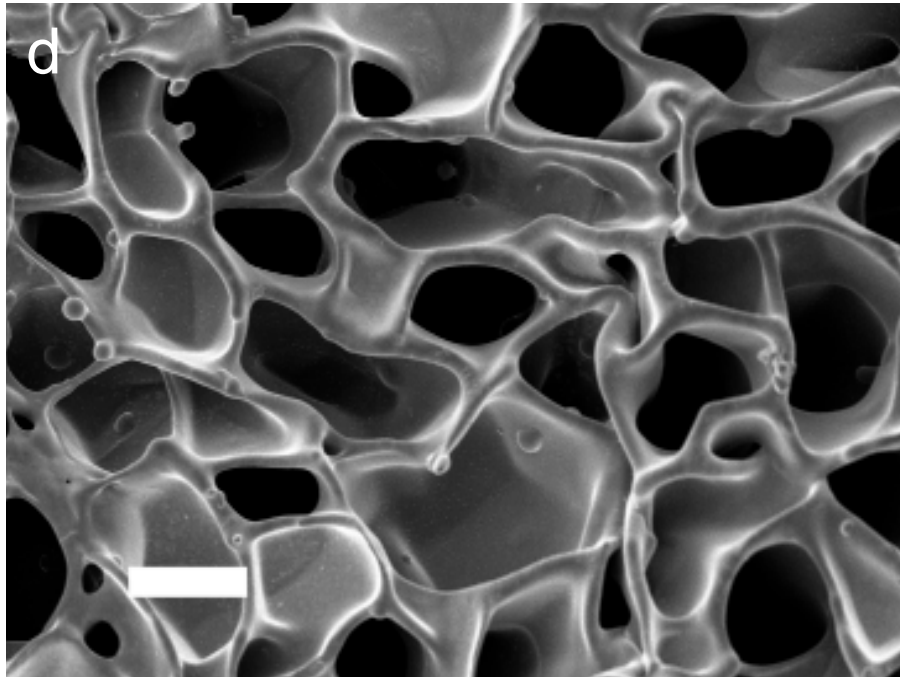
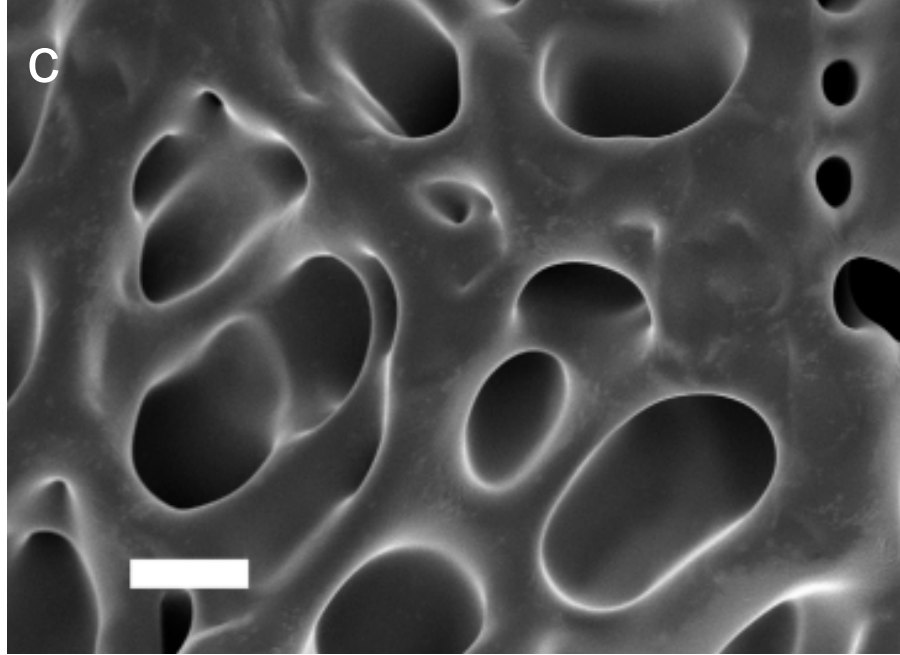
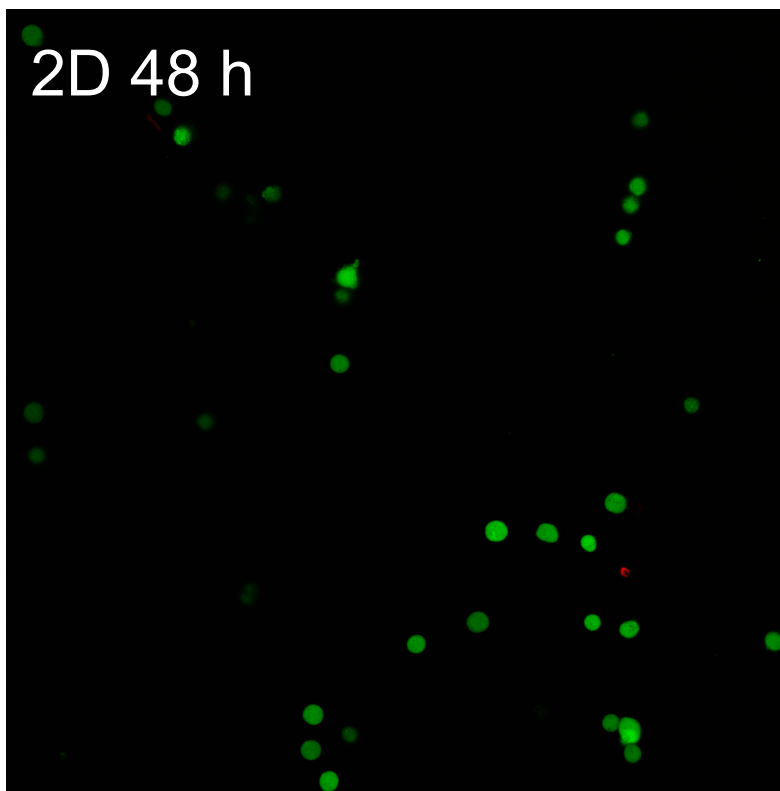
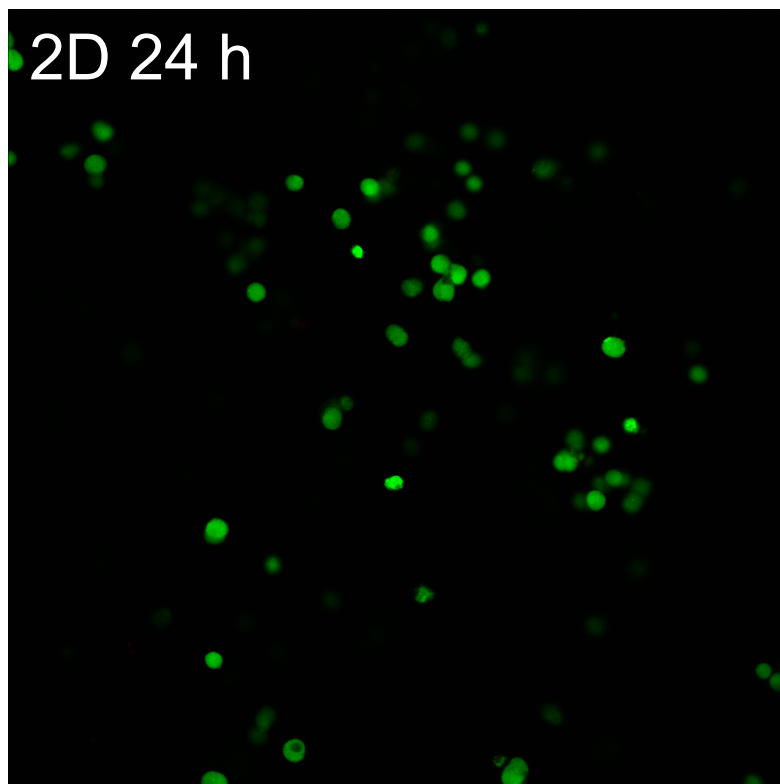
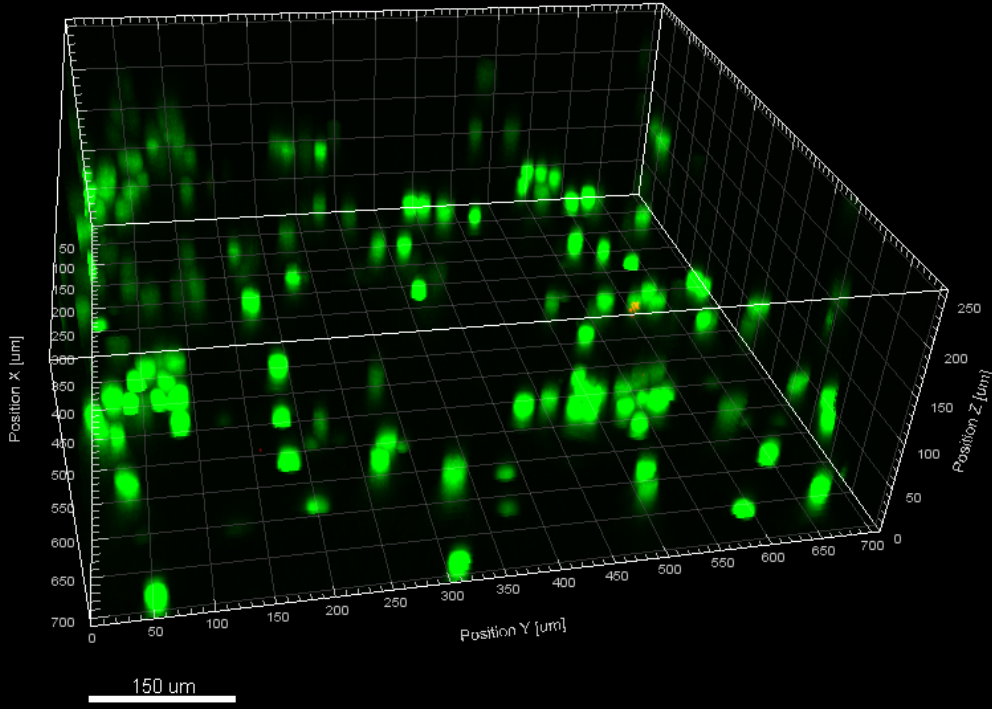


Figure 2-29 C:



# 3D 24 h



# 3D 48 h

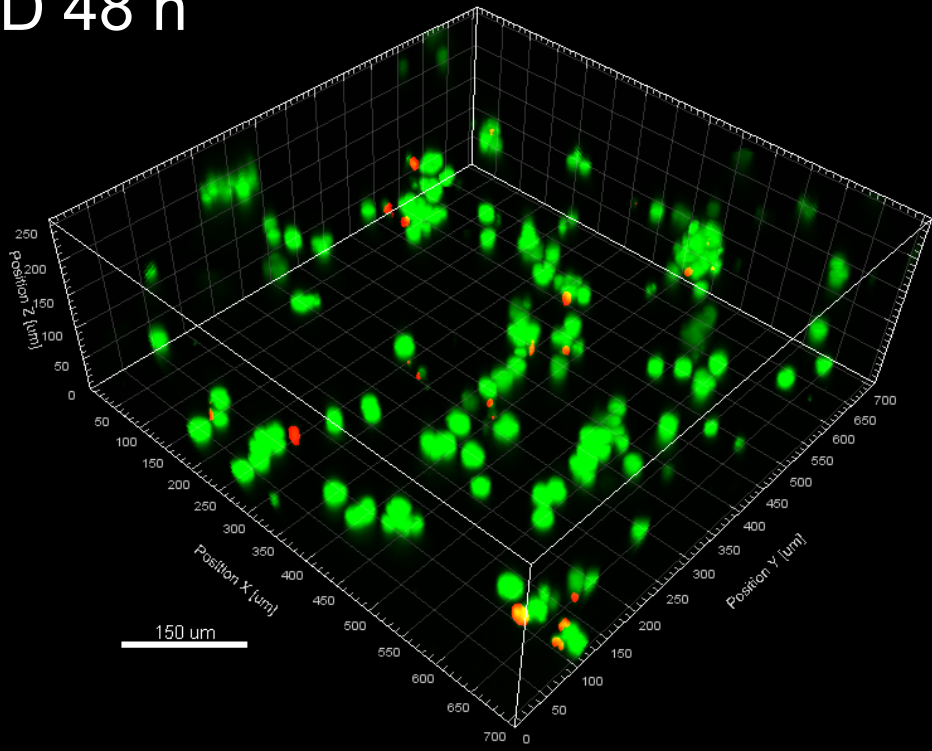
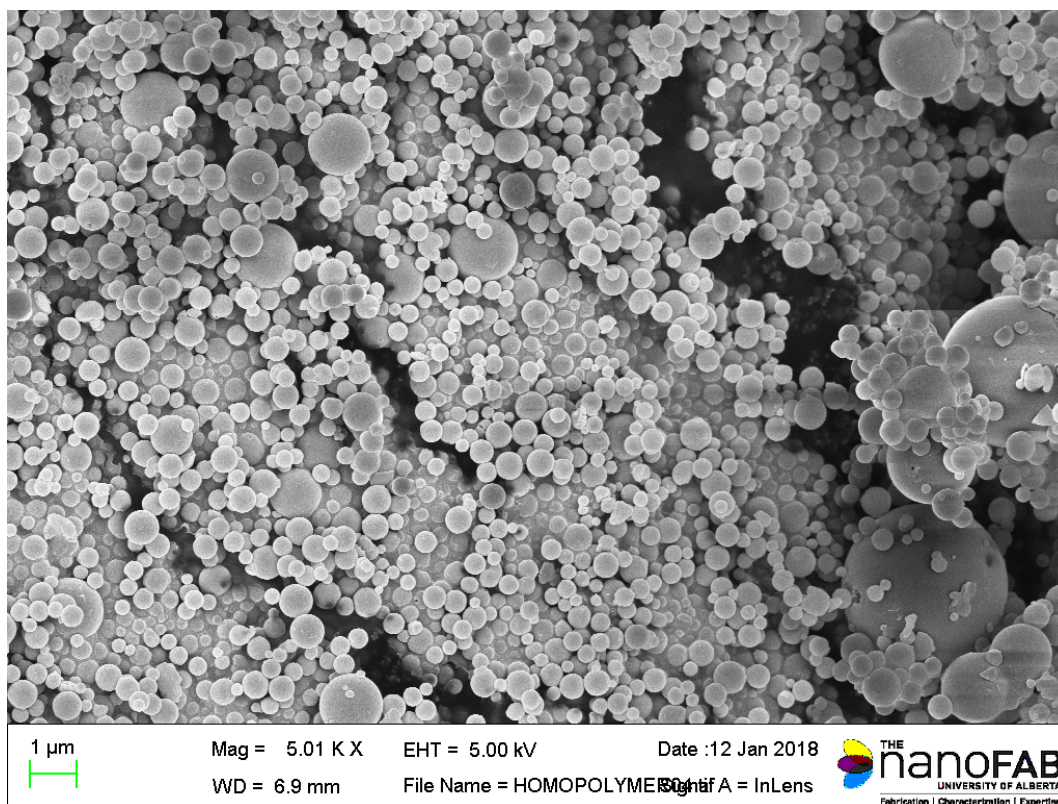
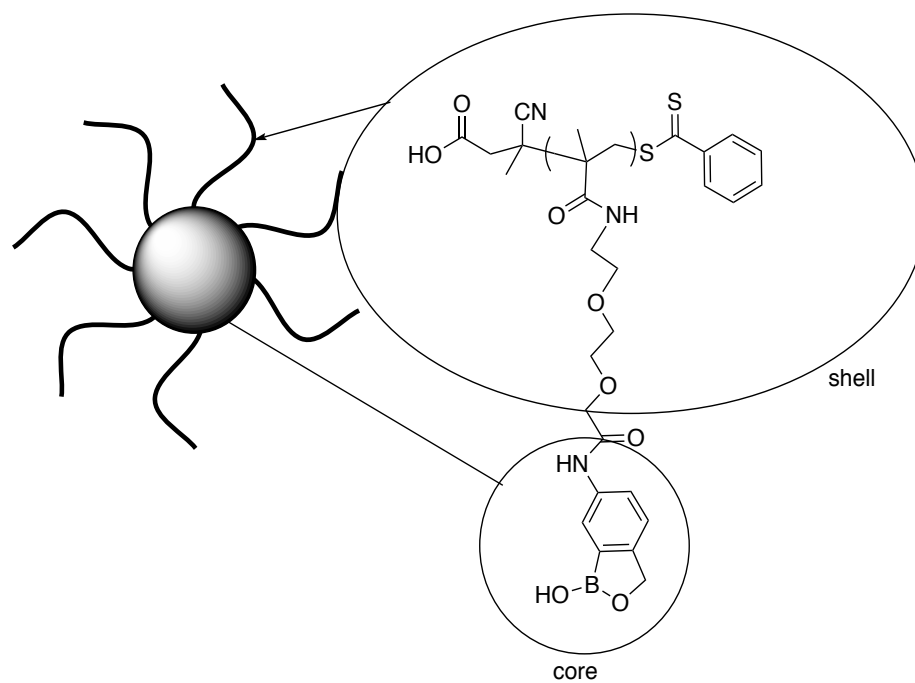


Figure 3-8:



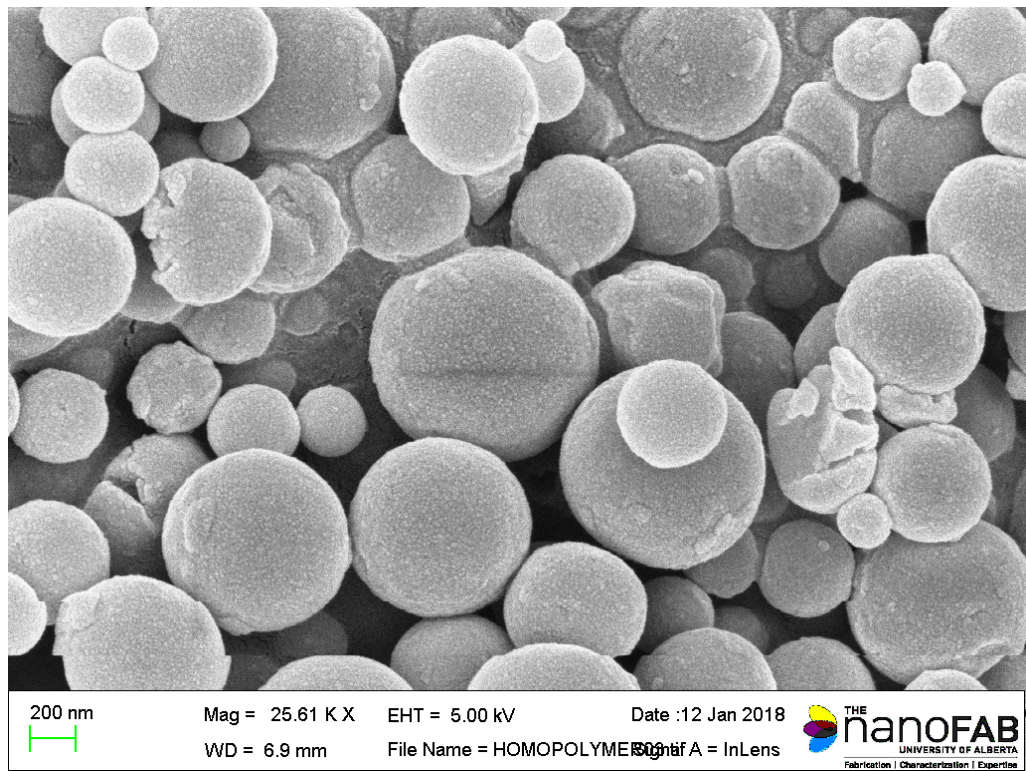
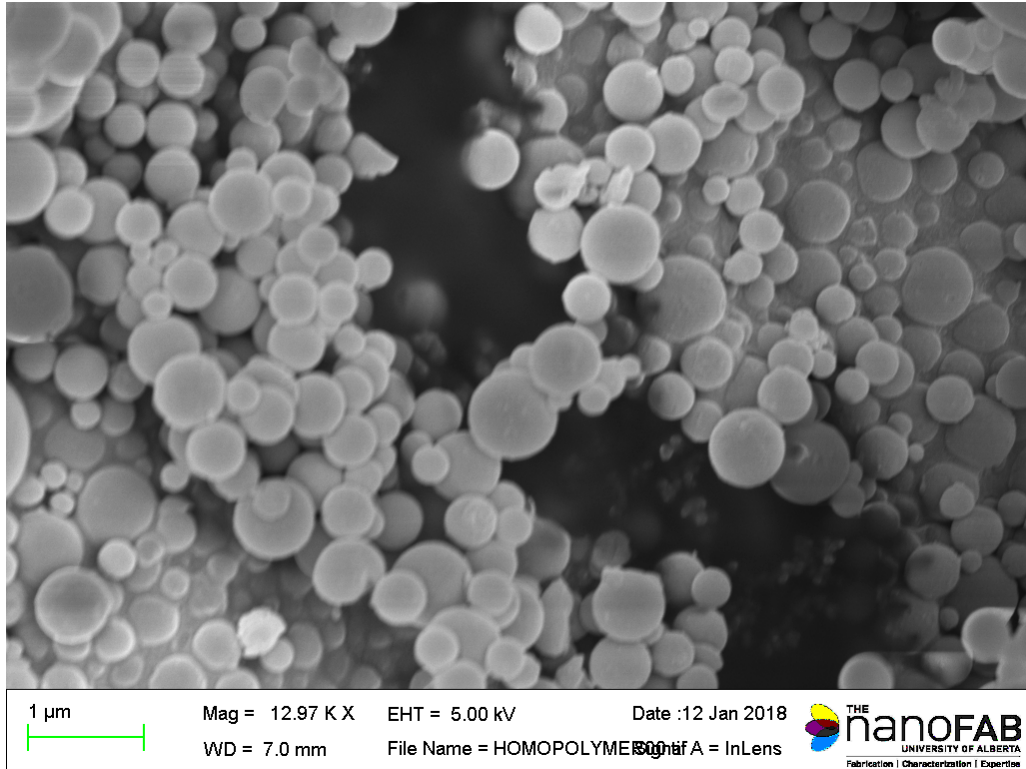
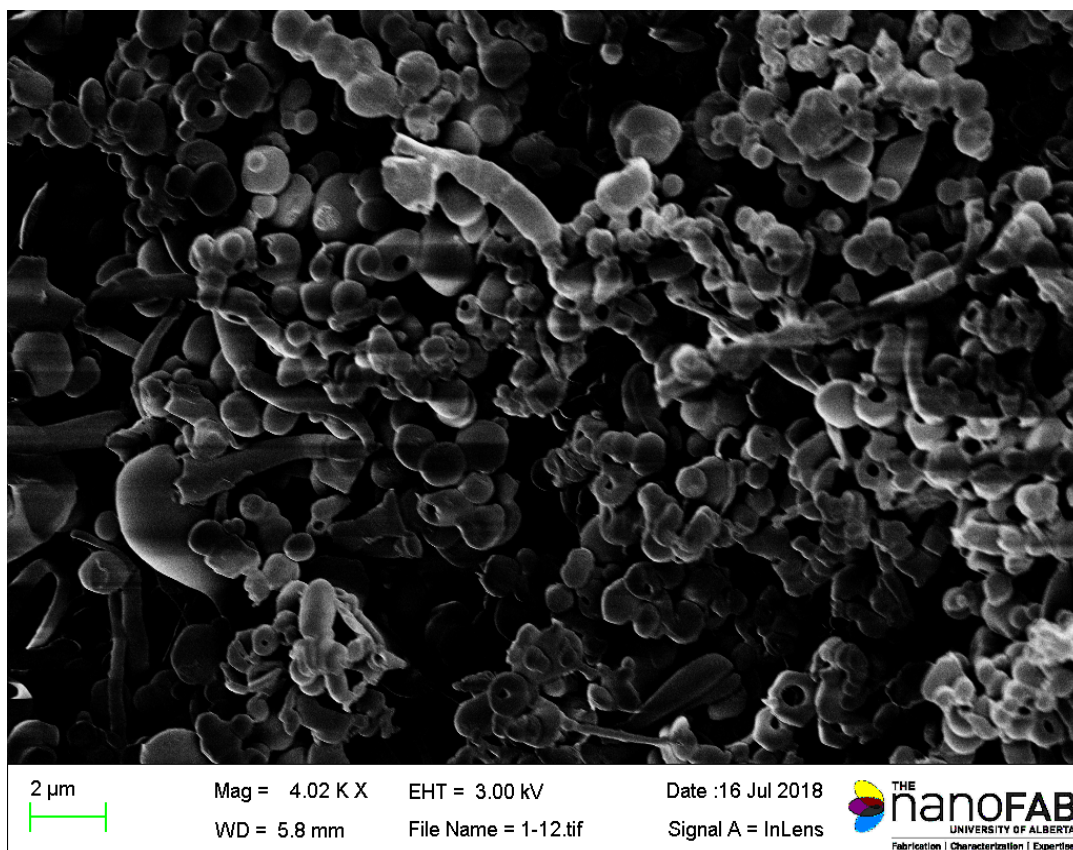
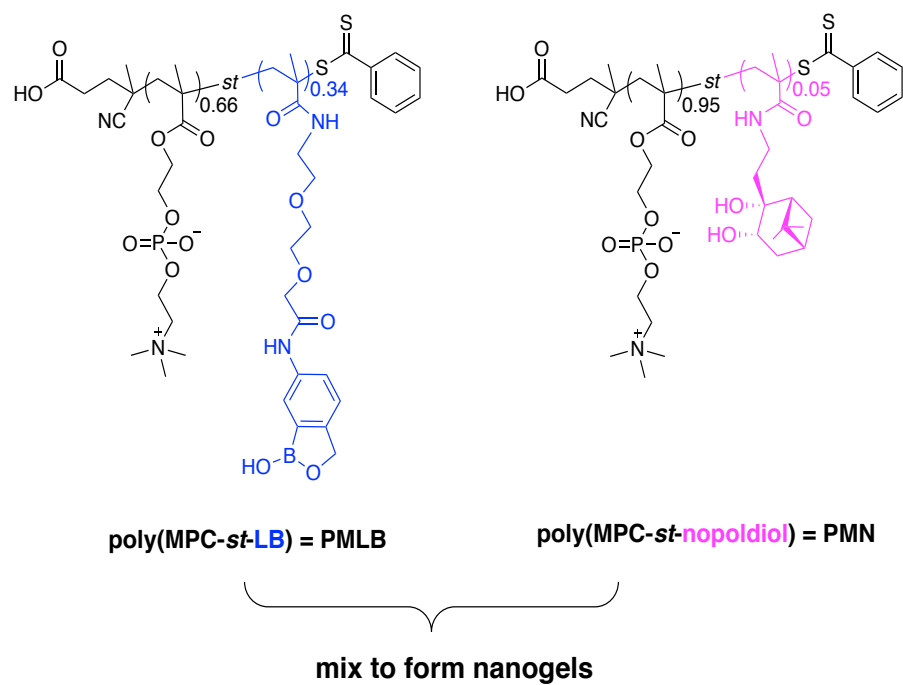
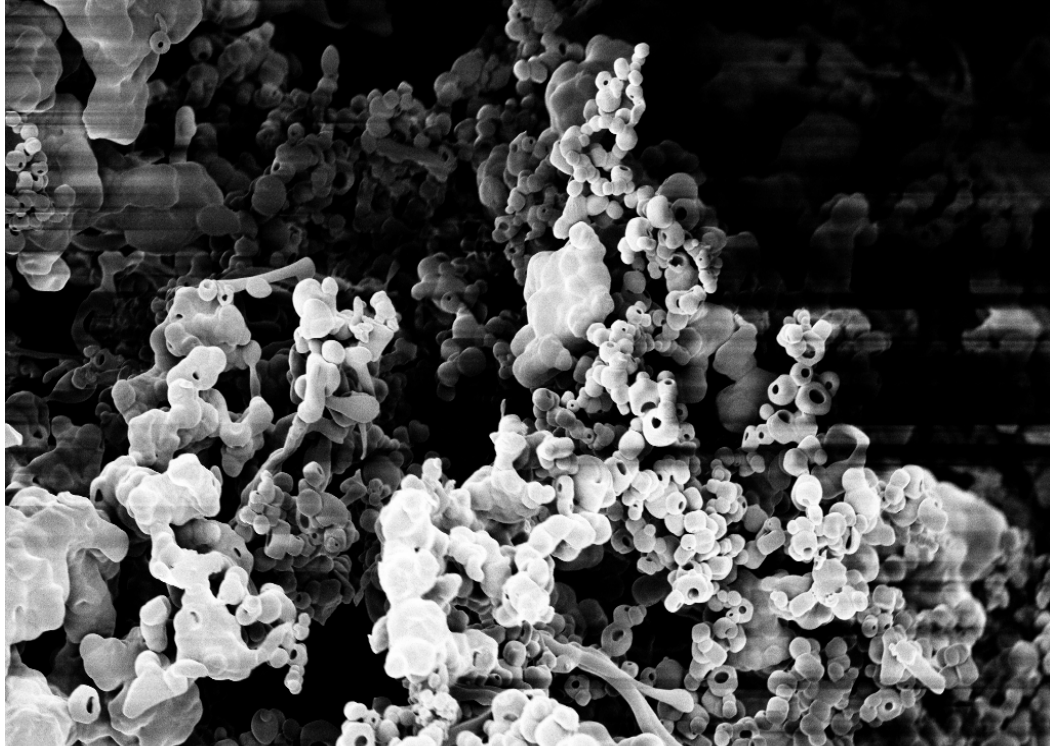


Figure 3-11:





2  $\mu$ m

Mag = 2.65 K X

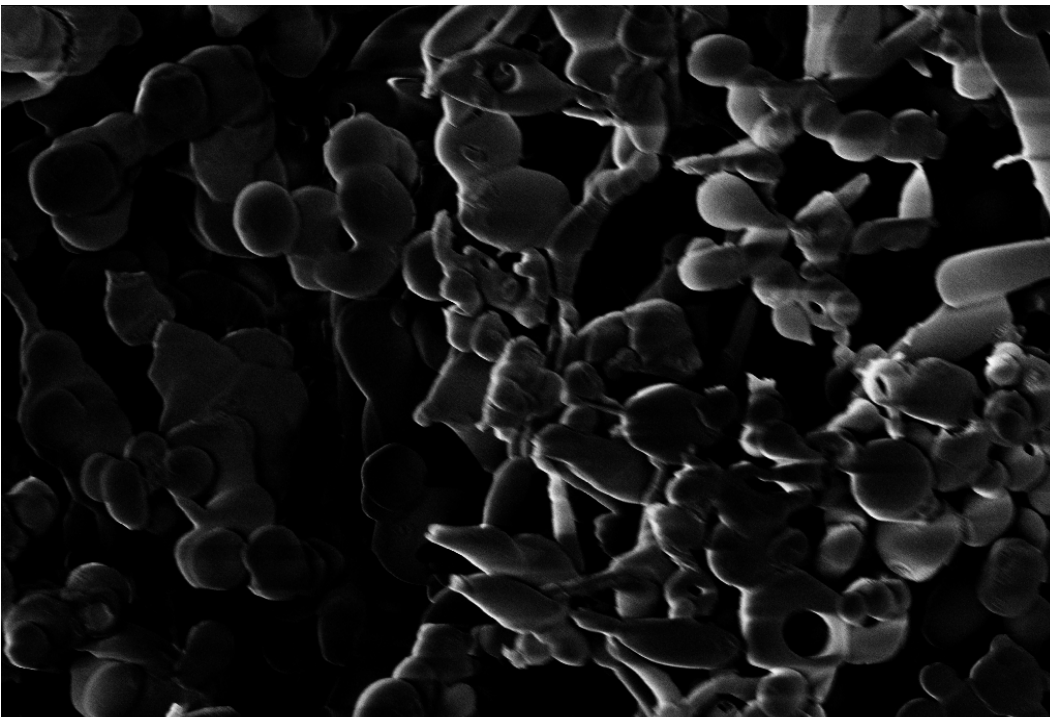
EHT = 3.00 kV

Date :16 Jul 2018

WD = 5.9 mm

File Name = 1-00.tif

Signal A = InLens



2  $\mu$ m

Mag = 7.99 K X

EHT = 3.00 kV

Date :16 Jul 2018

WD = 5.8 mm

File Name = 1-13.tif

Signal A = InLens

